



Sponsoring Agency Code FA4600-12-D-9000

EVALUATION OF MAXIMUM TIRE- PAVEMENT FRICTION COEFFICIENTS FOR A FORD CROWN VICTORIA

Submitted by

Cody S. Stolle, Ph.D., E.I.T.
Research Assistant Professor

Gabriela Perales, B.S.C.E.
Graduate Research Assistant

Laurence R. Rilett, Ph.D., P.E.
Professor and NTC Director

Ronald K. Faller, Ph.D., P.E.
Research Associate Professor and
MwRSF Director

James C. Holloway, M.S.C.E., E.I.T.
MwRSF Proving Grounds Manager

John D. Reid, Ph.D.
Professor

Ana L. Guajardo, B.S.M.E.
Graduate Research Assistant

MIDWEST ROADSIDE SAFETY FACILITY
130 Whittier Research Center
NEBRASKA TRANSPORTATION CENTER
262 Whittier Research Center
University of Nebraska-Lincoln
2200 Vine Street
Lincoln, Nebraska 68583-0853
(402) 472-0965

Submitted to

U.S. Army Corps of Engineers, Protective Design Center
1616 Capitol Avenue
Omaha, NE 68102

MwRSF Research Report No. TRP-03-341A-16

November 10, 2016

TECHNICAL REPORT DOCUMENTATION PAGE

1. Report No. TRP-03-341A-16	2.	3. Recipient's Accession No.	
4. Title and Subtitle Evaluation of Maximum Tire-Pavement Friction Coefficients for a Ford Crown Victoria		5. Report Date November 10, 2016	
		6.	
7. Author(s) Stolle, C.S., Perales, G., Rilett, L.R., Faller, R.K., Holloway, J.C., and Guajardo, L.A.		8. Performing Organization Report No. TRP-03-341A-16	
9. Performing Organization Name and Address Midwest Roadside Safety Facility (MwRSF) Nebraska Transportation Center University of Nebraska-Lincoln 130 Whittier Research Center 2200 Vine Street Lincoln, Nebraska 68583-0853		10. Project/Task/Work Unit No.	
		11. Contract © or Grant (G) No. FA4600-12-D-9000	
12. Sponsoring Organization Name and Address U.S. Army Corps of Engineers Protective Design Center 1616 Capitol Avenue Omaha, NE 68102		13. Type of Report and Period Covered Final Report: 2015-2016	
		14. Sponsoring Agency Code FA4600-12-D-9000	
15. Supplementary Notes Prepared with federal funds provided by USACE with assistance provided by USSTRATCOM and NSRI			
16. Abstract The U.S. Army Corps of Engineers (USACE) prepared a Threat Calculator to assist with estimation of a threat vehicle's worst-case travel time through Access Control Points (ACPs). A tire-pavement friction coefficient of 0.75 was used in the Calculator by default, leading to estimations for maximum possible accelerations during speeding up, slowing down, and turning (i.e., centripetal acceleration) of 0.35, 0.75, and 0.75 g's, respectively. Researchers at the University of Nebraska-Lincoln (UNL), in cooperation with the National Strategic Research Institute (NSRI), conducted a research study to determine the maximum rates of vehicle acceleration during speeding up, slowing down, and turning, and relate those accelerations to the maximum practical tire-ground coefficient of friction. The maximum 0.50-s average acceleration during braking for a single test and the average for all longitudinal acceleration tests were 1.03 and 1.01 g's, respectively. Likewise, the maximum centripetal acceleration for a single test and the average accelerations for all tests, approximating the as-driven radius at 106 ft, were 0.90 and 0.86 g's, respectively. The acceleration during speeding up declined as speeds increased, likely due to engine power limits and changes in transmission gears. Researchers recommend maximum braking and turning accelerations of 1.0 g's and 0.90 g's, respectively. These coefficients correspond to static (i.e., braking with anti-lock brakes, or ABS) and dynamic tire-pavement coefficients of friction of 1.00 and 0.90 g's, respectively. No changes are recommended for accelerations or frictions during speeding up.			
17. Document Analysis/Descriptors Vehicle Dynamics, Tire-Pavement Friction, Side Friction, Threat Calculator		18. Availability Statement Restricted. No portion of the report may be reproduced, copied, or transmitted without the explicit consent of USACE PDC.	
19. Security Class (this report) Unclassified	20. Security Class (this page) Unclassified	21. No. of Pages 128	22. Price

DISCLAIMER STATEMENT

This report was completed with funding provided by the United States Army Corps of Engineers (USACE), Protective Design Center (PDC), the National Strategic Research Institute (NSRI), and the U.S. Strategic Command (USSTRATCOM). The contents of this report reflect the views and opinions of the authors who are responsible for the facts and the accuracy of the data presented herein. The contents do not necessarily reflect the official views or policies of USACE PDC, NSRI, USSTRATCOM, or the U.S. Government. This report does not constitute a standard, specification, regulation, product endorsement, or an endorsement of manufacturers.

ACKNOWLEDGEMENTS

The authors wish to acknowledge several sources that made a contribution to this project: (1) USACE PDC for funding, guiding, and supporting this project; (2) MwRSF personnel for conducting the tests; (3) the Lincoln Airport Authority for providing access to the testing area; and (4) the Nebraska State Patrol, Lincoln Police Department, Lancaster County Sheriffs Office, and Nebraska Department of Roads for participating in the research effort and providing measurement equipment.

Acknowledgement is also given to the following individuals who made a contribution to the completion of this research project.

Midwest Roadside Safety Facility

M.A. Rasmussen, Laboratory Mechanic
E.W. Krier, Laboratory Mechanic
A.T. Russell, B.S.B.A., Shop Manager
D.S. Charroin, Laboratory Mechanic
C.J. Vargas, Undergraduate Research Assistant
B.D. Schroder, Undergraduate Research Assistant
K.A. Lechtenberg, M.S.M.E., E.I.T., Research Associate Engineer
R.W. Bielenberg, M.S.M.E., E.I.T., Research Associate Engineer
S.K. Rosenbaugh, M.S.C.E., E.I.T., Research Associate Engineer
J.D. Schmidt, Ph.D., P.E., Research Assistant Professor
S.M. Tighe, Laboratory Mechanic
Undergraduate and Graduate Research Assistants

USACE PDC

Brian W. Erickson
Robert Hallet
Mark Witloski

Nebraska State Patrol

Christopher Lutes
Frederick Storm
Major Brett Friesz
Tony Kavan

Lincoln Police Department

Captain Donald Scheinost
Sergeant Todd Kocian
Sergeant Mike Muff

Lancaster County Sheriffs Office

Investigator Drew Bolzer
Captain John Vik

Nebraska Department of Roads

Jeremy Weigel

TABLE OF CONTENTS

TECHNICAL REPORT DOCUMENTATION PAGE	i
DISCLAIMER STATEMENT	ii
ACKNOWLEDGEMENTS	iii
EXECUTIVE SUMMARY	1
1 INTRODUCTION	2
1.1 Background	2
1.2 Objective	3
1.3 Scope.....	4
2 LITERATURE REVIEW	5
2.1 Introduction.....	5
2.2 Federal Mandates	5
2.3 Policy and Road Design.....	5
2.4 Crash Reconstruction Measurements and Physical Testing Results.....	9
2.5 Tire and Friction Mechanics	11
2.5.1 Pavement Texture	12
2.5.2 Contact Patch and Tire Slip	12
2.5.3 Side Forces and Pneumatic Trail	15
2.5.4 Steering Models and Mechanics	18
2.6 Modifications for Enhanced Vehicle Performance.....	19
2.6.1 Vehicle Performance Modification Example No. 1: Ethanol	20
2.6.2 Vehicle Performance Modification Example No. 2: Braking Systems	21
2.7 Summary Evaluation of Factors Which Affect Tire-Pavement Friction Coefficients	22
3 FRICTION TESTING CONDITIONS	24
3.1 Test Layout	24
3.1.1 Threat Calculator Procedures.....	24
3.1.2 Test Layouts.....	25
3.2 Test Facility	28
3.3 Vehicle Navigation Conditions.....	28
3.4 Test Vehicles.....	28
3.5 Data Acquisition Systems	28
3.5.1 Accelerometers	28
3.5.2 VC4000DAQ	32
3.5.3 Digital Photography	32
3.6 External Instrumentation and Measurement Equipment.....	32
3.6.1 Skid Trailer (NDOR)	32
3.6.2 VC3000 (Lincoln Police Department)	33
3.6.3 Drag Sled (Lancaster County Sheriffs Office).....	34
3.7 Start and End of Test Determination	34
3.8 Data Processing.....	34

4 LONGITUDINAL FRICTION TEST RESULTS AND DISCUSSION	36
4.1 Weather Conditions	36
4.2 Test Details	36
4.3 Results.....	36
4.3.1 SLICE and VC4000	36
4.3.2 Locked Wheel Skid Trailer	45
4.3.3 Drag Sled	45
4.4 Comparisons with Threat Calculator Defaults.....	46
4.5 Conclusions, Discussion, and Recommendations.....	50
4.5.1 Threat Calculator Evaluation	50
4.5.2 Friction Measurement Methods	51
5 SIDE FRICTION TEST RESULTS AND DISCUSSION	52
5.1 Weather Conditions	52
5.2 Test Photography	52
5.3 Results.....	52
5.3.1 SLICE and VC4000	52
5.3.2 Locked Wheel Skid Trailer (NDOR)	65
5.3.3 Drag Sled (LSO)	65
5.4 Comparison with Threat Calculator.....	66
5.5 Discussion	70
6 SUMMARY, CONCLUSIONS, AND RECOMMENDATIONS	71
7 REFERENCES	72
8 APPENDICES	75
Appendix A. Test Results – Test No. LF-1	76
Appendix B. Test Results – Test No. LF-2.....	80
Appendix C. Test Results – Test No. LF-3.....	84
Appendix D. Test Results – Test No. LF-4	88
Appendix E. Test Results – Test No. LF-1b.....	92
Appendix F. Test Results – Test No. CF100-1	96
Appendix G. Test Results – Test No. CF100-2	100
Appendix H. Test Results – Test No. CF100-3	104
Appendix I. Test Results – Test No. CF100-b.....	108
Appendix J. Test Results – Test No. CF200-1.....	112
Appendix K. Test Results – Test No. CF200-2	116
Appendix L. Test Results – Test No. CF200-3.....	120
Appendix M. Test Results – Test No. CF200-1b.....	124

LIST OF FIGURES

Figure 1. AASHTO Green Book Tabulated Tests for Side Friction Factor [3].....	7
Figure 2. AASHTO Recommendations for Side Friction Factor for Design [3].....	7
Figure 3. Distances Required to Accelerate to Target Speed from a Reference Speed [3]	8
Figure 4. Braking Design Distances for Dry and Wet Pavements [3]	8
Figure 5. Braking Coefficient by Vehicle Model Year [12]	10
Figure 6. Distributions of Braking Coefficients of Friction by Brake Type [12]	10
Figure 7. Comparison of Longitudinal Braking Coefficient Distributions for ABS-Equipped Vehicles [12]	11
Figure 8. Effect and Size of Road Textures [9, 13]	12
Figure 9. Tire Slip Percentage vs. Effective Coefficient of Friction [9].....	13
Figure 10. Pressure, Friction, and Slip During Straight-Forward Braking [19]	14
Figure 11. Contact Patch Size and Mechanics (a) Steady-State, Straight-Line Driving and (b) Turning [17]	15
Figure 12. Suspension Relaxation and Camber Change During Cornering [19].....	16
Figure 13. Friction Circle Concept [22].....	16
Figure 14. Shear Force Generation on Tire Tread during Steady-State Cornering [17, 20].....	17
Figure 15. (a) Bicycle and (b) Four-Wheel Models of the Vehicle for Low-Speed, Large-Radius Turns [19]	18
Figure 16. Four-Bar Ackerman Steering Wheel Geometries for Forward, Left, and Right Turns (a) Ackerman Steering (b) Wheel Rotations [19].....	19
Figure 17. Test Layout and Parameters for LF Longitudinal Friction Test Series	26
Figure 18. Test Layout and Parameters for CF Side Friction Test Series	27
Figure 19. Test Vehicle, USACE Friction Tests.....	29
Figure 20. Vehicle Dimensions, USACE Friction Tests	30
Figure 21. Target Geometry, USACE Friction Tests	31
Figure 22. NDOR Locked Wheel Skid Trailer	33
Figure 23: ASTM E501 Ribbed Test Tire and ASTM E524 Smooth Test Tire	33
Figure 24. Sample Exterior Sequential Images (test no. LF-3 shown).....	37
Figure 25. Example Longitudinal Acceleration, Test No. LF-1	38
Figure 26. Example Braking Acceleration, Test No. LF-1	39
Figure 27. Comparison of Braking Accelerations for Test Nos. LF-1 through LF-4 and LF-1b.....	40
Figure 28. Acceleration vs. Speed, Test Nos. LF-1 through LF-4 and LF-1b.....	41
Figure 29. Detail View of Braking Acceleration vs. Speed (Note: X-axis reversed)	42
Figure 30. Example Velocity Comparison of Integrated SLICE Accelerations and VC4000 GPS and OBDII Port Speed Outputs for Test No. LF-1	43
Figure 31. Comparison of Longitudinal Velocity Results, Integrated SLICE and VC4000 GPS Output for Test Nos. LF-1 through LF-3.....	44
Figure 32. Comparison of Longitudinal Velocity Results, Integrated SLICE and VC4000 GPS Output for Test Nos. LF-4 and LF-1b	44
Figure 33. Braking Deceleration Comparison with USACE Threat Calculator Acceleration	47
Figure 34. Braking Speed Comparison with USACE Threat Calculator Calculated Speed Change	47
Figure 35. Test Distance Traveled While Braking Compared with USACE Threat Calculator Calculated Distance Traveled while Braking	48

Figure 36. Acceleration while Speeding Up Comparison with USACE Threat Calculator	49
Figure 37. Comparison of Test Results and USACE Threat Calculator Calculated Speed.....	49
Figure 38. Distance Traveled while Speeding Up Comparison with USACE Threat Calculator Calculated Distance.....	50
Figure 39. Example External Camera Sequential Images (test no. CF-100-3 shown)	53
Figure 40. Sample Occupant Compartment Sequential Images (test no. CF-100-3 shown)	54
Figure 41. Example Longitudinal and Lateral Acceleration, Test No. CF-100-3	55
Figure 42. Example Acceleration Magnitude, Test No. CF-100-1	55
Figure 43. Lateral Accelerations, Test Nos. CF-100-1 through CF-100-3 and CF-100-1b.....	56
Figure 44. Lateral Accelerations, Test Nos. CF-200-1 through CF-200-3 and CF-200-1b.....	57
Figure 45. GPS Speed Measurements, Test Nos. CF-100-1 through CF-100-3 and CF-100- 1b.....	58
Figure 46. GPS Speed Measurements, Test Nos. CF-200-1 through CF-200-3 and CF-200- 1b.....	59
Figure 47. Centripetal Accelerations, Test Nos. CF-100-1 through CF-100-3 and CF-100-1b	61
Figure 48. Centripetal Accelerations, Test Nos. CF-200-1 through CF-200-3 and CF-200-1b	61
Figure 49. Example Total and Magnitude of Lateral Acceleration (SLICE) and Calculated Centripetal Acceleration, Test No. CF-100-1	62
Figure 50. Example Total and Magnitude of Lateral Acceleration (VC4000) and Calculated Centripetal Acceleration, Test No. CF-100-1	62
Figure 51. Total Accelerations (SLICE), Test Nos. CF-100-1 through CF-100-3 and CF- 100-1b	63
Figure 52. Total Accelerations (SLICE), Test Nos. CF-200-1 through CF-200-3 and CF- 200-1b	63
Figure 53. Total Accelerations (VC4000), Test Nos. CF-100-1 through CF-100-3 and CF- 100-1b	64
Figure 54. Total Accelerations (VC4000), Test Nos. CF-200-1 through CF-200-3 and CF- 200-1b	64
Figure 55. Comparison of Test Lateral Accelerations and USACE Threat Calculator Limits for a 106-ft Average Radius.....	67
Figure 56. Comparison of Test Lateral Accelerations and USACE Threat Calculator Limits for a 208-ft Average Radius.....	67
Figure 57. Centripetal Acceleration Comparison with USACE Threat Calculator Limit for 106-ft Average Radius	68
Figure 58. Centripetal Acceleration Comparison with USACE Threat Calculator Limit for 208-ft Average Radius	68
Figure 59. Speed Comparison with USACE Threat Calculator for 106-ft Average Radius	69
Figure 60. Speed Comparison with USACE Threat Calculator for 208-ft Average Radius	69
Figure A-1. Longitudinal Acceleration, Test No. LF-1	77
Figure A-2. Braking Acceleration, Test No. LF-1	77
Figure A-3. Vehicle Speed, Test No. LF-1	78
Figure A-4. Speed During Acceleration, Test No. LF-1	78
Figure A-5. Speed During Braking, Test No. LF-1	79
Figure A-6. Distance Traveled, Test No. LF-1	79
Figure B-1. Longitudinal Acceleration, Test No. LF-2	81
Figure B-2. Braking Acceleration, Test No. LF-2	81

Figure B-3. Vehicle Speed, Test No. LF-2	82
Figure B-4. Speed During Acceleration, Test No. LF-2.....	82
Figure B-5. Speed During Braking, Test No. LF-2	83
Figure B-6. Distance Traveled, Test No. LF-2	83
Figure C-1. Longitudinal Acceleration, Test No. LF-3	85
Figure C-2. Braking Acceleration, Test No. LF-3	85
Figure C-3. Vehicle Speed, Test No. LF-3	86
Figure C-4. Speed During Acceleration, Test No. LF-3.....	86
Figure C-5. Speed During Braking, Test No. LF-3	87
Figure C-6. Distance Traveled, Test No. LF-3	87
Figure D-1. Longitudinal Acceleration, Test No. LF-4	89
Figure D-2. Braking Acceleration, Test No. LF-4.....	89
Figure D-3. Vehicle Speed, Test No. LF-4	90
Figure D-4. Speed During Acceleration, Test No. LF-4.....	90
Figure D-5. Speed During Braking, Test No. LF-4	91
Figure D-6. Distance Traveled, Test No. LF-4	91
Figure E-1. Longitudinal Acceleration, Test No. LF-1b	93
Figure E-2. Braking Acceleration, Test No. LF-1b	93
Figure E-3. Vehicle Speed, Test No. LF-1b	94
Figure E-4. Speed During Acceleration, Test No. LF-1b	94
Figure E-5. Speed During Braking, Test No. LF-1b.....	95
Figure F-1. Longitudinal Acceleration, Test No. CF100-1	97
Figure F-2. Lateral Acceleration, Test No. CF100-1	97
Figure F-3. Longitudinal and Lateral Acceleration, Test No. CF100-1	98
Figure F-4. Total Acceleration, Test No. CF100-1	98
Figure F-5. Speed, Test No. CF100-1	99
Figure G-1. Longitudinal Acceleration, Test No. CF100-2.....	101
Figure G-2. Lateral Acceleration, Test No. CF100-2	101
Figure G-3. Longitudinal and Lateral Acceleration, Test No. CF100-2.....	102
Figure G-4. Total Acceleration, Test No. CF100-2	102
Figure G-5. Speed, Test No. CF100-2	103
Figure H-1. Longitudinal Acceleration, Test No. CF100-3.....	105
Figure H-2. Lateral Acceleration, Test No. CF100-3	105
Figure H-3. Longitudinal and Lateral Acceleration, Test No. CF100-3	106
Figure H-4. Total Acceleration, Test No. CF100-3	106
Figure H-5. Speed, Test No. CF100-3	107
Figure I-1. Longitudinal Acceleration, Test No. CF100-b	109
Figure I-2. Lateral Acceleration, Test No. CF100-b.....	109
Figure I-3. Longitudinal and Lateral Acceleration, Test No. CF100-b	110
Figure I-4. Total Acceleration, Test No. CF100-b.....	110
Figure I-5. Speed, Test No. CF100-b.....	111
Figure J-1. Longitudinal Acceleration, Test No. CF200-1	113
Figure J-2. Lateral Acceleration, Test No. CF200-1	113
Figure J-3. Longitudinal and Lateral Acceleration, Test No. CF200-1	114
Figure J-4. Total Acceleration, Test No. CF200-1	114
Figure J-5. Speed, Test No. CF200-1	115
Figure K-1. Longitudinal Acceleration, Test No. CF200-2.....	117

Figure K-2. Lateral Acceleration, Test No. CF200-2	117
Figure K-3. Longitudinal and Lateral Acceleration, Test No. CF200-2.....	118
Figure K-4. Total Acceleration, Test No. CF200-2	118
Figure K-5. Speed, Test No. CF200-1	119
Figure L-1. Longitudinal Acceleration, Test No. CF200-3	121
Figure L-2. Lateral Acceleration, Test No. CF200-3.....	121
Figure L-3. Longitudinal and Lateral Acceleration, Test No. CF200-3	122
Figure L-4. Total Acceleration, Test No. CF200-3	122
Figure L-5. Speed, Test No. CF200-3.....	123
Figure M-1. Longitudinal Acceleration, Test No. CF200-1b	125
Figure M-2. Lateral Acceleration, Test No. CF200-1b	125
Figure M-3. Longitudinal and Lateral Acceleration, Test No. CF200-1b	126
Figure M-4. Total Acceleration, Test No. CF200-1b	126
Figure M-5. Speed, Test No. CF200-1b	127

LIST OF TABLES

Table 1. Examples of Aftermarket Vehicle Performance Improvements.....	20
Table 2. Ranking of Factors Affecting Friction and Approximate Reduction Factors (if applicable).....	23
Table 3. Weather Conditions, Test Nos. LF-1 through LF-4 and LF-1b.....	36
Table 4. Maximum Average Braking Accelerations, Test Nos. LF-1 through LF-4 and LF-1b.....	39
Table 5. Maximum Average Braking Acceleration Results Summary.....	40
Table 6. Skid Trailer Reported Skidding Coefficients of Friction, ASTM E501 Ribbed Tire.....	45
Table 7. Skid Trailer Reported Skidding Coefficients of Friction, ASTM E524 Smooth Tire.....	45
Table 8. Drag Sled Test Results.....	46
Table 9. Weather Conditions, USACE Friction Tests	52
Table 10. Maximum Test Speeds at 1 st and 2 nd Slip Conditions	60
Table 11. Range of Possible Maximum Centripetal Accelerations Based on Possible Trajectory Radii	60
Table 12. Locked Wheel Skid Trailer Friction Measurements in CF-100 and CF-200 Test Areas	65
Table 13. Drag Sled Pull Force Results, CF-100 Test Area	66
Table 14. Drag Sled Pull Force Results, CF-200 Test Area	66

EXECUTIVE SUMMARY

The U.S. Army Corps of Engineers (USACE) prepared a Threat Calculator to assist with estimation of a threat vehicle's worst-case travel time through Access Control Points (ACPs). A tire-pavement friction coefficient of 0.75 was used in the Calculator by default, leading to estimations for maximum possible accelerations during speeding up, slowing down, and turning (i.e., centripetal acceleration) of 0.35, 0.75, and 0.75 g's, respectively. Researchers at the University of Nebraska-Lincoln (UNL), in cooperation with the National Strategic Research Institute (NSRI), conducted a research study to determine the maximum rates of vehicle acceleration during speeding up, slowing down, and turning, and relate those accelerations to the maximum practical tire-ground coefficient of friction.

Five longitudinal acceleration and braking tests were conducted: test nos. LF-1 through LF-4 and LF-1b. The maximum test vehicle acceleration declined with increasing speed and time, as a result of gear changes and engine power limitations. The maximum 0.50-s average acceleration during braking for a single test and the average accelerations for all longitudinal tests were 1.03 and 1.01 g's, respectively. Researchers recommended a maximum longitudinal coefficient of braking of 1.0 g's for simplicity.

Eight circular curve tests were also conducted to determine the maximum available side friction. Drag sled and skid trailer friction measurements suggested that there was a lower total available friction in the circular test area by approximately 0.05. The maximum centripetal acceleration for a single test was 0.90 g's, and the average maximum centripetal accelerations for the CF100 and CF200 tests were 0.86 and 0.84 g's, respectively. Researchers recommended a maximum centripetal acceleration of 0.90 g's for use with the Threat Calculator.

The next step in the research process is to construct target test geometries which are similar to the inputs of the Threat Calculator and evaluate estimated and actual travel times and vehicle speeds throughout the test areas.

1 INTRODUCTION

1.1 Background

Military bases are designed to facilitate military and civilian traffic through Access Control Points (ACPs), which are traffic corridors leading into military bases. Military personnel observing the operations within an ACP must quickly react to unauthorized individuals and vehicles attempting to gain entry to a military base and determine which, if any, pose a threat to the security of the base. Identification of a possible threat vehicle by military personnel leads to the activation of deployable barriers at the end of the ACP, known as Active Vehicle Barriers (AVBs).

The Army Corps of Engineers (USACE) identified four worst-case threat vehicle behaviors (i.e., threat scenarios) which could occur as a threat vehicle navigates an ACP [1]:

- Scenario 1: Threat vehicle enters the ACP at the maximum entry speed which can still navigate through the ACP. Threat vehicle maneuvers through the ACP at maximum speed at all times.
- Scenario 2: Threat vehicle enters the ACP at a low speed to avoid detection from over-speed detectors. The threat vehicle navigates the remainder of the ACP at maximum speed. (This scenario is not applicable if over-speed detection is not used.)
- Scenario 3: Threat vehicle briefly stops at security checkpoint, but abruptly travels at maximum acceleration and speed through the Response Zone.
- Scenario 4: Threat vehicle is rejected at security checkpoint and acts as though it were attempting to leave ACP via turnaround lanes. Instead, the threat vehicle turns and travels at maximum acceleration and speed through the Response Zone.

USACE identified that up to 9 seconds may be required to adequately respond to the threat vehicle: 3 seconds for a guard in the Access Control Zone to identify and respond to a threat; 4 seconds for warning light activation; and 2 seconds to fully deploy an Active Vehicle Barrier (AVB) [1]. Subsequently, the Air Force Civil Engineering Center (AFCEC) evaluated minimum lengths of an ACP which will provide the necessary response time, depending on anticipated threat vehicle travel speeds [2]. Currently, USACE recommends that the maximum straight-line speed that a threat vehicle will be capable of sustaining in an ACP is 120 mph. Therefore, using the Scenario 1 assumptions, a long, straight ACP must be 1,584 ft to prevent the threat vehicle from bypassing the AVB. Purchasing and maintaining this amount of land for ACP use is likely cost-prohibitive for most bases, thus alternative passive safety techniques must be used to shorten the ACP and increase threat vehicle travel times, including introduction of curves, chicanes, or passive safety devices.

A tool for assessing various implementation of passive safety schemes in ACPs is the USACE Threat Calculator, a spreadsheet-based tool which allows the user to input a threat vehicle's starting speed and the geometry of its trajectory using tangent lines and circular curves. The Calculator then determines the maximum possible speeds throughout the trajectory. The Threat Calculator fundamentally uses the assumption that a threat driver will always attempt to accelerate¹

¹ Note: Acceleration refers to any time-varying difference in velocity magnitude or direction. Accelerations while speeding up are positive in the longitudinal direction, and accelerations while braking or slowing down are negative in the longitudinal direction. Left and right turns generate negative and positive lateral accelerations, respectively.

at the maximum possible rate, until reaching the maximum possible speed. USACE recommends a maximum possible speed of 120 mph. Currently, by default, the maximum accelerations during speeding up, slowing down, and turning (i.e., centripetal acceleration) are 11.3, 24.1, and 24.1 ft/s² (0.35, 0.75, and 0.75 g's), respectively. Because the Threat Calculator always assumes that the vehicle is either traveling at the maximum possible acceleration or the maximum speed of 120 mph, the behavior of the Threat Calculator vehicle model was deemed by researchers as the Maximum Threat Calculator Acceleration and Speed (MTCAS).

Newton's 2nd Law dictates that the net force acting on a vehicle is equal to its mass times net acceleration. By assuming that the ground is flat and that the weight of the vehicle remains constant, there is no net vertical acceleration, and thus the weight is exactly counterbalanced by the vertical (normal) force from the ground surface. A friction coefficient is universally described as the ratio of planar shear force to the normal force acting on a body:

$$\mu = \frac{F_s}{N} \quad (1)$$

μ = friction coefficient

F_s = magnitude of planar shear force

N = magnitude of normal force

If the friction force, F_s , is the only unbalanced force, then the friction coefficient can be related to the vehicle net acceleration by:

$$\mu = \frac{F_s}{N} = \frac{m|\mathbf{a}|}{mg} = a_g \quad (2)$$

$|\mathbf{a}|$ = magnitude of vehicle acceleration vector (note: acceleration is in horizontal plane)

a_g = acceleration measured in the units of g's (1 g = 32.2 ft/s² = 9.81 m/s²); $a_g = a/g$

Thus, the effective maximum coefficient of friction used in the Threat Calculator is 0.75 for longitudinal braking and 0.75 for side friction (i.e., related to maximum centripetal acceleration). Note that the friction applicable for speeding up is affected by engine power limits, tire-pavement friction, and the number of wheels powered by the engine (e.g., two wheel drive or 2WD). Therefore, the Threat Calculator limit for acceleration while speeding up is less than the maximum coefficient of tire-pavement friction.

Unfortunately, recent evidence has suggested that the effective maximum coefficient of friction of 0.75 may be less than what real threat drivers can achieve. If threat vehicles use more of the available friction throughout an ACP, it may be possible for the threat drivers to pass by the AVBs before they are deployed, even though the calculator suggests that there is enough time to respond. Thus, representatives at USACE PDC contacted researchers at the University of Nebraska-Lincoln to conduct tests to determine the maximum vehicle performance of a threat vehicle under practical worst-case driving conditions.

1.2 Objective

The objective of this research effort was to investigate factors affecting tire-pavement friction, determine the maximum vehicle acceleration limits, and critically evaluate whether or not the Threat Calculator could accurately estimate worst-case vehicle travel times.

1.3 Scope

To complete the project objectives, several tasks were undertaken:

- (1) A literature review was conducted to identify factors affecting tire-pavement friction, mechanics of friction, experimental and theoretical maximum friction values, and friction measurement techniques.
- (2) Researchers evaluated costs and availability of friction measurement devices and measurement techniques.
- (3) Tests were designed and drawn in CAD with the goal of calculating friction limits in the longitudinal and lateral directions, and were sent to USACE for approval.
- (4) Results were analyzed and effective maximum utilized friction values were determined and recommended to USACE.
- (5) Additional test setups were designed and drawn in CAD, with the goal of comparing estimates of Threat Calculator travel times to test travel times. Drawings and test conditions were submitted to USACE for review and approval.
- (6) Test results were analyzed and compared to Threat Calculator estimates. The Threat Calculator assumptions and methodology were evaluated.
- (7) Summary reports were written describing all test results and findings.

This report describes the results of the initial round of testing and analysis (tasks 1-4).

2 LITERATURE REVIEW

2.1 Introduction

Tire-pavement friction measurements have been conducted for many decades. Many contemporary roadway designs are based on the observed values of friction being used by drivers for many years [3]. Many pavement studies have also been conducted to evaluate existing tire-pavement friction and to determine what coatings, materials, or construction techniques can improve friction. Some examples of tire-pavement friction research and how various factors affect friction values are discussed in the following sections.

2.2 Federal Mandates

The Federal Mandate for the Federal Motor Vehicle Safety Standard (FMVSS) No. 105 requires that Portland Cement concrete surfaces be used to establish vehicle braking capacities which have a skid number of 81, which correlates to a tire-roadway fully-skidding coefficient of friction of approximately 0.81 [4]. This standard also requires that passenger cars be braked to a complete stop from 95 mph or more at an effective rate of at least 15 ft/s^2 (0.47 g's), which corresponds to an effective sustained coefficient of tire-pavement friction of 0.47. Motorcycles must satisfy similar requirements [5]. All passenger vehicle manufacturers exceed the minimum braking requirements of FMVSS 105 and 122 [4-5].

With the advent of anti-lock brake systems (ABS) and intelligent vehicles with active braking assist meant to reduce the risk of inattentive drivers crashing into objects ahead of or behind them, recent advances in braking technology have approached a factor of safety of nearly three (3) compared to FMVSS minimum requirements in terms of brake force capability. Nonetheless, the maximum brake force available at the brake rotor is typically higher than the maximum brake force achievable at the tire-pavement interface.

2.3 Policy and Road Design

Highway curve radii are selected such that, at the posted speed limit, vehicle traffic will not experience skidding on either wet or dry pavements [3]. To ensure that pavement will retain sufficient friction under various weather conditions as it ages, factors of safety are built into roadway and pavement design based on past experimental data.

Since the early 1930s, many experimental tests have been conducted to determine the range of side friction coefficients (i.e., centripetal accelerations) which drivers will comfortably and reliably utilize when reasonable to do so. These limits have been incorporated into the modern design guides, such as the *Policy on Geometric Design of Highways and Streets* (AASHTO Green Book) which is the contemporary guide for roadway construction and design in the U.S. [3]. Some examples of historical and contemporary design guidelines are provided below.

Stonex and Noble evaluated the limits of vehicle fleet capabilities and steering limitations on the Pennsylvania Turnpike in 1940 [6]. A total of 191 curves summing up to $50\frac{1}{2}$ miles in length with radii varying from 38,197 ft to 955 ft were analyzed. For these tests, drivers were asked to navigate around curve radii with speeds sufficient to produce 0.10 g's of centripetal acceleration, then gradually increase speeds during successive tests on the same radii. Speeds were recorded for each

test by measuring the crossing time of the vehicle at 200-ft increments throughout the curve. Accelerometers were also used to continuously estimate centripetal friction used. Tests were conducted with both wet and dry concrete pavements. The skidding coefficients of friction on the turnpike were measured by locking the rear wheels of the test vehicle and towing the test vehicle while recording the tow force with a dynamometer. With approximately 1,888 pounds over the rear axle, wet and dry pavement coefficients of friction were measured at 0.64 and 0.62, respectively. Stonex and Noble hypothesized that the unexpected lower coefficient of dry pavement friction was related to the melting lubrication of the tire while being towed.

Barnett developed a conservative measure of the maximum side friction a driver would tolerate by requiring drivers to navigate a series of curves and asking the drivers to identify the speed and radius combinations which produced a noticeable roll angle displacement [7]. Test results indicated that many drivers identified sensing a roll angle displacement at a centripetal acceleration of 0.16 g's at speeds up to 60 mph. For higher speeds, drivers identified sensing roll angles at smaller centripetal accelerations. On average, the centripetal acceleration at which roll angles were identified decreased by 0.01 g's for each increase of 5 mph.

A separate study evaluating 900 driving tests, predominantly using passenger cars, was used to study friction while cornering by recording the cornering speed [8]. The vehicle type, tire wear condition at test time, pavement type, and geographic location were varied during testing. In general, friction coefficients used during cornering maneuvers varied between 0.10 and 0.20, although results were limited for turns at speeds at or greater than 60 mph. Drivers also completed turns at higher speeds during dry conditions than during wet conditions.

As of September of 2016, the 2011 Green Book is the most recent version to be published [3]. This manual provides recommendations for the design of roadway curves based on design speeds and maximum utilized friction coefficients on turns, using tabulated results from studies dating back to the 1930s. Examples of roadway design coefficients for turning are shown in Figures 1 and 2.

In addition to tabulating the side friction testing and recommendations for design, the 2011 Green Book also tabulated distances associated with speeding up from rest to a target speed, as well as distances associated with braking from the target speed to a complete stop, as shown in Figures 3 and 4. The acceleration chart shown in Figure 3 used a declining acceleration as vehicle speed increased, ranging from approximately 0.13 g's (4.3 ft/s^2) at rest to approximately 0.1 g (3.2 ft/s^2) at 55 mph.

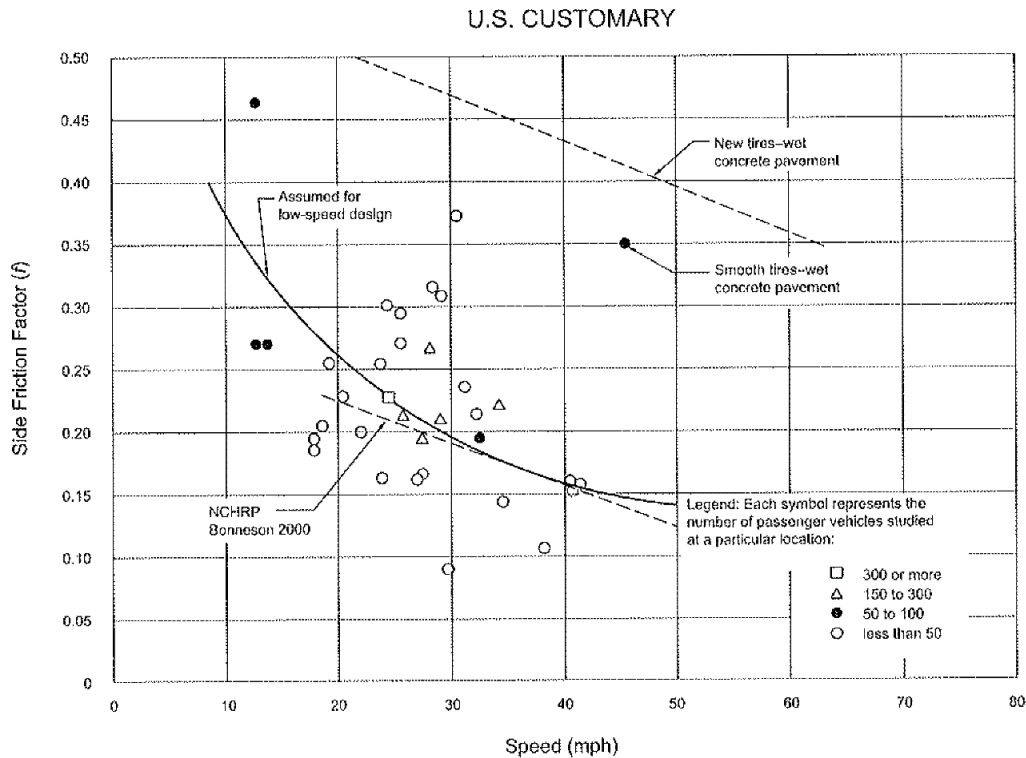


Figure 1. AASHTO Green Book Tabulated Tests for Side Friction Factor [3]

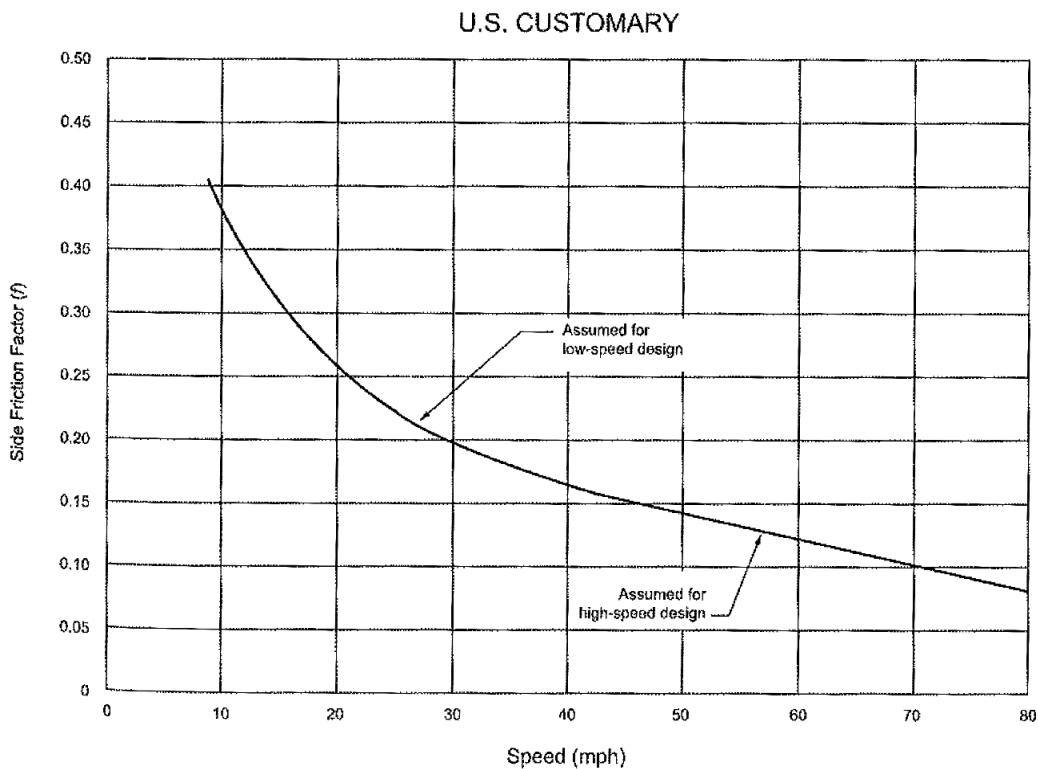


Figure 2. AASHTO Recommendations for Side Friction Factor for Design [3]

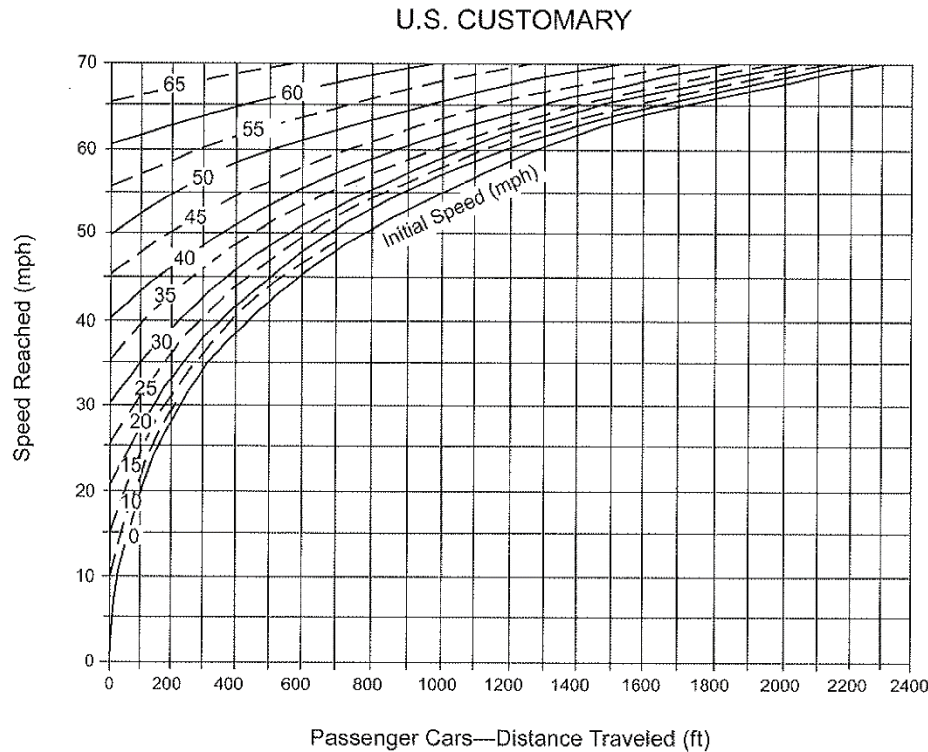


Figure 3. Distances Required to Accelerate to Target Speed from a Reference Speed [3]

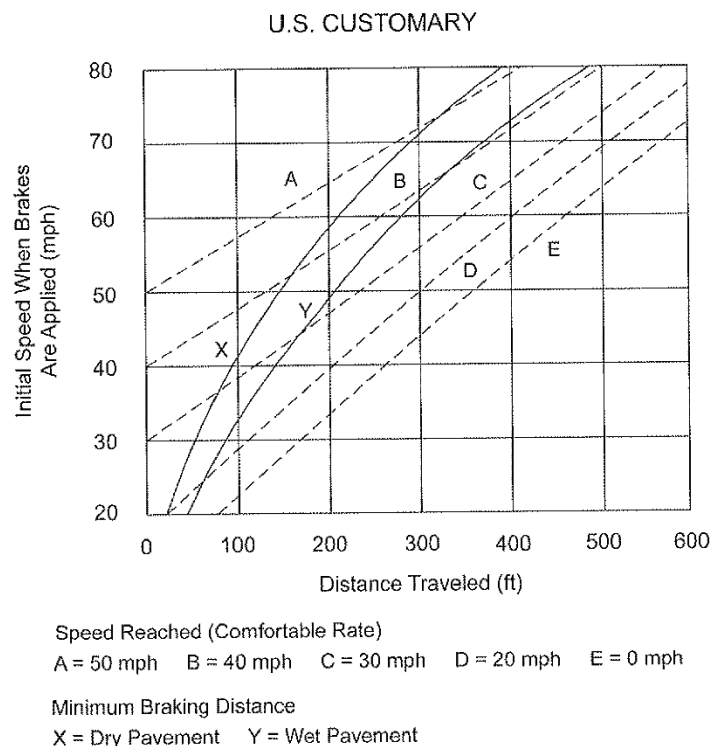


Figure 4. Braking Design Distances for Dry and Wet Pavements [3]

2.4 Crash Reconstruction Measurements and Physical Testing Results

Many crash reconstructionists have measured tire-pavement friction during crash investigations. To ensure that the measurements are fair to a defendant, typically only the lowest measured value is used to estimate pre-crash travel speeds when multiple pavement friction tests are conducted.

During a crash investigation, exemplar vehicles² are used whenever possible to estimate the prevailing tire-pavement friction at the time of the crash. If a satisfactory exemplar vehicle cannot be found or if the scene is affected by temporary environmental conditions (e.g., ice, wet ground or hydroplaning, etc), reconstructionists may perform simple tests with instruments such as a drag sled to calculate conservative³ estimates of friction coefficients. A drag sled may be a rubber strip or segment of a tire which is weighted down (e.g., with concrete) and which is dragged along the ground. The ratio of the pull force to the weight is equal to the sliding friction coefficient. The pull force may be recorded from a force gauge (such as a fish scale). This sliding coefficient is always less than or equal to the static, non-sliding coefficient of friction [e.g., 9, 10]. Alternatively, reconstructionists may utilize reference tables published in historical research which provide reasonable but below-average values intended to underestimate the probable real-world tire-pavement friction coefficient⁴ [11].

The Vericom Computers company is one example of a company which sells accelerometers for more robust assessments of vehicle accelerations. Company representatives demonstrating the use of their data recorders maintained a table of over 3,000 tests to identify tire-pavement friction values which included vehicle, location, and test dates from 1995 to the present (2016) [12]. With newer vehicle years, average tire-pavement frictions have increased, exceeding 1.0 on standard dry road conditions starting in 2013, as shown in Figures 5 through 7. Per discussions with the president of Vericom, most of the highest-friction tests conducted occurred on long, flat, freshly-paved surfaces such as roads which have been repaved but have not yet been reopened to the public, or on airport tarmacs with surface friction treatments. Thus, results may not be representative of all roadways and may overstate the attainable braking coefficients of friction, but are useful for comparing different types of vehicles as well as vehicles with ABS vs. locking brakes.

USACE uses a Ford Crown Victoria as the standard threat vehicle for numerical calculations. Thus, vehicles which shared a Ford Crown Victoria chassis, consisting of any of the Ford Crown Victoria, Lincoln Town Car, and Mercury Grand Marquis were considered separately from other vehicle types, as shown in Figures 5 and 6. Additional vehicle types were lumped broadly based on additional characteristics such as horsepower-to-weight ratio (i.e., performance cars) and

² An exemplar vehicle is a vehicle of similar make, model, production year, and maintenance condition.

³ For crash reconstructionists, conservative friction values are those which are typically lower than or equal to the expected value for friction.

⁴ In both law enforcement and engineering communities, there is a prevailing train of thought that friction values cannot exceed 1.0. Many contemporary tire-pavement tests have yielded friction values of 1.0 or higher, but these are often unreported or not included in reference tables [9]. As a result, most values reported and included in reconstructionist publications have tire-pavement friction values less than 1.0 for most road conditions. As more data becomes available, however, higher values will become more widely accepted.

manufacturer-recommended, new-vehicle starting price (i.e., economy cars) for comparison, as shown in Figure 7.

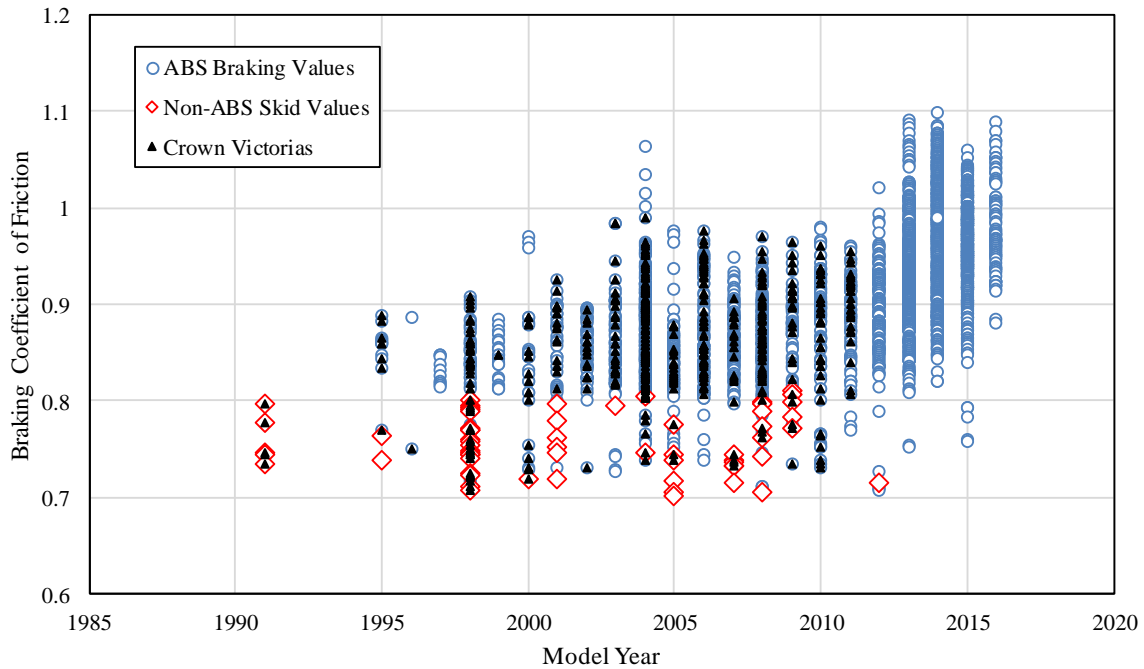


Figure 5. Braking Coefficient by Vehicle Model Year [12]

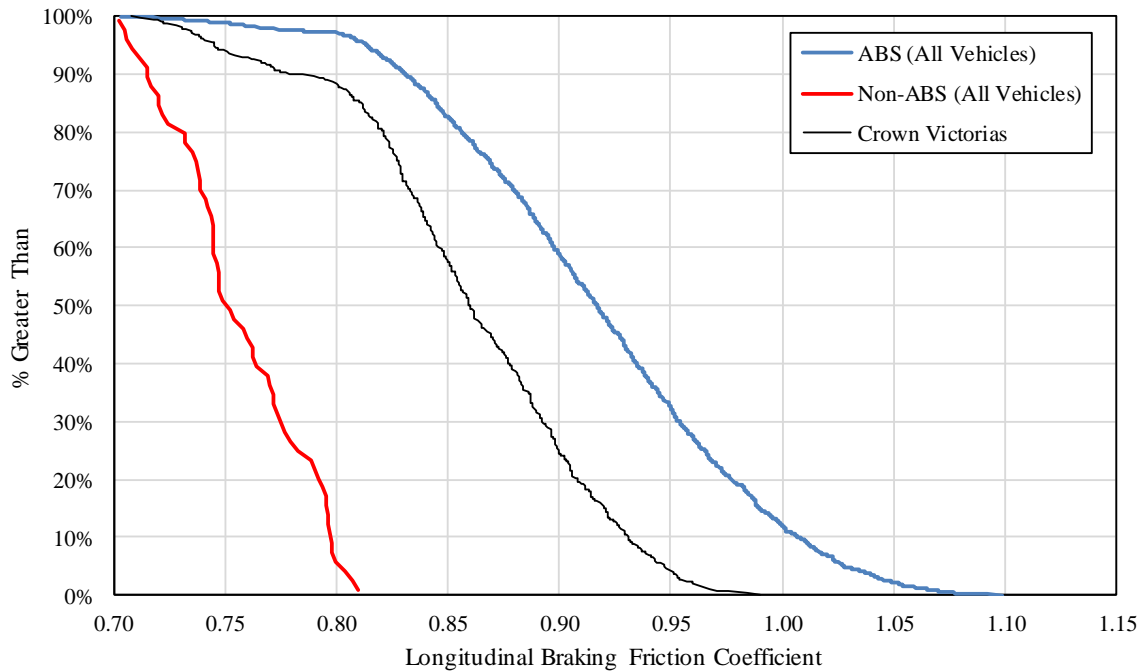


Figure 6. Distributions of Braking Coefficients of Friction by Brake Type [12]

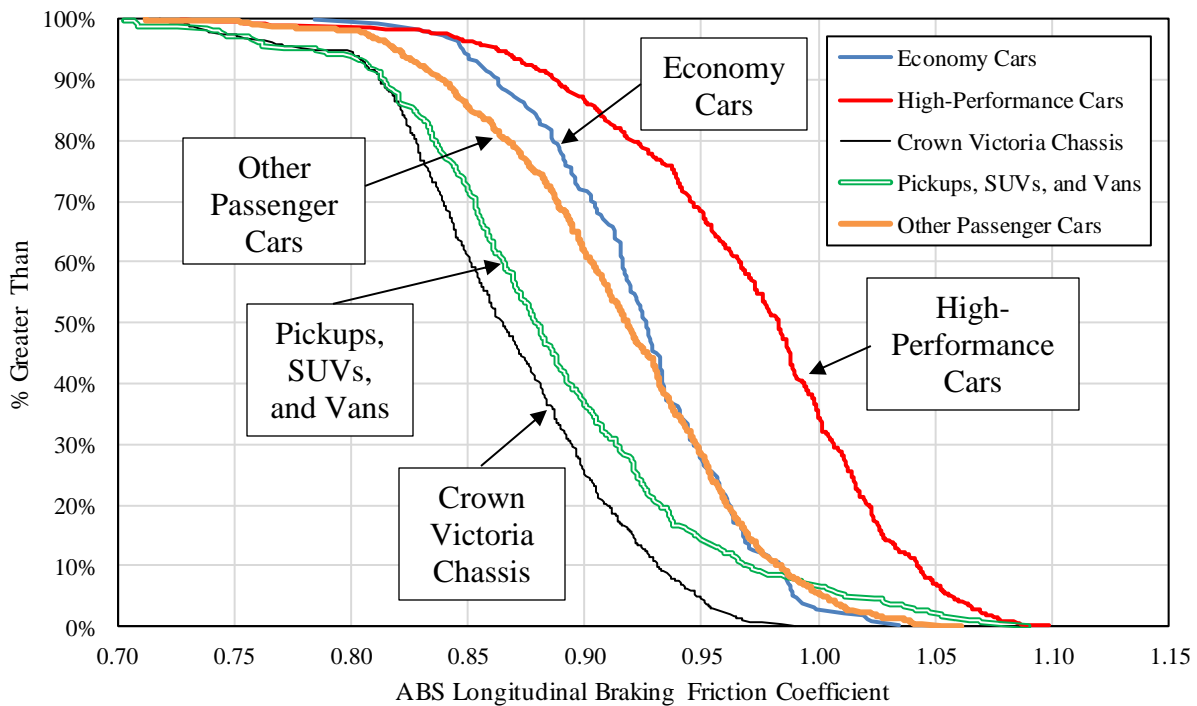


Figure 7. Comparison of Longitudinal Braking Coefficient Distributions for ABS-Equipped Vehicles [12]

Based on the available dataset, researchers concluded the following:

- Vehicles with ABS experienced higher rates of acceleration and thus higher effective braking friction values, on average, than vehicles without ABS equipped
- Ford Crown Victorias and vehicles built on the Crown Victoria chassis (Lincoln Town Car and Mercury Grand Marquis) had the lowest tabulated friction values. It is uncertain to what degree the lower-than-average friction values are affected by vehicle production factors or maintenance condition (i.e., the mechanical wear of the components and tires).
- High-performance vehicles are capable of generating much more braking friction than all other vehicle types. It is likely that the result is strongly related to the types of tires used with the vehicle and the pavement surfaces selected to conduct the tests.

2.5 Tire and Friction Mechanics

Researchers investigated the mechanisms of shear force transmission at the tire-pavement interface to identify conditions associated with the highest tire-pavement friction. Significant tire-pavement friction factors include: the cement binder material; aggregate geometry, material, and smoothness; smoothness of the road; and tire production factors.

Moisture has the strongest influence on tire-pavement friction. On-road debris, such as dirt, gravel, sand, leaves, grass clippings, and other elements can also lubricate the contact surface or create an intermediate contact interface between the tire and pavement. Although moisture and debris effects are significant, they are not considered further in this report. In contrast, no conclusive link could

be established to determine how significant tire temperature (which is related to operating time), pavement temperature (which is related to sun exposure and time of day), and ambient temperature, amongst other factors, were also significant.

2.5.1 Pavement Texture

Pavement texture has been shown to influence tire-pavement friction coefficients via microtexture, macrotexture, and megatexture [e.g., 9, 13-14]. Mega-texture refers to the waviness of the roadway often associated with tire vibration, such as in locations where big trucks are forced to stop for intersections. Mega-texture typically has wavelengths on the order of 2 to 20 in. (50 to 500 mm) with amplitudes up to 2 in. (50 mm). Macrotexture refers to the shape and sizes of the aggregates used in the pavement mixture, grooving, and the degree of polishing on the surface of the pavement. Microtexture refers to the roughness of the surface of the aggregate, with wavelengths less than 0.02 in (0.5 mm).

Microtexture dominates the tire-aggregate interface at lower speeds due to rubber adhesion. For speeds above 20 mph, macrotexture plays an increasingly important role as the tire is acting under centripetal acceleration and does not completely deform around the surface of every piece of aggregate. At very high speeds, mega-texture can adversely affect the average friction by causing tires to “hop” between peak amplitudes in the road surface. The effect of texture sizes on road friction is demonstrated schematically in Figure 8.

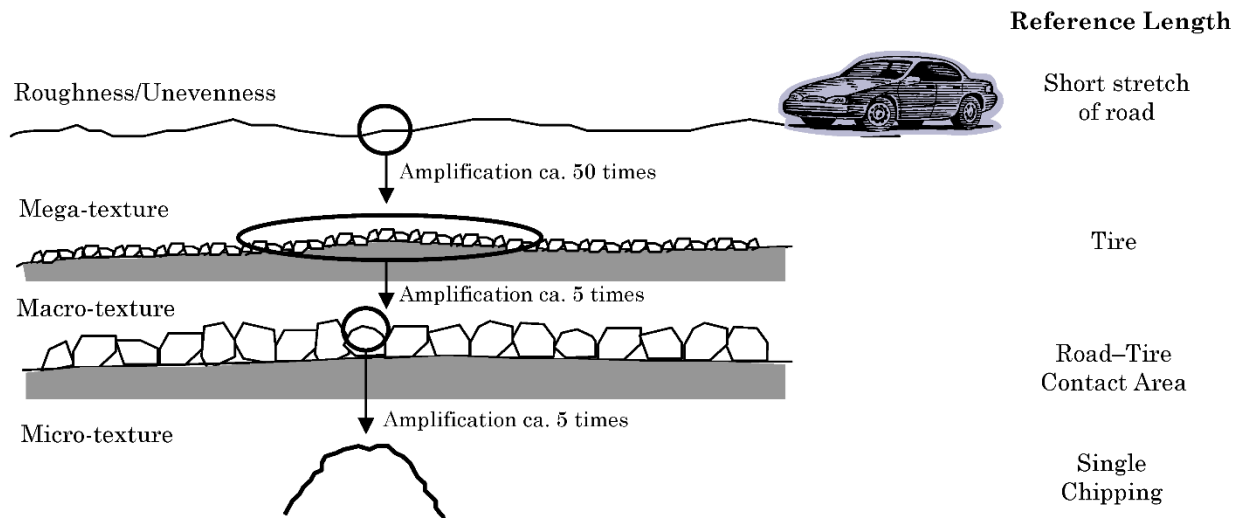


Figure 8. Effect and Size of Road Textures [9, 13]

2.5.2 Contact Patch and Tire Slip

Pneumatic tires have two stiffnesses: one based on the materials, geometry, and structural interaction of the components of the wheel, and one based on the pneumatic air pressure [15-16]. At low velocities, a tire which does not slip is relatively flexible and the deformation of the tire is predominantly based on the air pressure. As a result, the tire partly flattens and contacts the ground via a “contact patch” [17]. Very often, tires have tread blocks cut into the contact area of the tire,

with grooves (channels) and holes (sipes) in the tread to increase flexibility and to channelize water from the center of the tire out to the sides [15].

As a vehicle speeds up or slows down, shear forces are developed in the contact patch region. Braking torque or engine torque apply a moment at the axle-to-wheel connection, which results in a shear force acting at the contact patch. Ignoring the rotational acceleration of the wheel, the brake torque or accelerating torque is equal to the product of the axle-to-contact patch distance times the mass of the vehicle times the net acceleration, as shown in Equations 3 and 4.

$$\vec{F}_{net} = m\vec{a}_{net} \quad (3)$$

$$\vec{T}_w = \sum r_{w,i} (\vec{F}_{net})_i = r_{w,avg} (m\vec{a}_{net})_i \quad (4)$$

As the shear forces are transmitted through the tire, the flexible rubber material is distorted in the contact patch, and a portion of the contact patch slips with respect to the ground. Tire slip forces ramp up almost linearly at first, then typically reach a peak value in the range of 15 to 20% slip [9, 11, 15-20]. Increased tire slip beyond this rate is unstable, and tire shear force drops, as the effective friction coefficient approaches purely sliding. The relationship between tire slip and friction force is shown schematically in Figure 10.

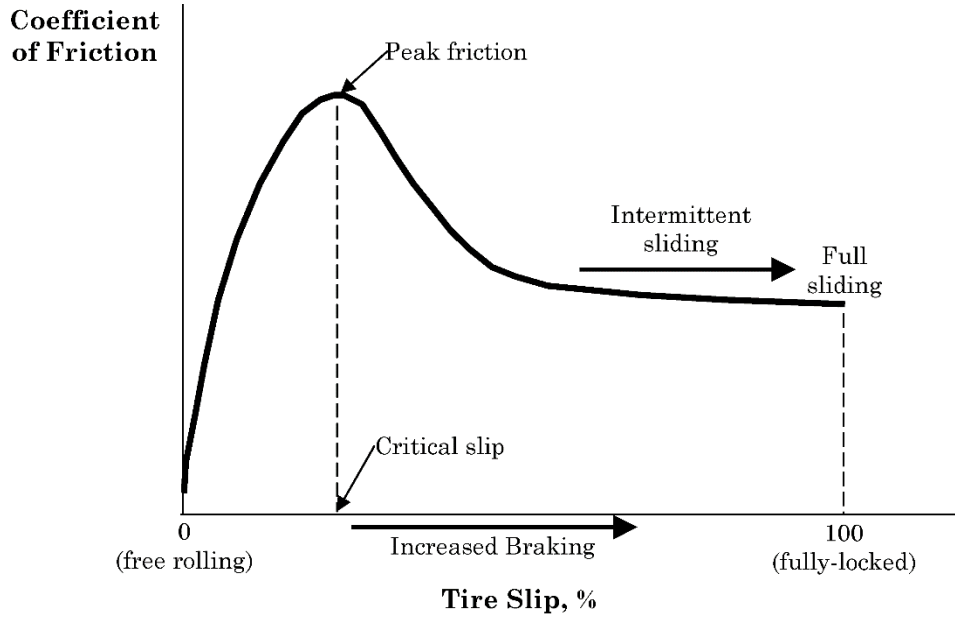


Figure 9. Tire Slip Percentage vs. Effective Coefficient of Friction [9]

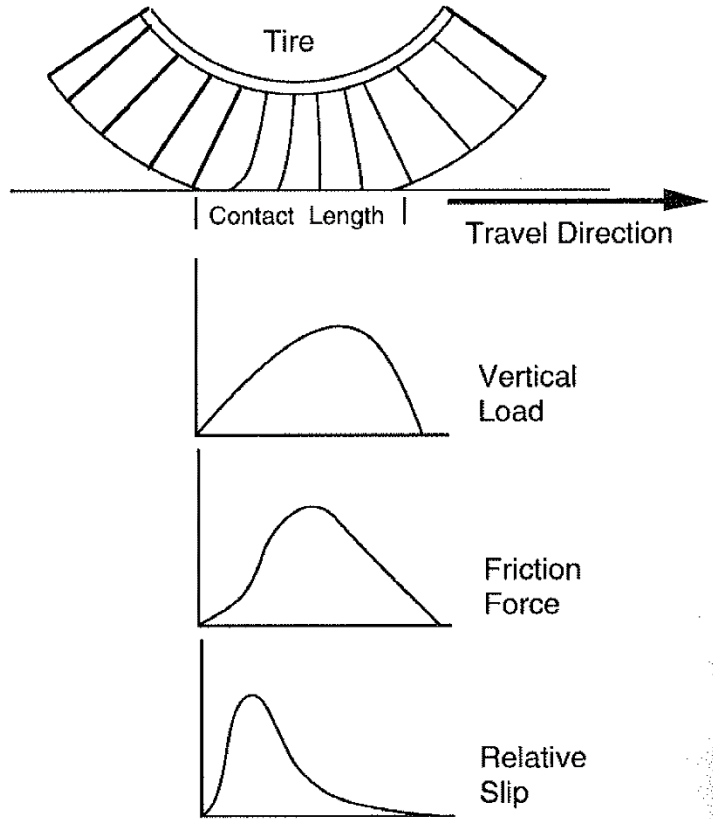


Figure 10. Pressure, Friction, and Slip During Straight-Forward Braking [19]

Automotive engineers took advantage of the higher shear forces available at small slip percentages to develop anti-lock brake systems (ABS). The concept was first conceived and applied for aeronautical vehicles during landing, as fully-locked wheels wore down quickly and deposited a layer of tire rubber on the landing strip, decreasing tire-pavement friction for subsequent landings [21]. ABS-assisted braking causes the vehicle to partially slip, but prevents the tire force from exceeding the unstable maximum slip range and locking up. The result is that fully-braked wheels have monitors which observe wheel slip and which reduce brake pressure if the tire slip becomes too large. This creates some pulsing oscillation during braking but also increases average brake force and decreases stopping distances.

Tires at normal inflation pressures and with tread experience an effective contact patch with the ground which is limited to the outer surface of a segment of the tread blocks, as shown in Figure 11. Under equilibrium driving conditions, the contact patch remains relatively static and slip between the tire tread and the ground is minimal. As a result, using a coordinate frame in which the ground is fixed, the contact patch temporarily has no net velocity as it rolls. Thus, the available friction that can act on the contact patch under normal rolling conditions is proportional to the maximum static coefficient of friction multiplied by the orthogonal contact force.

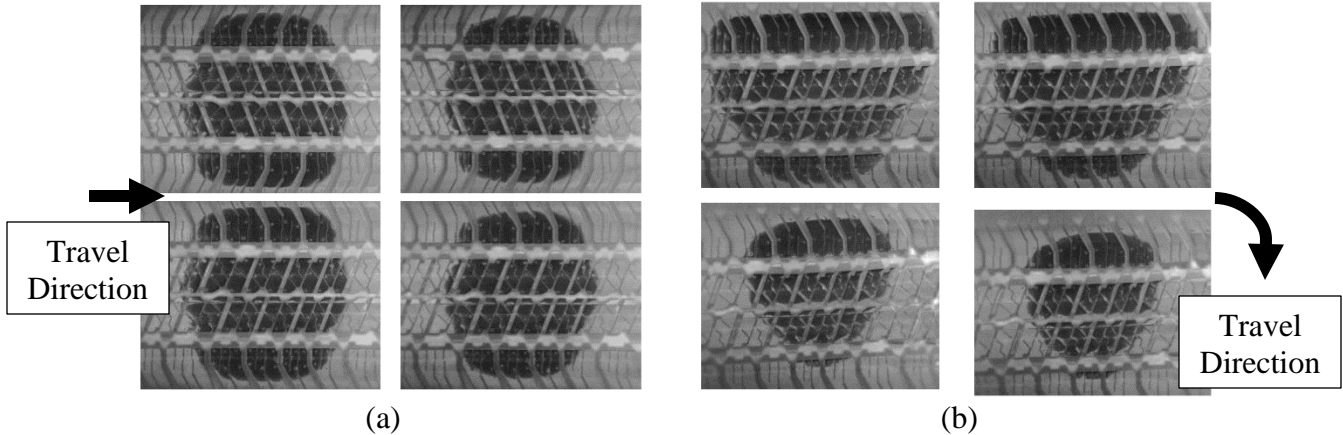


Figure 11. Contact Patch Size and Mechanics (a) Steady-State, Straight-Line Driving and (b) Turning [17]

While a vehicle is turning, some of the vertical load on the tires on the interior side of the turn is transferred to the tires on the outside of the turn to compensate for the turning roll moment, as shown in Figure 11. The decrease in load on the interior-side turns results in a smaller contact patch, whereas the increase in load on the tires on the outside of the turn radius contribute to a larger contact patch.

2.5.3 Side Forces and Pneumatic Trail

When a vehicle steers, lateral shear forces are developed on the tire tread blocks, causing them to distort laterally. The centripetal acceleration relates to the turn radius:

$$a_{cent} = \frac{V^2}{R} \quad (5)$$

a_{cent} = centripetal acceleration

V = velocity

R = turn radius

Forces and accelerations acting in the direction of travel cause a vehicle to speed up or slow down, whereas lateral shear forces acting on a car perpendicular to the direction of travel causes the vehicle to steer, but do not affect speed. Shear forces which develop at the tire-ground interface contribute to a roll moment at the vertical CG location, causing the vehicle to roll to one side. Vehicle roll angle, as well as the roll moment, cause the suspension to extend on the side of the vehicle facing toward the origin (center) of the curve, and to compress on the side of the vehicle facing to the outside of the turn, as shown in Figure 12.

The motion of the suspension likewise contributes to wheel camber angle change [19-20]. Camber is the tilt angle of the wheel when viewed parallel to the longitudinal axis of the vehicle. Camber reduces the effectiveness of the tread by concentrating load on the inner or outer edges of the tire. Although features such as antiroll bars⁵ reduce the amount of vehicle roll angle displacement by

⁵ Other common names for the antiroll bar include anti-twist bars, roll bars, stabilizer bars, sway bars, and anti-sway bars.

transferring more load to the interior turning wheel, roll angular displacement cannot be completely prevented.

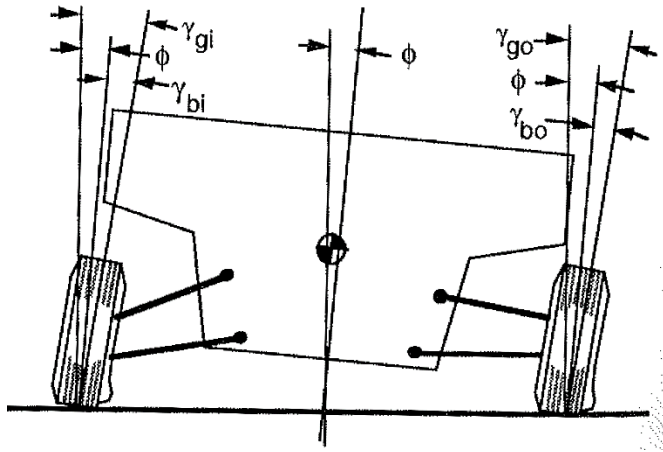


Figure 12. Suspension Relaxation and Camber Change During Cornering [19]

The frictional force acting on a tire is equal to the integral of the shear force over the area of the tire. Tire slip in the contact patch “wastes” some of the available friction for acceleration. A “friction circle” concept is often utilized, in which the total available friction (i.e., normal force times friction coefficient) is a circle residing in the X-Y plane of lateral and longitudinal friction forces, respectively. An example of a friction circle is shown in Figure 13.

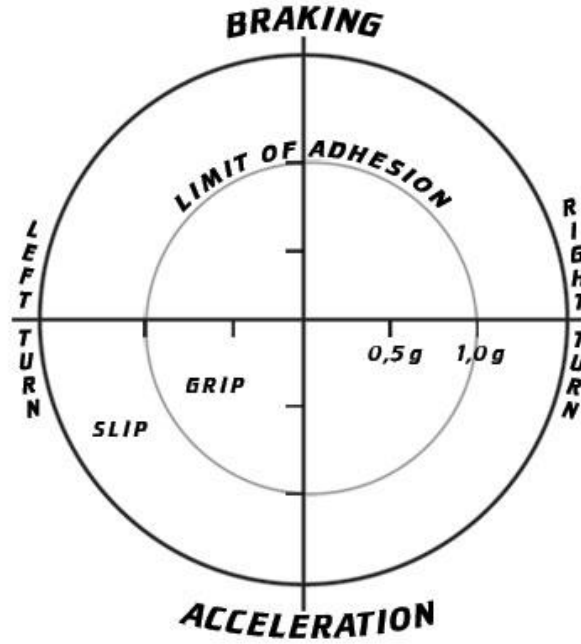


Figure 13. Friction Circle Concept [22]

In addition, the deformation of the tire tread block and contact patch due to lateral shear does not follow the same pressure or force profile that the longitudinal accelerations caused. Shear causes a shear distortion on the tire from the start of the contact patch. The distortion is fairly linear initially, but reaches a maximum point and quickly declines to zero shear at the trailing edge of the contact patch [15-19]. As a result, the center of shear force on the tire is located at a distance known as the “pneumatic trail” behind the central axis of the wheel. This effect generates a counter-steering moment which is known as the “self-aligning torque”. For a vehicle with proper tire alignment (balanced toe in, camber, and caster), self-aligning torque will always resist turning and will gradually straighten a vehicle’s path.

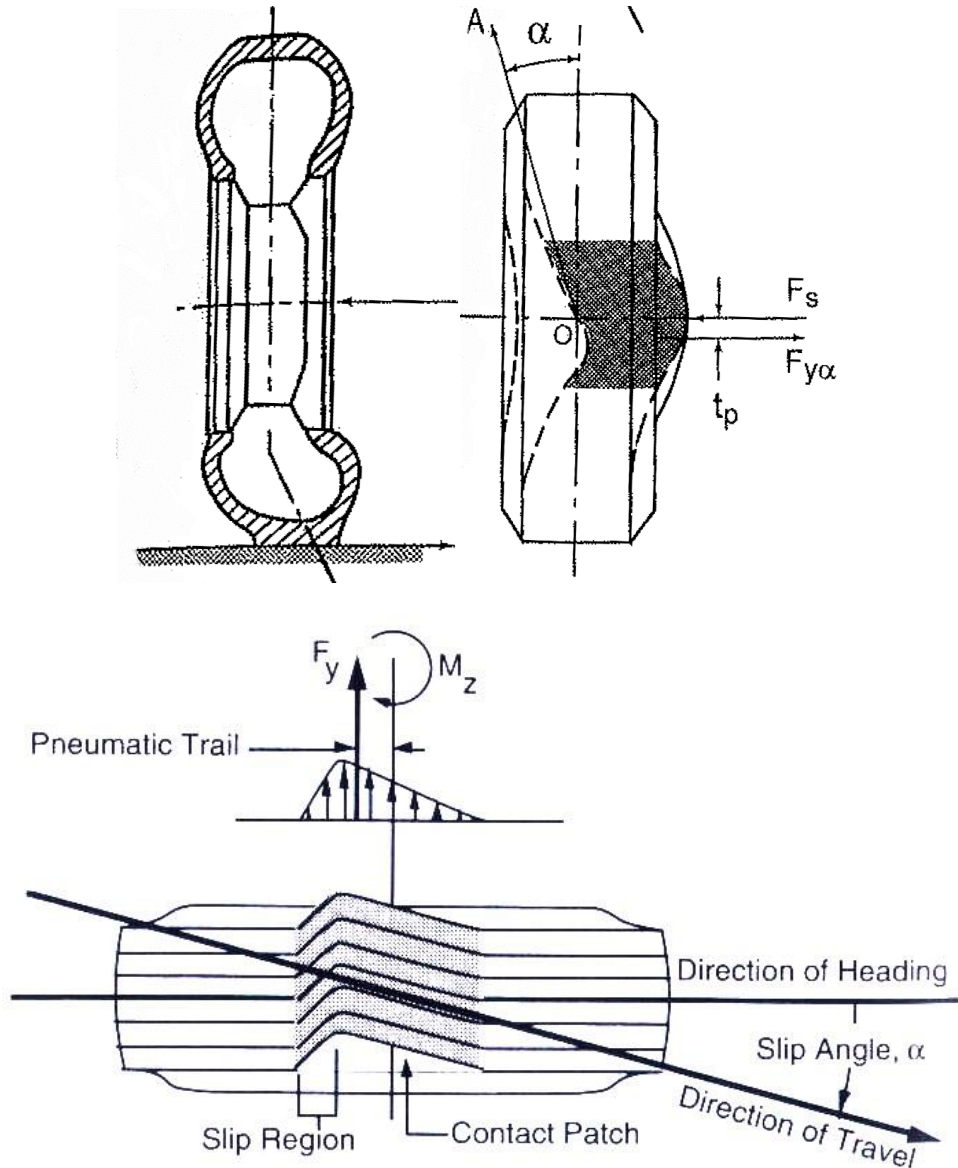


Figure 14. Shear Force Generation on Tire Tread during Steady-State Cornering [17, 20]

2.5.4 Steering Models and Mechanics

For large-radius, low-speed turns, the vehicle acts similar to a rigid body and the shear force losses due to turning are minimized [19]. For some radii, wheelbase, and speed combinations, or where simplified modeling is acceptable, the vehicle can be analyzed as if it were a two-wheel bicycle, as shown in Figure 15. If the steer angles of individual wheels must be known, a more complicated four-wheel vehicle model may be used.

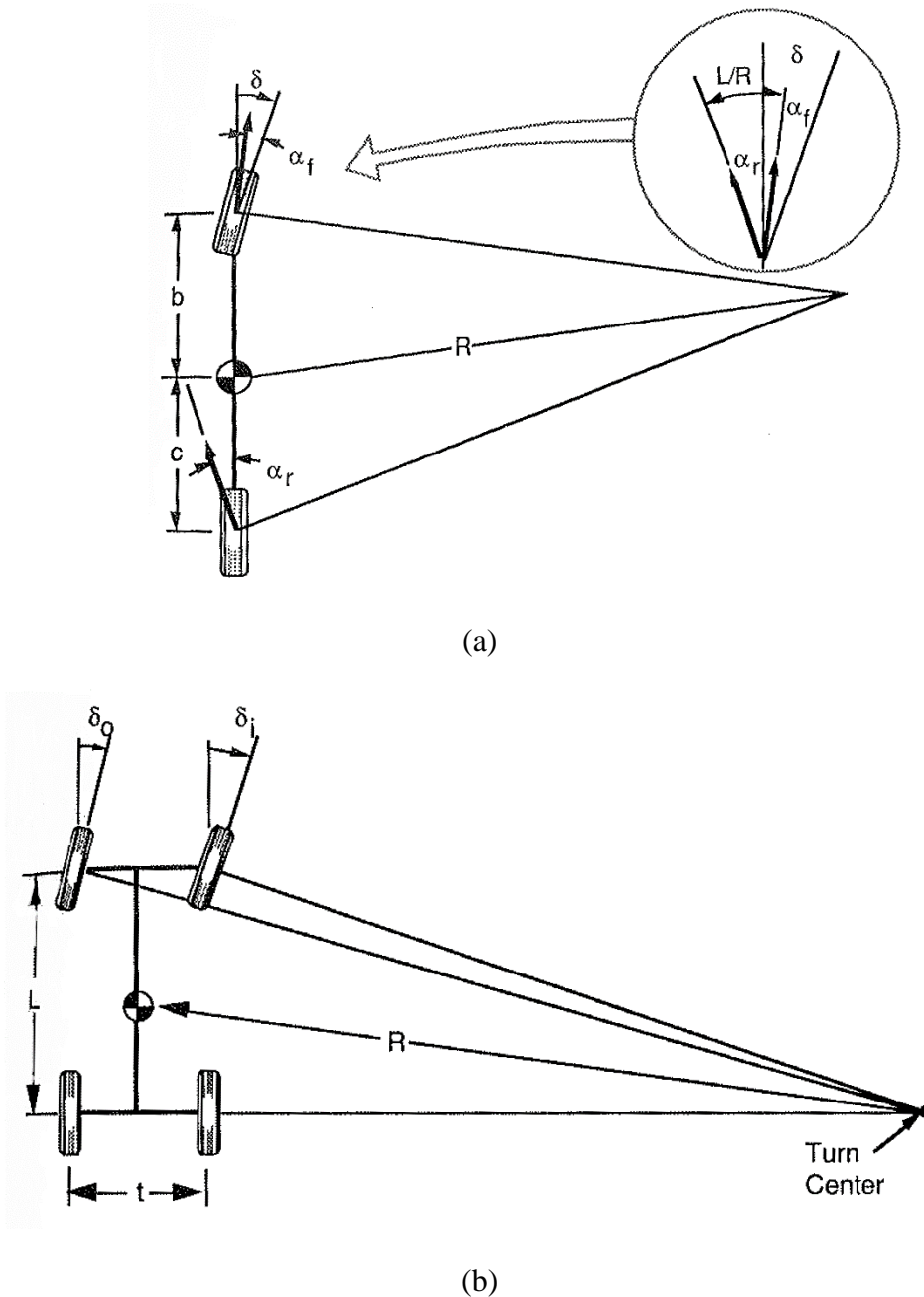


Figure 15. (a) Bicycle and (b) Four-Wheel Models of the Vehicle for Low-Speed, Large-Radius Turns [19]

The four-wheel vehicle model can be thought of as a rigid body with five points of interest: the centerpoints of the contact patches of each of the four wheels, and the center-of-mass (CM, also known as CG⁶). For simplicity and convenience, CG will be used. The vehicle CG rotates around a single convergent point in space during steady-state, constant-radius cornering, which is known as the turn center. For limited slip conditions at the wheels to apply, a radial line drawn from the turn center to the wheel center should be parallel with the rotational axis of the wheel. This requires that the two front wheels steer at different angles to minimize slip, as shown in Figure 16. Most vehicles are not constructed with independent rear wheel steering, thus both rear wheels rotate along the same axis, which must also be parallel with the line extending to the turn center. This is true for most solid rear axle vehicles, such as passenger cars and front-wheel drive SUVs or trucks. A steering configuration which satisfies these directional constraints is known as Ackerman steering.

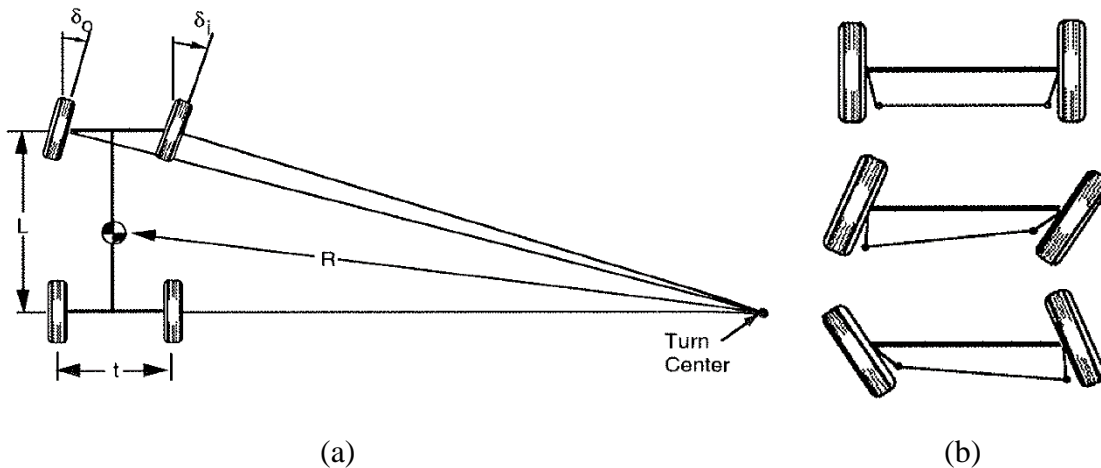


Figure 16. Four-Bar Ackerman Steering Wheel Geometries for Forward, Left, and Right Turns
(a) Ackerman Steering (b) Wheel Rotations [19]

As the turn radius decreases and/or speeds increase, slip develops in the wheels regardless of Ackerman steer. The turn center shifts forward with respect to the rear axle and every tire experiences some slip. The result is to diminish the friction available for the vehicle to turn and a loss of turning efficiency.

2.6 Modifications for Enhanced Vehicle Performance

There are many modifications that can be made to vehicles to improve their performance. Because vehicle customization is used daily in racing circuits and for hobbyists and enthusiasts, there is a large market for aftermarket modifications to improve vehicle performance. Modifications include optimized components, high-end fuels, modified air-fuel ratios, higher compression ratios, lighter engine and frame materials, and modified tires. Some of the modifications are summarized and described in Table 1.

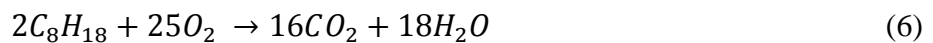
⁶ CG: Center of Gravity. For bodies which are much smaller than the radius of the earth (less than 500 ft, for example), the gravitational force acting on a mass is nearly identical regardless of the elevation of the mass. Thus, the center of gravitational force, or CG, is at a location which is nearly identical to a body's center-of-mass, or CM.

Table 1. Examples of Aftermarket Vehicle Performance Improvements

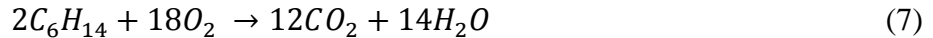
Modification	Components Affected	Result
Lighter, stronger materials	Pistons, connecting rods (conrods), crankshafts, and flywheels Cylinders and engine blocks Suspension arms and frame	Less weight: increased responsiveness, increased acceleration, less inertia Vehicle is more unstable (reduced mass moments of inertia)
Higher-energy fuels	Piston, conrod, crankshaft, and cylinder Valves (tappets) Gaskets Lubricants (e.g., engine oil) and coolants	Higher combustion temperature Higher cylinder pressures Optimized coolant and/or lubricant dispersal system and fluids required
Superchargers, turbochargers, and increased compression ratios	Pistons, conrods, crankshafts, and cylinders Engine mounts and stabilizers Power transmission belts Exhaust system (turbochargers) Axles and transmissions	Increased air and fuel pressure prior to start of combustion process More output torque on crankshaft
Racing tires (“slicks”)	Tires, axles	Improved grip on dry, clean, sharp roads Reduced traction in wet conditions Sensitive to debris, dust, and films on road
Suspension kits (specifically drop kit)	Load-bearing suspension components (control arms, swing arms, etc) Springs and shocks Tires, axles, steering control arms, and brakes	Decreased ground clearance and stiffer springs and shocks reduces steering compliance and improves cornering efficiency, speeds Requires modified tires and suspension components
Power transmission	Transmission CVT: continuously-varying transmission; reduces engine speed reduction due to gear switching by continuously varying engine speed-to-wheel speed ratio Electric motor: high speed range reduces need for gearing, allows close connection to wheels Axles, universal joints, and bearings	Constant torque output independent of vehicle speed Reduced power transmission losses from bearings, couplings, and joints Possibility for regenerative braking (i.e., braking stores power for subsequent engine use) Four-wheel drive (4WD) and all-wheel drive (AWD) increase total traction while speeding up
High-performance braking systems	Brake rotor Brake pads and hydraulic lines Brake power-assist motor	Minimal brake fade during periods of intense, frequent braking Maintain high coefficient of friction at higher temperatures Faster brake application with less foot pressure

2.6.1 Vehicle Performance Modification Example No. 1: Ethanol

An example of how fuels can affect accelerations is provided below. Using ethanol-based fuels can produce more power if a richer air-fuel ratio is used (i.e., fuel-to-air ratio is increased). Non-ethanol-enhanced gasoline (standard 87-octane mix) is a distilled hydrocarbon mix of mostly octane (C_8H_{18}) and hexane (C_6H_{14}). Stoichiometry dictates that each octane molecule requires $12\frac{1}{2} O_2$ molecules to fully combust into CO_2 and H_2O :

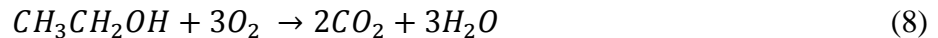


Likewise for hexane:

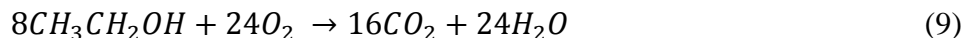


However, standard ambient air near the equator is only approximately 20% oxygen by volume at sea level, decreasing with altitude [e.g., 23]. Air is mostly nitrogen, ranging from 75% to 79% depending on factors such as humidity and gaseous solutes (contaminants, such as dust). Thus, to combust two octane molecules, 25 oxygen molecules are accompanied by 100 N₂ molecules which absorb some of the combustion energy but which do not participate in the combustion process. Thus, the maximum temperature achieved during combustion is limited.

In contrast, the hydroxide chain associated with ethanol fuel (CH₃CH₂OH) contains one oxygen atom already present in the molecule. To fully combust one ethanol molecule would require 3 O₂ molecules from air:



The same amount of carbon and hydrogen is combusted if the reaction is scaled up by a factor of 8:



This means that to combust ethanol requires 4% less externally-supplied oxygen (i.e., 4% less air for a similar amount of fuel). With less inactive elements (e.g., N₂) present, the combustion temperature can be higher, but with less total combustion product and inactive gases, the combustion pressure could also be lower as well. Cylinder pressure is required to move the pistons, producing engine torque and rotating the crankshaft. To increase cylinder pressure, the fuel flow rate has to increase, meaning that more fuel has to be burned per engine cycle. In addition, to manage the increased cylinder temperatures associated with combusting ethanol, specialized coolants and lubricants may be required. Exotic fuel blends which require less ambient air are therefore often associated with higher fuel flow rates and much more robust engine cooling systems. Thus, unmodified engines and unmodified fuel flow rates could actually decrease the effectiveness of higher-efficiency fuel blends.

2.6.2 Vehicle Performance Modification Example No. 2: Braking Systems

The brake system is the most powerful system in a vehicle, converting vehicle kinetic energy into heat, electrical energy, or pneumatic pressure. Extensive automotive improvements over time improved brake performance on factory cars and trucks to vastly exceed minimum FMVSS requirements [4,5]. Large brake rotors, exotic cooling systems, improved brake pad materials, better power-assist modules and motors to increase brake sensitivity, and wider, stiffer tires will improve braking efficiency. During adverse weather events or when roads are moisture- or debris-covered, tire tread can also improve braking efficiency.

For a threat vehicle traveling in an ACP, the short-duration over which the vehicle is expected to drive in a hostile or threatening manner could diminish any potential gains from high-performance brake systems. Varying tire geometries and tread types could assist in the event that moisture or debris covers ACP roadways, but mitigation of factors which could adversely affect tire friction,

such as debris and moisture, does not improve traction under worst-case (i.e., ideal friction) conditions and may actually decrease dry-travel condition traction. Brake modifications may not be a significant concern for most current ACP configurations.

2.7 Summary Evaluation of Factors Which Affect Tire-Pavement Friction Coefficients

The results of the literature review, experience of the UNL experts, and the opinions of long-serving crash reconstructionists in law enforcement were evaluated to determine an approximate ranking system for various factors affecting friction. Although it is impossible to determine the extent to which each factor affects the overall tire-pavement friction, approximate reduction factors were noted in Table 2, when sufficient evidence or experience supported that determination. The data in Table 2 is not considered an absolute reference but rather a philosophical and loosely empirical relationship between factors which have the most, and least, effect on the tire-pavement friction available to drivers.

The friction coefficient research conducted to date has largely focused on two aspects of friction: braking (deceleration) and turning/cornering. Both have strong safety implications. However, the lowest coefficient of friction used in the Threat Calculator is the “effective” friction associated with increasing speed (acceleration). Any modification which increases the rate at which a vehicle will increase speed will generally have a stronger influence on predicted maximum speed and time to navigate an ACP configuration. Thus, the friction which affects a vehicle’s ability to speed up will be very meaningful in addition to braking and turning (cornering) coefficients of friction.

Table 2. Ranking of Factors Affecting Friction and Approximate Reduction Factors (if applicable)

Road Condition	Significance ¹	Approximate Reduction Factor ^{2,3}
BASELINE (MAXIMUM FRICTION) ⁴ :	-	1.0 to 1.4 (Portland cement concrete) 0.9 to 1.2 (clean, new, sharp asphalt) 0.5 to 0.8 (sand, gravel, dry dirt at small vehicle accelerations) 0.35 to 0.55 (dry, mowed and maintained grass)
Moisture or Debris on Road	1	-0.15 to -0.5 (wet) -0.5 to -1.0 (icy) -0.4 to -1.0 (snow/slush) Variable (debris, e.g., sand, dirt)
Pavement Quality and Texture ⁵	2	-0.2 to -0.4 (excessive tar) -0.2 to -0.3 (heavy cracking) -0.2 to -0.5 ("glassy" smooth) Variable (micro and macrotexture)
Pavements and Materials ⁵	3	-0.1 to -0.4 (based on aggregate types, smoothness, pavement binder quality) -0.1 to -0.25 (pothole fillers) Unknown (surface coatings, including pavement paints)
Vehicle Systems and Components	4	~ -0.1 to -0.15 (ABS age and quality) -0.1 to -0.25 (skidding instead of ABS) -0.05 to -0.1 (tire inflation pressure) Unknown (effects of ESC, intelligent braking controls, other brake or wheel systems) -0.1 to -0.2 (worn or corroded brakes) -0.05 to -0.15 (brand new or unburnished brakes) Variable (tire wear, tread wear, or tire damage)
Other Effects	5	Variable but small (ambient temperature, air pressure) Variable (high speeds; generally reduction of 5% for every 5 mph increment above 40 mph is assumed) Unknown (foreign objects embedded in tire tread, such as rocks or gravel)

1. Significance refers to a relative ranking for the extent of the reduction factor, frequency of observation (such as annual, monthly, daily, or hourly frequencies), the number of vehicles which will be affected by the factor, and how well a factor has been studied.
2. Reduction factors subtract from the baseline (maximum friction) scenario. Reduction factors are approximate and based on a combination of literature review, empirical testing, and anecdotal and empirical evidence from crash reconstructionists and law enforcement.
3. Reduction factors do not necessarily sum together to quantify the uncertainty range. For example, an aged, "glassy" asphalt road under wet conditions and with a fully-skidding car has an empirical tire-pavement friction coefficient of approximately 0.40 to 0.55 [24]. By summing the respective reduction factors and their respective tolerances (i.e., uncertainties), the possible range of friction coefficients would be $0.0 \leq \mu \leq 0.75$. While the correct friction range is contained within this uncertainty, the resulting friction range estimate is extremely broad. The reduction factors are most accurate when other factors are controlled.
4. Maximum friction conditions (i.e., zero reduction factors apply).
5. Pavement quality and texture effects are strongly affected by precipitation and moisture. When ice, snow, or hydroplaning conditions are present, the quality and age of the roadway, micro and macrotextures, and binder material (asphalt or Portland cement) have minimal effect.

3 FRICTION TESTING CONDITIONS

3.1 Test Layout

Simple geometries were selected for threat vehicle trajectories in order to record tire-pavement friction in longitudinal and lateral directions. All test configurations were conducted to be representative of threat calculator procedures and setup.

3.1.1 Threat Calculator Procedures

USACE's Threat Calculator is a program to estimate threat vehicle travel time based on the geometries of the threat vehicle path. The Excel-based program operates with several critical assumptions and simplifications [25]:

Threat Vehicle Limitations

- The threat vehicle is a Ford Crown Victoria
- The tire-roadway friction coefficient is 0.75
- The vehicle's acceleration while speeding up is constant, independent of speed, roadway crowning, and changes in grade and curvature, and is equal to 11.4 ft/s^2 (0.35 g's)
- The vehicle's acceleration while braking is constant, independent of speed, roadway crowning, and changes in grade and curvature, and is equal to 24.1 ft/s^2 (0.75 g's)
- The vehicle's limiting centripetal acceleration magnitude is identical to the braking acceleration magnitude, and is equal to 24.1 ft/s^2 (0.75 g's)
- Longitudinal and lateral accelerations are decoupled (vehicle may accelerate and brake on a turn so long as it is traveling slower than the maximum stable cornering speed)

Path Geometry

- All threat vehicle trajectory segments can be represented with a series of straight (tangent) lines and circular curves

Threat Vehicle Behavior

- The vehicle always maximizes accelerations in lateral (centripetal) and longitudinal directions (i.e., threat vehicle travels at MTCAS⁷)
- A vehicle will always turn at the maximum stable cornering speed (i.e., maximum centripetal acceleration)
- The vehicle remains stable and in contact with the ground at all times (i.e., no launching, rollover, etc.)
- The threat driver will:
 - instantaneously transition between accelerating, decelerating, and turning
 - identify the optimum (i.e., worst-case) trajectory, including the exact locations to change steering angles as well as to depress the gas and brake pedals
 - perform maneuvers at the acceleration limits and is not affected by g-loading nor any environmental distractions or influences

⁷ MTCAS: Maximum Threat Calculator Acceleration and Speed

The threat vehicle behaviors are conservative, as all real drivers undergo a transition between different behaviors (e.g., between speeding up and slowing down). Moreover, drivers are rarely able to sustain the maximum acceleration for even a moderate amount of time. Professional race drivers, which operate primarily near the boundaries of the friction circle, nonetheless struggle to prevent low-acceleration periods as it can be physiologically difficult to maintain large accelerations indefinitely. Accelerations are the result of net forces acting on a mass, and a 0.75-g force acting on a driver in the longitudinal or lateral direction will raise the “effective weight” of the driver (i.e., total force acting on the driver including vertical load due to gravity) by 25%.

However, whereas most of the assumptions are conservative, the longitudinal coefficient of friction of 0.75 may underestimate real tire-roadway coefficients of friction in ACPs. As discussed in Chapter 2, historical limits for tire-pavement friction underestimate common measurements for modern vehicles [12, 24]. In addition, the constant acceleration rate of 11.4 ft/s^2 (0.35 g's) may not be a conservative measure of linear acceleration for many passenger cars [25].

3.1.2 Test Layouts

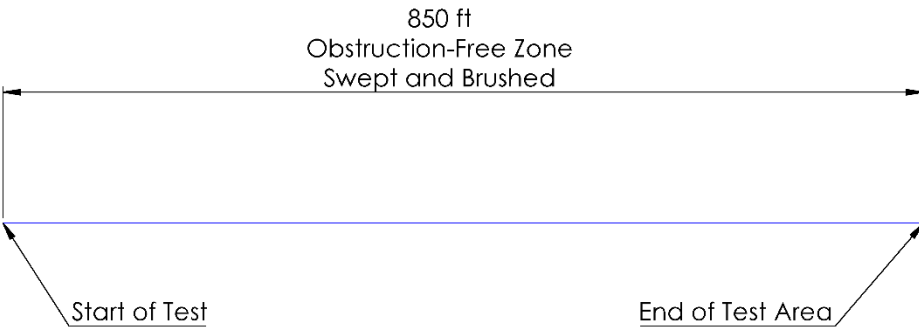
To evaluate the adequacy of the tire-pavement friction coefficient used in USACE’s Threat Calculator, a series of tests were conducted using a combination of tangent and circular curve path layouts to isolate longitudinal and lateral acceleration limits, respectively. The target vehicle trajectories for each test are shown in Figures 17 and 18.

Test nos. LF-1 through LF-4 and LF-1b utilized a long, tangent path layout. The test vehicle accelerated in a straight line from rest to 60 mph at full throttle (i.e., maximum acceleration possible), released the accelerator to bring the vehicle near constant-speed equilibrium, and then fully braked the vehicle (i.e., 100% braking) to a complete stop, then the test was completed. The speed of the vehicle and accelerations were recorded throughout the event. The test designation “LF” referred to “Linear Friction”, because the path of the vehicle was a straight line throughout the test. For test no. LF-1b, 219 lb was added to the trunk of the vehicle to represent the mass of a bomb (payload), per sponsor request.

Test nos. CF-100-1 through CF-100-3 and CF-100-1b utilized a 100-ft radius. The test procedure was to accelerate slowly around the circle until the vehicle was near slipping, then gradually increase speed until the vehicle lost traction on the circle and drifted off of the path. Then, the vehicle was to slow down and rejoin the circular path once again, subsequently increasing speed until the vehicle slid off of the target path again. After that point, the test was concluded, and the vehicle was brought to a complete stop. The test designation “CF” referred to “Circular Friction”, because the path of the vehicle was a constant-radius circular line throughout the test. For test no. CF-100-1b, a total mass of 219 lb was added to the trunk of the vehicle to represent the mass of a bomb (payload), per sponsor request.

Test nos. CF-200-1 through CF-200-3, and CF-200b were identical to test nos. CF-100-1 through CF-100-3 and CF-100b, except that the radius was increased to 200 ft. For test no. CF-200-1b, 219 lb was added to the trunk of the vehicle to represent the mass of a bomb, per sponsor request.

Test Names	Test Parameters	Test Vehicle	Live Driver?	Instrumentation
LF-1-4 & LF-1b	Accelerate to 60 mph, hold speed for 3 sec, decelerate to stop	Ford Crown Victoria (Police Interceptor)	Yes	Accelerometers, rate gyro



850 ft
Obstruction-Free Zone
Swept and Brushed

Start of Test End of Test Area

NOTES:

- Vehicle shall start from rest and accelerate as fast as possible to 60 mph, let off of the accelerator (i.e., coast) for 3 seconds, and then brake as quickly as possible to a stop. Two straight-line acceleration and deceleration tests are required.
- Test vehicle is a Ford Crown Victoria, Police Interceptor is preferred. Vehicle shall be equipped with new or very good condition tires designed for clean, dry road conditions. Racing tires are also acceptable.
- Obstruction-Free Zone shall be swept and brushed with stiff-bristle or wire bristle broom/sweeper until the surface of the tarmac is clean and roughened (i.e., not glassy).

	T00054 USACE Friction Study	S-1: 1 sf ²
Midwest Roadside Safety Facility	Straight-Line Accel & Braking Tests	2016/08/25
ORG. NAME: USACE-Friction-Casta-RS	SCA F. #: 500	DRAWN BY: OSS
UN. S. #: 4A3	REV. BY:	

Figure 17. Test Layout and Parameters for LF Longitudinal Friction Test Series

Test Names	Test Parameters	Test Vehicle	Live Driver?	Instrumentation
CF100-1-3 & CF100-1b	Accelerate slowly around 100-ft radius circle until vehicle cannot maintain radius	Ford Crown Victoria (Police Interceptor)	Yes	Accelerometers, rate gyro
CF200-1-3 & CF200-1b	Accelerate slowly around 200-ft radius circle until vehicle cannot maintain radius	Ford Crown Victoria (Police Interceptor)	Yes	Accelerometers, rate gyro

NOTES:

- Vehicle shall slowly accelerate while maintaining the left side of the vehicle on or very nearly on the inside edge of a marked circle. The speed at which the vehicle is no longer able to maintain the turn around the circle will be recorded. Speed shall be reported by driver, recorded by speed trap, and tracked by overhead camera.
- Two radii are required: 100 ft and 200 ft. Two tests shall be conducted with each radius size.
- Test vehicle is a Ford Crown Victoria, Police Interceptor is preferred. Vehicle shall be equipped with new or very good condition tires designed for clean, dry road conditions. Racing tires are also acceptable.
- An area 15 ft wider than the test radius shall be swept and brushed with stiff-bristle or wire bristle broom/sweeper until the surface of the tarmac is clean and roughened (i.e., not glassy).

MwRSF	T00054 USACE Friction Study	S: 1 2 p ² 2
Midwest Roadside Safety Facility	Lateral Friction Tests (Skid Pad)	2010/09/25
Dwg. NAME: USACE-friction-test--r5	SCA F: 1/800 UN S: 1	REV. BY: 4A3

Figure 18. Test Layout and Parameters for CF Side Friction Test Series

3.2 Test Facility

The testing facility is located at the Lincoln Air Park on the northwest side of the Lincoln Municipal Airport and is approximately 5 miles (8.0 km) northwest of the University of Nebraska-Lincoln. The testing facility contained concrete tarmac originally constructed as part of an Air Guard military base.

3.3 Vehicle Navigation Conditions

A driver weighing approximately 190 lb drove the vehicle for all of the tests. The driver who was selected had previous experience driving sprint cars around tracks as well as participating in competitive motorcycle and drag racing. A passenger weighing approximately 100 lb was also present and used to arm instrumentation systems and turn on instruments as needed, and to log test conditions and times to document each test individually.

3.4 Test Vehicles

For test nos. LF-1 through LF-4, LF-1b, C100-1 through C100-3, CF100b, C200-1 through C200-3, and CF200b, a 2009 Ford Crown Victoria was used as the test vehicle. The curb and test inertial vehicle weights were 4,026 lb and 3,929 lb, respectively. The test vehicle is shown in Figure 19, and vehicle dimensions are shown in Figure 20.

The longitudinal component of the center of gravity (c.g.) was determined using the measured axle weights. The vertical component of the c.g. for the 1100C vehicle was determined utilizing a procedure published by SAE [26], and was subsequently verified using data from 4N6XPRT Expert Autostats [27]. The location of the final c.g. is shown in Figure 21.

Square, black-and-white-checkered targets were placed on the vehicle for reference to be viewed from the digital video cameras, as shown in Figure 21. Round, checkered targets were placed on the center of gravity on the left-side door, the right-side door, and the roof of the vehicle.

New tires were placed on the vehicle and the tires were “broken in” by performing test maneuvers repeatedly. The distance put on the tires was approximately 50 miles of high-friction travel. Researchers believed that this was roughly equivalent to 200 or more miles of typical highway travel, which is the distance recommended to break in locked wheel skid trailer tires, per recommendations provided by ASTM [28].

3.5 Data Acquisition Systems

3.5.1 Accelerometers

One environmental shock and vibration sensor/recorder system was used to measure the accelerations in the longitudinal, lateral, and vertical directions. The accelerometer system was mounted near the center of gravity of the test vehicle.



Figure 19. Test Vehicle, USACE Friction Tests

Date: <u>3/2/2016</u>	Test Number: <u>Friction Tests</u>	Model: <u>Crown Victoria</u>	
Make: <u>Ford</u>	Vehicle I.D.#: <u>2fahp71v59x129213</u>		
Tire Size: <u>235/55 R17</u>	Year: <u>2009</u>	Odometer: <u>121605</u>	
Tire Inflation Pressure: <u>35 psi</u>			
*(All Measurements Refer to Impacting Side)			
Vehicle Geometry -- in. (mm)			
a <u>71 7/8</u> (1826)	b <u>59 1/2</u> (1511)		
c <u>212 1/2</u> (5398)	d <u>55</u> (1397)		
e <u>114 1/2</u> (2908)	f <u>43</u> (1092)		
g <u>23 2/5</u> (594)	h <u>49 7/8</u> (1267)		
i <u>13 3/4</u> (349)	j <u>20 1/2</u> (521)		
k <u>16</u> (406)	l <u>26</u> (660)		
m <u>63 1/8</u> (1603)	n <u>65 1/2</u> (1664)		
o <u>33</u> (838)	p <u>5 5/8</u> (143)		
q <u>26</u> (660)	r <u>17</u> (432)		
s <u>12</u> (305)	t <u>75 1/2</u> (1918)		
Wheel Center Height Front <u>12 3/4</u> (324)			
Wheel Center Height Rear <u>12 3/4</u> (324)			
Wheel Well Clearance (F) <u>28 1/4</u> (718)			
Wheel Well Clearance (R) <u>29 3/8</u> (746)			
Frame Height (F) <u>14</u> (356)			
Frame Height (R) <u>17 1/2</u> (445)			
Engine Type <u>8 cyl. Gas</u>			
Engine Size <u>4.6 L</u>			
Transmission Type: <u>Automatic</u>			
Drive Axle: <u>RWD</u>			
Mass Distribution lb. (kg)			
Gross Static	LF <u>N/A</u>	RF <u>N/A</u>	
	LR <u>N/A</u>	RR <u>N/A</u>	
Weights lb. (kg)	Curb	Test Inertial	Gross Static
W-front	<u>2276</u> (1032)	<u>2229</u> (1011)	<u>N/A</u> <u>N/A</u>
W-rear	<u>1750</u> (794)	<u>1720</u> (780)	<u>N/A</u> <u>N/A</u>
W-total	<u>4026</u> (1826)	<u>3949</u> (1791)	<u>N/A</u> <u>N/A</u>
GVWR Ratings			
Front	<u>2750</u>		
Rear	<u>2900</u>		
Total	<u>5650</u>		
Driver Data			
Name: <u>Eugene Kreier</u>			
Mass: <u>190</u>			
Seat Position: <u>Driver</u>			
Note any damage prior to test: _____			

Figure 20. Vehicle Dimensions, USACE Friction Tests

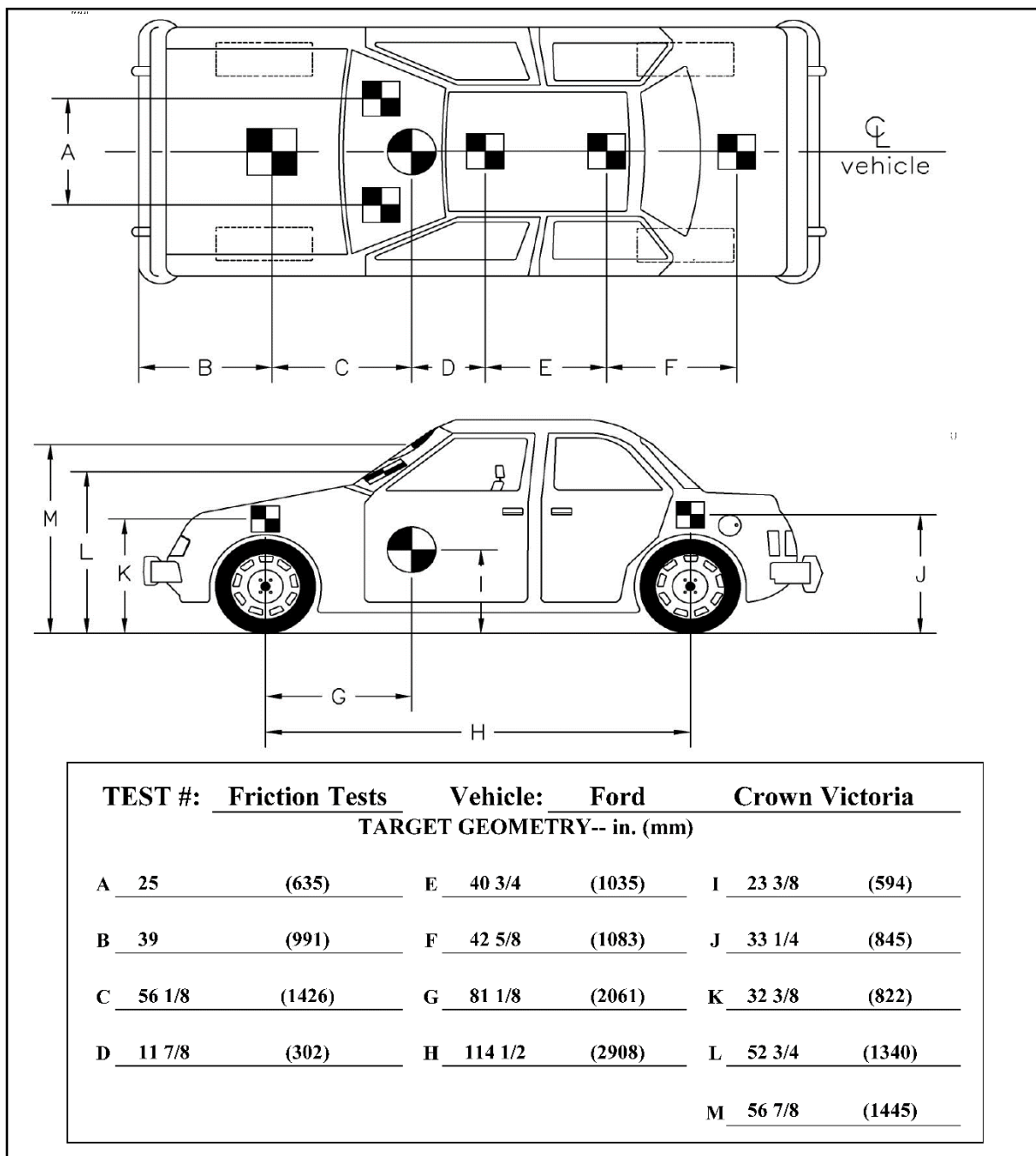


Figure 21. Target Geometry, USACE Friction Tests

The SLICE-1 unit was a modular data acquisition systems manufactured by DTS of Seal Beach, California [29]. The acceleration sensors were mounted inside the body of a custom built SLICE 6DX event data recorder and recorded data at 10,000 Hz to the onboard microprocessor. Each SLICE 6DX was configured with 7 GB of non-volatile flash memory, a range of ± 500 g's, a sample rate of 100 Hz. The "SLICEWare" computer software programs and a customized Microsoft Excel worksheet were used to analyze and plot the accelerometer data.

3.5.2 VC4000DAQ

A portable onboard accelerometer, the VC4000DAQ, produced by Vericom Computers, Inc., was installed on the test vehicle's windshield and used to record acceleration, GPS-calculated speed, and angular rotations [30]. The recording rate of the unit was 1,000 Hz when using the "Monitor" test type. A 30-deg/sec gyro was included with the VC4000 and used to auto-correct test data. Data was exported to Excel and processed using a customized data analysis spreadsheet.

3.5.3 Digital Photography

One onboard GoPro digital video camera and one external JVC digital video camera were utilized to document the USACE friction tests. The GoPro video camera had a frame rate of 59 frames per second, and the JVC digital video camera had a frame rate of 29.97 frames per second. A Nikon D50 digital still camera was also used to document pre- and post-test conditions for all tests.

3.6 External Instrumentation and Measurement Equipment

3.6.1 Skid Trailer (NDOR)

A locked wheel skid trailer was used to measure and record friction at various increments within the test area. The trailer was a Dynatest 1295 Pavement Friction Tester unit equipped with hydraulic power-assisted disc brakes, and was towed by a 2006 Chevrolet C3500 extended cab pickup truck with an 8.1L V8 engine and an automatic transmission, as shown in Figure 22. The skid trailer recorded friction by fully braking the left wheel such that the wheel was 100% skidding (i.e., non-rotating). The resistance force on the tire was recorded with a torque transducer. Torque results are converted by the 1295 Friction Tester software to a skid number, which is equivalent to the friction coefficient multiplied by a factor of 100. The left tire of the Dynatest 1295 skid trailer was alternated between an ASTM E501 ribbed tire and an ASTM E524 smooth tire [28], in order to gauge the differences between tire types on dry surfaces.

The Dynatest 1295 skid trailer typically operates by dispensing water in front of the locked wheel to record wet tire-pavement friction to represent a non-ABS vehicle braking on wet pavement. For all tests conducted in the LF and CF test locations, no water was dispensed in order to estimate the dry tire-ground skidding coefficient of friction. The tire was fully locked for approximately two (2) seconds at a time. By limiting the locked wheel skid time, temperature buildup and localized tire deformations (e.g., grinding and flattening) were limited.



Figure 22. NDOR Locked Wheel Skid Trailer



Figure 23: ASTM E501 Ribbed Test Tire and ASTM E524 Smooth Test Tire

3.6.2 VC3000 (Lincoln Police Department)

A portable onboard accelerometer, the VC3000, produced by Vericom Computers, Inc., was installed on the test vehicle's windshield and used to record acceleration, GPS-calculated speed,

and angular rotation [30]. The VC3000 was owned and operated by the Lincoln Police Department (LPD). Longitudinal, lateral, and vertical accelerations, as well as pitch and yaw rate, were recorded at 100 Hz for every test.

The VC3000 unit automatically zeroed the accelerometers and rate transducers at the start of the recording. The unit was oriented such that the X-axis (perpendicular to the LCD display) was approximately aligned with the vehicle centerline, and the Z-axis was approximately parallel to the yaw axis of the vehicle.

3.6.3 Drag Sled (Lancaster County Sheriffs Office)

A drag sled was also used to estimate the effective skidding tire-pavement friction. The drag sled consisted of a cut section of tire, 8-in. tall, and partially filled with concrete. The weight of the drag sled was 17 lb. The drag sled was pulled using a spring scale with a nearly perpendicular force, and the pull force in the scale was recorded five times per friction test location (straight line, 100-ft arc, and 200-ft arc) for a total of 15 measurements.

Note that although the precision of the drag sled was limited compared to some of the other frictional methods, this tool was low cost and easy to use, and required minimal setup. As a result, it can be quickly and inexpensively used to estimate tire-pavement.

3.7 Start and End of Test Determination

For all tests, there was no official start or end time based on an impact criterion. For longitudinal acceleration and braking tests, the start of the test was initially selected as the first point of significant vehicle acceleration. Subsequently, a braking start time was established based on significant changes in the longitudinal (or “X”) acceleration of the vehicle in the negative direction. The end of the event was selected as the time at which the vehicle came to a stop.

For circular tests, there was no distinguishable period of event start or end times. Thus, the start of the event was selected as the start of the vehicle initial acceleration. The end of the circular test events was determined to be the time at which the vehicle came to a complete stop.

3.8 Data Processing

Braking and acceleration events require many seconds to conduct. As such, some of the data measurement and processing techniques established in SAE J211 which are typically used for full-scale crash testing were not applicable [31]. Researchers utilized 100-ms moving averages to filter the acceleration data. For the longitudinal acceleration and braking tests, the longitudinal accelerations were integrated to find the velocity and displacement of the vehicle. The longitudinal and lateral accelerations could not be integrated to find velocities or displacements of the vehicle during the circular tests, because there is ambiguity of the vehicle’s centerline orientation with respect to a tangent line to path at a given instant. Without knowing how much the vehicle’s yaw angle deviated from the tangent line to the circular path, it was impossible to differentiate the longitudinal accelerations which modified speed (i.e., speeding up) from a component of centripetal acceleration acting along the longitudinal axis of the recorder.

An onboard GPS unit located within the VC4000 also recorded distance traveled and speed maintained throughout the event. The VC4000 GPS has a position accuracy of approximately +/- 1.5 m (5 ft) in space, but is accurate to approximately 0.2 mph for speed [30]. The VC4000 was also equipped with an OBDII port connector which monitored vehicle-reported speed and distance traveled throughout the event.

4 LONGITUDINAL FRICTION TEST RESULTS AND DISCUSSION

4.1 Weather Conditions

Test nos. LF-1 through LF-4 and LF-1b were conducted between 10 and 11:30 am on March 2, 2016. The weather conditions as per the National Oceanic and Atmospheric Administration (station 14939/LNK) were reported and are shown in Table 3.

Table 3. Weather Conditions, Test Nos. LF-1 through LF-4 and LF-1b

Temperature	48° F
Humidity	46%
Wind Speed	21 mph
Wind Direction	170° from True North
Sky Conditions	Sunny
Visibility	10 Statute Miles
Pavement Surface	Dry, swept, and wire brushed
Previous 3-Day Precipitation	0.00 in.
Previous 7-Day Precipitation	0.00 in.

4.2 Test Details

For all tests, a 4,026-lb Ford Crown Victoria was operated by a driver and passenger weighing approximately 190 and 100 lb, respectively, at or near to its acceleration and braking performance limits. For test no. LF-1b, 219 lb of additional mass was added to the trunk of the vehicle to represent a bomb, at the request of the sponsors. Videos were taken of the tests from external viewpoints and from within the occupant compartment. Sample sequential photographs of the tests are shown in Figures 24. The SLICE accelerometer was attached to the frame of the car using a bolt-down plate and was located near the vehicle's CG. A Vericom VC4000 was mounted to the center of the windshield using a vacuum-sealed suction cup, and a Vericom VC3000 was mounted to the windshield to the right of the VC4000 using two vacuum-sealed suction cups.

Following the vehicle acceleration and braking tests, a drag sled was pulled along the surface of the test area and the friction was recorded. In addition, the locked wheel skid trailer was pulled along the surface without spraying water in front of the test tire, and the skidding resistance was also recorded.

4.3 Results

4.3.1 SLICE and VC4000

Accelerometer results were extracted, filtered, and analyzed for all tests. Similar tests were grouped for analysis. The VC3000 data was extracted and processed, but was a backup to the VC4000 collection system. Because results were similar to VC4000 data, but the precision and tolerances were slightly lower, those results are not shown here.



Figure 24. Sample Exterior Sequential Images (test no. LF-3 shown)

Despite filtering the data sets, the acceleration traces were noisy for all the data sets collected. Example SLICE and VC4000 longitudinal accelerations using filtered data from test no. LF-1 are shown in Figure 25. VC4000 and SLICE results for test nos. LF-1 through LF-4 and LF-1b are provided in Appendices A through E.

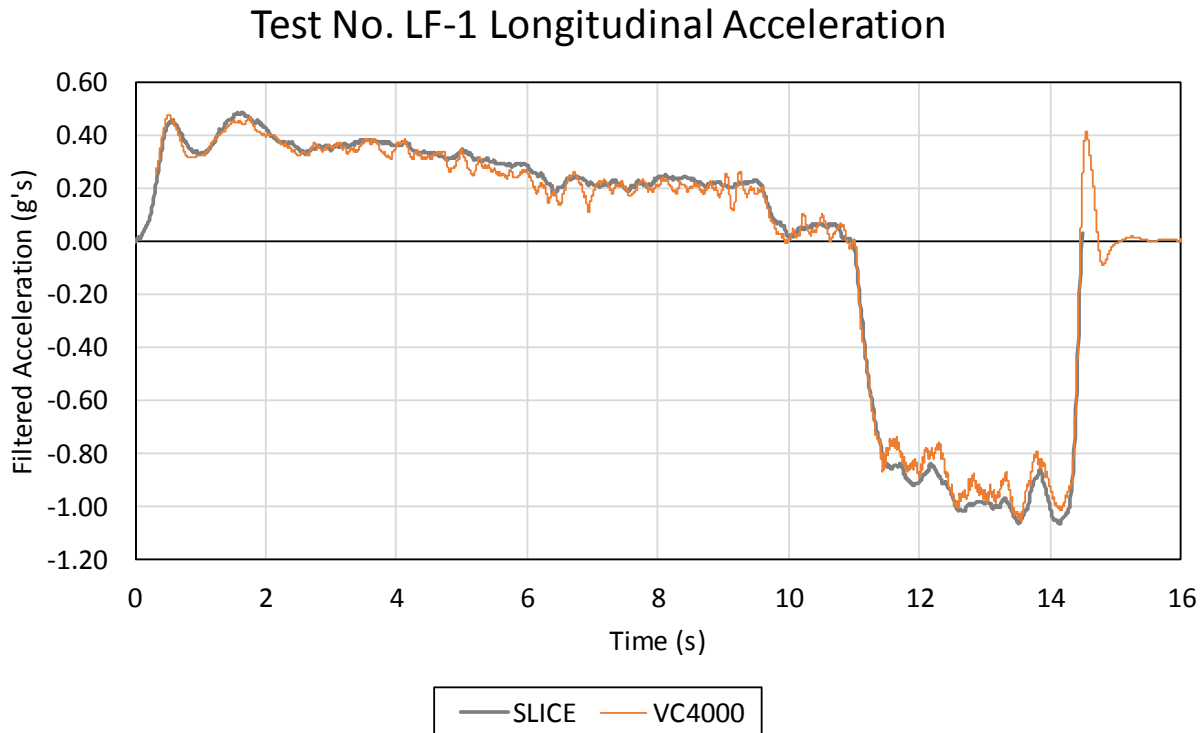


Figure 25. Example Longitudinal Acceleration, Test No. LF-1

Using these observations, the maximum tire-pavement friction coefficient for tangent (straight forward) braking conditions was estimated by extracting the acceleration trace during the braking event. Researchers identified the portion of the event at which the acceleration trace rapidly changed in the negative direction. The last positive acceleration data point prior to the negative signal was selected as the braking start time. An example of an extracted braking data set is shown in Figure 26.

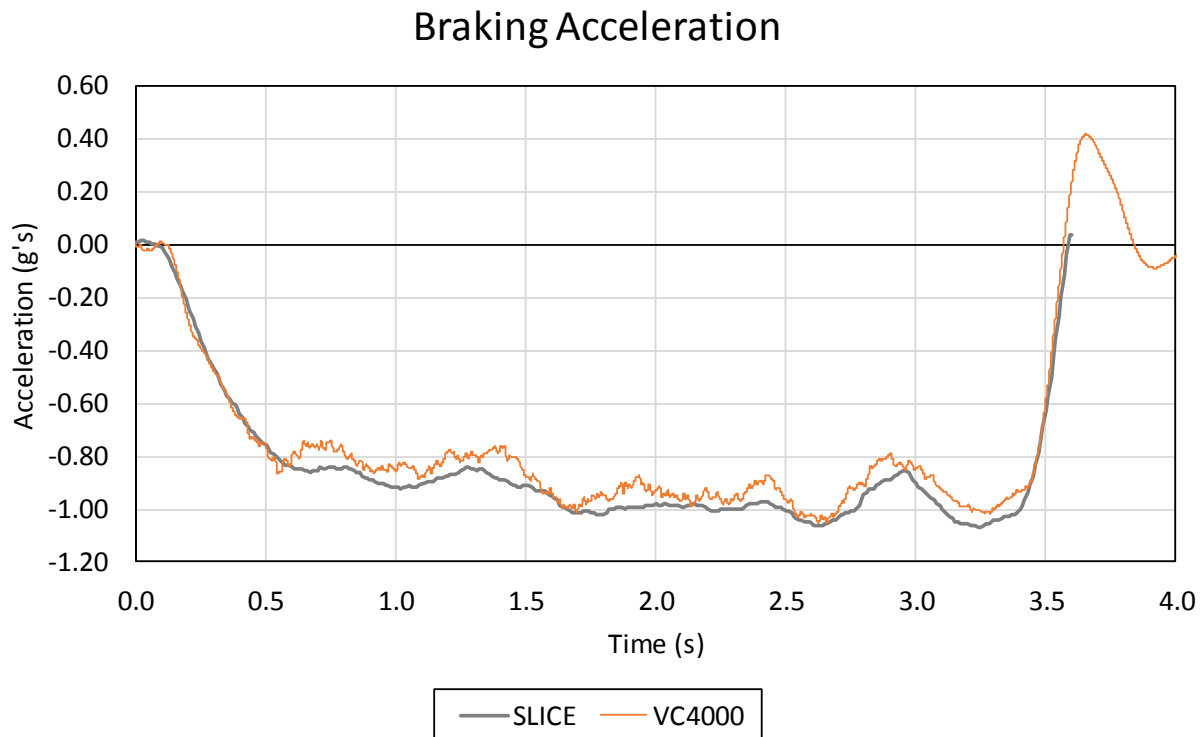


Figure 26. Example Braking Acceleration, Test No. LF-1

The maximum braking acceleration magnitude (and thus friction coefficient utilized) from test no. LF-1 was -1.069 g's and -1.052 g's for the SLICE and VC4000 units, respectively. Nonetheless, the maximum or minimum value of the acceleration curve is not an accurate method of identifying what the maximum sustainable friction value was. Due to the pulsing action of the vehicle's anti-lock brakes (ABS), the vehicle acceleration recorded by the SLICE unit fluctuated between -0.893 and -1.07 g's. The maximum sustainable friction would be considered the average friction utilized by the vehicle over a meaningful time interval. Maximum average braking accelerations were recorded using average intervals spanning between 0.50 and 3.00 s for test nos. LF-1 through LF-4 and LF-1b, and are tabulated in Table 4. A summary of the acceleration results is shown in Table 5. Braking accelerations for all of the tests are shown in Figure 27.

Table 4. Maximum Average Braking Accelerations, Test Nos. LF-1 through LF-4 and LF-1b

Time Average	LF-1 (g's)		LF-2 (g's)		LF-3 (g's)		LF-4 (g's)		LF-1b (g's)	
	SLICE	VC4000	SLICE	VC4000	SLICE	VC4000	SLICE	VC4000	SLICE	VC4000
0.50 sec	-1.013	-0.969	-0.982	-0.942	-1.011	-0.954	-1.026	-0.986	-1.022	-0.976
1.00 sec	-1.004	-0.955	-0.970	-0.925	-1.001	-0.943	-1.019	-0.975	-0.995	-0.951
1.50 sec	-0.992	-0.938	-0.965	-0.912	-0.990	-0.934	-1.007	-0.957	-0.979	-0.935
2.00 sec	-0.987	-0.936	-0.959	-0.901	-0.981	-0.927	-0.991	-0.941	-0.965	-0.923
2.50 sec	-0.967	--0.912	-0.950	-0.891	-0.978	-0.923	-0.981	-0.931	-0.953	-0.914
3.00 sec	-0.946	-0.893	-0.928	-0.875	-0.941	-0.896	-0.952	-0.911	-0.924	-0.890

Table 5. Maximum Average Braking Acceleration Results Summary

Time Average	LF-1 through LF-4 and LF-1b Average	
	SLICE	VC4000
0.50 sec	-1.011	-0.965
1.00 sec	-0.998	-0.950
1.50 sec	-0.987	-0.935
2.00 sec	-0.976	-0.926
2.50 sec	-0.966	-0.914
3.00 sec	-0.938	-0.893

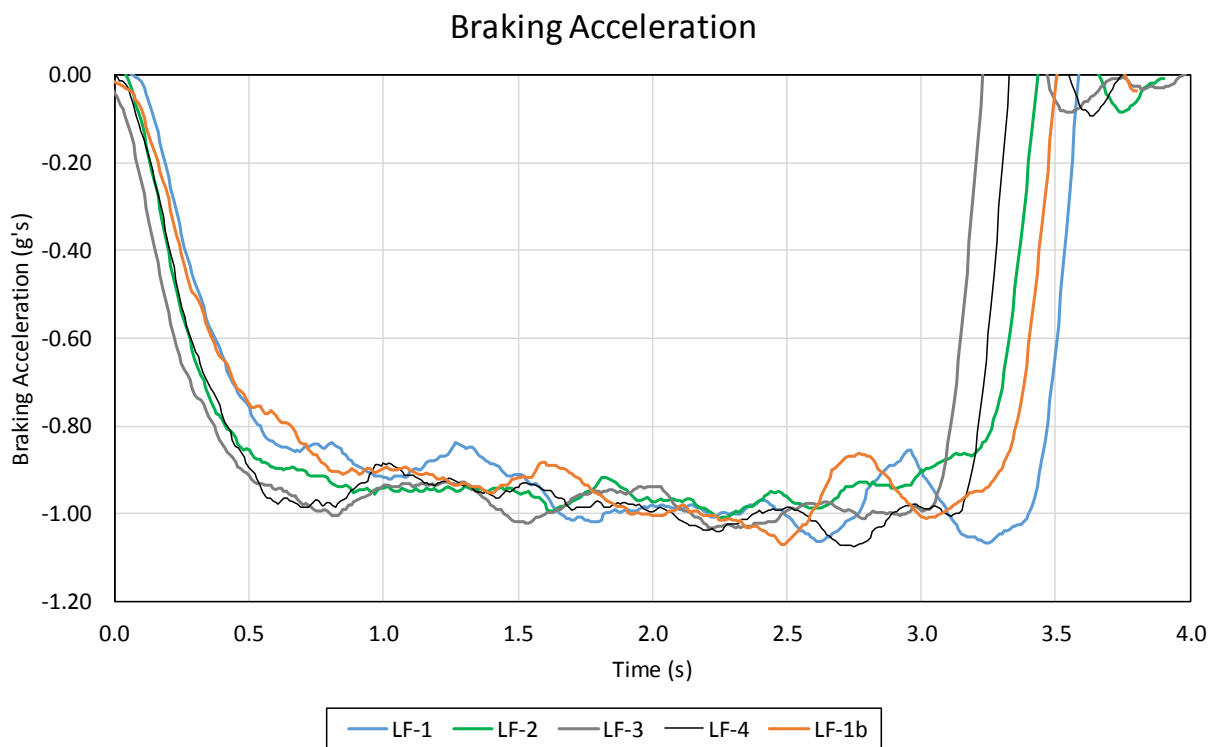


Figure 27. Comparison of Braking Accelerations for Test Nos. LF-1 through LF-4 and LF-1b

For all tests, the vehicle started braking at a speed of approximately 60 mph, then decelerated to a complete stop. Likewise, for all braking acceleration curves, the maximum braking acceleration (largest absolute value of the negative acceleration) always occurred near the end of the event, when the vehicle had significantly slowed down. To confirm this finding, the vehicle speed was estimated by integrating the acceleration vs. time curve, and the braking acceleration was plotted against the speed, as shown in Figures 28 and 29. Based on test results, it can be concluded that the instantaneous braking coefficient of friction is influenced by vehicle speed.

Not surprisingly, for test no. LF-1b, the vehicle sped up more slowly due to the increased weight, but experienced no net reduction in braking efficiency. The brake torque capacity at the wheel is typically much higher than the brake torque produced at the tire-pavement interface, because the brake pad must still stop a fully-loaded vehicle in compliance with the FMVSS standards. Speeding up, however, is limited to the available vehicle power, which is the rate of change of kinetic energy. By adding mass but keeping a constant maximum power, the vehicle will not be able to speed up as quickly when it is fully loaded, as shown in Figure 29.

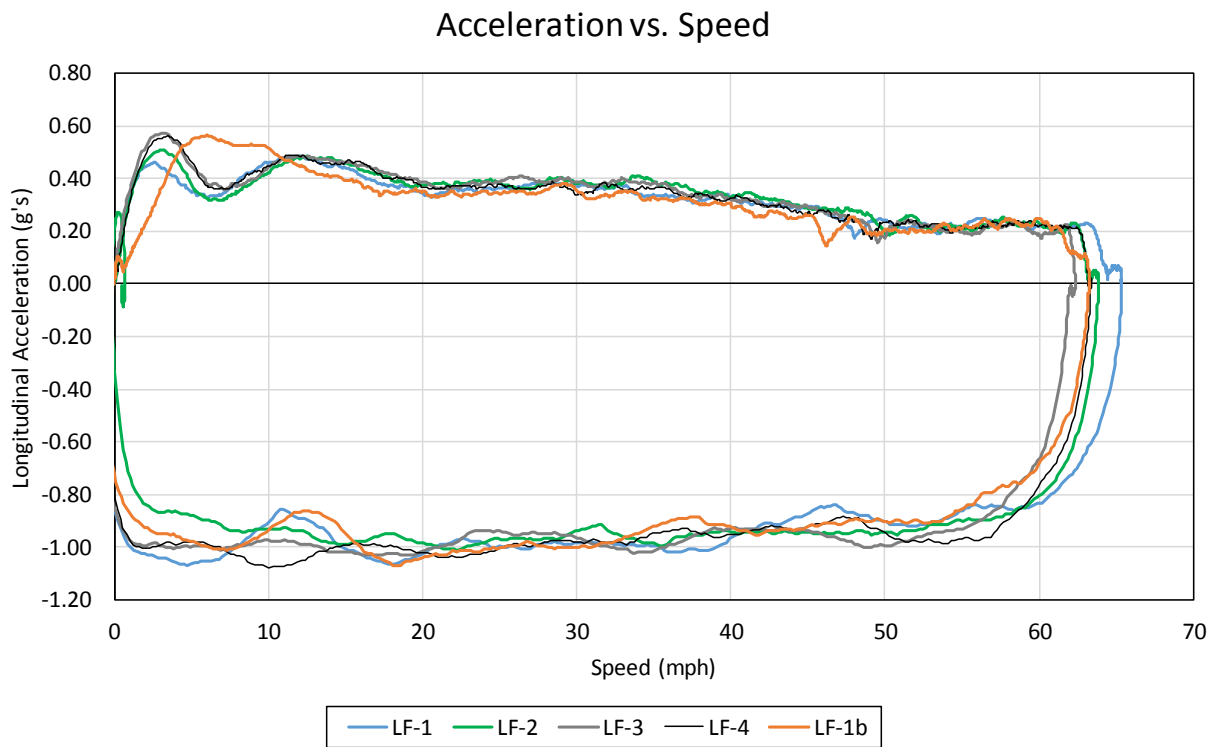


Figure 28. Acceleration vs. Speed, Test Nos. LF-1 through LF-4 and LF-1b

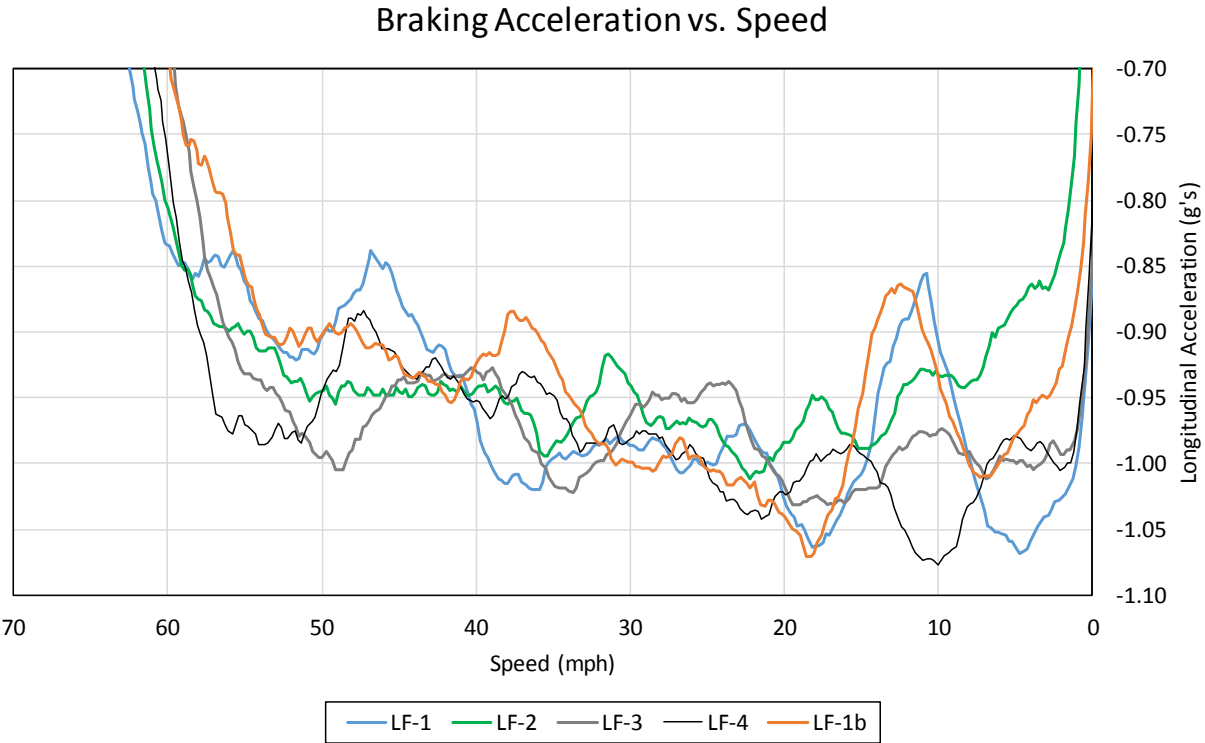


Figure 29. Detail View of Braking Acceleration vs. Speed (Note: X-axis reversed)

The velocity estimates obtained by integrating the SLICE acceleration curves were compared to the onboard GPS-reported and vehicle OBDII port-reported speeds. A sample comparison is shown in Figure 30. In general, the OBDII and GPS speeds were similar for all tests. Some deviation existed because of wheel slip which affected the OBDII reported speed. This conclusion was supported by a previous investigation of onboard OBDII and GPS speed reports for 2010 and 2011 Toyota Camry vehicles [32].

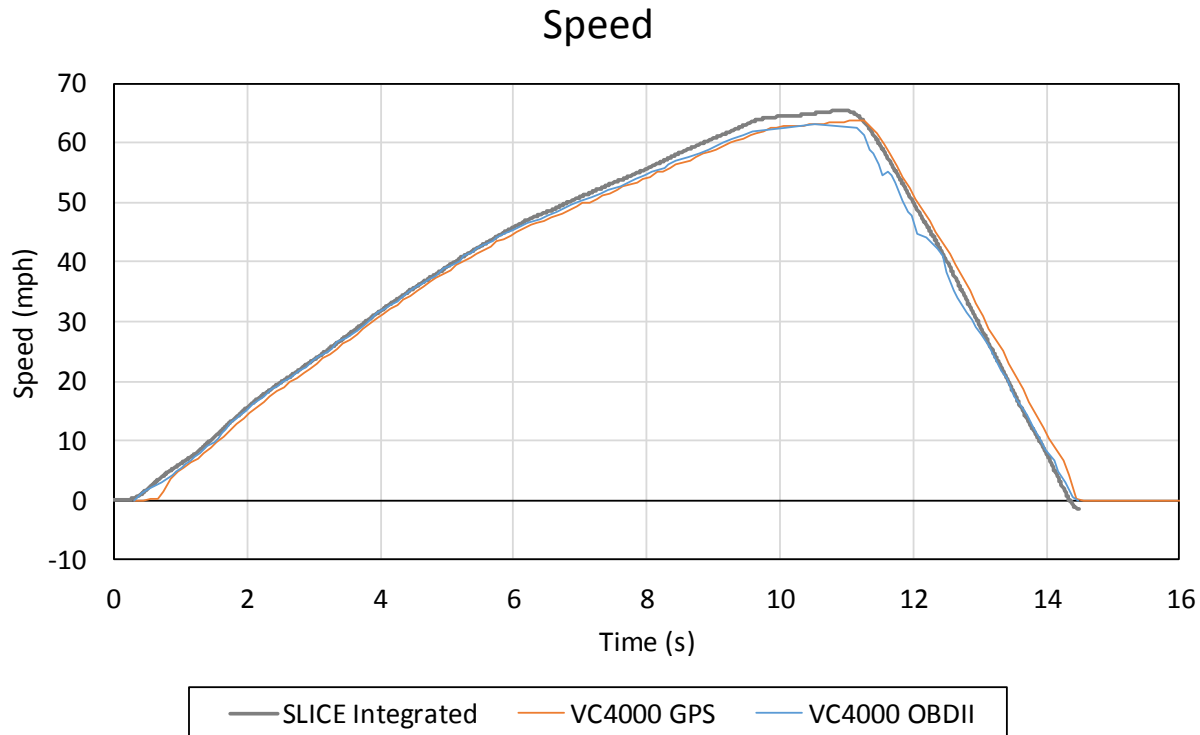


Figure 30. Example Velocity Comparison of Integrated SLICE Accelerations and VC4000 GPS and OBDII Port Speed Outputs for Test No. LF-1

For all tests, the integrated SLICE curves indicated a higher maximum speed than the GPS and OBDII port speeds. Nonetheless, the maximum deviation between the maximum speed identified using the integrated SLICE accelerometer data and the maximum GPS speed was 2.97 mph during Test No. LF-2, or a 4.9% difference.

Researchers observed that the GPS speeds were likely more accurate than the integrated SLICE or OBDII output. Integrating the SLICE data can result in error introduced due to even a very small bias in the signal. Bias could be introduced due to low-frequency, low-amplitude voltage oscillation in the SLICE recorder, variations in environmental noisy signals present around the recorder, or perhaps most importantly, minor deviations in forward pitch due to acceleration, braking, and occupant movement. Even a 1-degree pitch change can result in a 0.017 g acceleration error which can accumulate in the data set. Over the course of one second, a 0.017-g bias error can result in a net difference in speed of 0.37 mph. For each sustained second of variation, the speed uncertainty increases.

A vehicle subjected to full-throttle acceleration would experience rearward load transfer and a small upward pitch. Likewise, a forward load transfer and pitch downward at the front of the vehicle is expected during full braking. Former tests investigating the pitch behavior of a Ford Taurus indicated that under 0.9-g fully-braked conditions, the forward pitch was as large as 2.8 deg [33]. Thus, some pitching-related error is likely. Unfortunately, the accuracy of the rate transducer was insufficient for such small angle motions and the pitch-related bias could not be accurately estimated. A comparison of output speeds is shown in Figures 31 and 32.

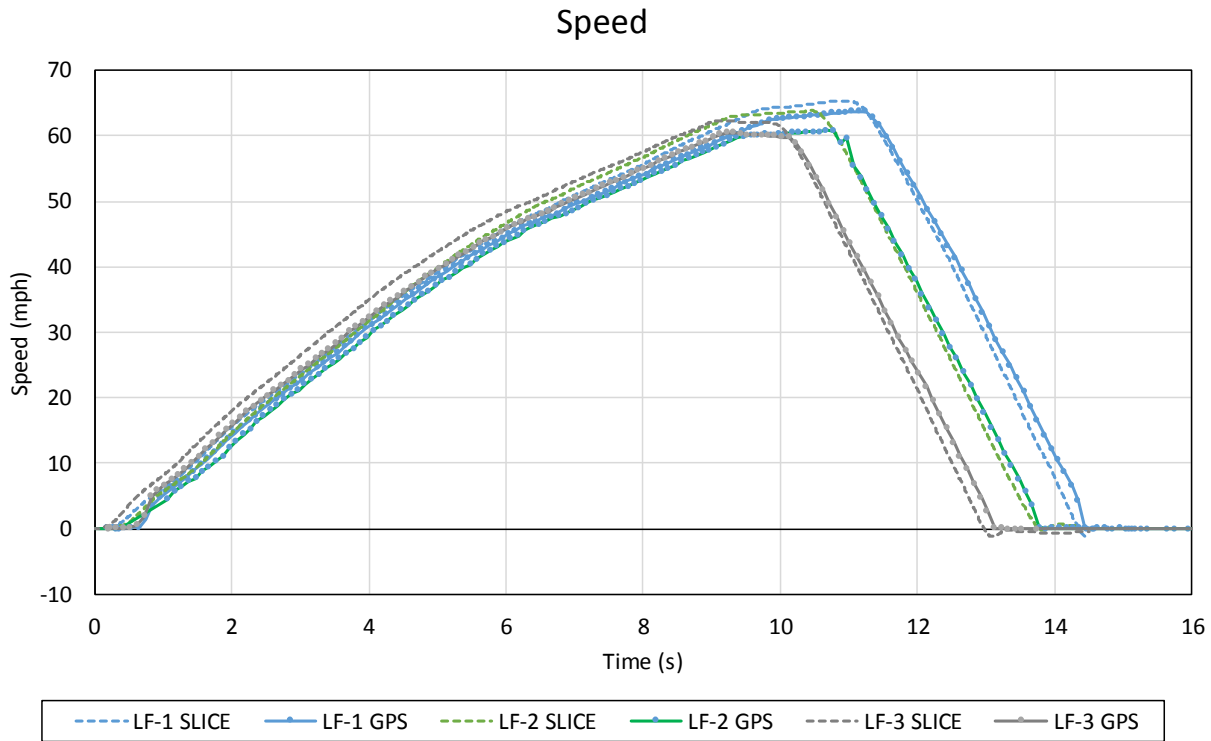


Figure 31. Comparison of Longitudinal Velocity Results, Integrated SLICE and VC4000 GPS Output for Test Nos. LF-1 through LF-3

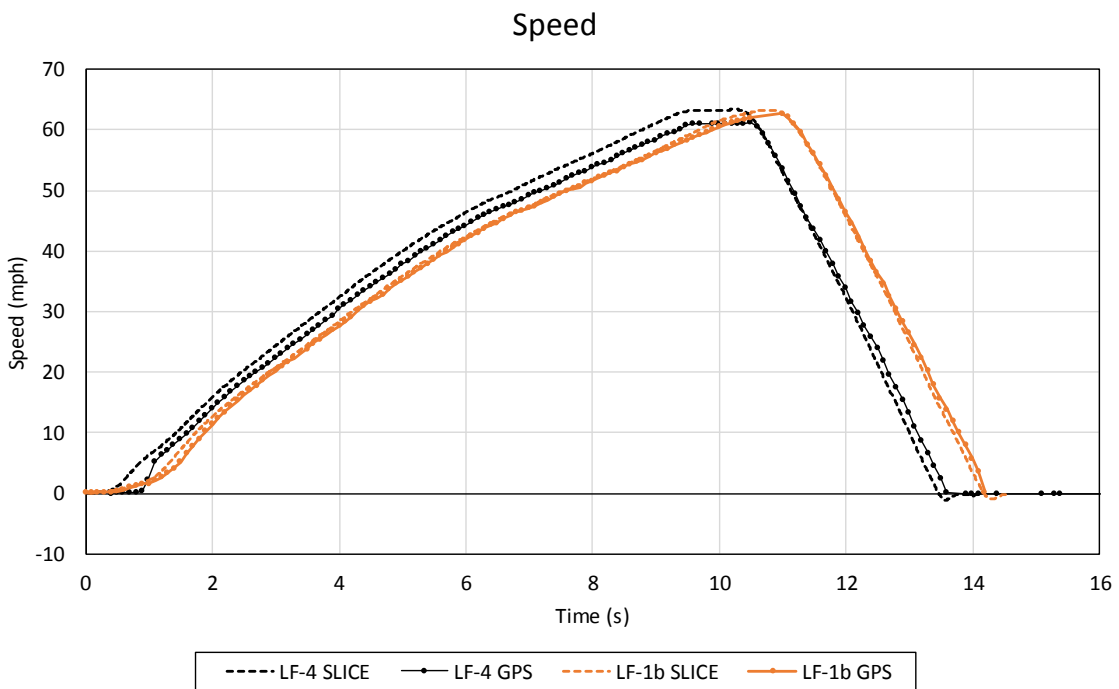


Figure 32. Comparison of Longitudinal Velocity Results, Integrated SLICE and VC4000 GPS Output for Test Nos. LF-4 and LF-1b

4.3.2 Locked Wheel Skid Trailer

The locked wheel skid trailer, owned and operated by the Nebraska Department of Roads (NDOR), was pulled at approximately 45 mph along the test area and the trailer wheel was locked for approximately 2 sec per test. Approximately 9 tests were conducted for each of the ASTM ribbed (E501) and smooth (E524) tires [28]. Results were provided in terms of a Skid Number (SN), which is equivalent to the coefficient of sliding friction multiplied by 100.

The average locked wheel skid trailer friction was 0.85 for the ribbed tire and 0.94 for the smooth tire. Although the smooth tire demonstrated substantially more resistance due to less tread compliance, as expected, test results were not representative of a locked, treaded tire. Thus remaining skid trailer tests only used the E501 ribbed tire.

Table 6. Skid Trailer Reported Skidding Coefficients of Friction, ASTM E501 Ribbed Tire

Measurement	Trailer Weight (lb)	F (lbf)	Average SN	Average μ
1	451	383.4	85.0	0.850
2	451	388.3	86.1	0.861
3	451	386.5	85.7	0.857
4	451	385.2	85.4	0.854
5	451	385.6	85.5	0.855
6	451	400.0	88.7	0.887
7	451	383.8	85.1	0.851
8	451	375.2	83.2	0.832
9	451	377.5	83.7	0.837
10	451	384.7	85.3	0.853
Average				0.854

Table 7. Skid Trailer Reported Skidding Coefficients of Friction, ASTM E524 Smooth Tire

Measurement	Trailer Weight (lb)	F (lbf)	Average SN	Average μ
1	451	420.8	93.3	0.933
2	451	427.1	94.7	0.947
3	451	422.6	93.7	0.937
4	451	427.1	94.7	0.947
Average				0.941

4.3.3 Drag Sled

The 17-lb drag sled, owned by the Lancaster County Sheriffs Office (LSO), was pulled along the surface of the longitudinal test area using a 30-lb fishing spring scale in 50-ft increments. Results are shown in Table 8, and varied by approximately 0.5 lb along the test area. The average sliding friction coefficient for the concrete-filled tire was approximately 0.87.

Table 8. Drag Sled Test Results

Drag Sled Pull Force (lb)	Effective Friction Coefficient
14.5	0.85
15	0.88
14.75	0.87
15	0.88
15	0.88
Average	0.87

4.4 Comparisons with Threat Calculator Defaults

The Threat Calculator limits for speeding up and braking are 11.4 ft/s^2 (0.35 g's) and 24.1 ft/s^2 (0.75 g's), respectively. Thus, since the vehicle is assumed to travel at MTCAS⁸, the acceleration during speeding up and braking will be constant. Likewise, the speed and the displacement of the vehicle during speeding up and accelerating can be calculated:

$$V = V_0 + at \quad (10)$$

$$\Delta s = V_0 t + \frac{1}{2} a t^2 \quad (11)$$

V= velocity (speed)

V_0 = initial speed

a = acceleration

t = time

Δs = change in displacement

The Threat Calculator braking defaults were compared to the test results, as shown in Figures 33 through 35. The maximum accelerations in the tests had a 25% higher magnitude than the Threat Calculator, but required nearly $\frac{1}{2} \text{ s}$ to transition between zero and the maximum braking rate (approximately -1.0 g's), as shown in Figure 33.

The speed change for the braking period was also plotted, as shown in Figure 34. During the driver's brake application period of 0.5 s, the threat vehicle decelerated from 60 to 52 mph. However, after the brakes were fully depressed, the test vehicle came to a stop more quickly than the Threat Calculator vehicle for every test, even when the initial speed was higher than the targeted 60 mph.

In addition, the braking distance was plotted, as shown in Figure 35. Although the test vehicles stopped more quickly (time) than the Threat Calculator vehicle, the Threat Calculator vehicle stopped in less distance.

⁸ MTCAS: Maximum Threat Calculator Acceleration and Speed

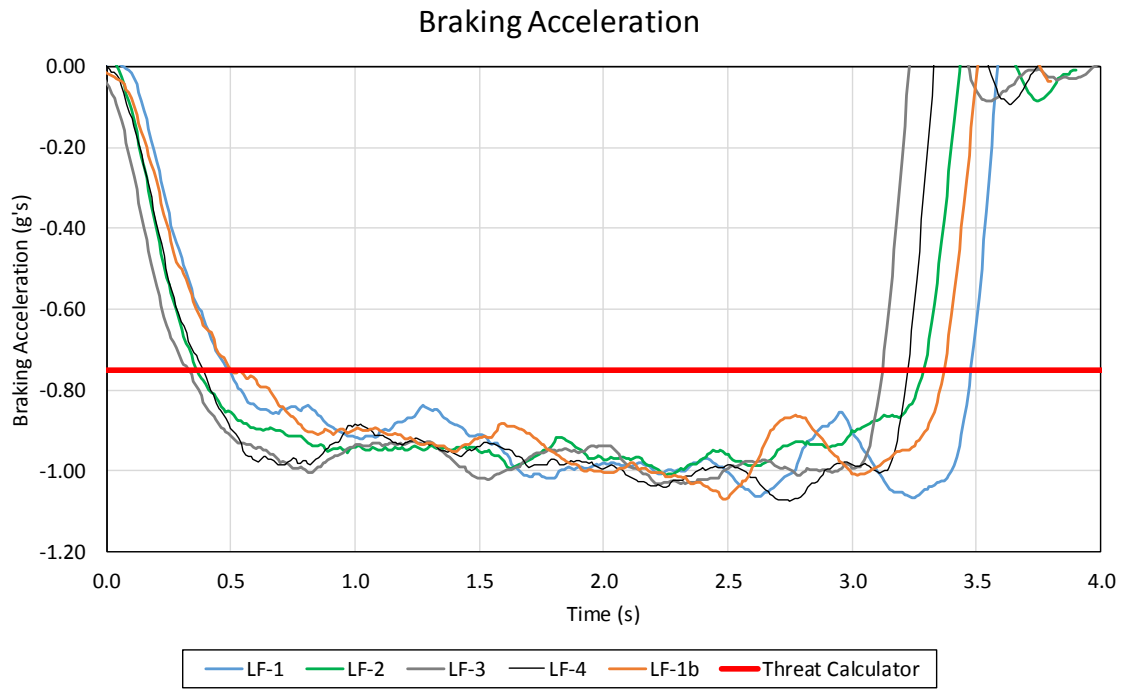


Figure 33. Braking Deceleration Comparison with USACE Threat Calculator Acceleration

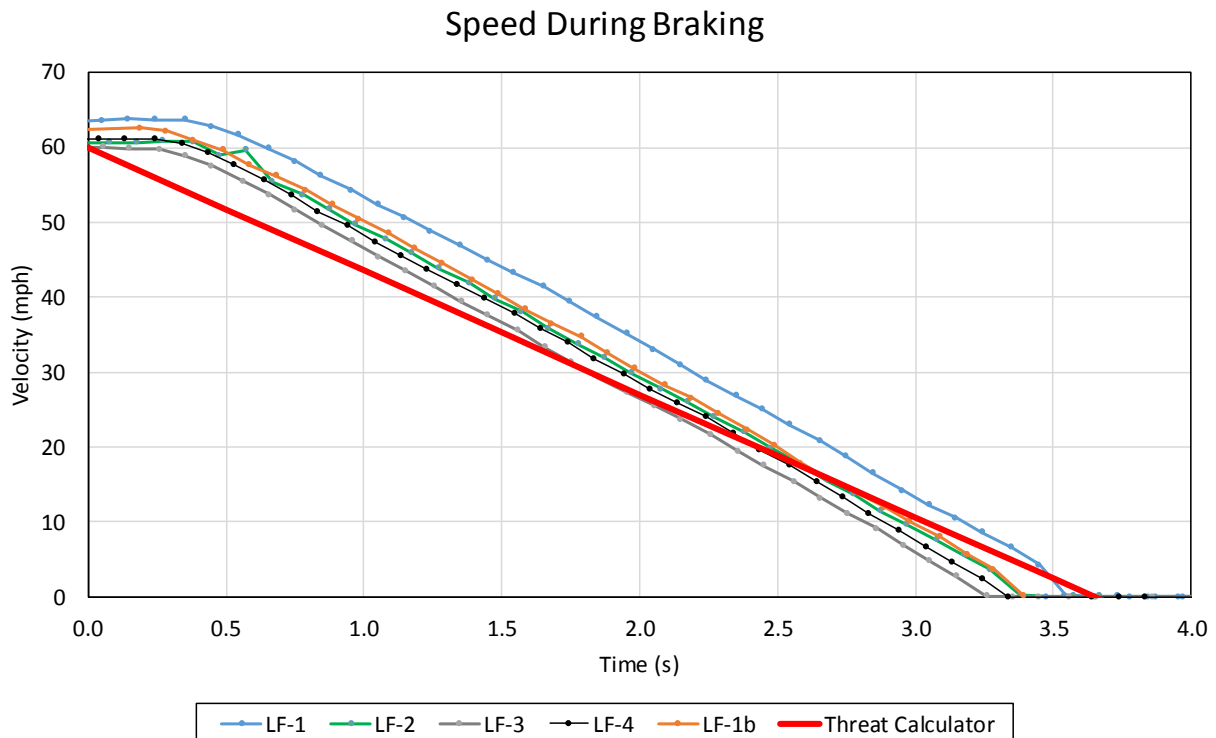


Figure 34. Braking Speed Comparison with USACE Threat Calculator Calculated Speed Change

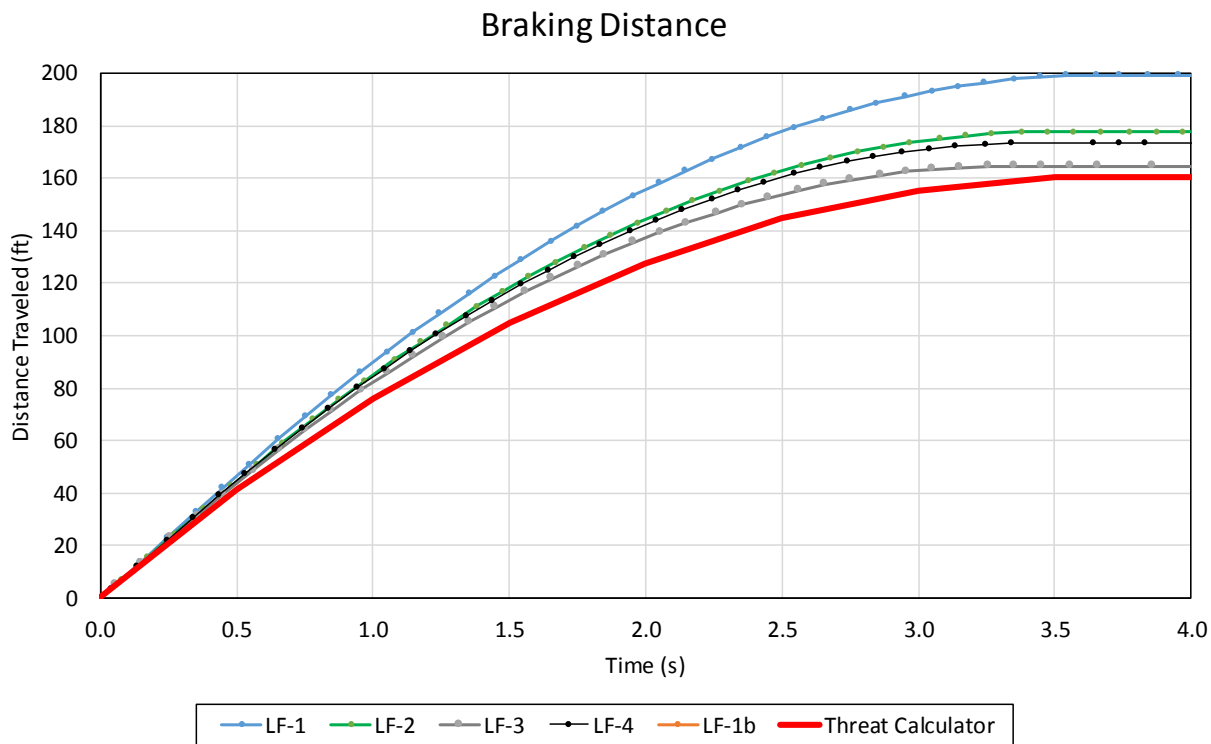


Figure 35. Test Distance Traveled While Braking Compared with USACE Threat Calculator Calculated Distance Traveled while Braking

Accelerations while speeding up, speeds, and distances traveled were plotted and compared, as shown in Figures 36 through 38. The driver of the test vehicle fully depressed the gas pedal (i.e., full throttle acceleration), but there was a distinguishable period of approximately $\frac{1}{2}$ s in which the acceleration increased from zero (stopped) to the maximum value of approximately 0.55 g's. The initial acceleration of the test vehicles was higher than the 0.35-g constant rate of the threat vehicle. However, after approximately 2 s, the test vehicle accelerations approached the Threat Calculator vehicle acceleration, and at approximately 5 s, the test vehicle accelerations all dropped below the Threat Calculator limits. The variations in the test vehicle acceleration were likely related to gear changes in the test vehicle transmission as well as power limitations from the engine.

Because of the initial acceleration ramp-up period, the test vehicle speed lagged the Threat Calculator speed until approximately 1 s, as shown in Figure 36. Between 1 s and 5 s, the test vehicle speed and Threat Calculator speed were nearly equal, but after 5 s, the Threat Calculator speed increased more quickly than the test vehicle speeds. The test vehicle speed never exceeded the Threat Calculator speed estimate in any test at 7.8 s, when the Threat Calculator speed estimate peaked at 60 mph, although the vehicle in test no. LF-3 briefly exceeded the Threat Calculator speed estimate.

The distance traveled by the test vehicles and Threat Calculator vehicle during speeding up are shown in Figure 38. The Threat Calculator vehicle traveled 50 ft farther than the test vehicles,

while speeding up after 7.8 sec (corresponding to the time when the Threat Vehicle reached 60 mph) than occurred during the tests, on average.

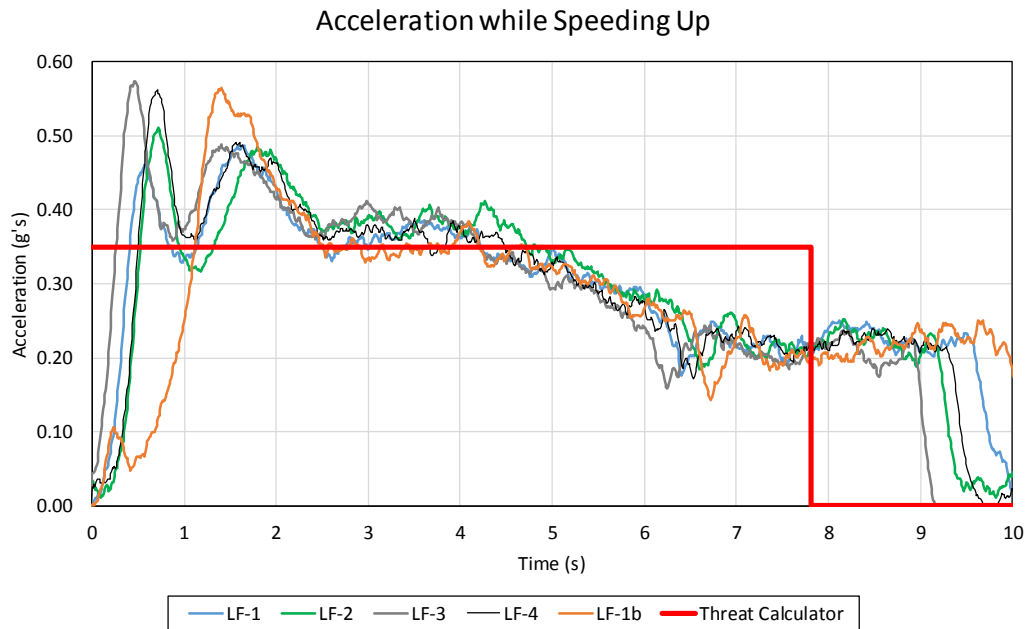


Figure 36. Acceleration while Speeding Up Comparison with USACE Threat Calculator

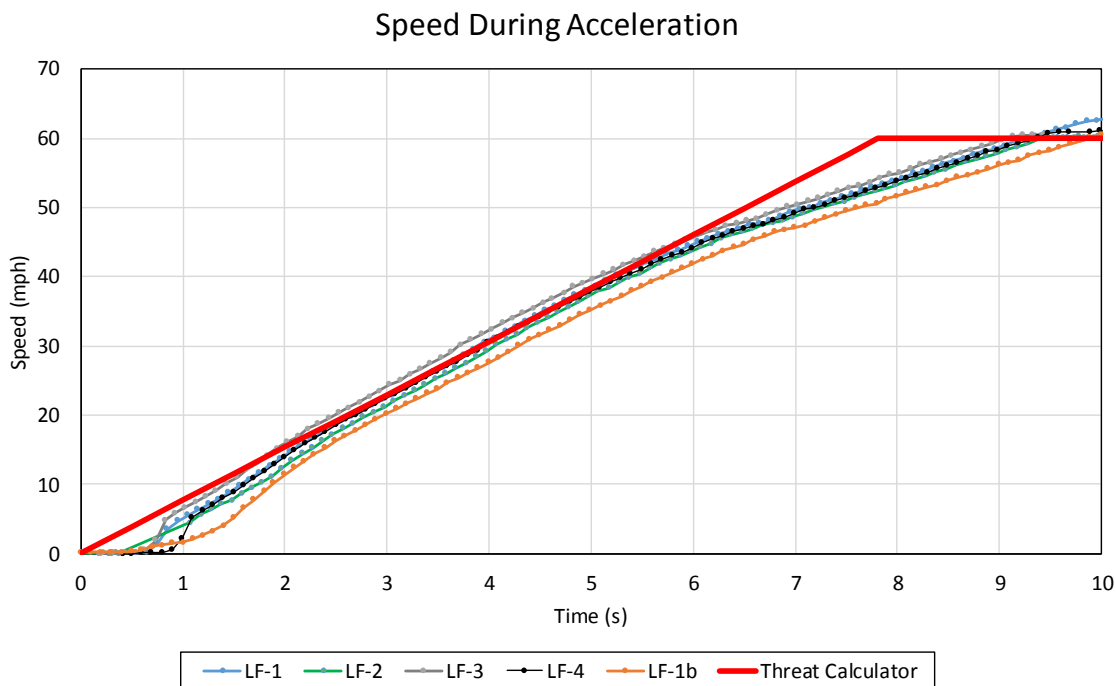


Figure 37. Comparison of Test Results and USACE Threat Calculator Calculated Speed

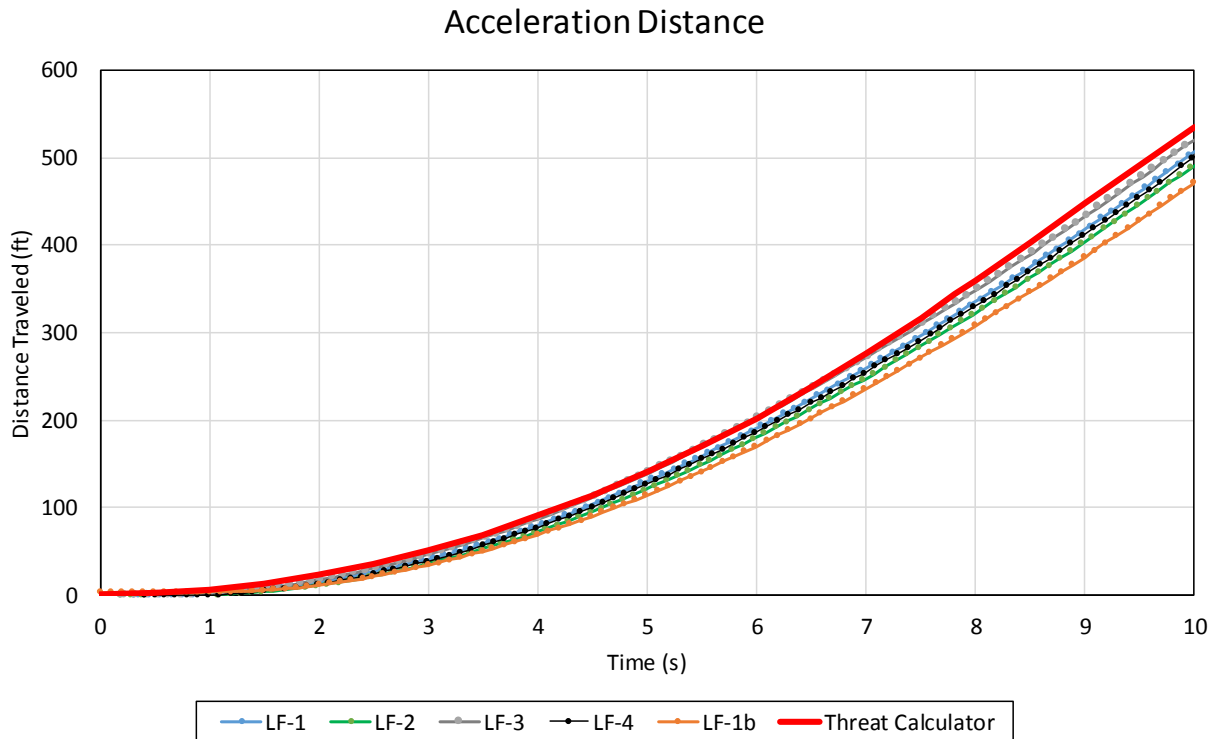


Figure 38. Distance Traveled while Speeding Up Comparison with USACE Threat Calculator Calculated Distance

4.5 Conclusions, Discussion, and Recommendations

4.5.1 Threat Calculator Evaluation

The objective of these tests was to determine the optimal value of tire-friction coefficient to utilize with the Threat Calculator, which is conservative but still reasonably representative of real vehicle driving behaviors. The USACE default braking acceleration of 0.75 g's was less than the braking accelerations observed in every test. The maximum acceleration while speeding up was lower than the test vehicle average at first, but rapidly exceeded the test vehicle average at 2.5 s, corresponding to a speed of approximately 20 mph. For accelerations beyond 5 s, corresponding to a speed of approximately 40 mph, the Threat Calculator acceleration estimate was higher than the test average. Thus, researchers recommend a maximum braking coefficient of friction and corresponding maximum braking acceleration of 1.0 and 1.0 g's, respectively.

Researchers recommend a straight-line (tangent) tire-pavement friction coefficient of 1.0 for the USACE Threat Calculator.

Although the numerical Threat Calculator vehicle outperformed the real test vehicle in every test, outcomes were heavily influenced by transitions between steady-state (no acceleration) and application of the gas and brake pedals. This indicates that the Threat Calculator assumptions are

The Threat Calculator assumption for instantaneous transition between braking and speeding up is conservative, but still reasonable.

conservative, but maximum values observed during the tests had larger magnitudes than the Threat Calculator. During the tests, the driver was instructed to release the gas and brake pedals between every maneuver. Thus, the test conditions prohibited the driver from using both feet simultaneously. “Two-pedal driving”, in which the gas and brake pedals are operated independently by the right and left feet, respectively, allows professional racers an opportunity to more quickly transition between accelerating and braking behaviors. It is not reasonable to assume that real drivers will have the same delay between steady-state and fully-braked or full-throttle speeding up conditions, though some delay could be expected. Therefore researchers recommend that no changes be

made to the Threat Calculator behavior assumption regarding instantaneous transitions between speeding up and braking.

4.5.2 Friction Measurement Methods

It may be meaningful for military personnel to investigate real-world friction in ACPs. The easiest method for recording friction on dry pavement is to use the drag sled. This device is very inexpensive and requires very little training to use. However, results underpredict the maximum ABS tire-pavement friction braking coefficient by between 15 and 20%. A reasonable ABS braking coefficient of friction is approximately 1.17 times larger than the drag sled estimate.

The second preferred method for measuring and recording friction was the VC4000 windshield-mounted accelerometer, which requires that a vehicle slam on the brakes to estimate the maximum friction coefficient. Although more expensive than the drag sled, results were 17% higher on average than the skidding tire friction, and provided a reasonable estimate of friction.

A skid trailer may be used if available, but the method requires considerable training to utilize and results underestimate the maximum friction during ABS braking conditions. In addition, the skid trailer is itself fairly expensive. The highest precision instrument, the SLICE triaxial accelerometer, was likely the most accurate method of estimating friction but is very expensive, can be difficult to use, requires considerable training to obtain meaningful data from, and likely is excessive for purposes of measuring friction. These units provide very precise results but their use may not be required for all personnel and all ACP configurations.

5 SIDE FRICTION TEST RESULTS AND DISCUSSION

5.1 Weather Conditions

Test nos. CF-100-1 through CF-100-3, CF-100-1b, CF-200-1 through CF-200-3, and CF-200-1b were conducted between 10 and 11:30 am on March 2, 2016 and immediately following the longitudinal tests. The weather conditions as per the National Oceanic and Atmospheric Administration (station 14939/LNK) were reported and are shown in Table 9.

Table 9. Weather Conditions, USACE Friction Tests

Temperature	48° F
Humidity	46%
Wind Speed	21 mph
Wind Direction	170° from True North
Sky Conditions	Sunny
Visibility	10 Statute Miles
Pavement Surface	Dry
Previous 3-Day Precipitation	0.00 in.
Previous 7-Day Precipitation	0.00 in.

5.2 Test Photography

The 4,026-lb Ford Crown Victoria was operated at or near to its performance limits for all tests. Videos were taken of the tests from external viewpoints and from within the occupant compartment. Sample sequential photographs of the tests are shown in Figure 40.

5.3 Results

5.3.1 SLICE and VC4000

Accelerometer results were extracted, filtered, and analyzed for all tests. Similar tests were grouped for analysis. The VC3000 data was extracted and processed, but because results were similar to VC4000 data, those results are not shown here.

Despite filtering the data sets, the acceleration traces were noisy for all the data sets collected. Example longitudinal and lateral accelerations and the magnitude of the resultant acceleration are shown in Figures 41 and 42. In general, VC4000 accelerations matched the behavior of the SLICE accelerations. The full data sets for test nos. CF-100-1 through CF-100-3, CF-100-1b, CF-200-1 through CF-200-3, and CF-200-1b are shown in Appendices F through M.

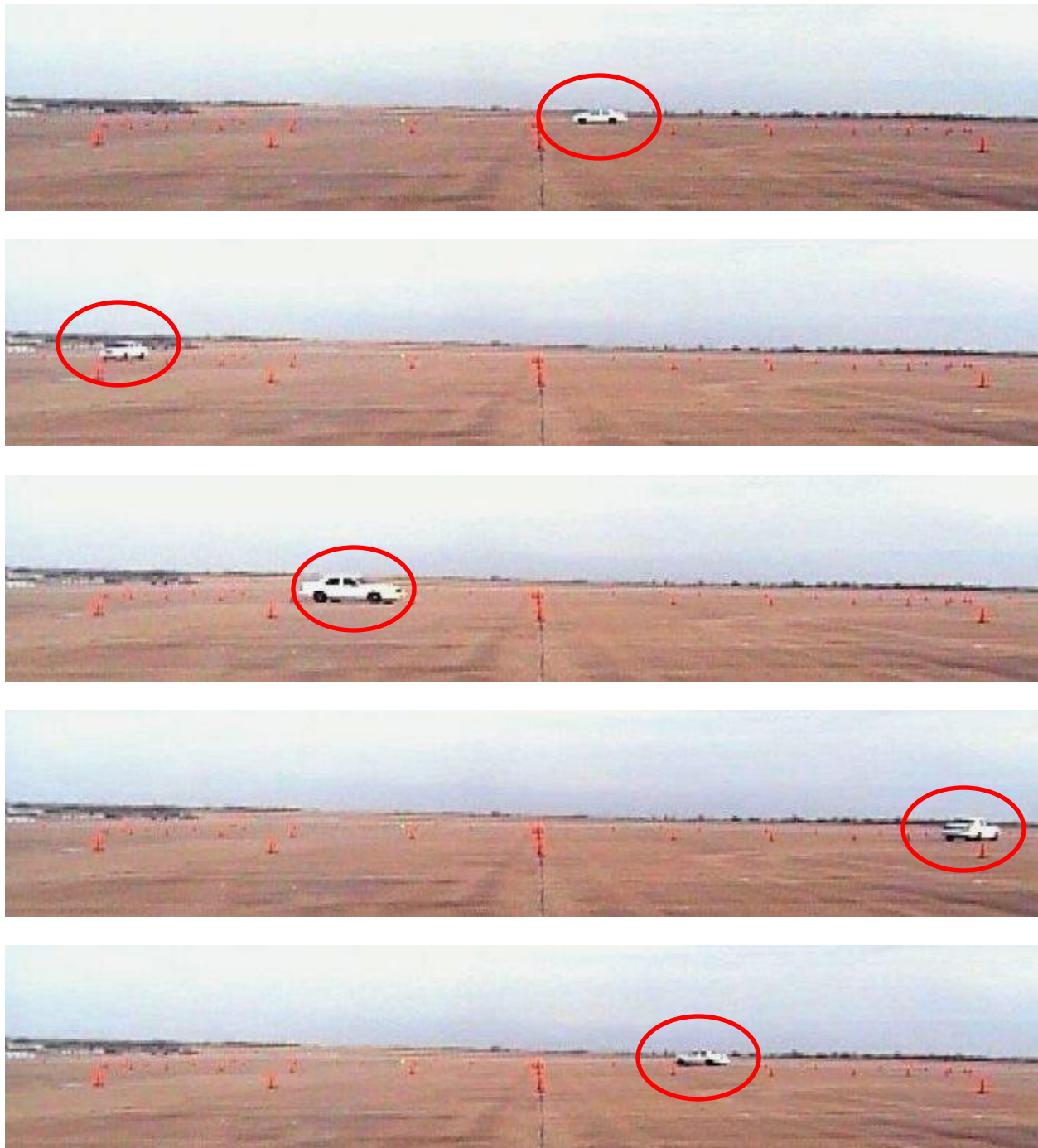


Figure 39. Example External Camera Sequential Images (test no. CF-100-3 shown)



Figure 40. Sample Occupant Compartment Sequential Images (test no. CF-100-3 shown)

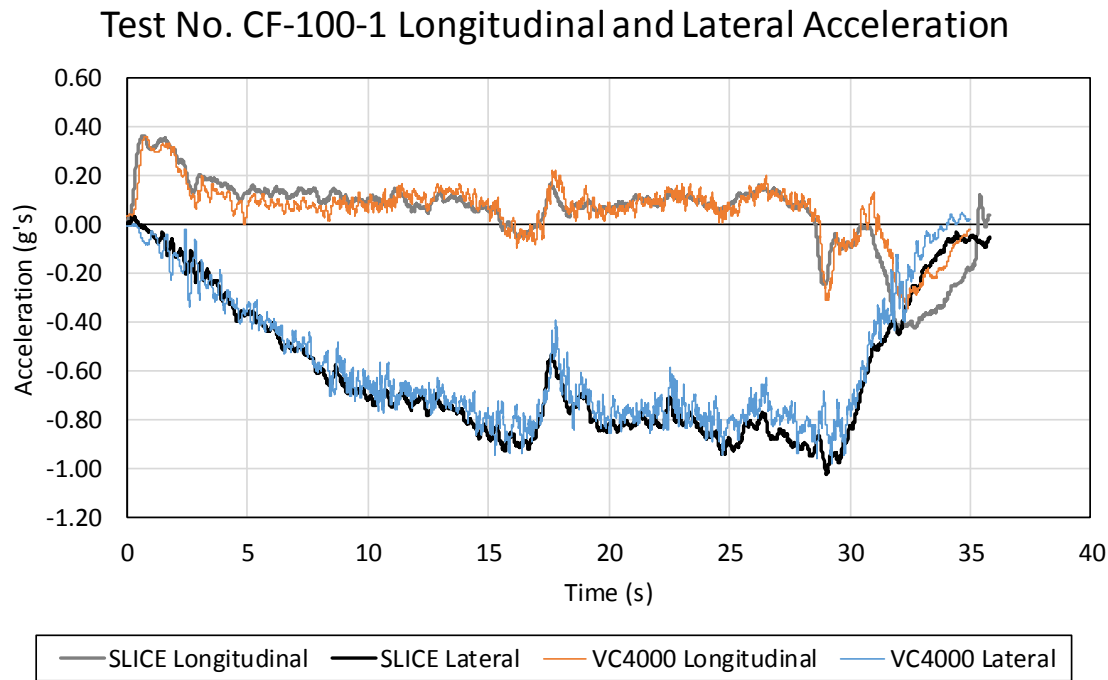


Figure 41. Example Longitudinal and Lateral Acceleration, Test No. CF-100-3

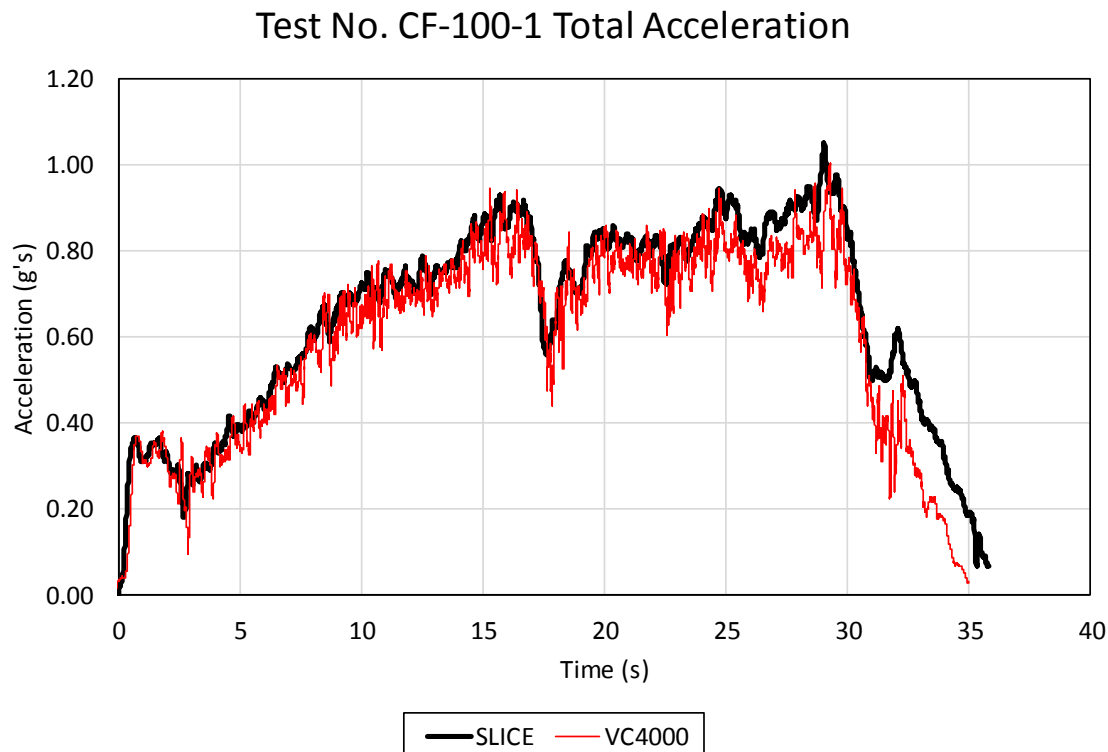


Figure 42. Example Acceleration Magnitude, Test No. CF-100-1

The tests were characterized by an initial longitudinal acceleration similar to the longitudinal (tangent) tests, and a lateral acceleration which increased in magnitude in the negative (i.e., left-hand) direction. The tests were conducted by driving in a left-hand circle so that the driver could accurately monitor his position relative to the interior, target circular path. Note that a right-hand turn would have produced a positive lateral acceleration.

After 15 s, the lateral acceleration neared a peak and the driver slowed the rate of increasing speed due to impending skid. Skidding was characterized by an abrupt transition in the longitudinal acceleration from positive (or near zero) to a negative number. When the vehicle stopped skidding, the lateral acceleration magnitude dropped sharply. The filtered lateral accelerations taken from the SLICE data of the CF-100 and CF-200 tests are shown in Figures 43 and 44, respectively.

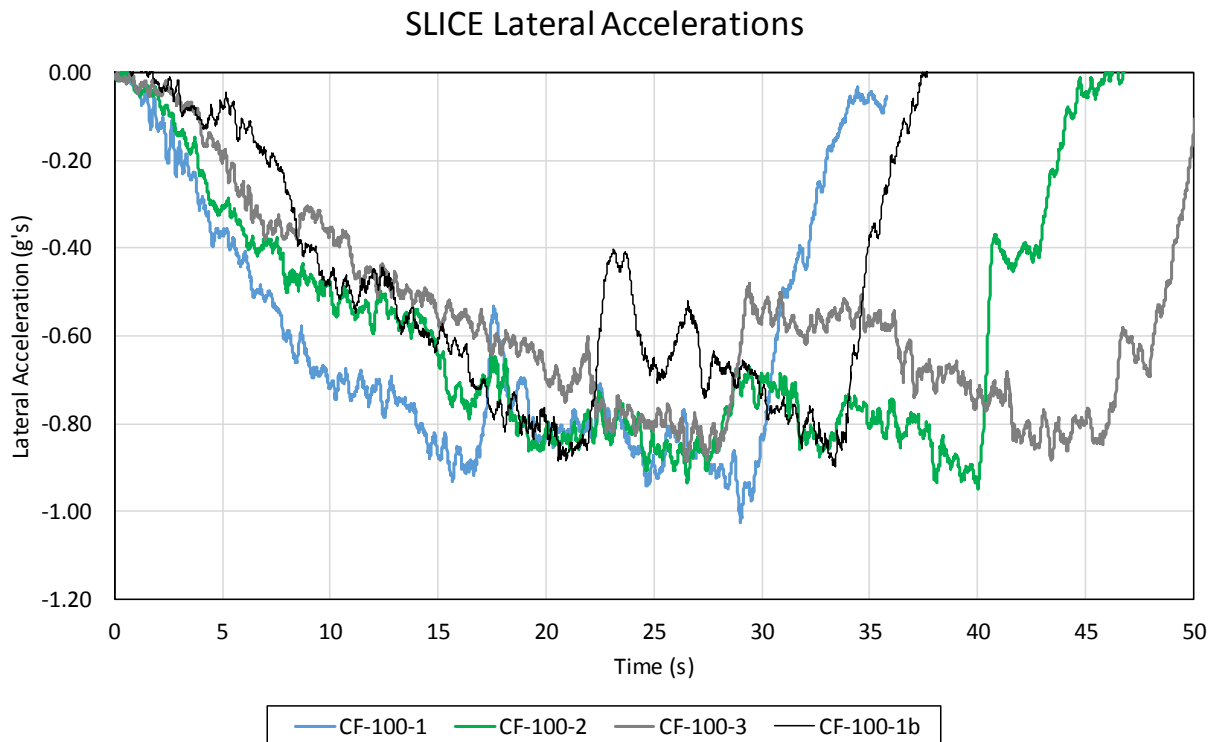


Figure 43. Lateral Accelerations, Test Nos. CF-100-1 through CF-100-3 and CF-100-1b

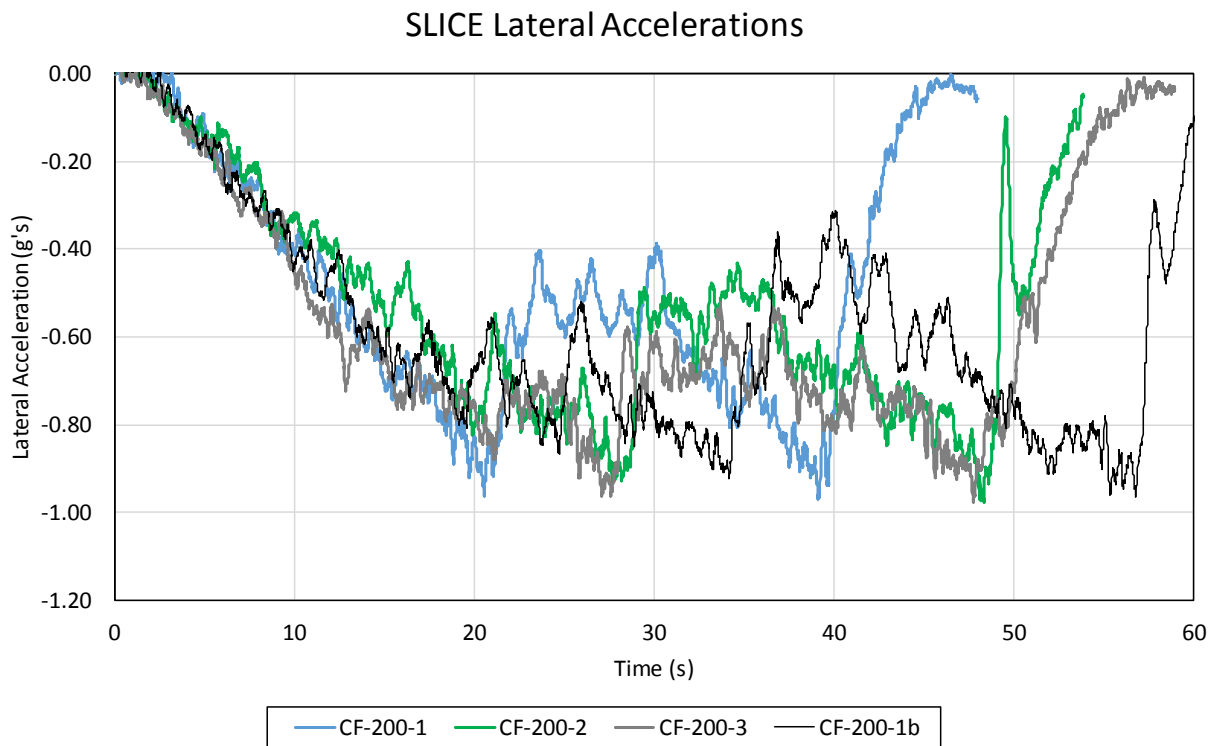


Figure 44. Lateral Accelerations, Test Nos. CF-200-1 through CF-200-3 and CF-200-1b

While it is certainly appealing to select the maximum lateral acceleration as the maximum side friction, the filtered lateral acceleration was noisy and the absolute maximum magnitude cannot be considered equal to the actual available friction. Possible reasons for the noise in the lateral acceleration signal include:

- Although the surface of the tarmac was mostly smooth, it was comprised of concrete slabs measuring 25 ft x 25 ft which were poured over 70 years prior to conducting the tests. Over time the slabs have shifted a little causing minor variations in elevation at the intersection of adjacent slabs. This could have contributed to signal noise.
- Tires are stiff in the longitudinal direction, but are generally more compliant (flexible) in the lateral direction [18-20]. Vibrations in the tire caused by compliance may have also increased noise in the acceleration signals.
- The SLICE accelerometer was bolted to the frame of the vehicle, and the VC4000 was mounted to the windshield. As a result, vibrations in the frame and body of the vehicle, and variations in mounting heights, could add noise to the output signals.
- The SLICE and VC4000 have some intrinsic lateral compliance. As the vehicle completed turns, resonant excitation frequencies in the lateral bending or translation direction could have introduced additional noise into the signal.
- Both SLICE and VC4000 units utilize highly sensitive piezoelectric accelerometers, which may experience external voltage excitation contributing to a noisy signal resulting from broadcast transmissions, magnetic field disruptions, and engine outputs.

The noisy lateral acceleration signal may mask the true maximum lateral (i.e., centripetal) acceleration. Researchers utilized a more fundamental estimate of the maximum side friction based on turn radius and vehicle speed:

$$a_{cent} = \frac{V^2}{R} \quad (12)$$

a_{cent} = centripetal acceleration

V = velocity

R = turn radius

Therefore, researchers investigated the speeds of the test vehicles based on the VC4000 GPS with a 10-Hz update and the vehicle's internally-estimated speed via the OBDII port readout. The precision of the VC4000 GPS was superior to the OBDII readout, because the vehicle could not discern tire slip and thus overestimated speeds at the point of slip. The VC4000 GPS-reported speeds of the vehicle for the CF-100 and CF-200 tests are shown in Figures 45 and 46.

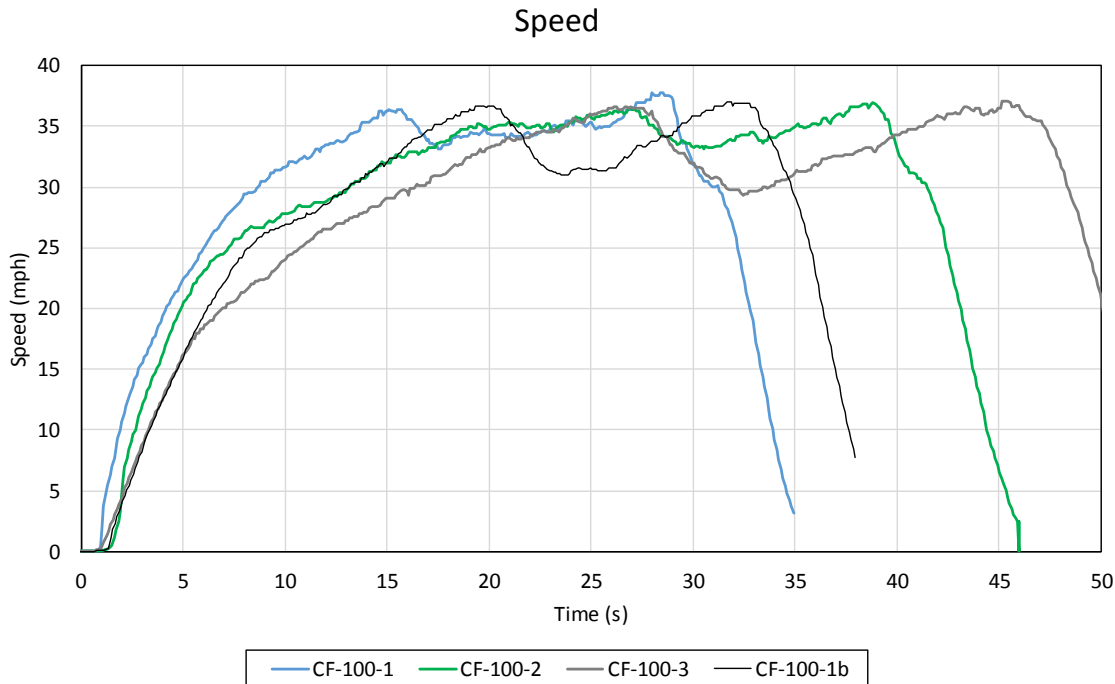


Figure 45. GPS Speed Measurements, Test Nos. CF-100-1 through CF-100-3 and CF-100-1b

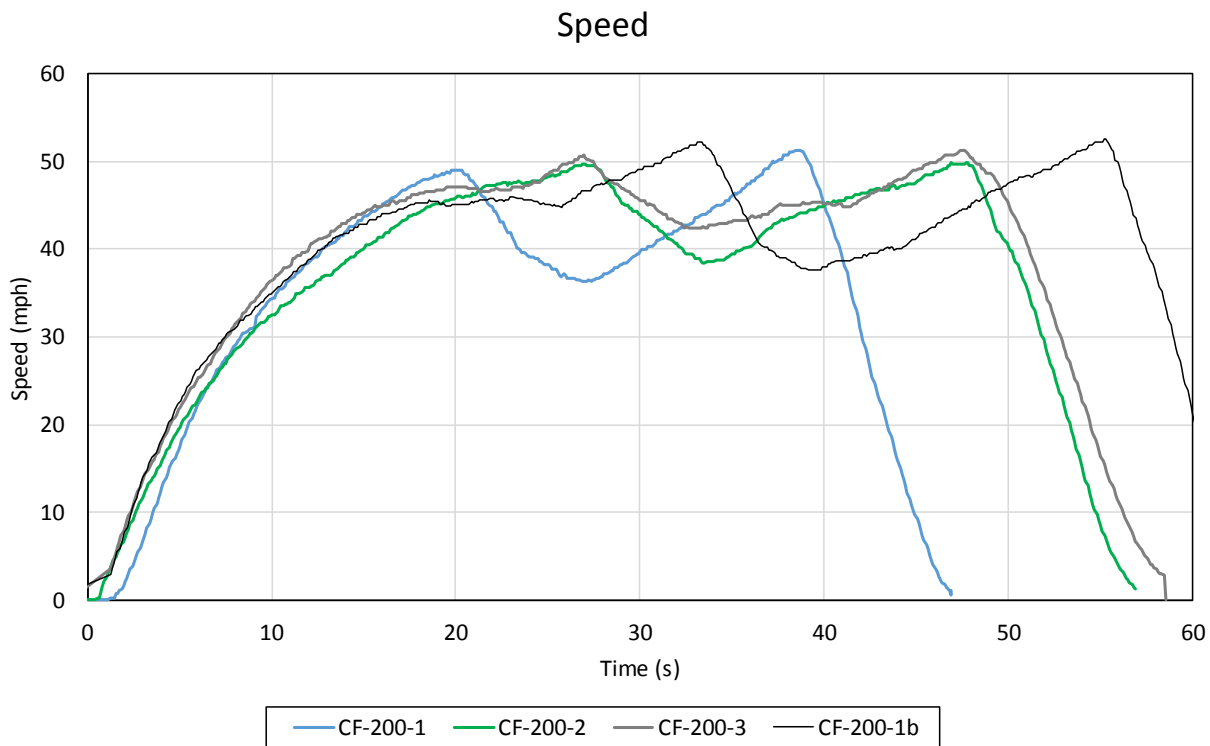


Figure 46. GPS Speed Measurements, Test Nos. CF-200-1 through CF-200-3 and CF-200-1b

The target test radius for the CF-100 tests was 100 ft, and the target test radius for the CF-200 tests was 200 ft. During the tests, guidance cones were placed exactly at the target test radius. Thus, if the vehicle was tracking with the left-side tires at the interior cones, the radius of the center of the turn to the vehicle's CG would be approximately 3 ft larger (i.e., 103 ft for the CF-100 test series and 203 ft for the CF-200 test series). Based on photographic data, the vehicle maintained an offset between 3 and 10 ft from the cones. Therefore, to calculate the range of possible maximum centripetal accelerations used, researchers used radii of 103, 106, 110, and 115 ft for the CF-100 test series, and 203, 206, 210, and 215 ft for the CF-200 test series, respectively, to calculate centripetal accelerations. Furthermore, since the vehicle skidded off of the target turn radius twice, two maximum effective centripetal accelerations were calculated for each test. Maximum test speeds and the maximum centripetal accelerations at the first and second slip conditions are shown in Tables 10 and 11, respectively.

The increased weight in the trunk of the vehicle did not significantly affect the results of test no. CF-100-1b compared to test nos. CF-100-1 through CF-100-3. However, the maximum achievable speed for test no. CF-200-1b was 2.1 mph faster (i.e., 8.3% larger) than the average of test nos. CF-200-1 through CF-200-3. The calculated centripetal accelerations are shown in Figures 47 and 48.

Referring back to the Friction Circle concept, the combination of lateral and longitudinal components of friction should be equal to the total available friction at the time of slip. Therefore, the total friction utilized at the point of slip should be very close to the effective maximum

centripetal acceleration. Example comparisons between the maximum centripetal accelerations and maximum total accelerations are shown in Figures 49 and 50. The total accelerations for the CF-100 and CF-200 test series are shown in Figures 51 through 54.

Table 10. Maximum Test Speeds at 1st and 2nd Slip Conditions

Test Name	Maximum Speed (mph)		
	1 st Slip	2 nd Slip	AVERAGE
CF-100-1	36.4	37.8	37.1
CF-100-2	36.5	36.9	36.7
CF-100-3	36.6	37.1	36.9
CF-100-1b	36.7	37.0	36.9
<i>Average for CF-100 Test Series</i>			36.9 mph
CF-200-1	49.0	51.3	50.2
CF-200-2	49.6	49.8	49.7
CF-200-3	50.7	51.3	51.0
CF-200-1b	52.2	52.6	52.4
<i>Average for CF-200 Test Series</i>			50.8 mph

Table 11. Range of Possible Maximum Centripetal Accelerations Based on Possible Trajectory Radii

Test Name	Maximum Centripetal Acceleration (g's)							
	1 st Slip	2 nd Slip	1 st Slip	2 nd Slip	1 st Slip	2 nd Slip	1 st Slip	2 nd Slip
<i>CF-100 Series</i>	<i>103 ft radius</i>		<i>106 ft radius</i>		<i>110 ft radius</i>		<i>115 ft radius</i>	
CF-100-1	0.861	0.928	0.836	0.901	0.806	0.869	0.771	0.831
CF-100-2	0.862	0.884	0.838	0.859	0.808	0.828	0.772	0.792
CF-100-3	0.872	0.894	0.847	0.869	0.816	0.837	0.781	0.801
CF-100-1b	0.875	0.890	0.850	0.865	0.819	0.833	0.784	0.797
<i>Average</i>	0.883 g's		0.858 g's		0.827 g's		0.791 g's	
<i>CF-200 Series</i>	<i>203 ft radius</i>		<i>206 ft radius</i>		<i>210 ft radius</i>		<i>215 ft radius</i>	
CF-200-1	0.791	0.866	0.780	0.854	0.765	0.838	0.747	0.818
CF-200-2	0.811	0.818	0.800	0.806	0.784	0.790	0.766	0.772
CF-200-3	0.846	0.866	0.834	0.854	0.818	0.837	0.799	0.818
CF-200-1b	0.897	0.911	0.884	0.898	0.867	0.881	0.847	0.860
<i>Average</i>	0.851 g's		0.839 g's		0.823 g's		0.803 g's	

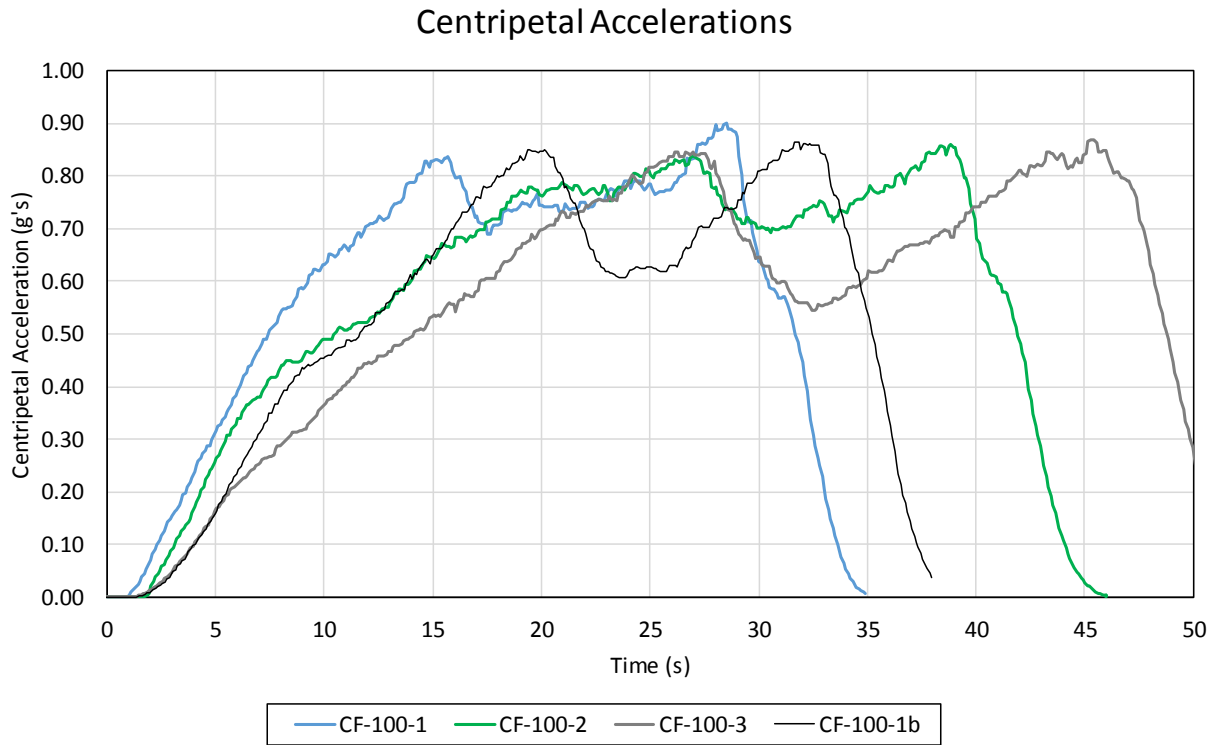


Figure 47. Centripetal Accelerations, Test Nos. CF-100-1 through CF-100-3 and CF-100-1b

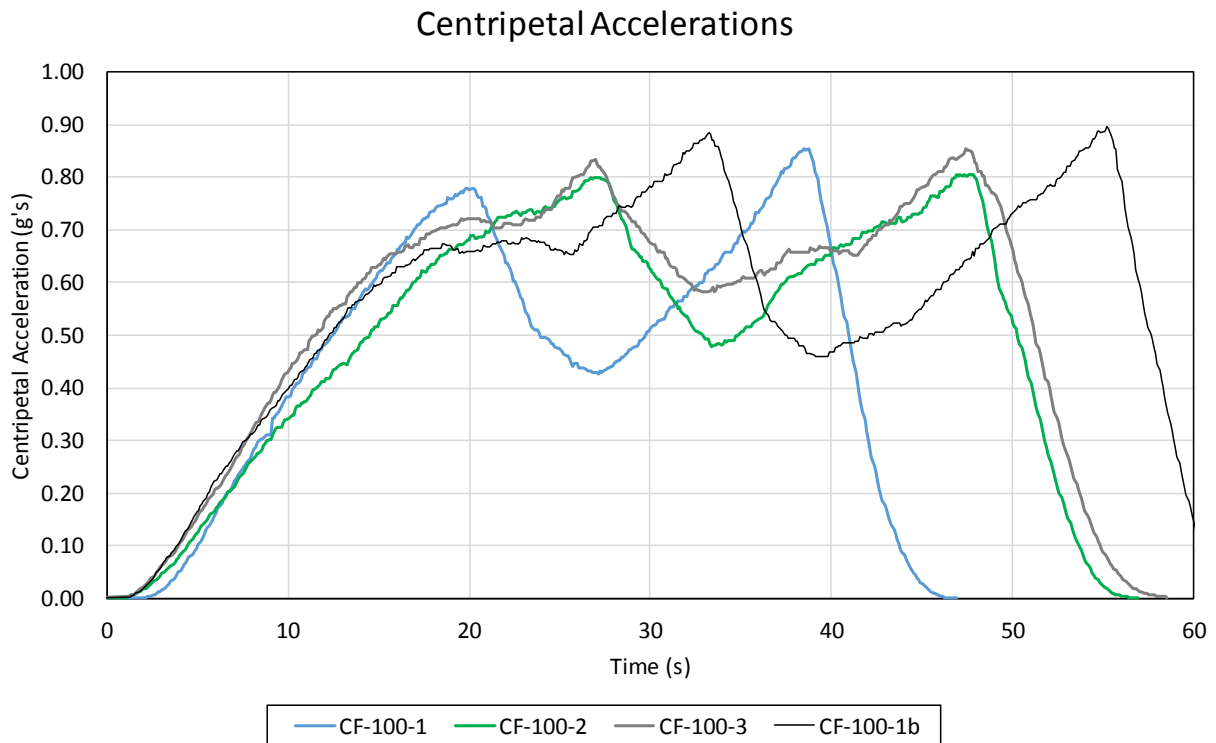


Figure 48. Centripetal Accelerations, Test Nos. CF-200-1 through CF-200-3 and CF-200-1b

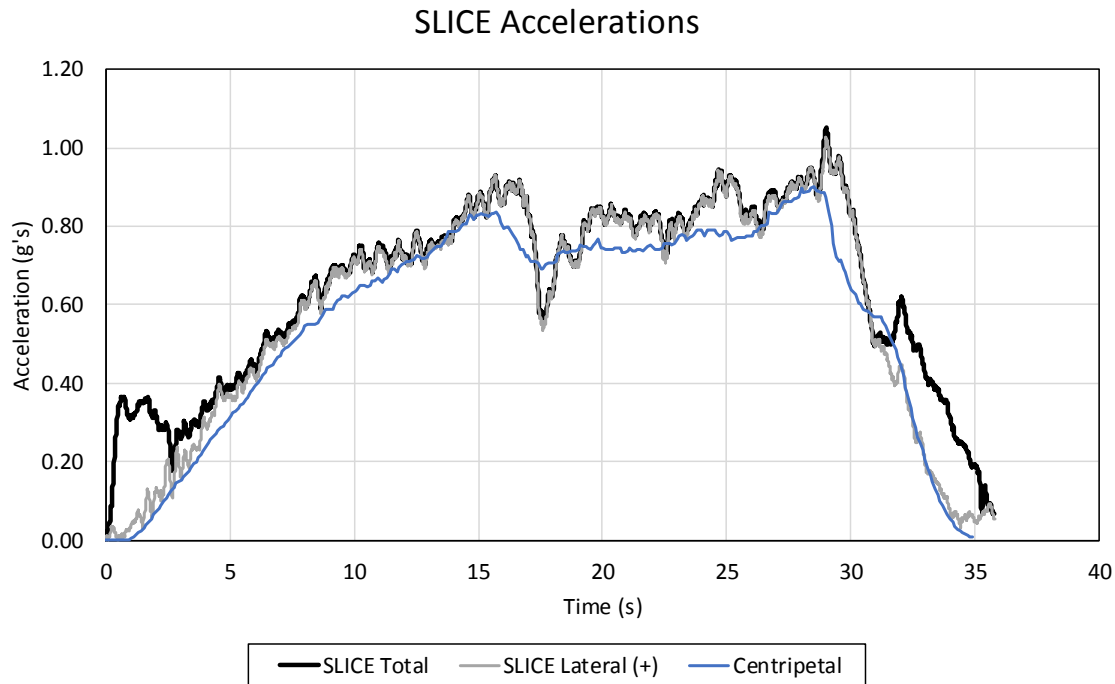


Figure 49. Example Total and Magnitude of Lateral Acceleration (SLICE) and Calculated Centripetal Acceleration, Test No. CF-100-1

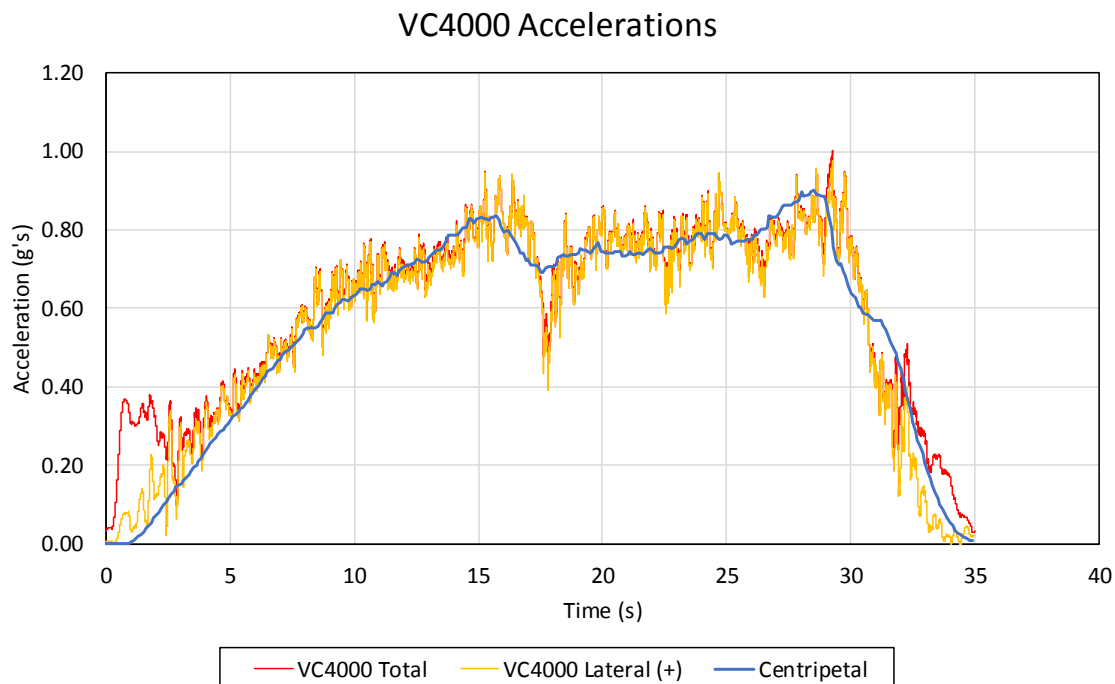


Figure 50. Example Total and Magnitude of Lateral Acceleration (VC4000) and Calculated Centripetal Acceleration, Test No. CF-100-1

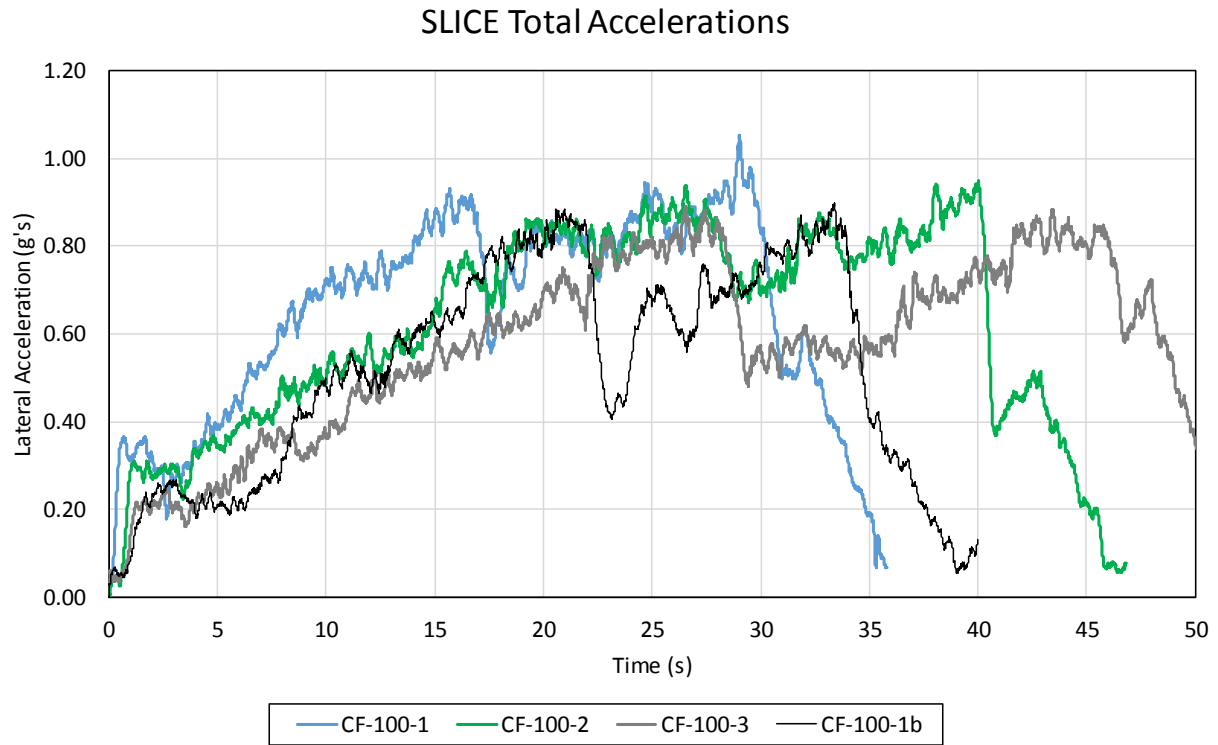


Figure 51. Total Accelerations (SLICE), Test Nos. CF-100-1 through CF-100-3 and CF-100-1b

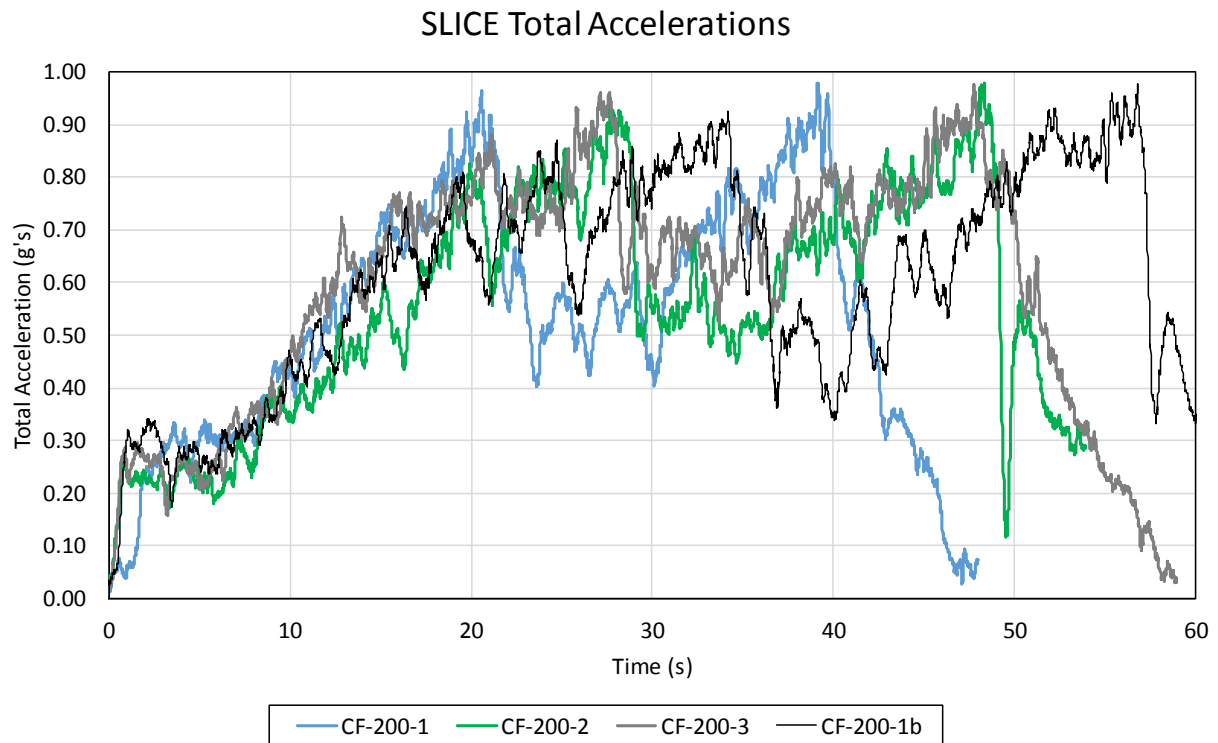


Figure 52. Total Accelerations (SLICE), Test Nos. CF-200-1 through CF-200-3 and CF-200-1b

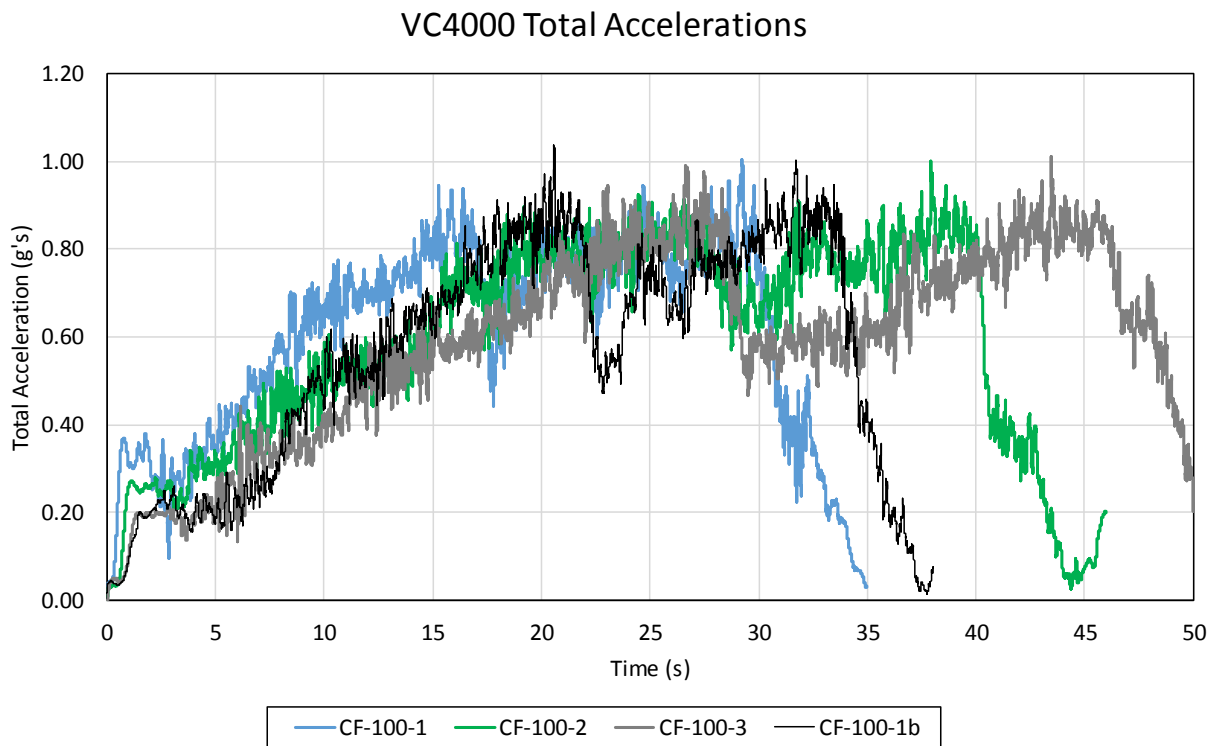


Figure 53. Total Accelerations (VC4000), Test Nos. CF-100-1 through CF-100-3 and CF-100-1b

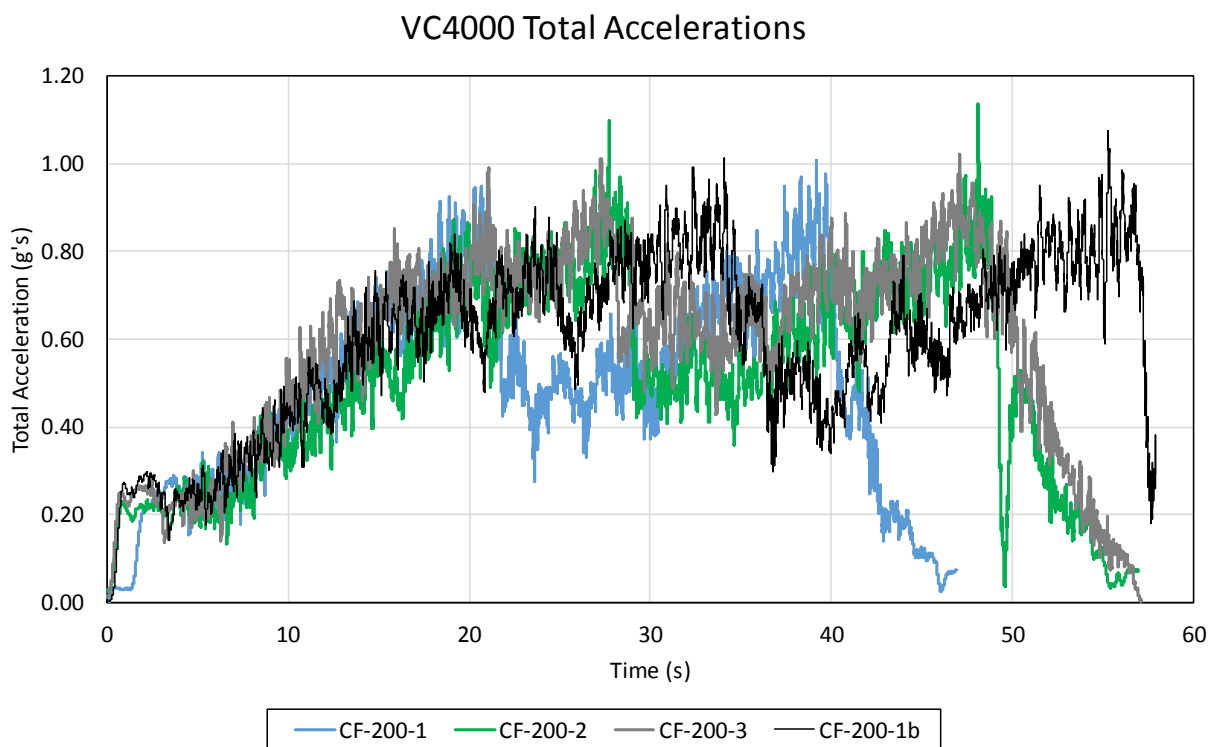


Figure 54. Total Accelerations (VC4000), Test Nos. CF-200-1 through CF-200-3 and CF-200-1b

Based on the test results, a conservative value of the maximum side friction would be approximately 0.90, corresponding to the maximum value of side friction obtained from the centripetal acceleration in all tests. The objective of the skid tests was to determine the maximum speed and radius combinations at which the threat vehicle could travel. Because the threat vehicle could reach, but not exceed, a centripetal acceleration of 0.90, it is reasonable to assume that no threat vehicle will exceed this value during real driving conditions.

5.3.2 Locked Wheel Skid Trailer (NDOR)

The skid trailer was also pulled through the test areas for the CF-100 and CF-200 driving tests, similar to what was done for the longitudinal test area. Due to the limited amount of space available to measure the friction and the inability of the skid trailer to navigate the curve while accurately recording the friction, fewer friction measurements were taken from both of the circular friction test areas. Test results are shown in Table 12.

Table 12. Locked Wheel Skid Trailer Friction Measurements in CF-100 and CF-200 Test Areas

Measurement	Test Area	Average SN	Average μ
1	CF-100	88.9	0.889
2	CF-100	85.4	0.854
3	CF-200	89.9	0.899
4	CF-200	90.0	0.900

Note that only the smooth tire was used for this test configuration. The effective frictions were lower for the circular test area than for the longitudinal test area, but the distance over which the tire could be locked and the location conducive to measure the test were much shorter than for the longitudinal test area. The average locked-wheel friction measurement was 0.886, which was approximately 0.05 lower than for the longitudinal area.

5.3.3 Drag Sled (LSO)

Drag sled results are shown in Tables 13 and 14. The drag sled was pulled in the location of the circular test area after the conclusion of the tests. Unfortunately, measurement error was introduced during drag sled measurement in the CF100 and CF200 test areas, as the drag sled was pulled with an inclined angle. By inclining the angle of the drag sled, some of the pull force acted to reduce the weight and thus effective normal force acting on the drag sled; thus the resistance force acting on the pull spring was reduced as well. Nonetheless, drag sled skidding friction results were lower than those observed in the longitudinal friction test area by approximately 0.10.

Table 13. Drag Sled Pull Force Results, CF-100 Test Area

100-ft Radius		
Measurement No.	Pull Force (lbf)	Effective Friction Coefficient
1	12	0.71
2	12	0.71
3	11.5	0.68
4	12.5	0.74
5	12.5	0.74
Average		0.72

Table 14. Drag Sled Pull Force Results, CF-200 Test Area

200-ft Radius		
Measurement No.	Pull Force (lbf)	Effective Friction Coefficient
1	11	0.65
2	12	0.71
3	12	0.71
4	13	0.76
5	13	0.76
Average		0.72

5.4 Comparison with Threat Calculator

The USACE Threat Calculator uses a default friction coefficient of 0.75 for centripetal acceleration. Using the relationship for maximum speed and centripetal acceleration, the corresponding Threat Calculator maximum speeds on the 100-ft and 200-ft radii are 33.5 and 47.4 mph, respectively.

However, it was known that during the test, the vehicle could not maintain the interior radius of the curve (without impacting the cones) and drifted as far as 15 ft away from the target radius. For 106-ft and 206-ft radii, the maximum speeds for the Threat Calculator vehicle would be 34.5 mph and 48.1 mph, respectively.

Comparisons between the test results and the Threat Calculator limits are shown in Figures 55 through 60. The lateral accelerations were observed to be as large as 0.95 g's (before slipping), which is 0.20 g's or 27% higher than the Threat Calculator limits, as shown in Figures 55 and 56. Likewise, when centripetal accelerations were calculated based on speeds, the maximum centripetal accelerations were up to 0.15 g's or 20% higher than the Threat Calculator results as well, as shown in Figures 57 and 58. All of the maximum speeds at the slip points for the nominal 100-ft and 200-ft tests were larger than the Threat Calculator maximum speeds, as shown in Figures 59 and 60.

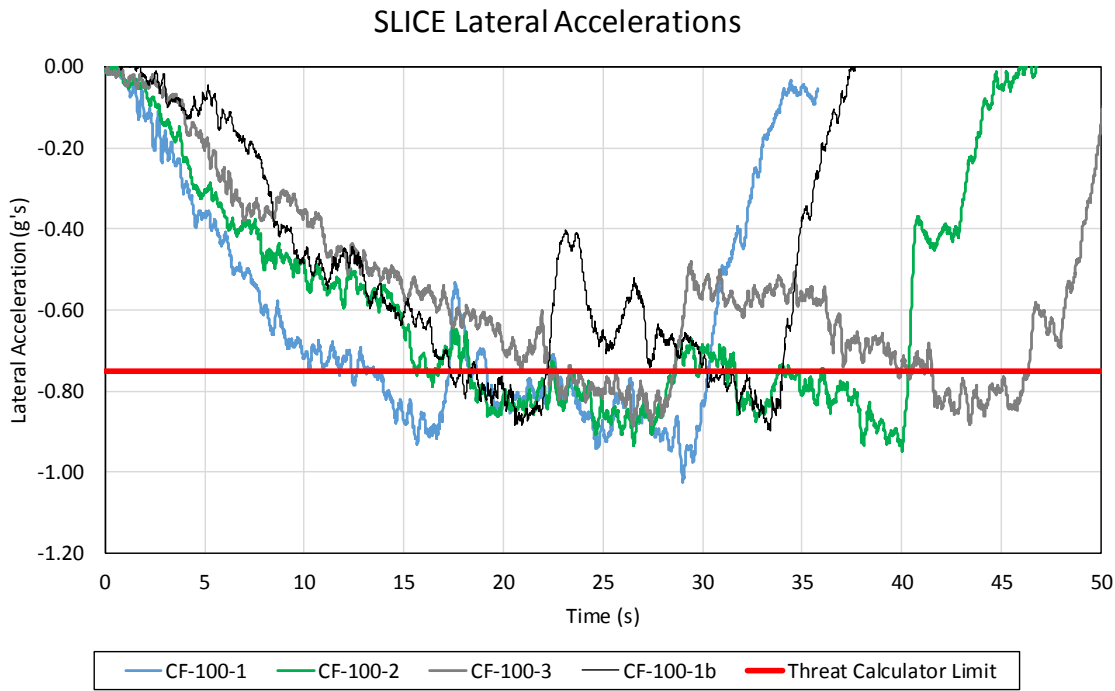


Figure 55. Comparison of Test Lateral Accelerations and USACE Threat Calculator Limits for a 106-ft Average Radius

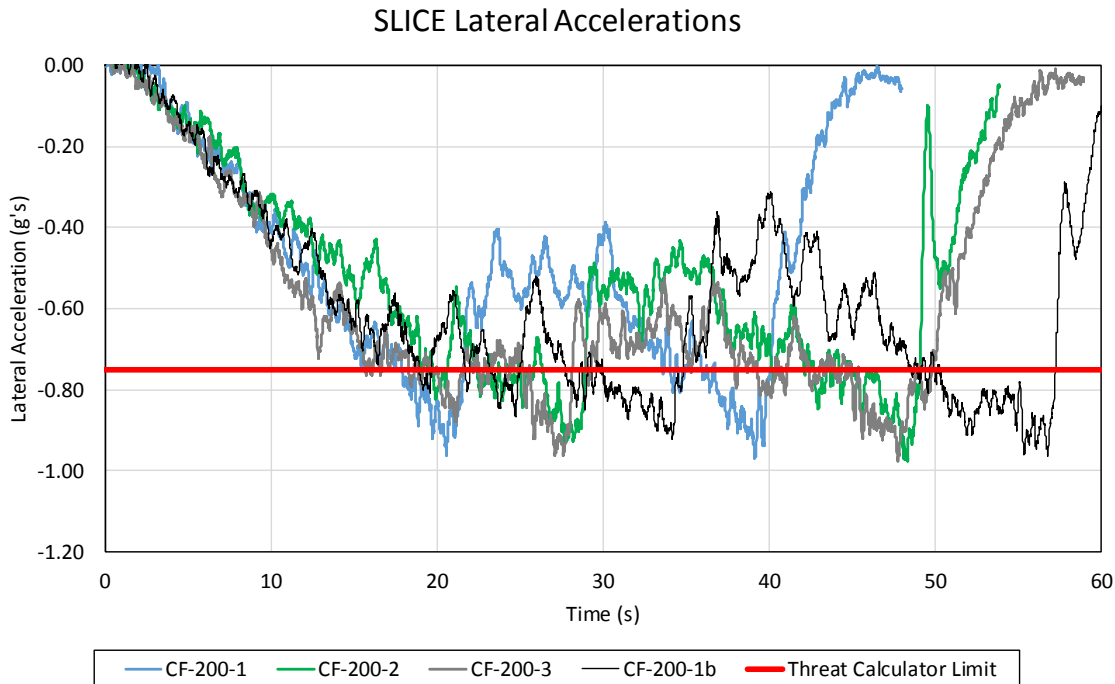


Figure 56. Comparison of Test Lateral Accelerations and USACE Threat Calculator Limits for a 208-ft Average Radius

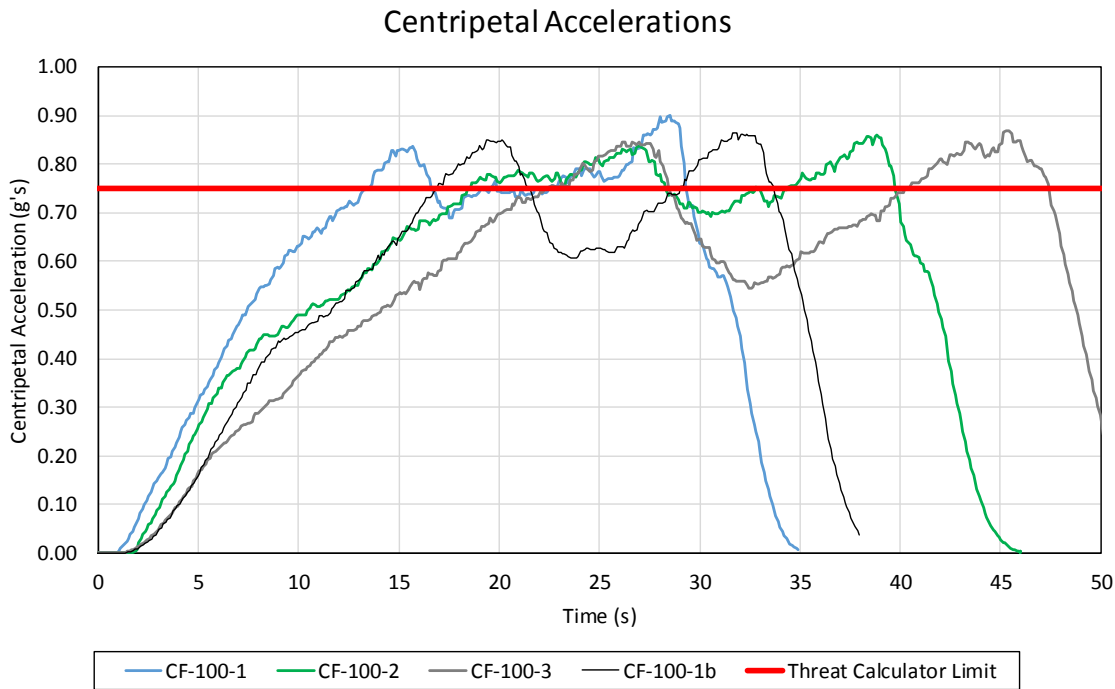


Figure 57. Centripetal Acceleration Comparison with USACE Threat Calculator Limit for 106-ft Average Radius

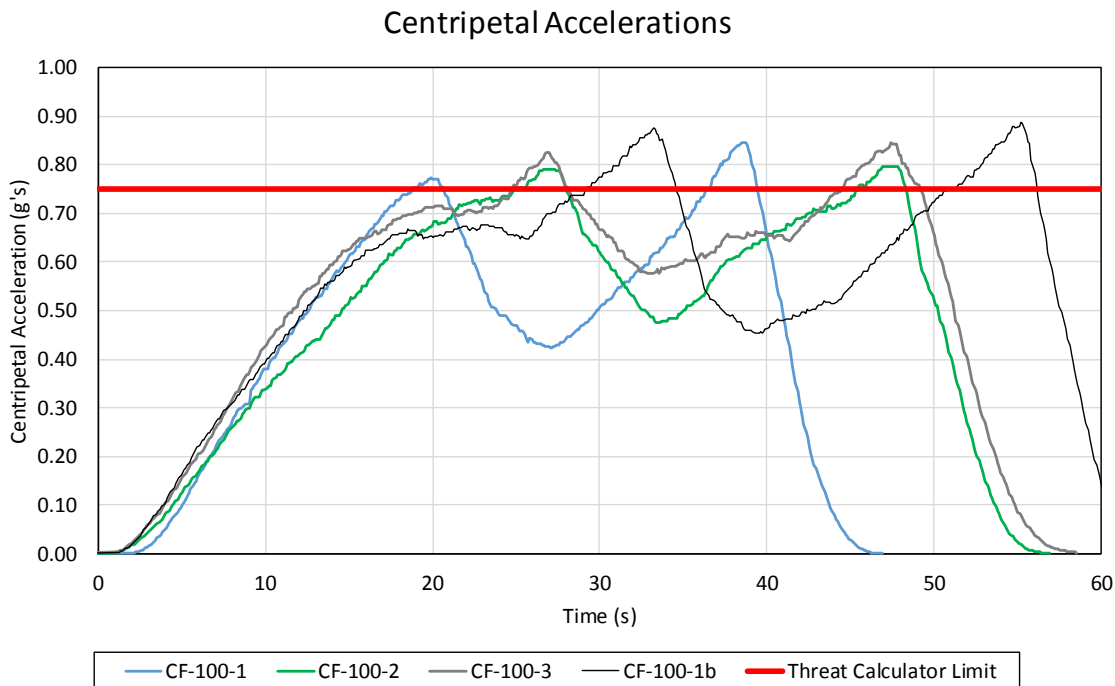


Figure 58. Centripetal Acceleration Comparison with USACE Threat Calculator Limit for 208-ft Average Radius

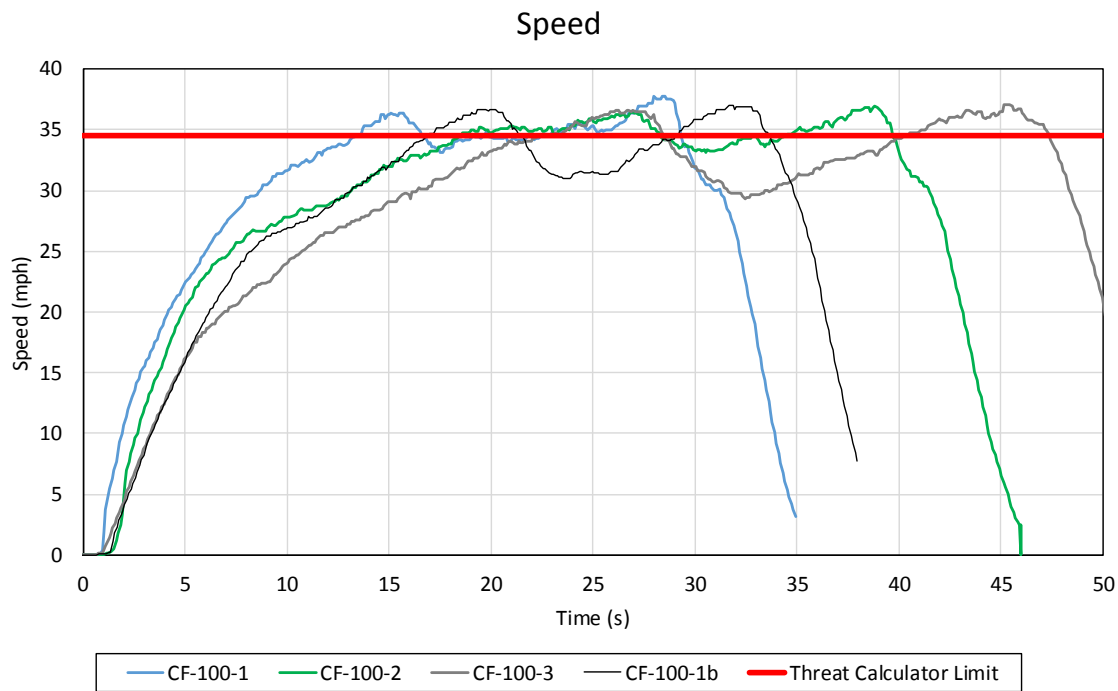


Figure 59. Speed Comparison with USACE Threat Calculator for 106-ft Average Radius

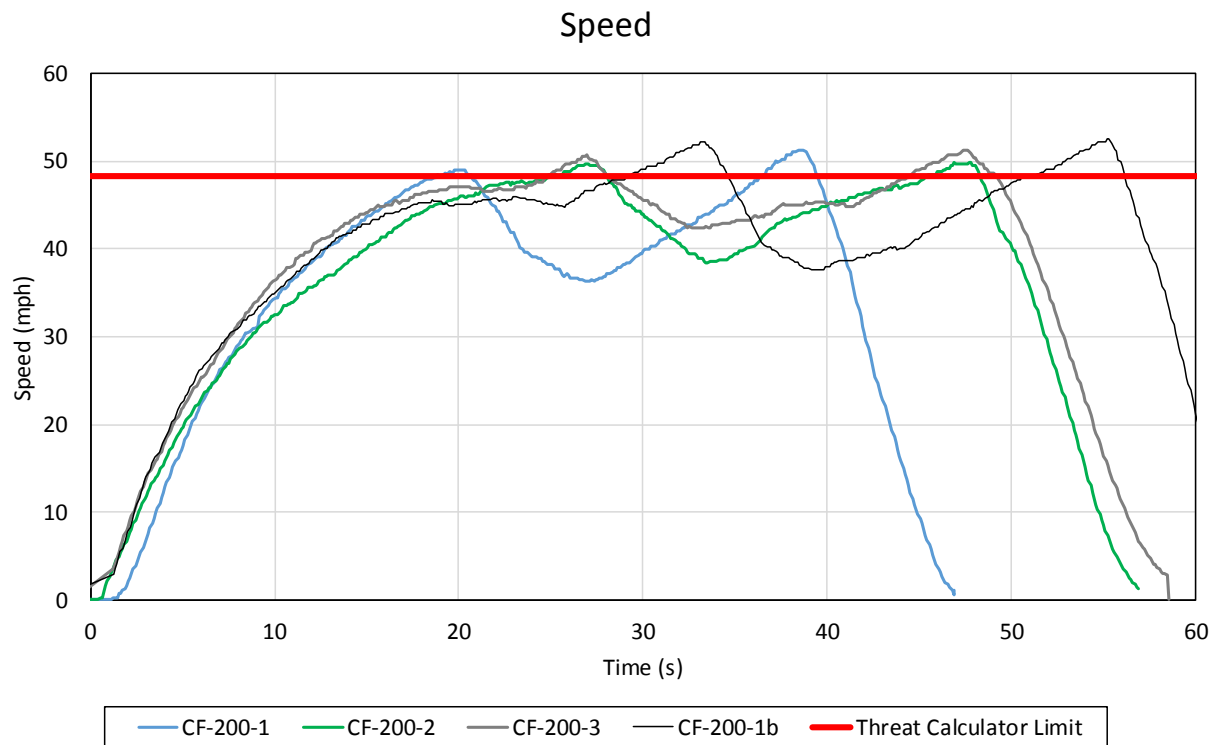


Figure 60. Speed Comparison with USACE Threat Calculator for 208-ft Average Radius

Based on test results, the recommended centripetal acceleration limit (and therefore side friction) for use in the Calculator was 0.90 g's. Using this limit, the maximum Threat Calculator estimated turning speeds for 106-ft and 206-ft radii were 36.9 and 52.7 mph, respectively, which closely match test data, as shown in Figures 59 and 60 and Tables 10 and 11.

5.5 Discussion

Results of the locked wheel trailer and drag sled friction tests suggested that the tire-pavement friction coefficient was lower in the circular test area than for the longitudinal test area. Both the drag sled and skid trailer may have underestimated the available friction in the circular test area due to measurement procedure difficulties, but nonetheless suggest that there was some spatial variability of the useable friction coefficient in the test area.

The centripetal acceleration calculation was most meaningful and stable methods of measuring the side friction. Lateral accelerations were noisy and choosing the absolute maximum lateral friction was misleading due to vibrations. Researchers recommend a maximum side friction estimate of 0.90, corresponding to a maximum centripetal acceleration of 0.90 g's, for analysis with the Threat Calculator.

Researchers recommend a maximum centripetal (side) friction coefficient of 0.90.

It should also be noted that the current version of the Threat Calculator uses one friction value to represent the acceleration limits of the threat vehicle in tangent and circular conditions, and that the threat vehicle always follows MTCAS⁹ philosophy. Real side friction coefficients will always be less than the total possible longitudinal coefficients of friction. Nonetheless, it is likely very conservative to use the same value in the longitudinal and lateral directions of 1.0 g's for Threat Calculator estimates. Further testing will be conducted in the second portion of this research study to evaluate how conservative these values are during representative threat driving conditions.

⁹ MTCAS: Maximum Threat Calculator Acceleration and Speed

6 SUMMARY, CONCLUSIONS, AND RECOMMENDATIONS

The objective of this study was to identify the factors affecting tire-pavement friction capabilities, conduct tests to determine the maximum frictional coefficient for the Ford Crown Victoria threat vehicle, and to recommend values for use in the USACE Threat Calculator program. This was accomplished by performing a literature review and interviewing experts with experience in measuring friction coefficients, identifying practical test conditions for maximizing the tire-pavement friction coefficient, and conducting tests to identify the longitudinal and lateral coefficients of friction.

Five longitudinal acceleration and braking tests were conducted: test nos. LF-1 through LF-4 and LF-1b. The accelerations during speeding up and braking were recorded and analyzed. It was observed that the vehicle was power-limited and that the acceleration curves closely resembled an inverse curve for speeds above 15 mph. In contrast, braking friction was less variable with speed, although higher friction values were obtained for lower travel speeds. If a single, conservative coefficient of friction is desired, using the friction coefficient for the lowest travel speeds, of 1.0 would be reasonable.

Eight circular curve tests were also conducted to determine the maximum available side friction. Although the linear straight-line skidding coefficients of friction were lower in the circular test area by between 5 and 10 percent, the vehicle still managed to achieve frictional coefficients during sliding which were comparable to the longitudinal braking coefficients. In addition, the maximum side friction coefficient was 0.90 for 100-ft and 200-ft radius curves.

The next step in the research process is to construct target test geometries, which are similar to the inputs of the Threat Calculator and evaluate estimated and actual travel times and vehicle speeds throughout the test areas. Target speeds and test geometries should be based on the braking and side friction coefficients observed in this study. With a comparison of realistic driving conditions and Threat Calculator procedures, researchers should be able to identify if the current and proposed values of friction coefficients for the Threat Calculator are conservative or require additional consideration.

7 REFERENCES

1. *Army Access Control Points Standard Design/Criteria*, U.S. Army Corps of Engineers (USACE) Protective Design Center, Omaha, Nebraska, 2009.
2. Nielsen, J., and Coughlin, T., *9 Seconds to Act: Design and Location of Active Vehicle Barriers*, Air Force Civil Engineer Volume 21 No. 3, 2013.
3. American Association of State Highway and Transportation Officials. *A Policy on Geometric Design of Highways and Streets*. Washington: AASHTO, 2011. Print.
4. *Standard No. 105; Hydraulic and electric brake systems*. Federal Motor Vehicle Safety Standard (FMVSS) No. 571.105, October 1, 2011.
5. *Standard No. 122; Motorcycle brake systems*. Federal Motor Vehicle Safety Standards (FMVSS) No. 571.122, October 1, 2011.
6. Stonex, K.A., and C.M. Noble. "Curve Design and Tests on the Pennsylvania Turnpike," *Proceedings HRB*, Vol. 20, Highway Research Board, 1940: 429-451.
7. Barnett, J. "Safe Side Friction Factors and Superelevation Design," *Proceedings HRB*, Vol.16, Highway Research Board, 1936: 69-80.
8. Henry J. J. (2000) "Evaluation of Pavement Friction Characteristics, a Synthesis of Highway Practice." NCHRP Synthesis 291, pp. 7.
9. Hall, J.W., Smith, K.L., Titus-Glover, L., Wambold, J.C., and Rado, Z., *Guide for Pavement Friction*, NCHRP Web-Only Report No. 108, Final Report to the National Cooperative Highway Research Program, February 2009.
10. Flintsch, G.W., McGhee, K.K., Izeppi, E.L., and Najafi, S., *The Little Book of Tire Pavement Friction*, Summary Report of the Pavement Surface Properties Consortium, September 2012.
11. Fricke, L.B., and Baker, J.S., "Drag Factor and Coefficient of Friction in Traffic Accident Reconstruction," Traffic Accident Investigation Manual, Chapter Topic 862. Northwestern University Traffic Institute.
12. *2015 Drag Factor Table*, Vericom Computers, Inc., Rogers, Minnesota, November 2015.
13. Sandberg, U., *Influence of Road Surface Texture on Traffic Characteristics Related to Environment, Economy and Safety*, Final Report to the Swedish National Road Administration, Swedish National Road and Transport Institute, October 1998.
14. Fuentes, L., Gunaratne, M., and Hess, D., "Evaluation of the Effect of Pavement Roughness on Skid Resistance", *Journal of Transportation Engineering*, Volume 136, July 2010, pp. 640-653.

15. *The Physics of Tire Traction: Theory and Experiment*, SAE, Warrendale, PA 2002; Ed Hays, D.F., and Browne, A.L., Symposium at the General Motors Research Laboratories, Warren, Michigan, 1974.
16. Walter, J.D., *Tire Construction and Materials Lecture*, University of Akron, Online Symposium and Seminar Series, Virginia Tech University, June 8-22, 2015.
17. Taheri, S., McIntyre, J., and Kennedy, R., *Tire and Vehicle Dynamics*, Online Symposium and Seminar Series, Virginia Tech University, June 8-22, 2015.
18. Pacejka, H.B., *Tire and Vehicle Dynamics*, Society of Automotive Engineers, Butterworth Heineman, Woburn, Massachusetts, 2002.
19. Gillespie, T.D., *Fundamentals of Vehicle Dynamics*, Society of Automotive Engineers, Inc., Warrendale, PA, 1992.
20. Wong, J.Y., *Theory of Ground Vehicles*, 3rd Ed., Wiley Interscience, New York, 2001.
21. Skorupka, Z., “ABS System Use Impact on Brake Torque in Aviation Brake”, *Journal of KONES Powertrain and Transport*, Volume 21 No. 1, December 2014, pp. 259-265.
22. “Oversteer and Understeer”, Drifting Street, 2015. <http://www.driftingstreet.com/oversteer-understeer-physics.html>
23. “The Effective Amount of Oxygen at Different Altitudes”, Higher Peak Altitude Training, 2015. <http://www.higherpeak.com/altitudechart.html>
24. *Accident Reconstruction, 2010*, Society of Automotive Engineers, Document No. SP-2267, Warrendale, Pennsylvania, April 2010.
25. Rilett, L.R., Stolle, C.S., Faller, R.K., and Reid, J.D., *Threat Delay Calculator Assumptions*, Technical Memo to the U.S. Army Corps of Engineers, Protective Design Center, Nebraska Transportation Center and Midwest Roadside Safety Facility, February 10, 2015.
26. MacInnis, D., Cliff, W., and Ising, K., *A Comparison of the Moment of Inertia Estimation Techniques for Vehicle Dynamics Simulation*, SAE Technical Paper Series – 970951, Society of Automotive Engineers, Inc., Warrendale, Pennsylvania, 1997.
27. Expert Autostats, 4N6XPRT Systems, La Mesa, California, 2012.
28. ASTM E274/E274M-15 *Standard Test Method for Skid Resistance of Paved Surfaces Using a Full-Scale Tire*, ASTM International, West Conshohocken, PA, 2015, http://dx.doi.org/10.1520/E0274_E0274M-15. Accessed May 9, 2016.
29. *SLICE User’s Manual*, DTS, 2011, pp. 6-16.
30. VC4000DAQ Performance and Braking Test Computer Owner’s Manual. Vericom, 2015, pp. 39-47.

31. Society of Automotive Engineers (SAE), *Instrumentation for Impact Test – Part 1 – Electronic Instrumentation*, SAE J211/1 MAR95, New York City, NY, July, 2007.
32. Ruth, R., Bartlett, W., and Daily, J., “Accuracy of Event Data in the 2010 and 2011 Toyota Camry During Steady State and Braking Conditions”, *SAE International Journal of Passenger Cars – Electronics and Electrical Systems*, Version 5 Issue 1, 2012, pp. 358-372.
33. Winkelbauer, B., Stolle, C.S., Faller, R.K., Lechtenberg, K.A., Reid, J.D., and Bielenberg, R.W., *Cable Guardrail with Strong J-Bolts*, Final Report to the New York State Department of Transportation (NYSDOT), MwRSF Research Report No. TRP-03-299-14, Midwest Roadside Safety Facility, University of Nebraska-Lincoln, Lincoln, Nebraska, May 2014.

For additional friction safety references:

34. Morral, J. F., Talarico, R. J., “Side Friction Demanded and Margin of Safety on Horizontal Curves,” *Journal of the Transportation Research Board*, 1994, pp. 145-152.
35. Henry J. J. (2000) “Evaluation of Pavement Friction Characteristics, a Synthesis of Highway Practice.” *NCHRP Synthesis 291*, 7p.

8 APPENDICES

Appendix A. Test Results – Test No. LF-1

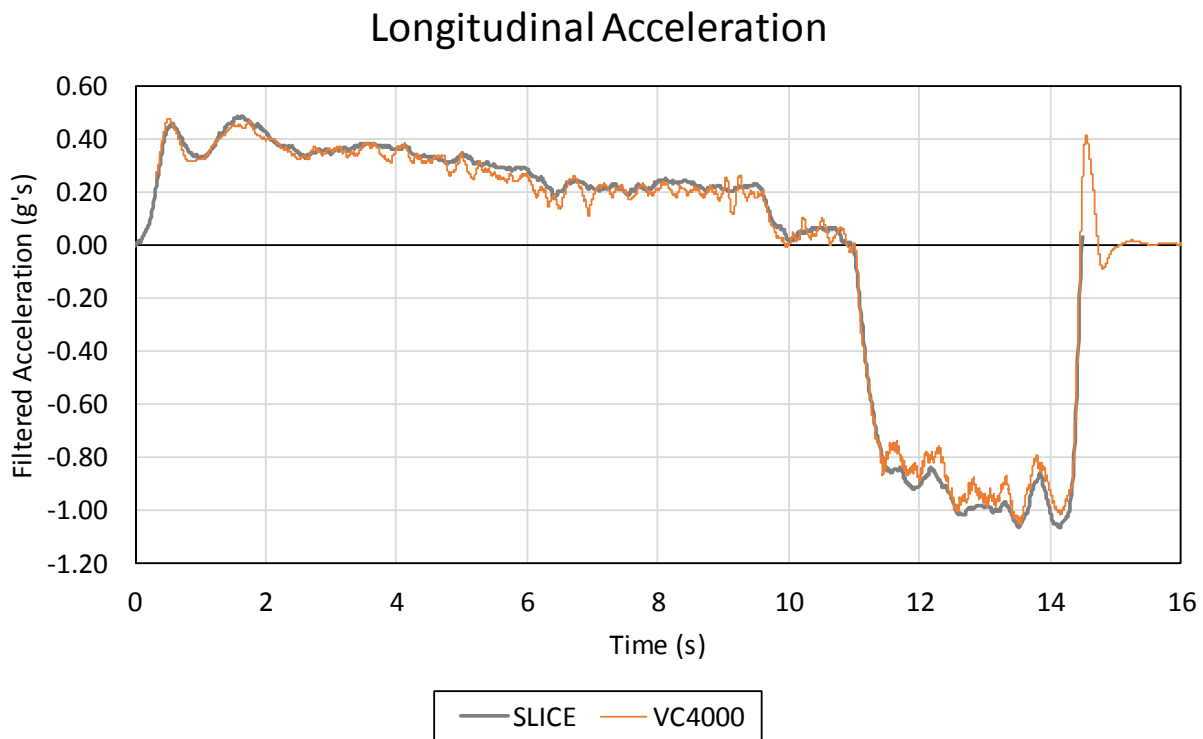


Figure A-1. Longitudinal Acceleration, Test No. LF-1

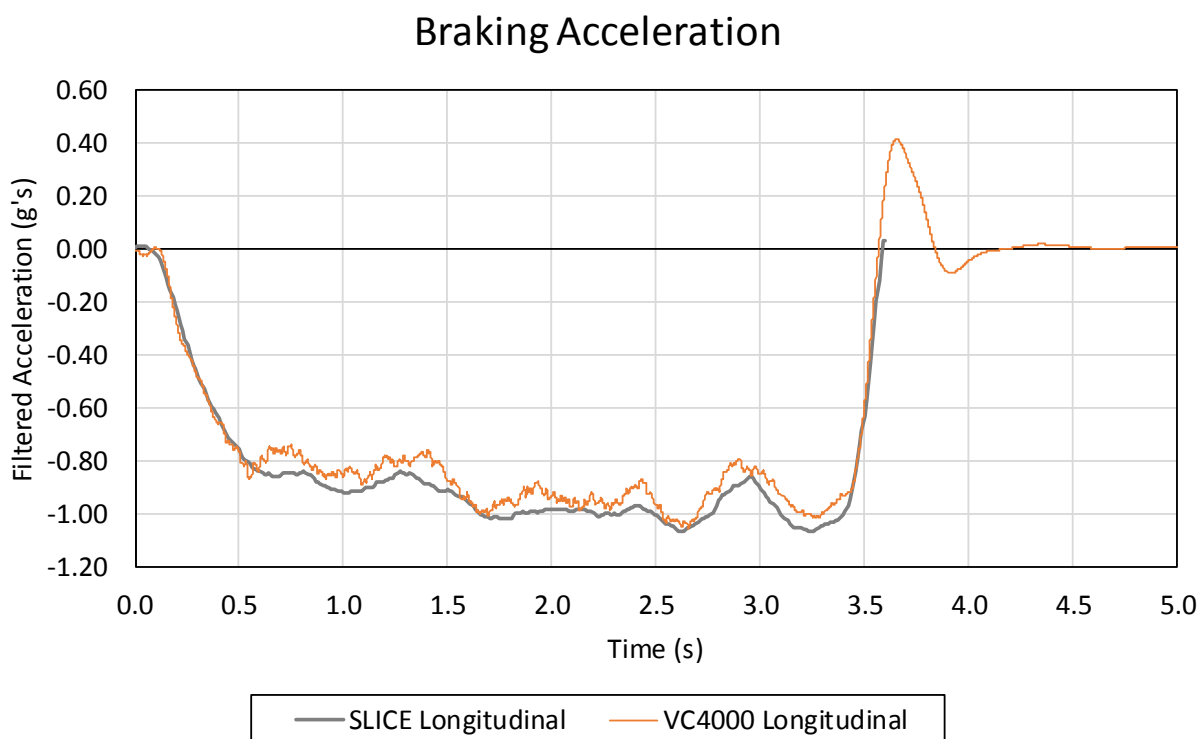


Figure A-2. Braking Acceleration, Test No. LF-1

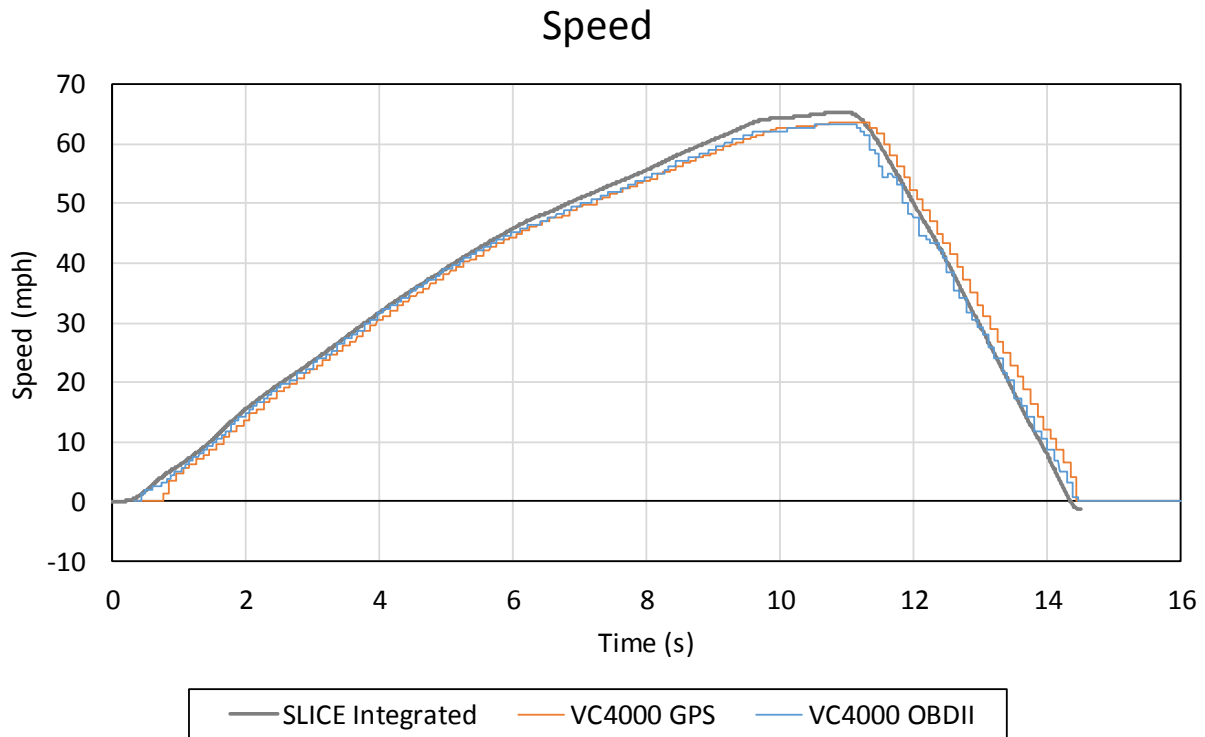


Figure A-3. Vehicle Speed, Test No. LF-1

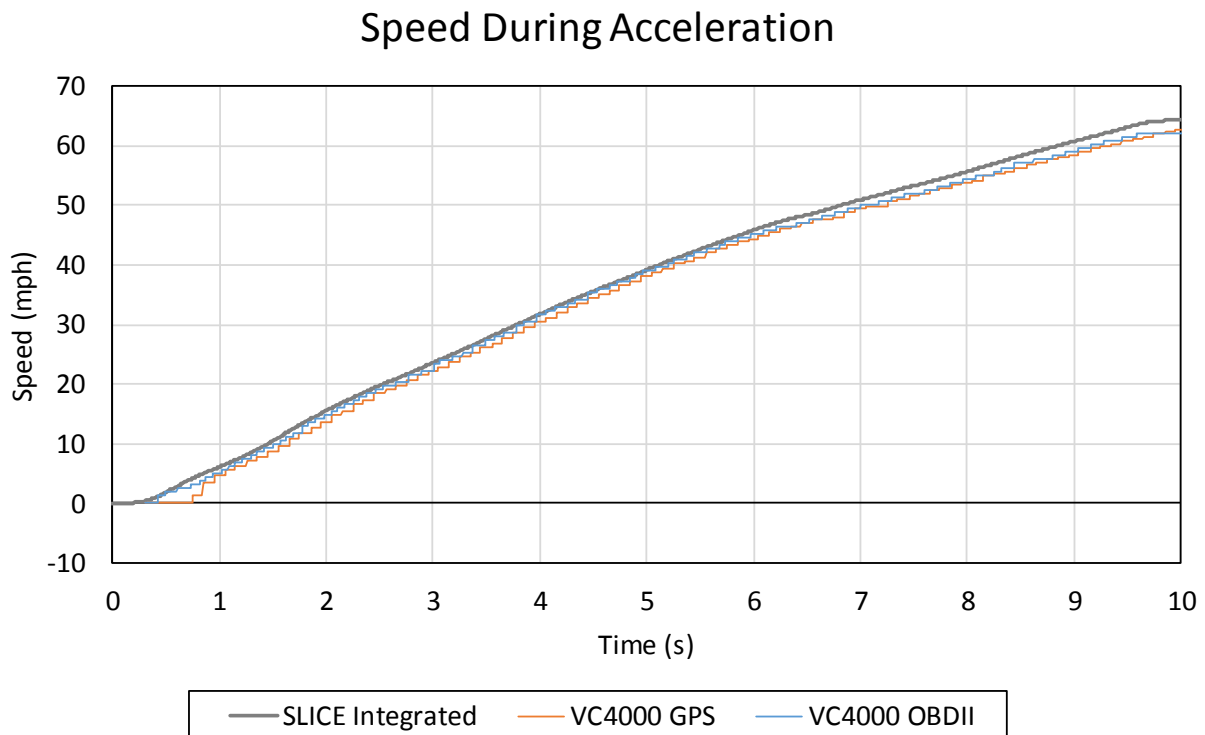


Figure A-4. Speed During Acceleration, Test No. LF-1

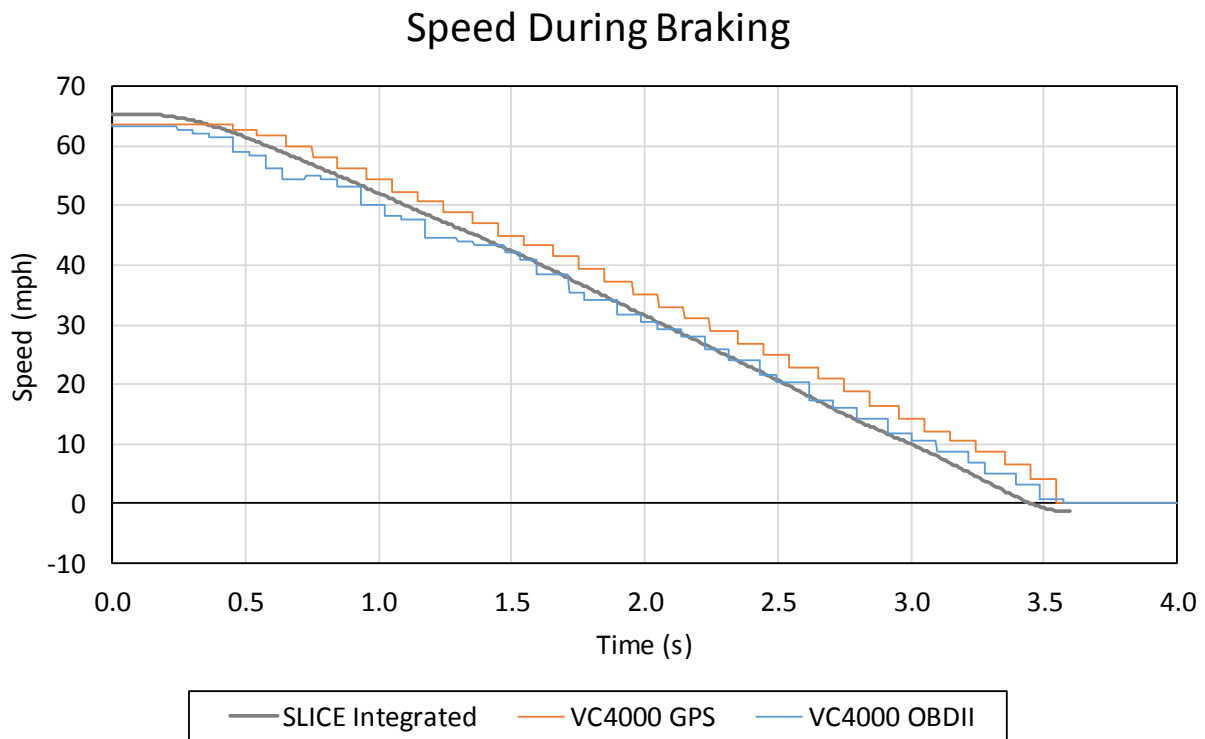


Figure A-5. Speed During Braking, Test No. LF-1

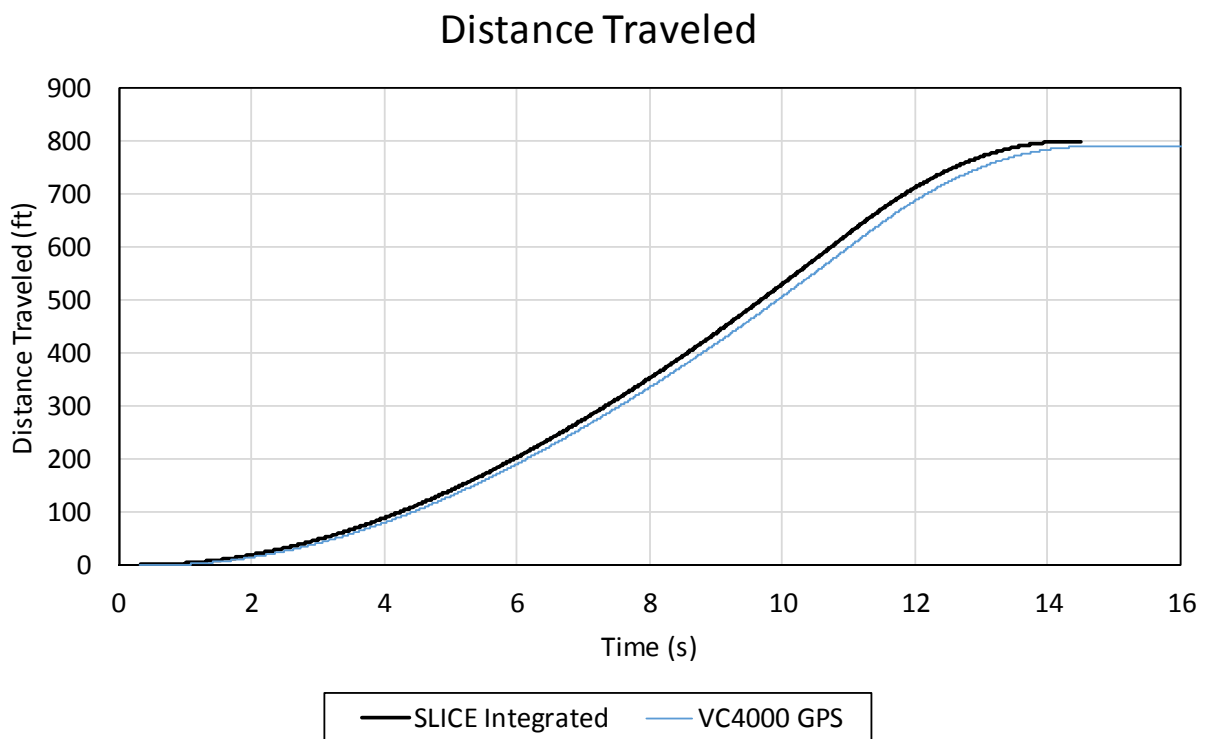


Figure A-6. Distance Traveled, Test No. LF-1

Appendix B. Test Results – Test No. LF-2

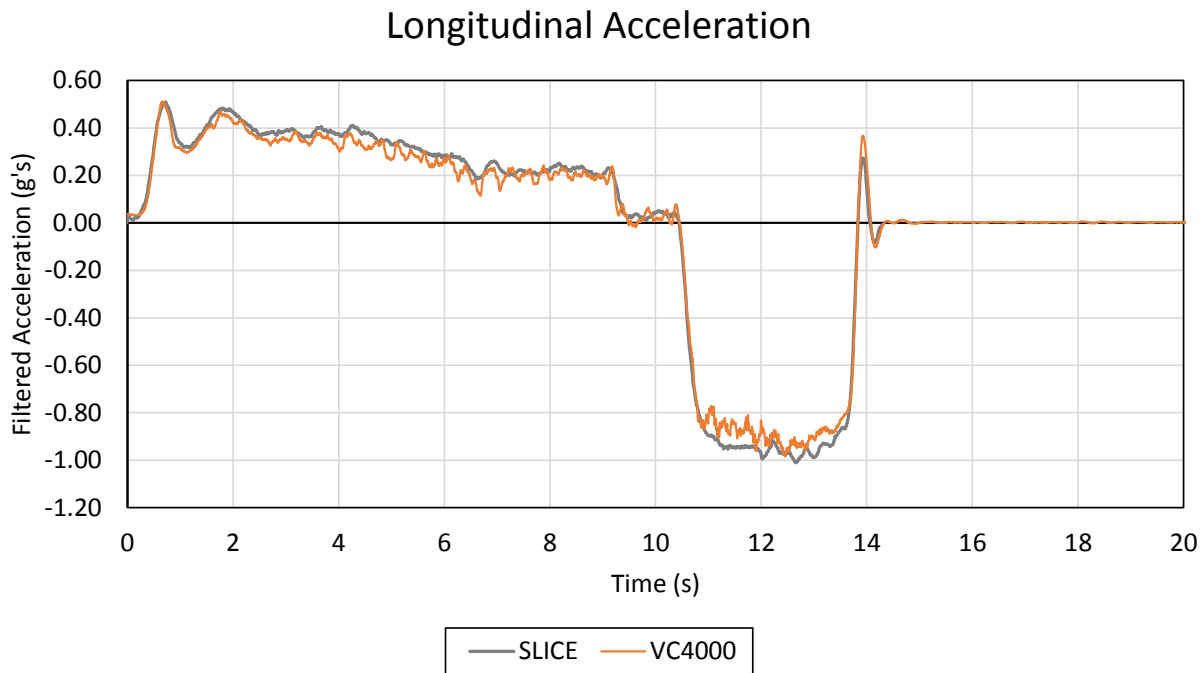


Figure B-1. Longitudinal Acceleration, Test No. LF-2

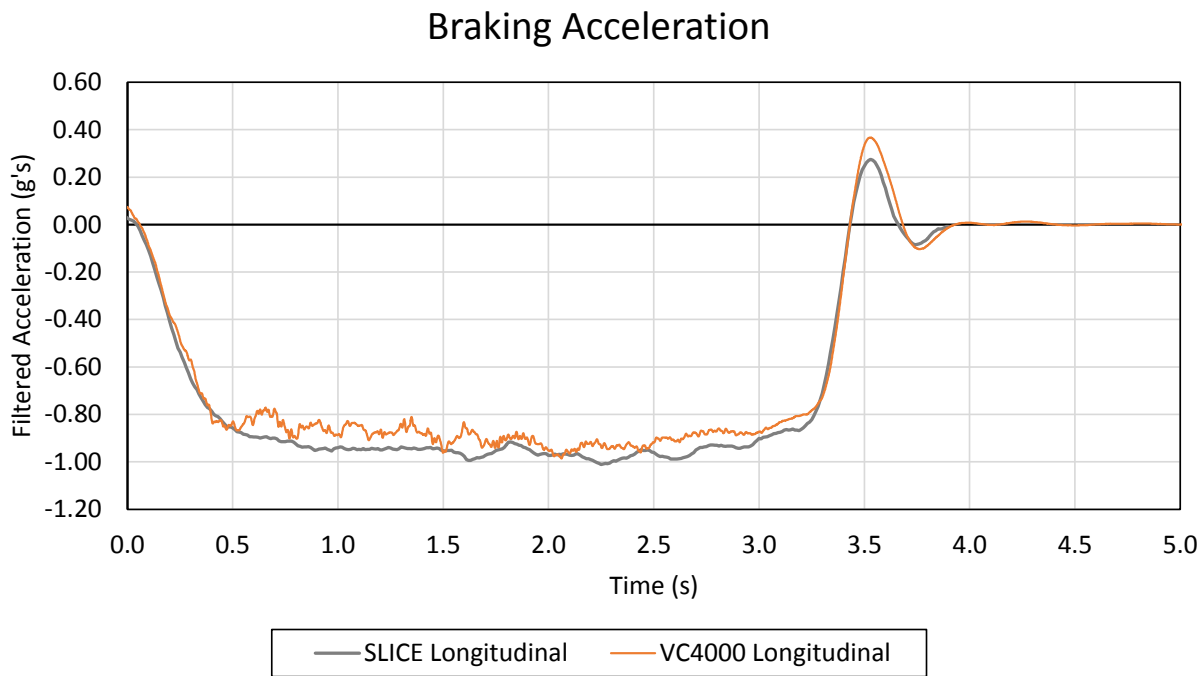


Figure B-2. Braking Acceleration, Test No. LF-2

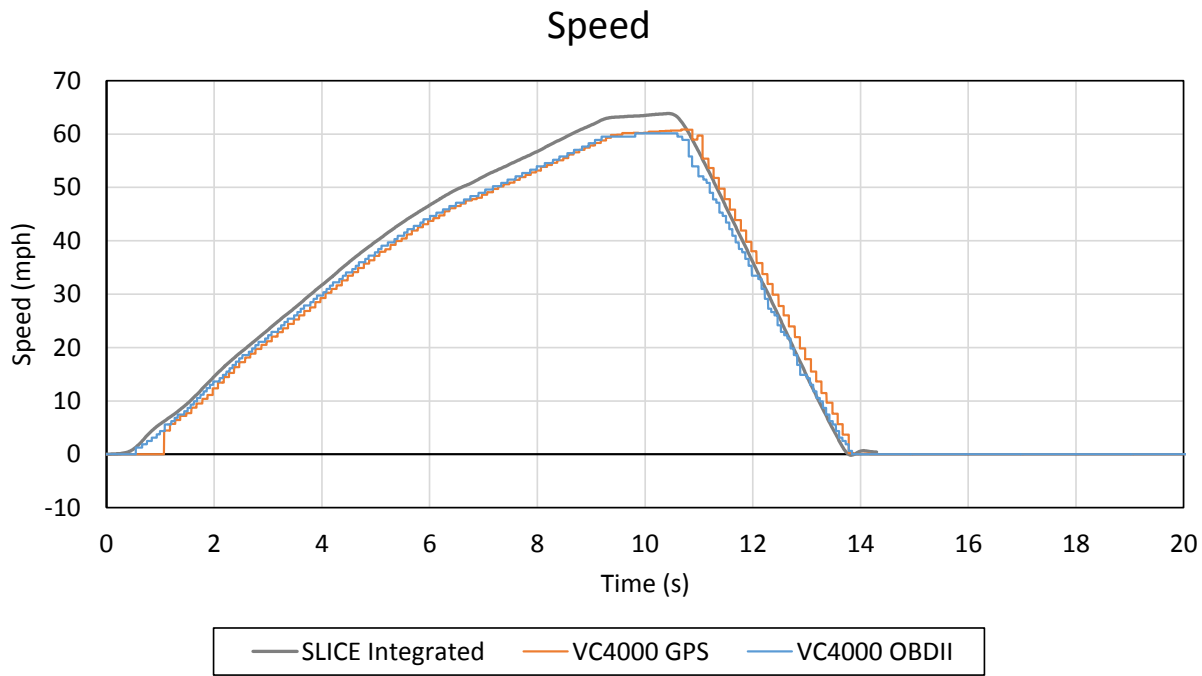


Figure B-3. Vehicle Speed, Test No. LF-2

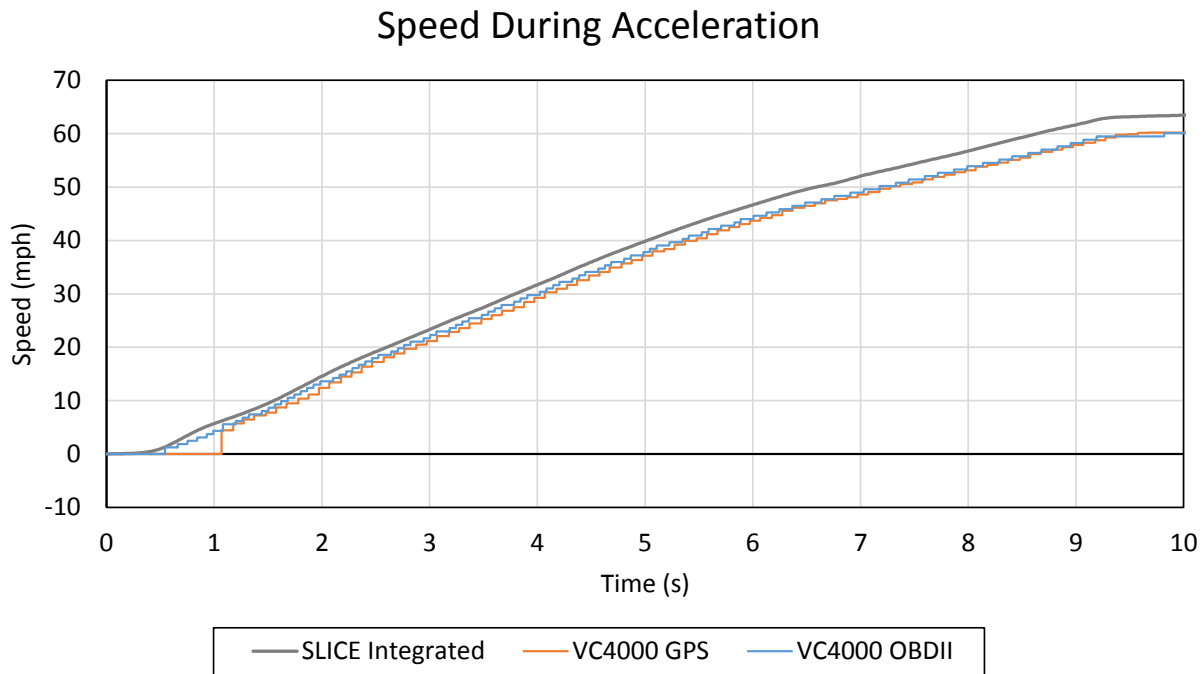


Figure B-4. Speed During Acceleration, Test No. LF-2

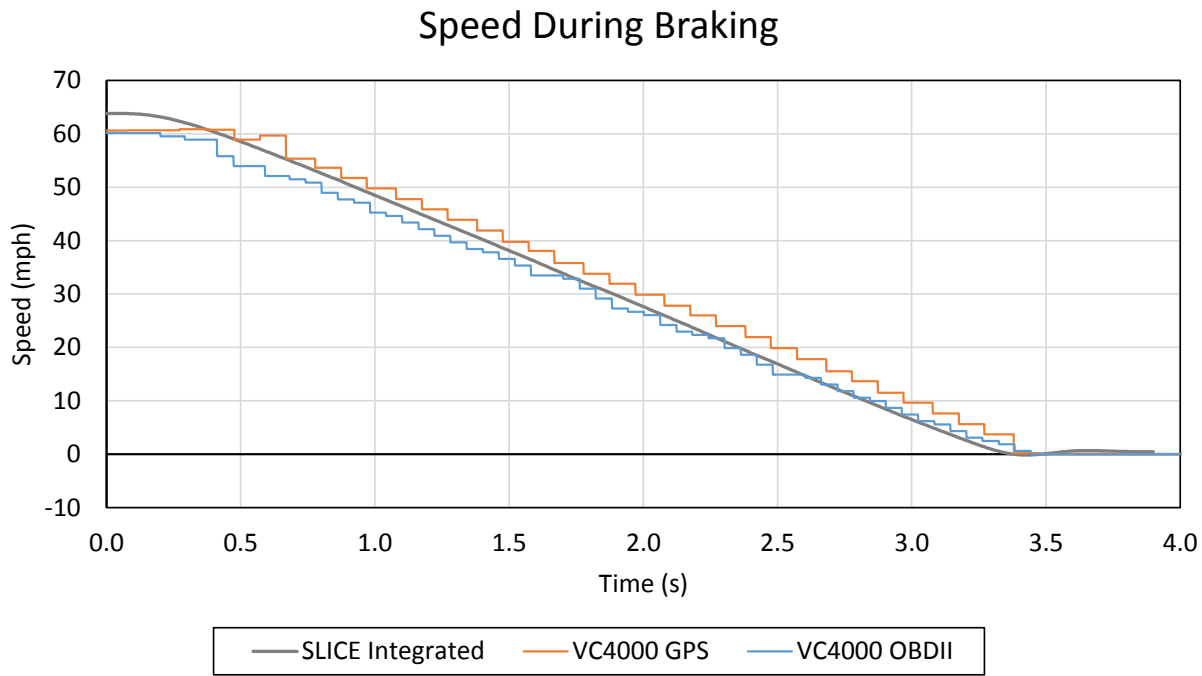


Figure B-5. Speed During Braking, Test No. LF-2

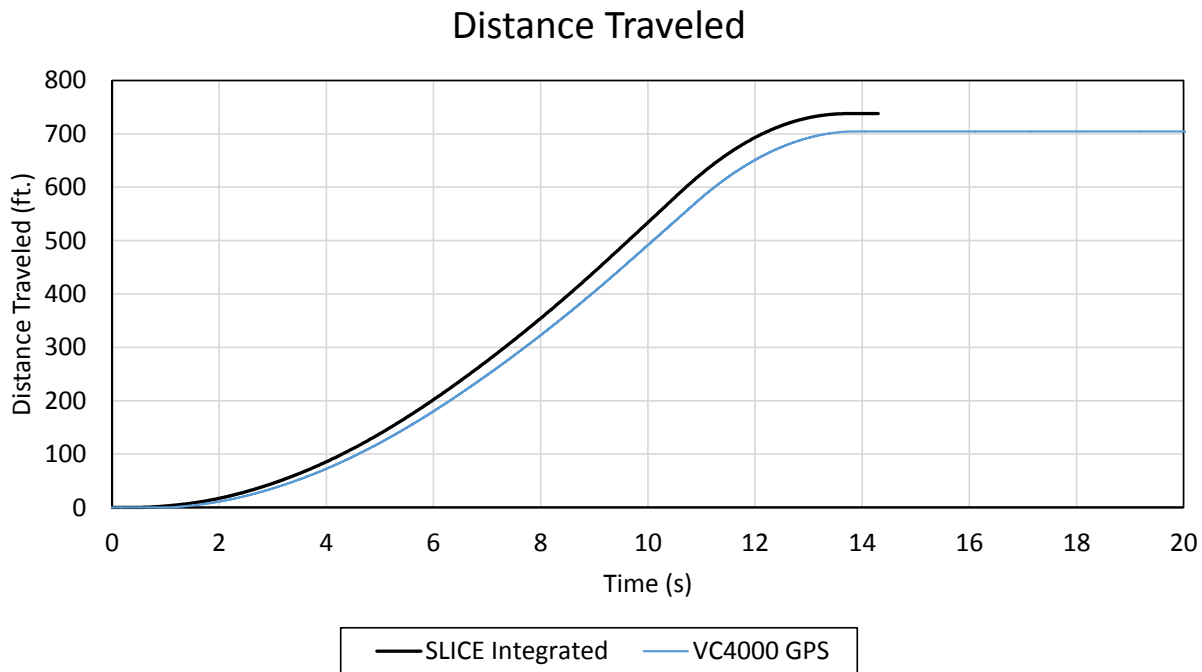


Figure B-6. Distance Traveled, Test No. LF-2

Appendix C. Test Results – Test No. LF-3

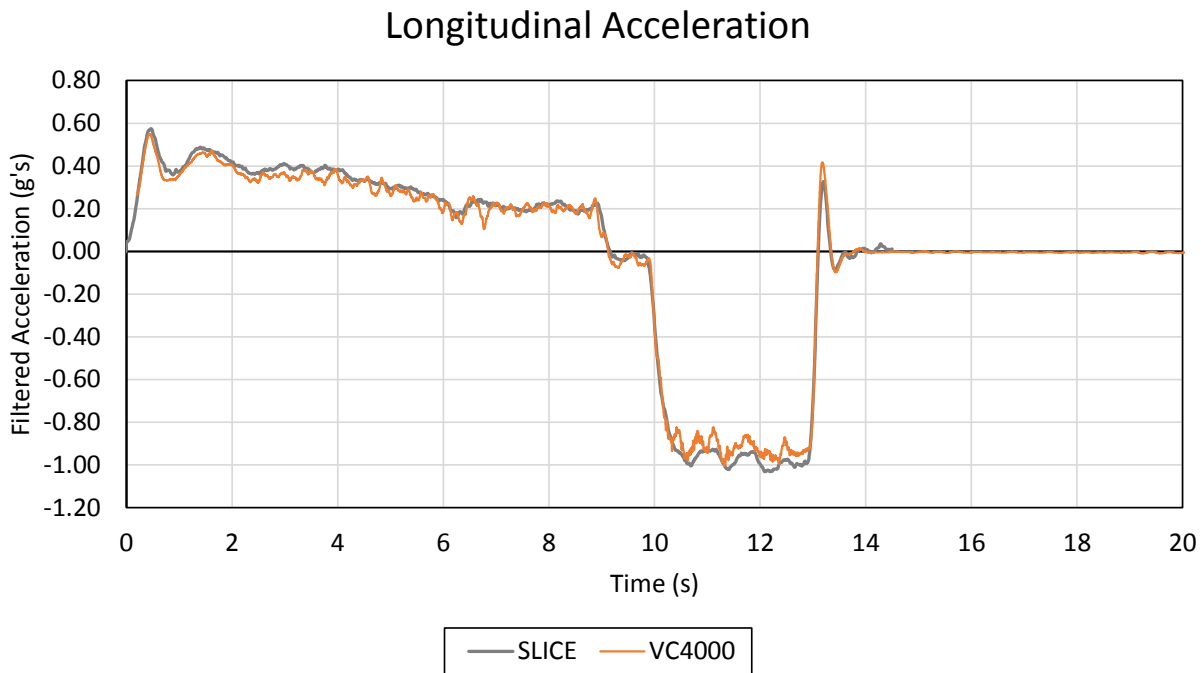


Figure C-1. Longitudinal Acceleration, Test No. LF-3

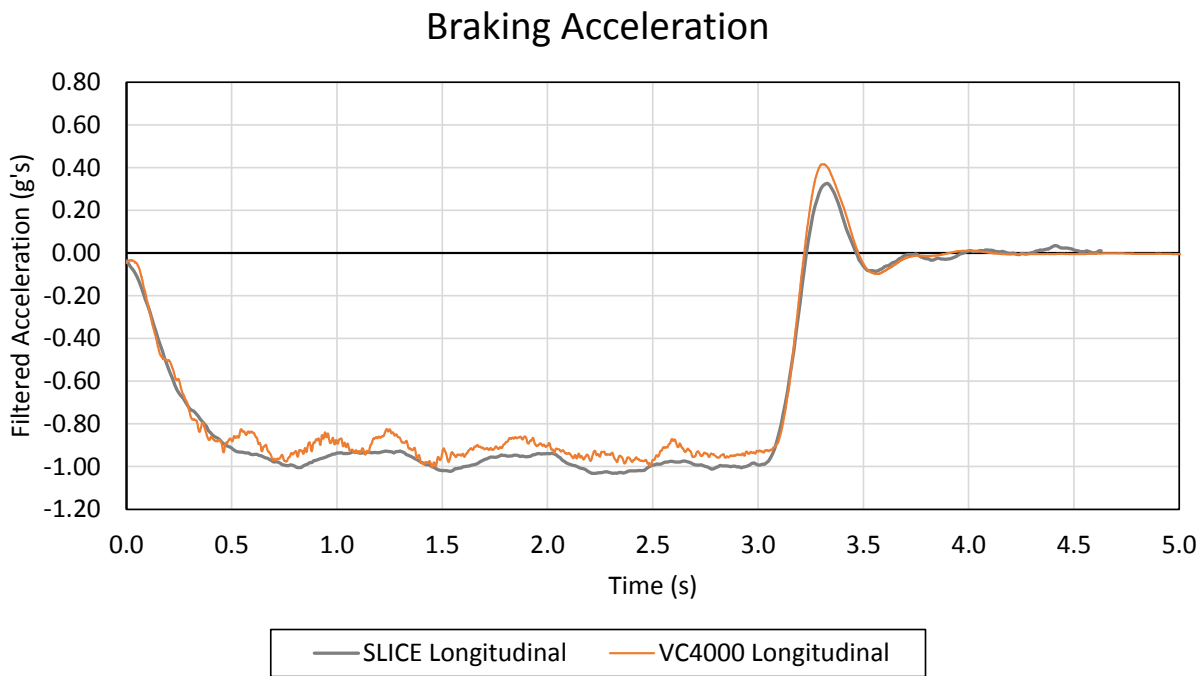


Figure C-2. Braking Acceleration, Test No. LF-3

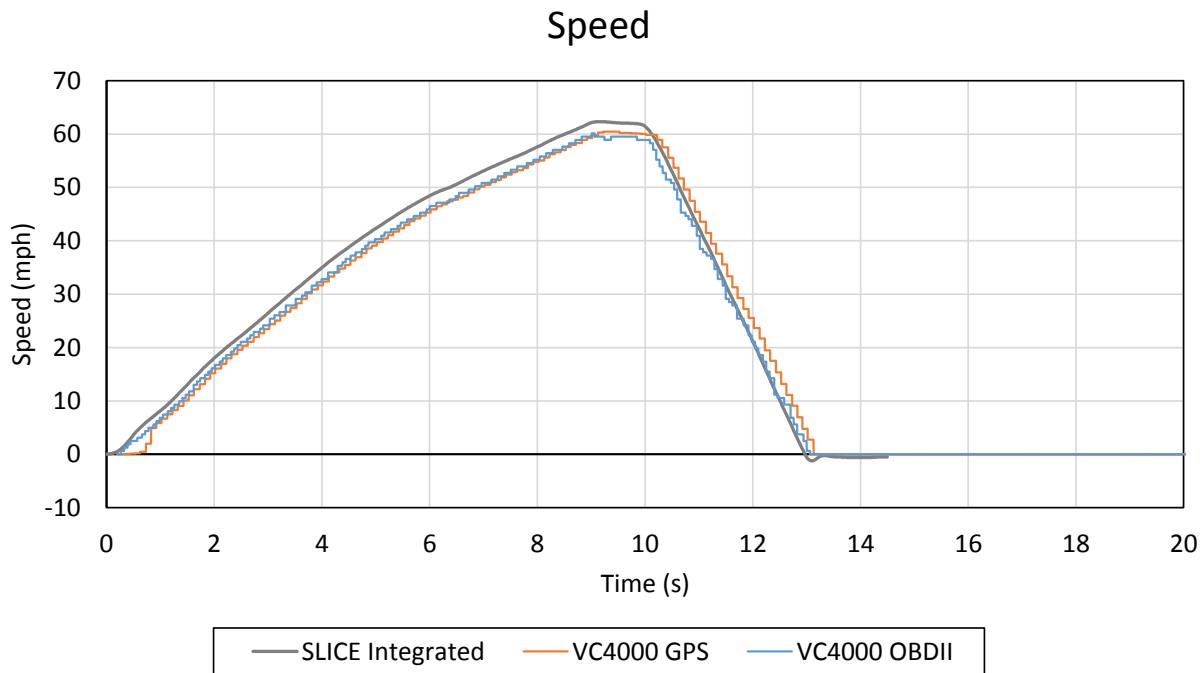


Figure C-3. Vehicle Speed, Test No. LF-3

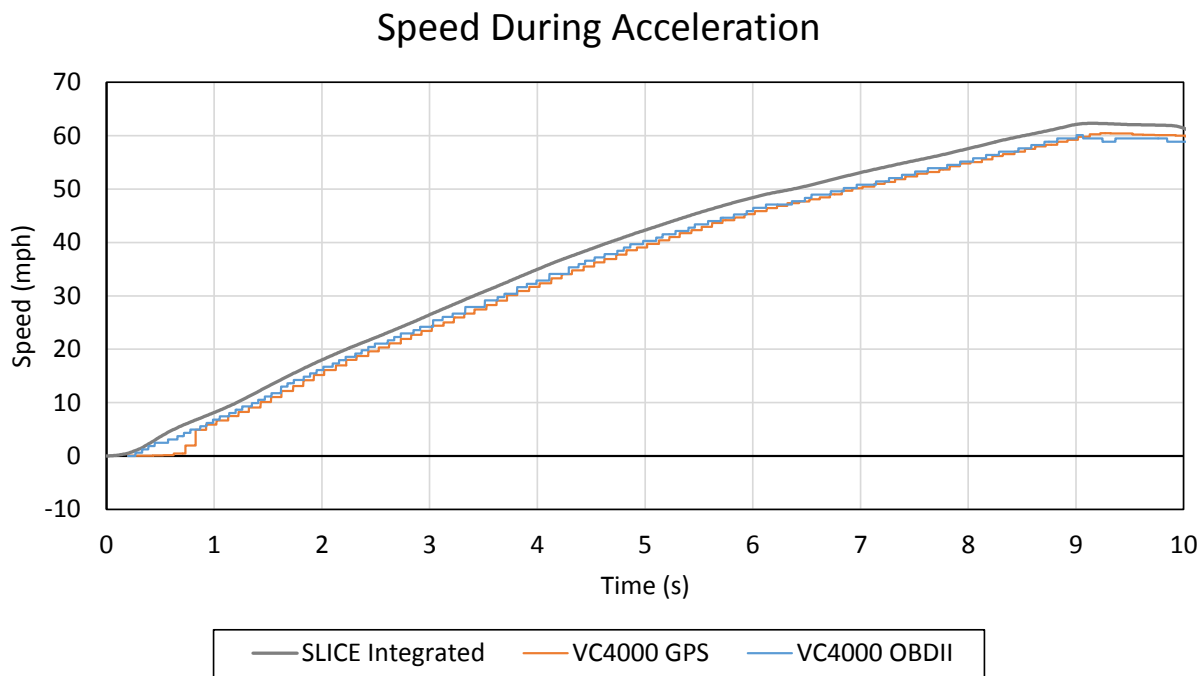


Figure C-4. Speed During Acceleration, Test No. LF-3

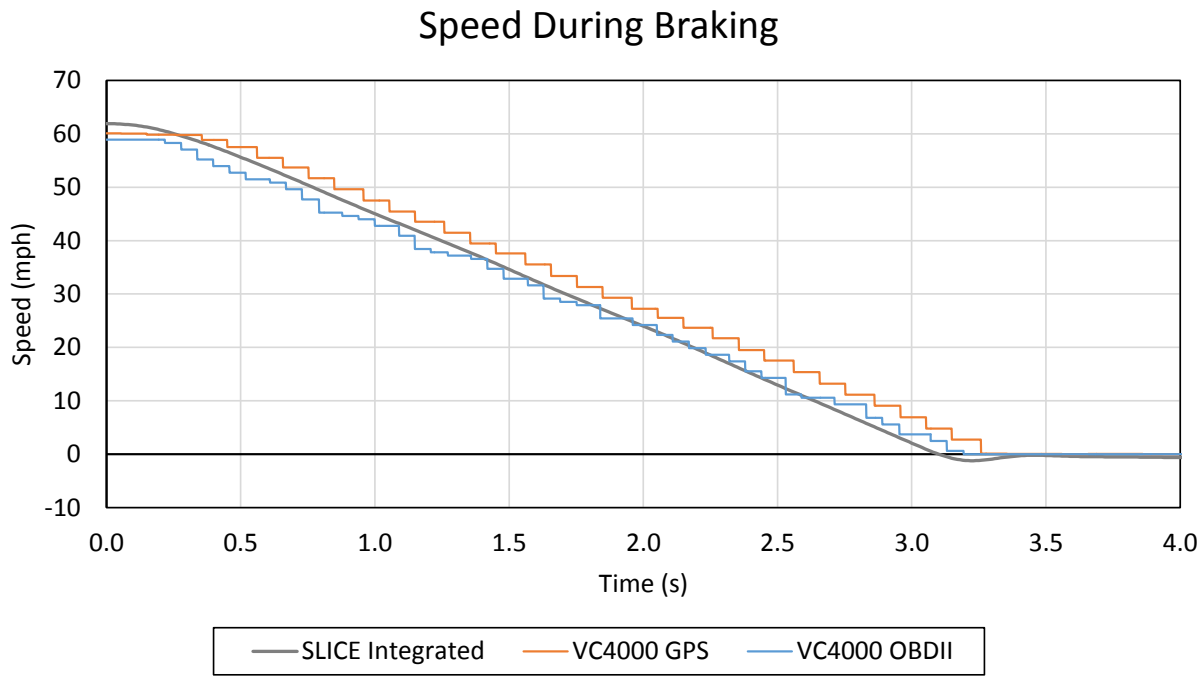


Figure C-5. Speed During Braking, Test No. LF-3

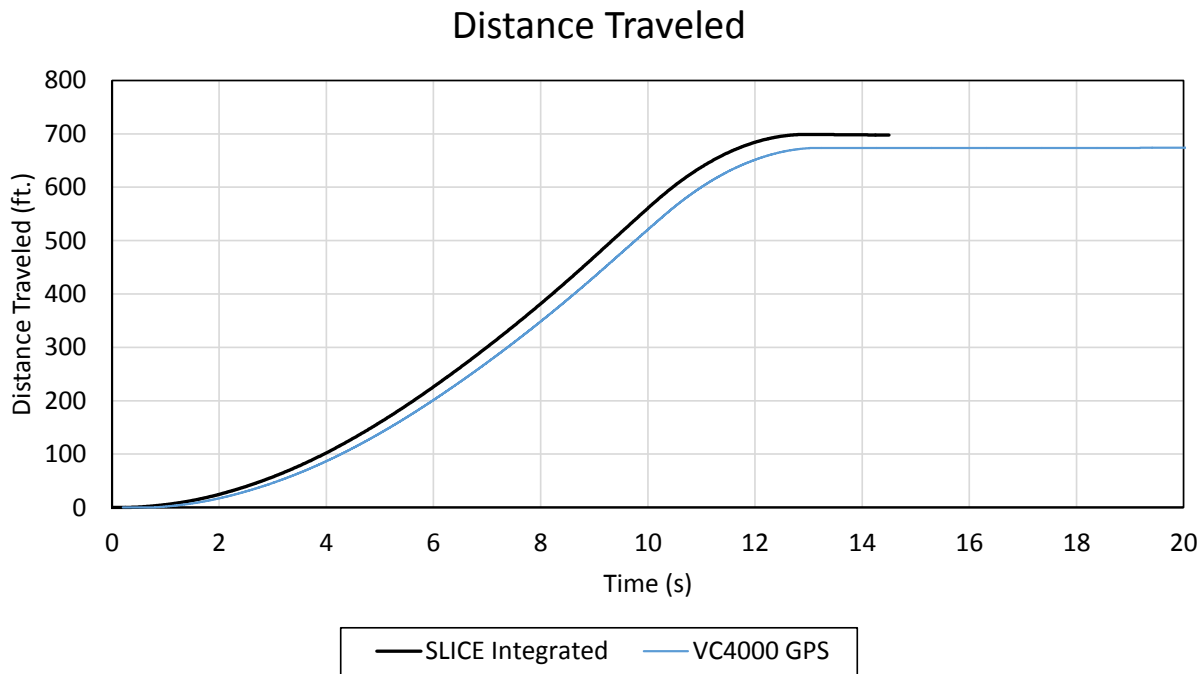


Figure C-6. Distance Traveled, Test No. LF-3

Appendix D. Test Results – Test No. LF-4

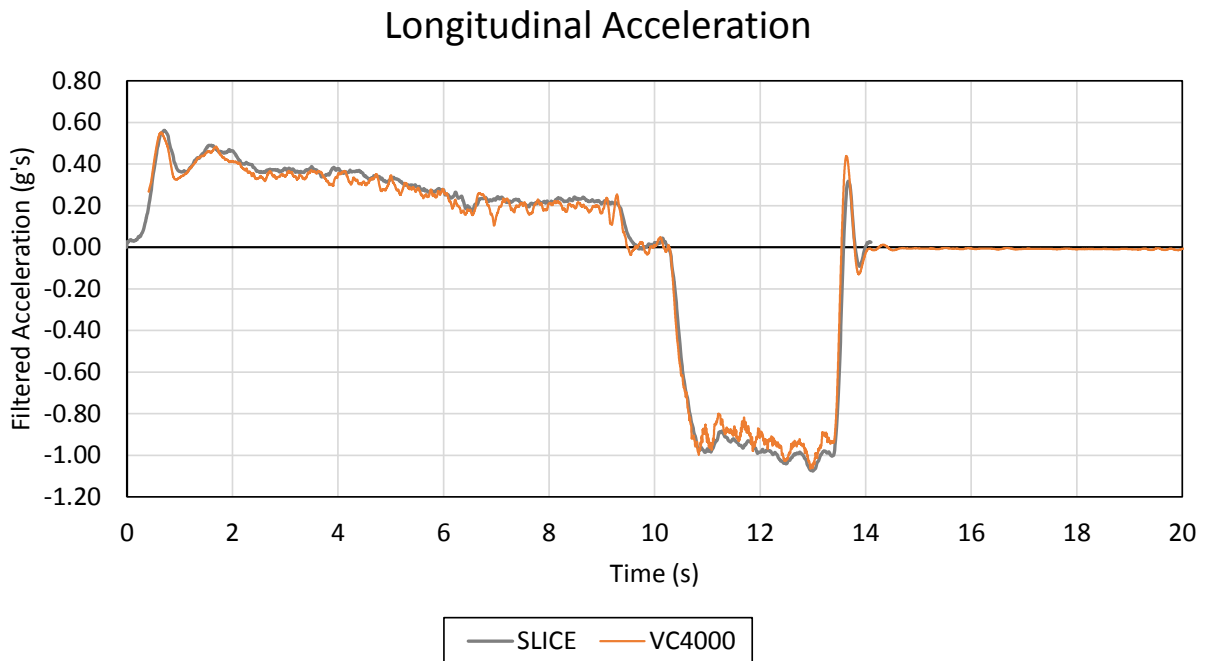


Figure D-1. Longitudinal Acceleration, Test No. LF-4

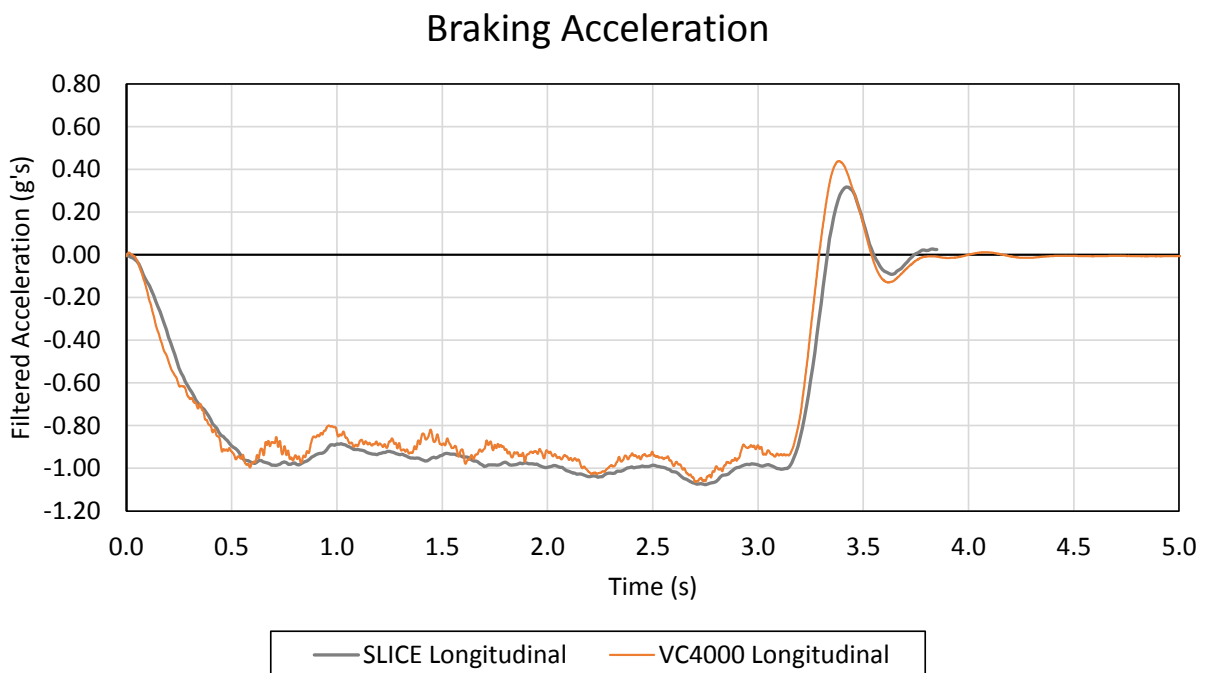


Figure D-2. Braking Acceleration, Test No. LF-4

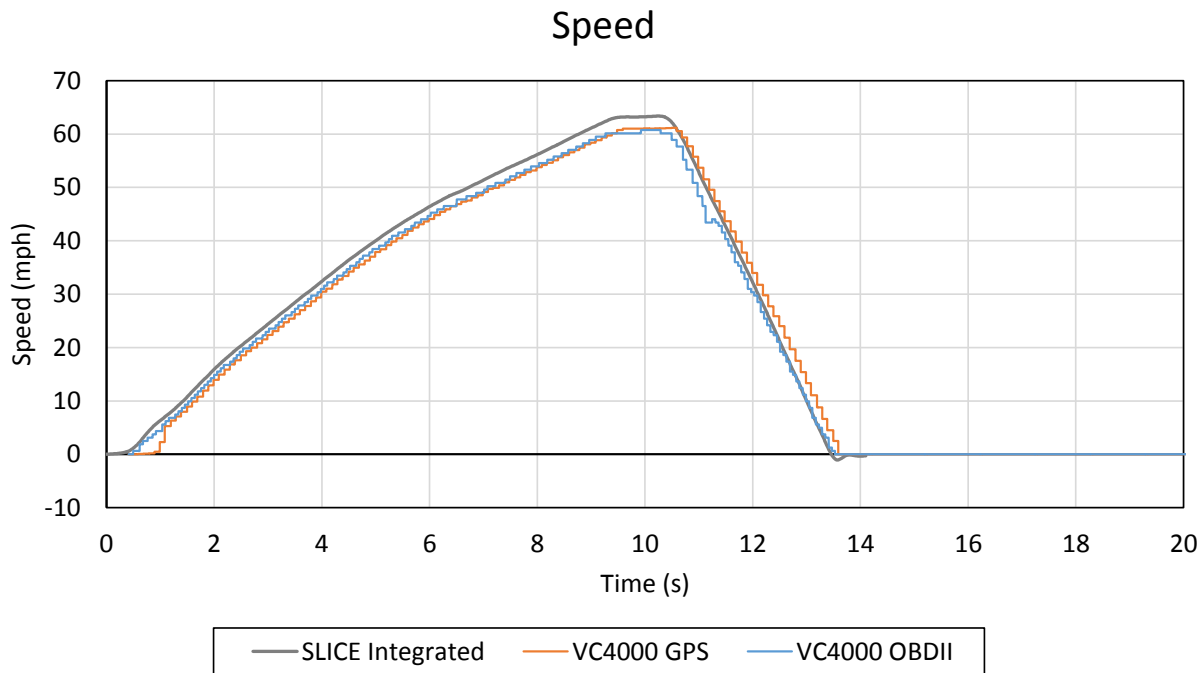


Figure D-3. Vehicle Speed, Test No. LF-4

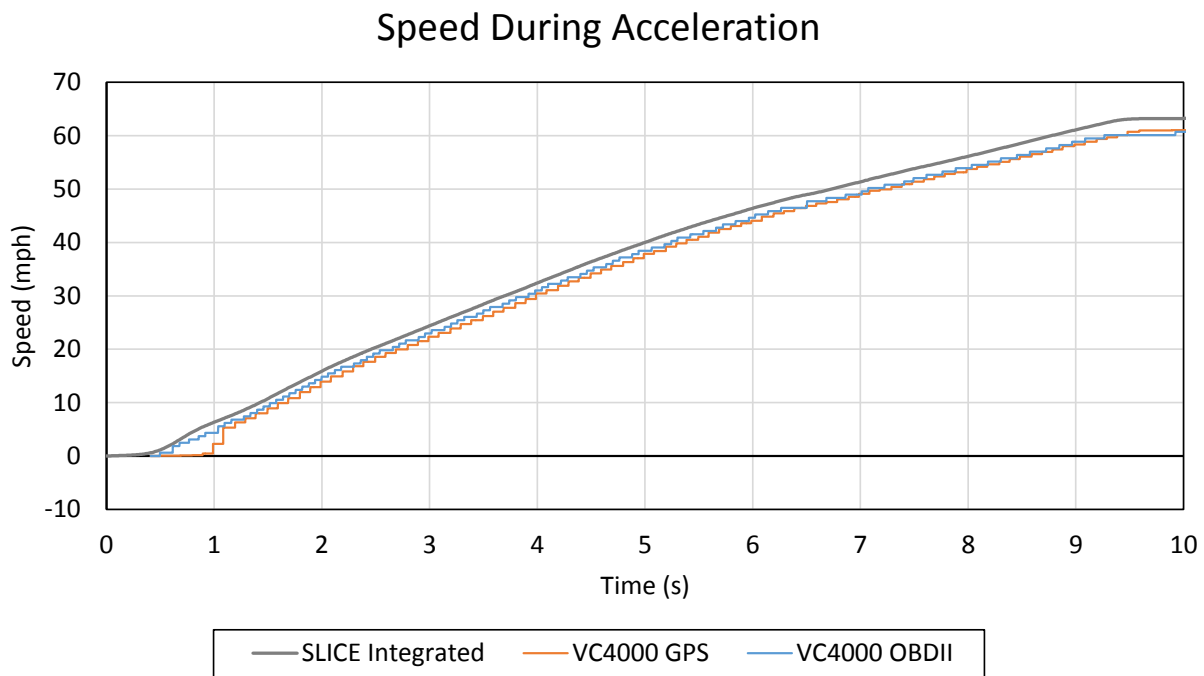


Figure D-4. Speed During Acceleration, Test No. LF-4

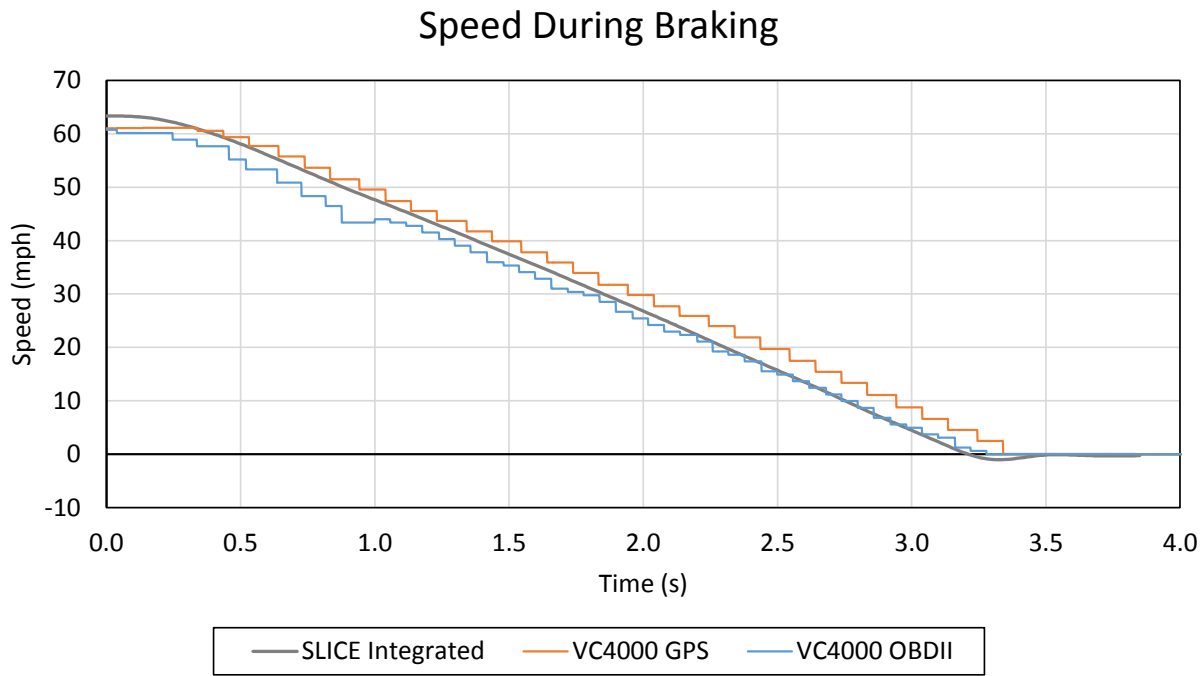


Figure D-5. Speed During Braking, Test No. LF-4

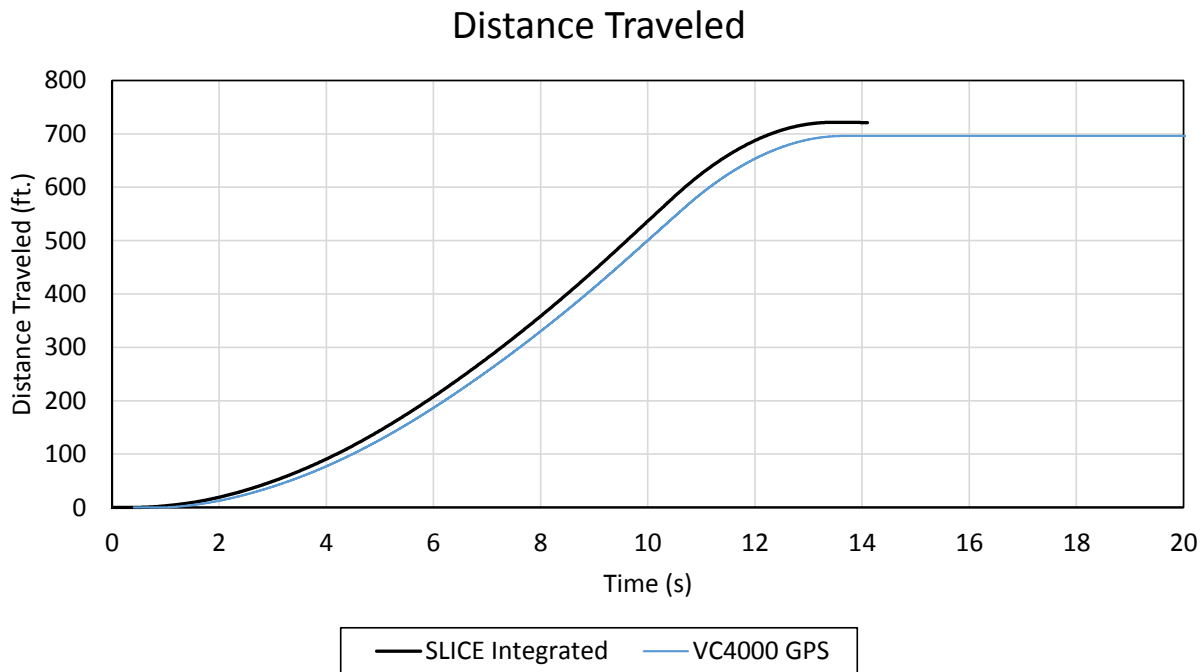


Figure D-6. Distance Traveled, Test No. LF-4

Appendix E. Test Results – Test No. LF-1b

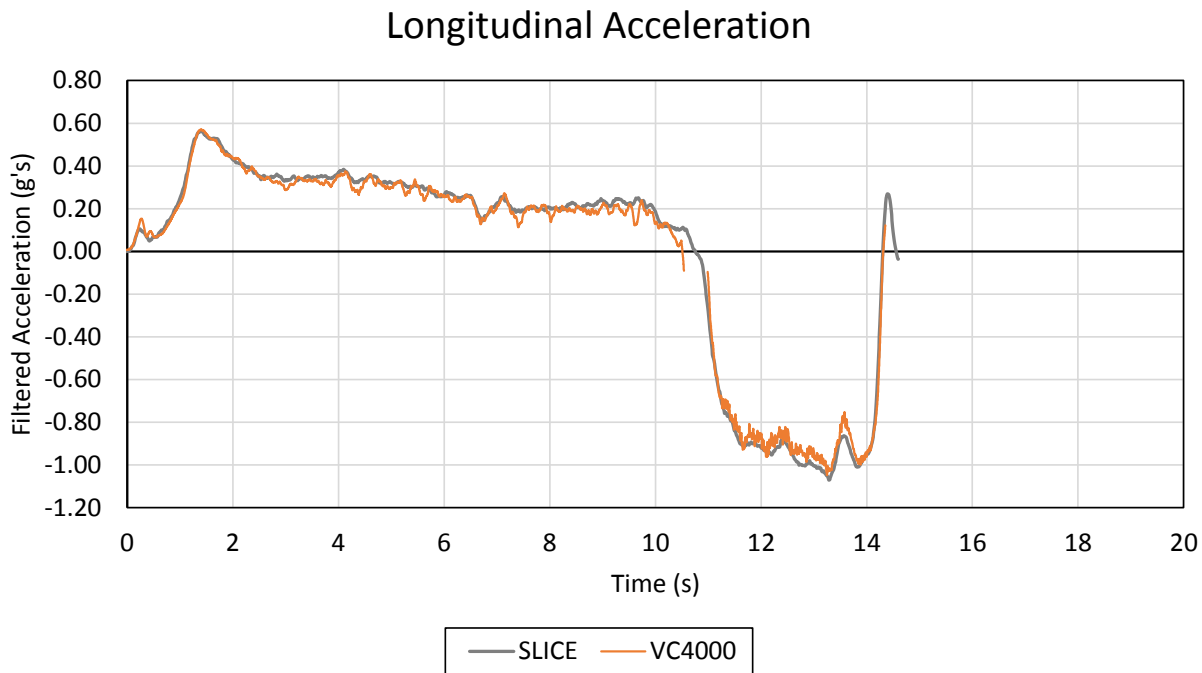


Figure E-1. Longitudinal Acceleration, Test No. LF-1b

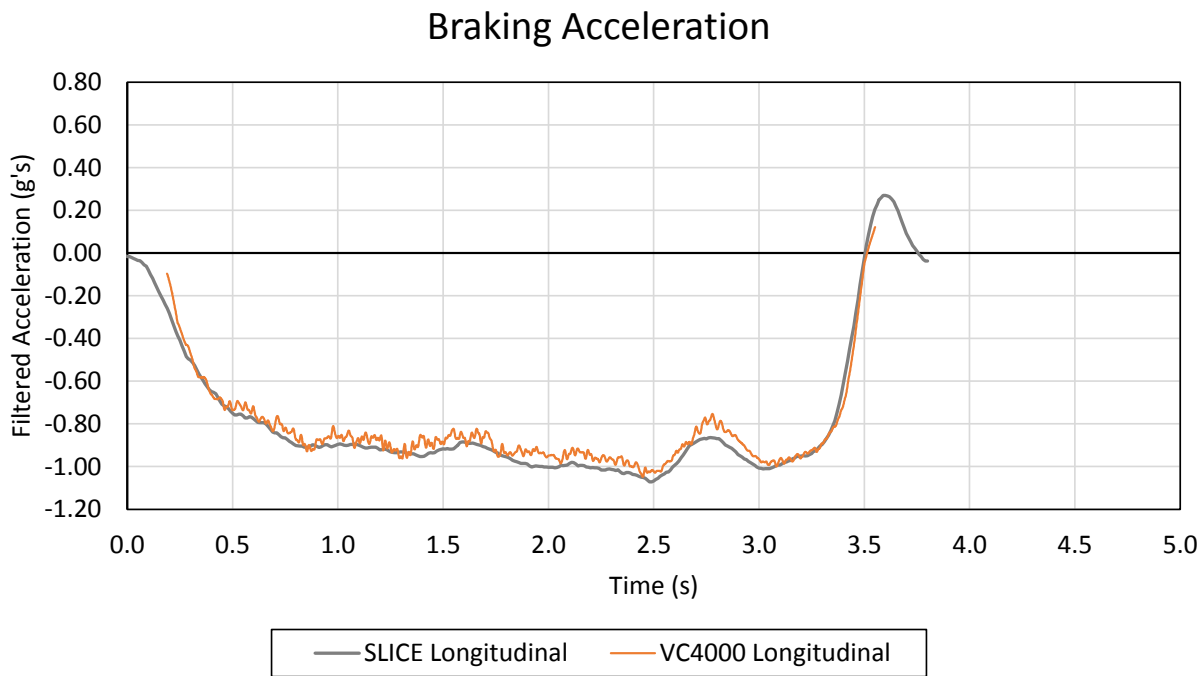


Figure E-2. Braking Acceleration, Test No. LF-1b

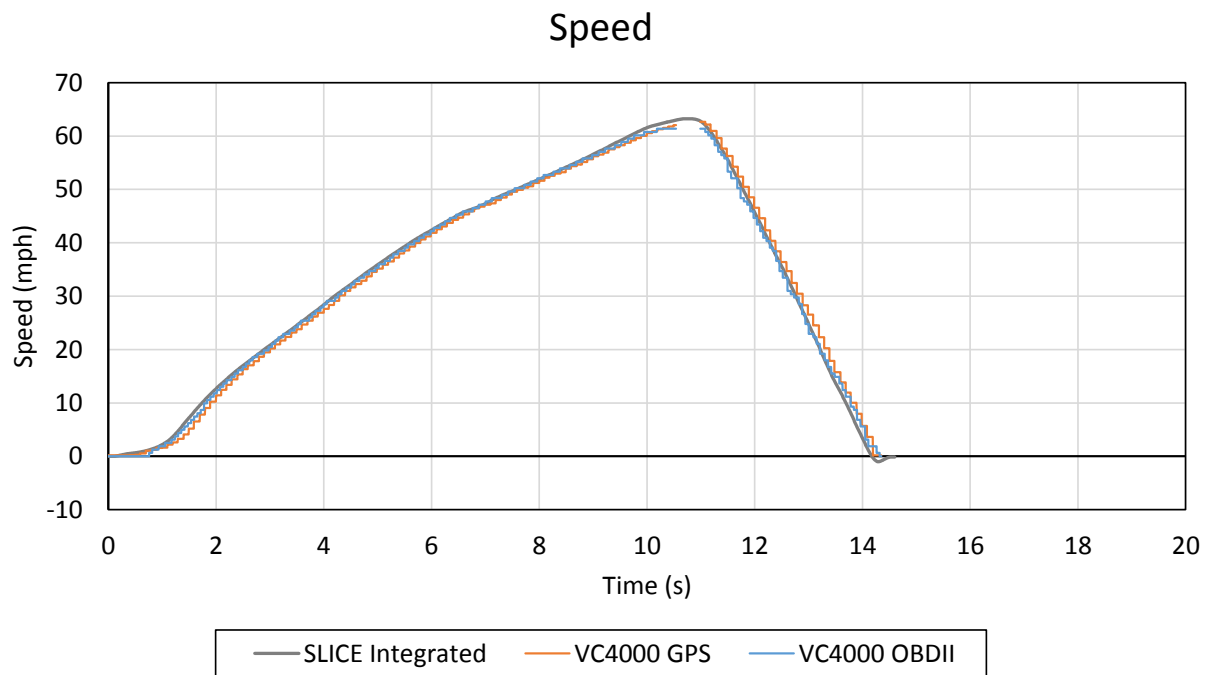


Figure E-3. Vehicle Speed, Test No. LF-1b

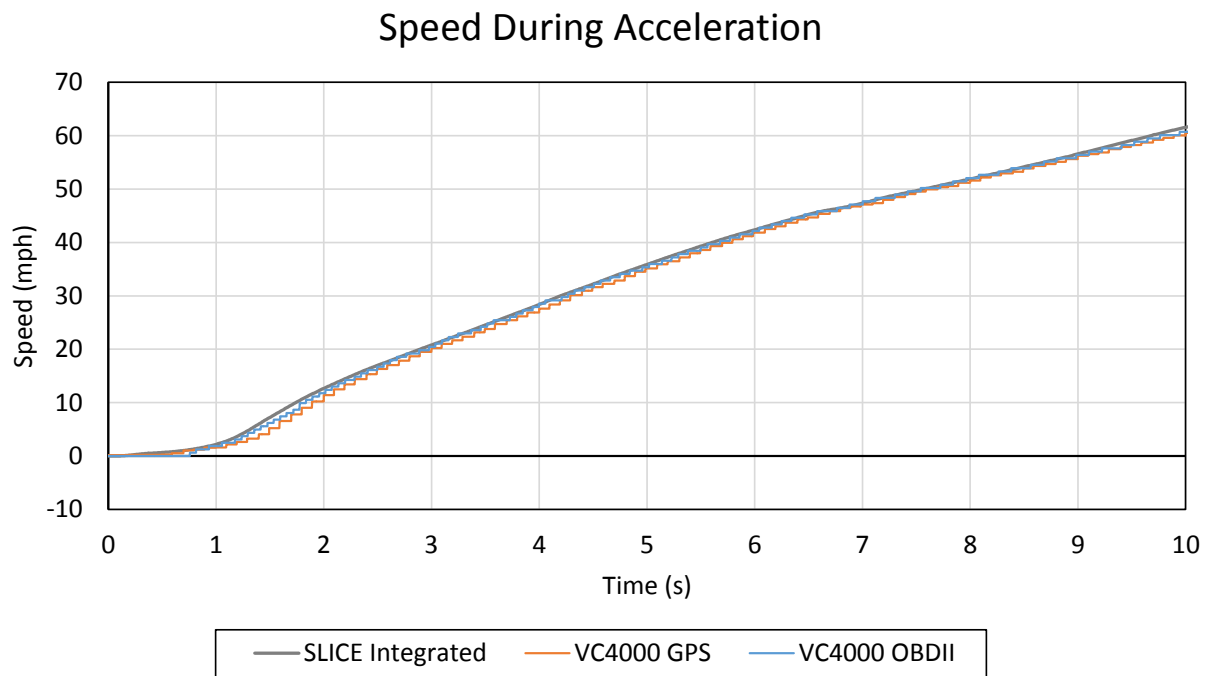


Figure E-4. Speed During Acceleration, Test No. LF-1b

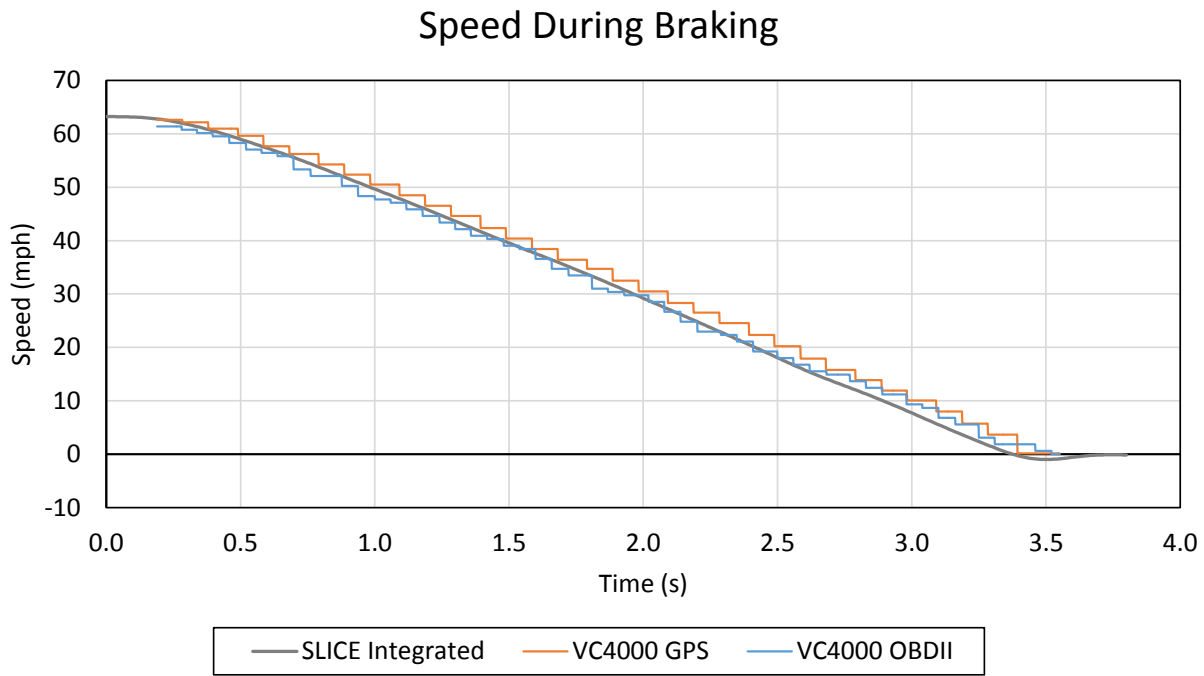
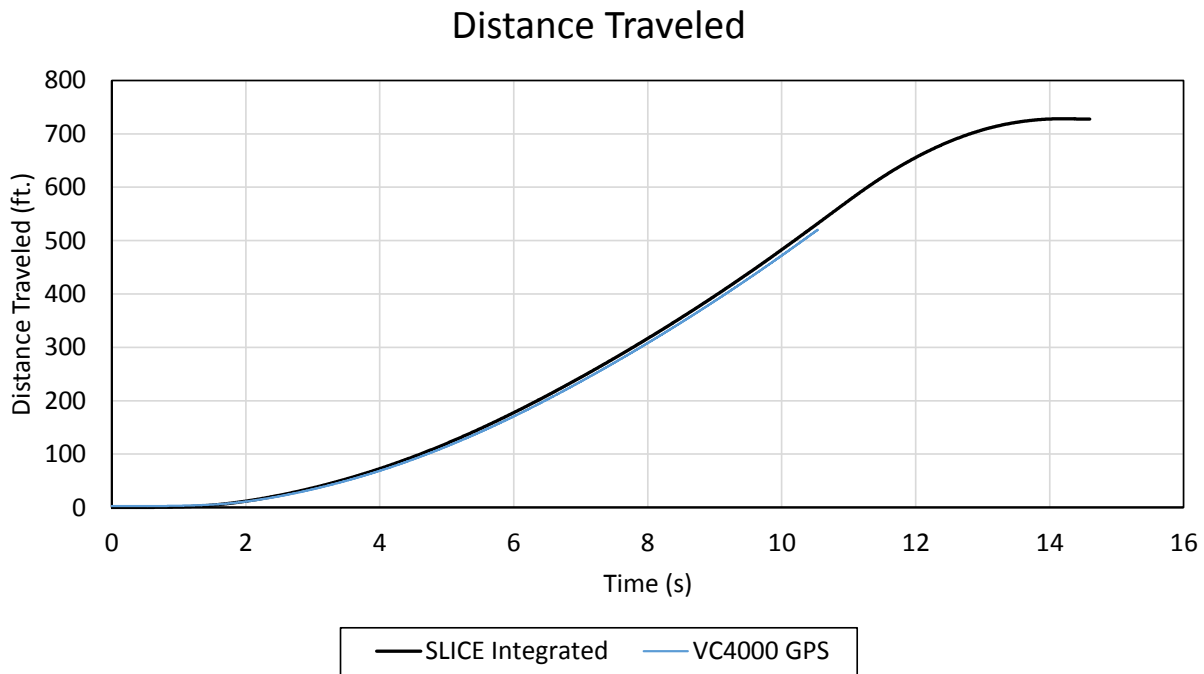


Figure E-5. Speed During Braking, Test No. LF-1b



Distance Traveled, Test No. LF-1b

Appendix F. Test Results – Test No. CF100-1

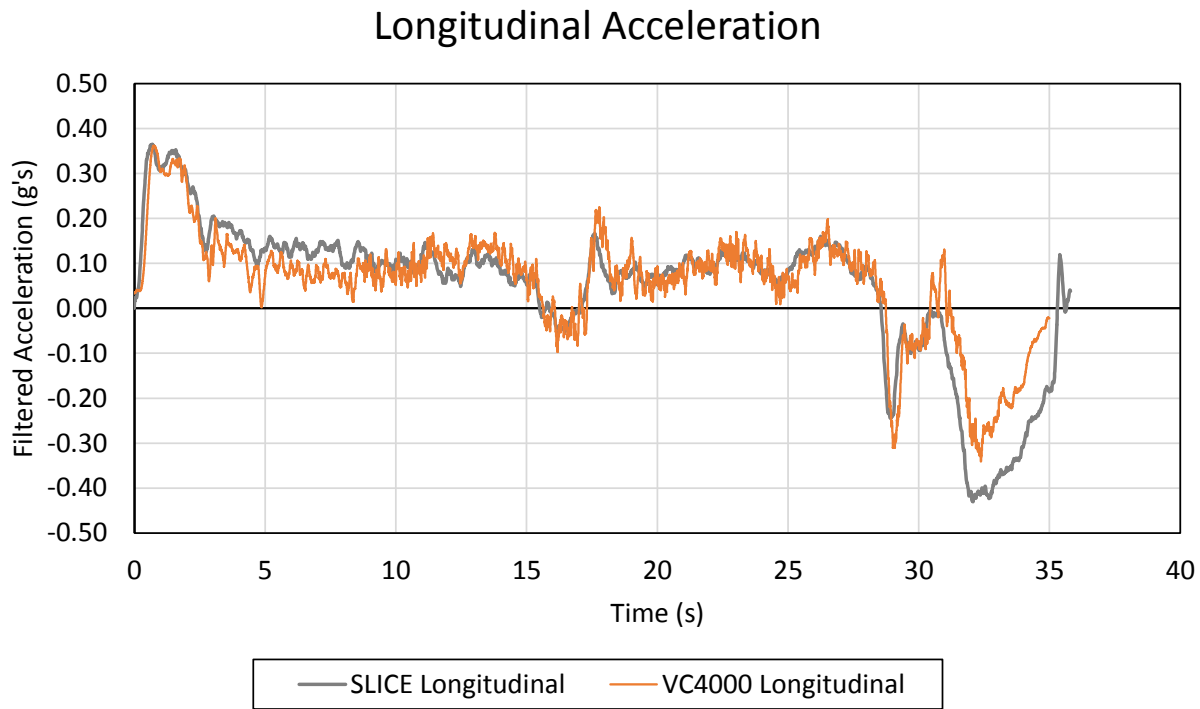


Figure F-1. Longitudinal Acceleration, Test No. CF100-1

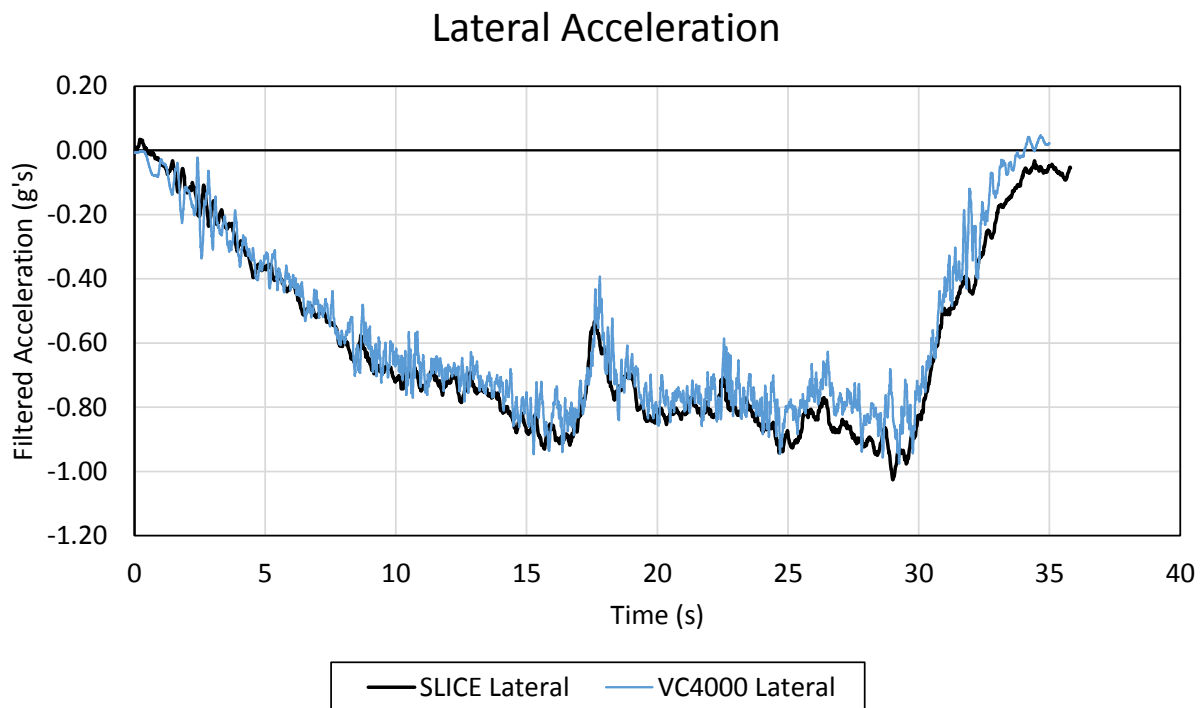


Figure F-2. Lateral Acceleration, Test No. CF100-1

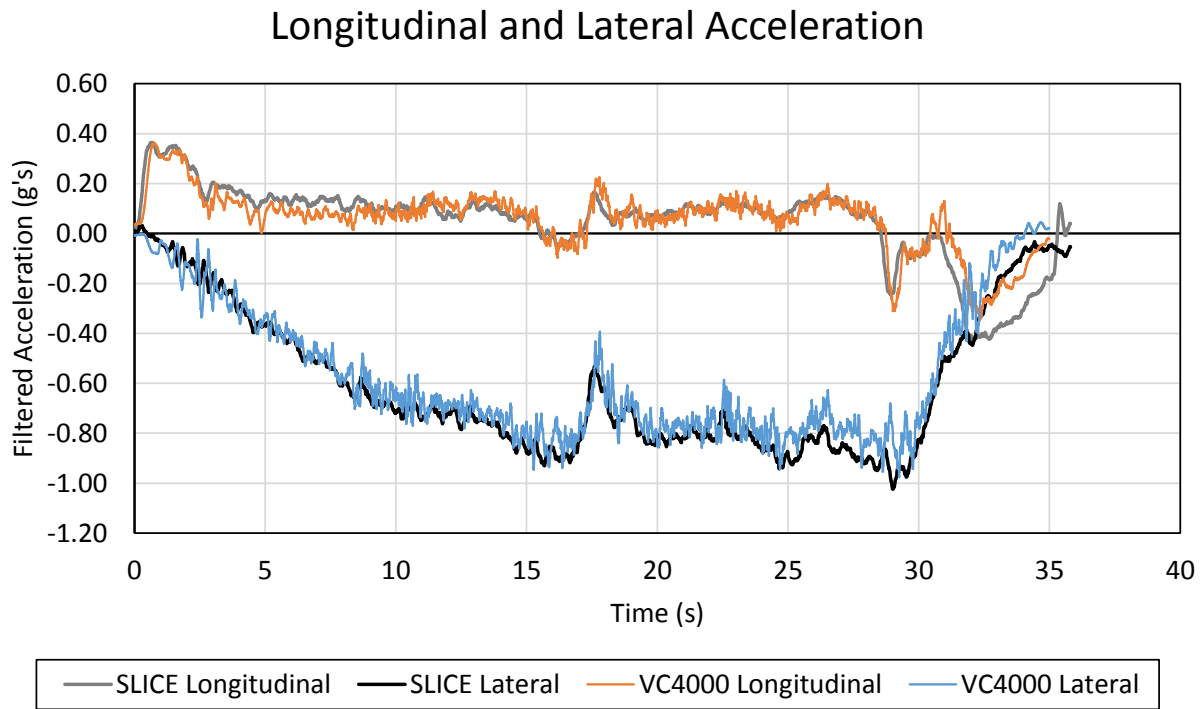


Figure F-3. Longitudinal and Lateral Acceleration, Test No. CF100-1

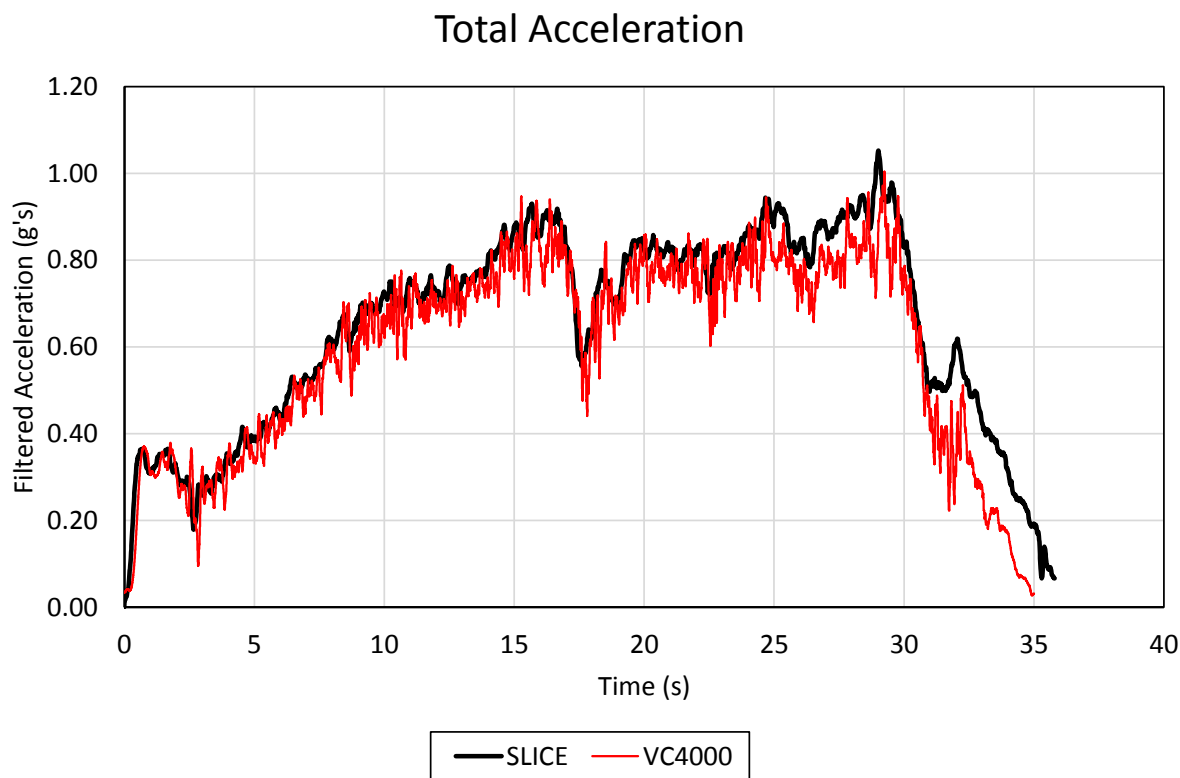


Figure F-4. Total Acceleration, Test No. CF100-1

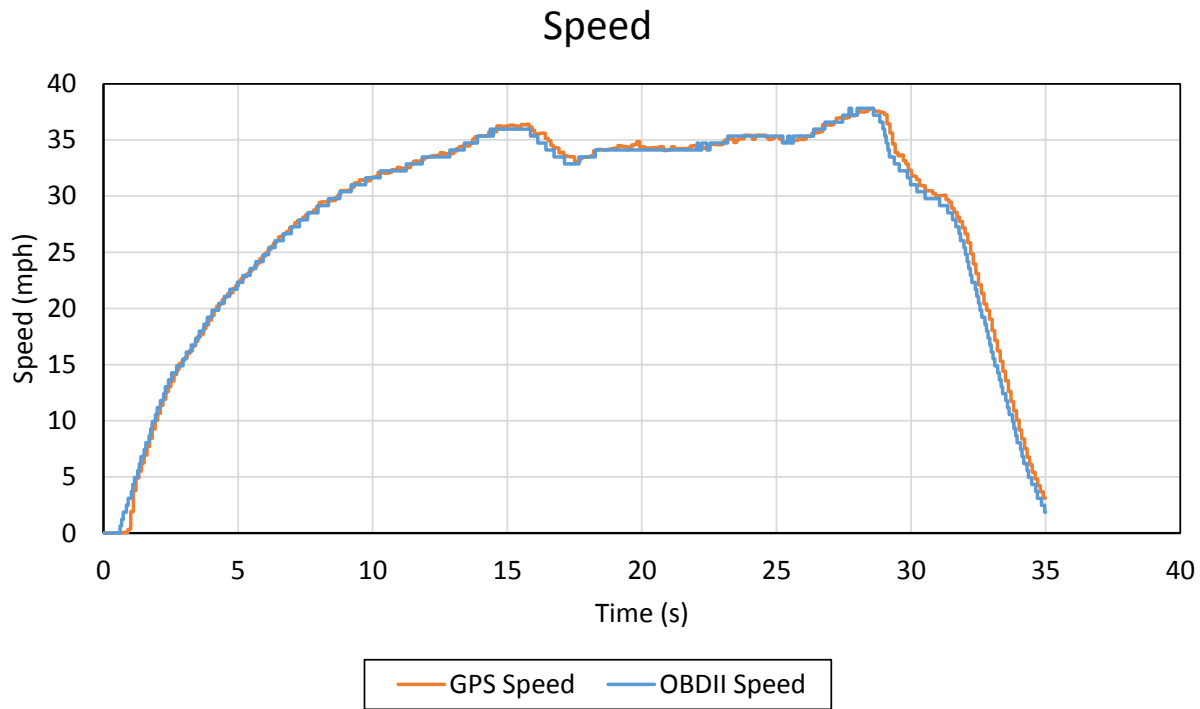


Figure F-5. Speed, Test No. CF100-1

Appendix G. Test Results – Test No. CF100-2

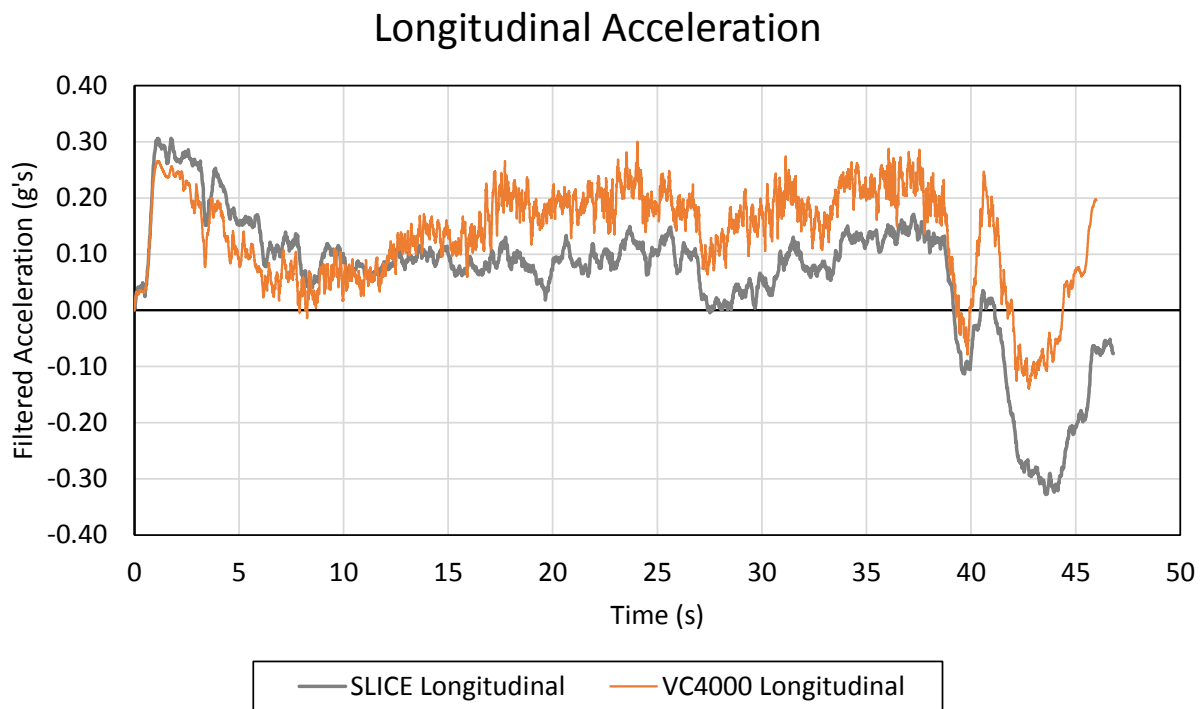


Figure G-1. Longitudinal Acceleration, Test No. CF100-2

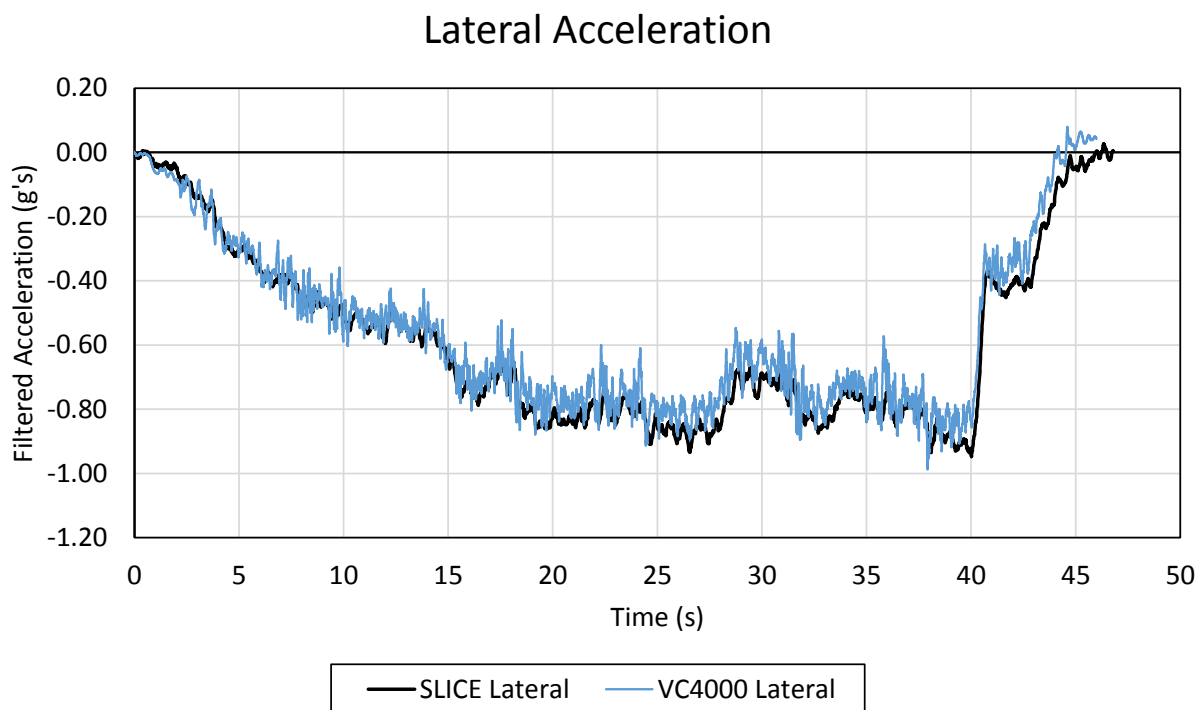


Figure G-2. Lateral Acceleration, Test No. CF100-2

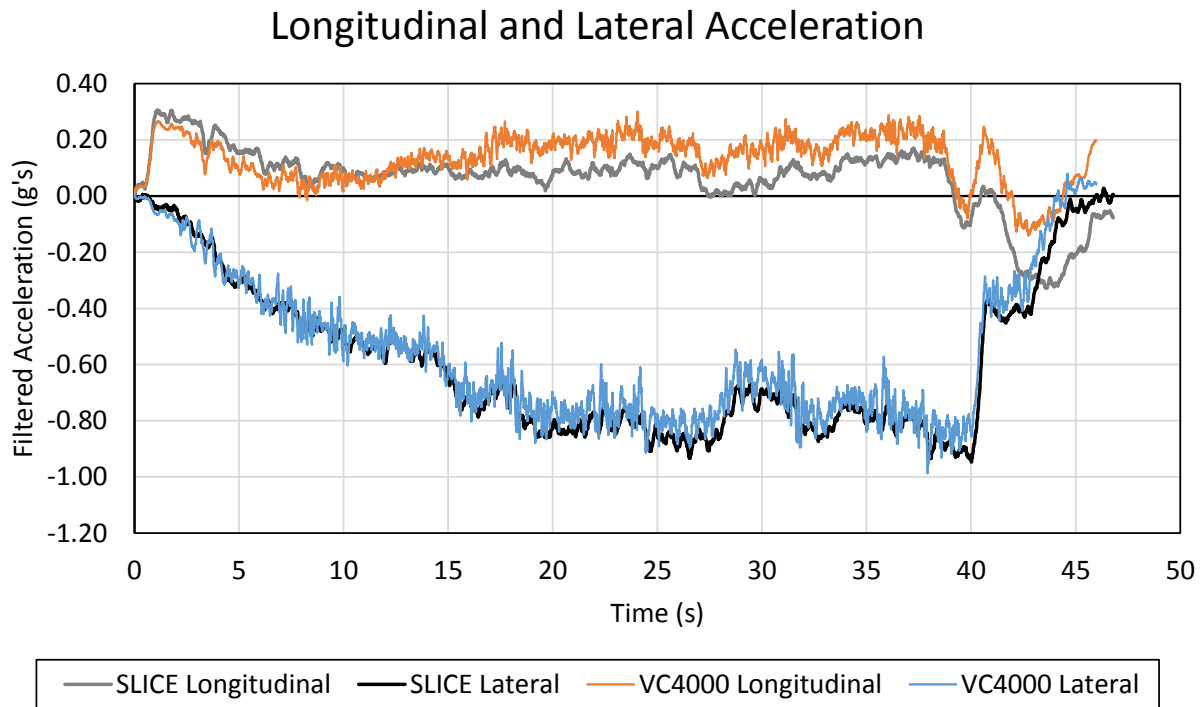


Figure G-3. Longitudinal and Lateral Acceleration, Test No. CF100-2

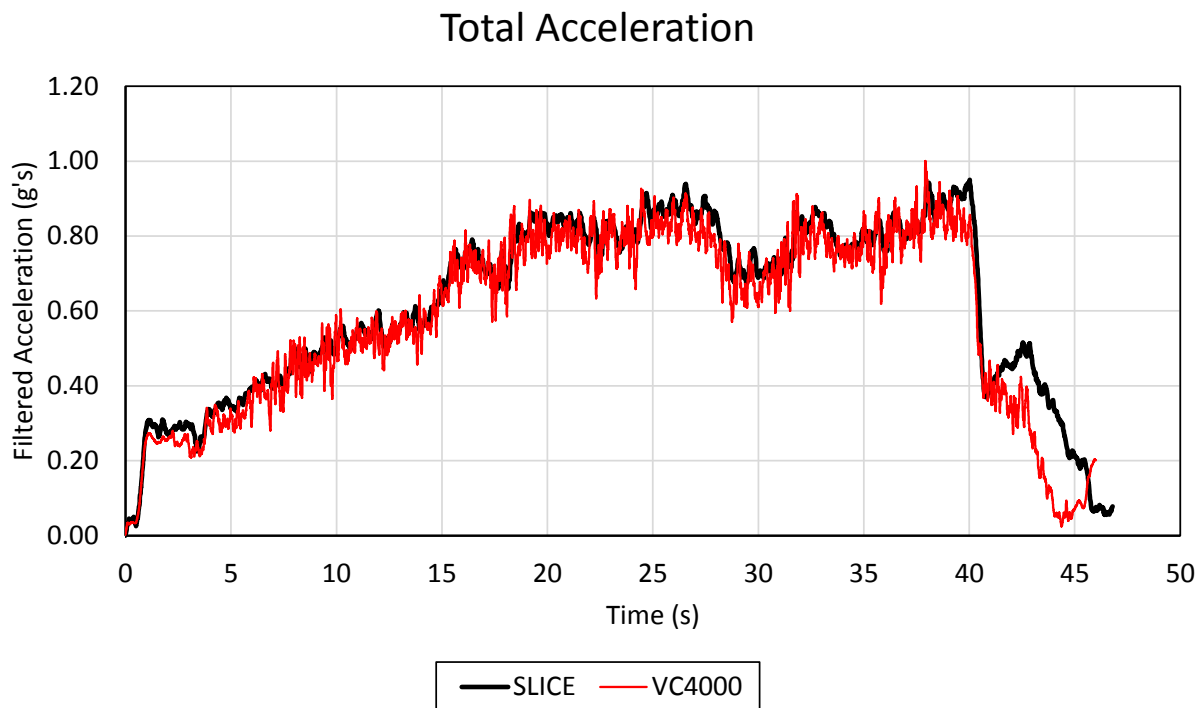


Figure G-4. Total Acceleration, Test No. CF100-2

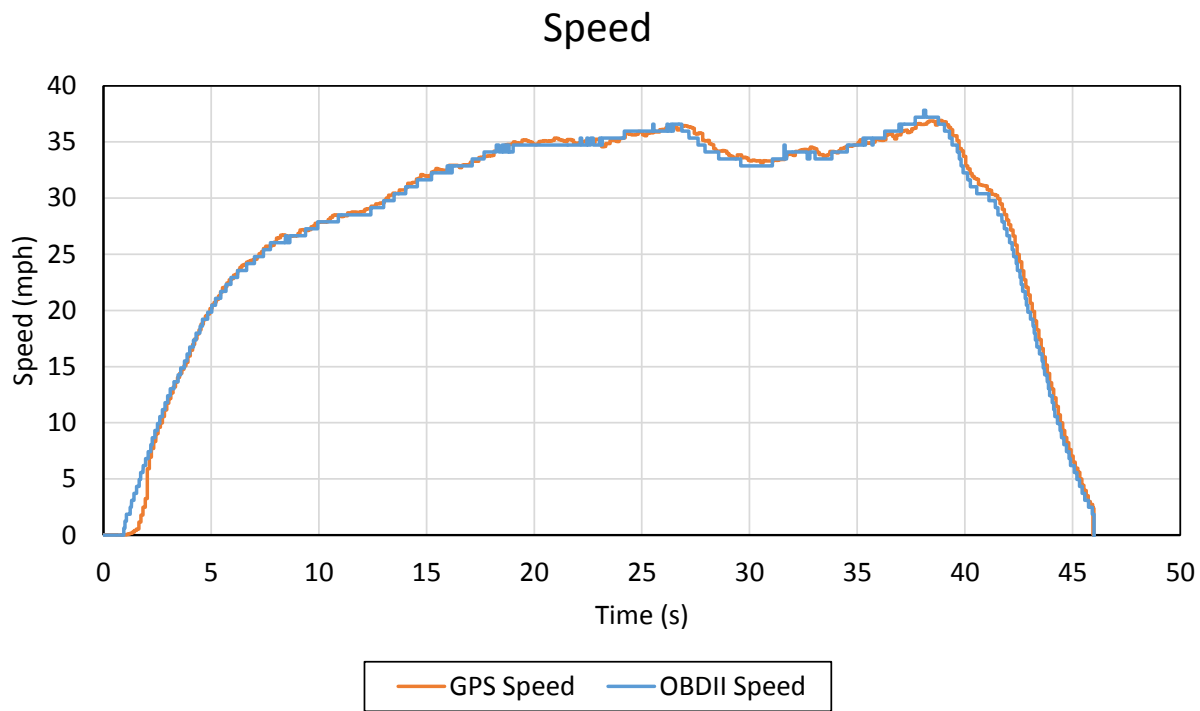


Figure G-5. Speed, Test No. CF100-2

Appendix H. Test Results – Test No. CF100-3

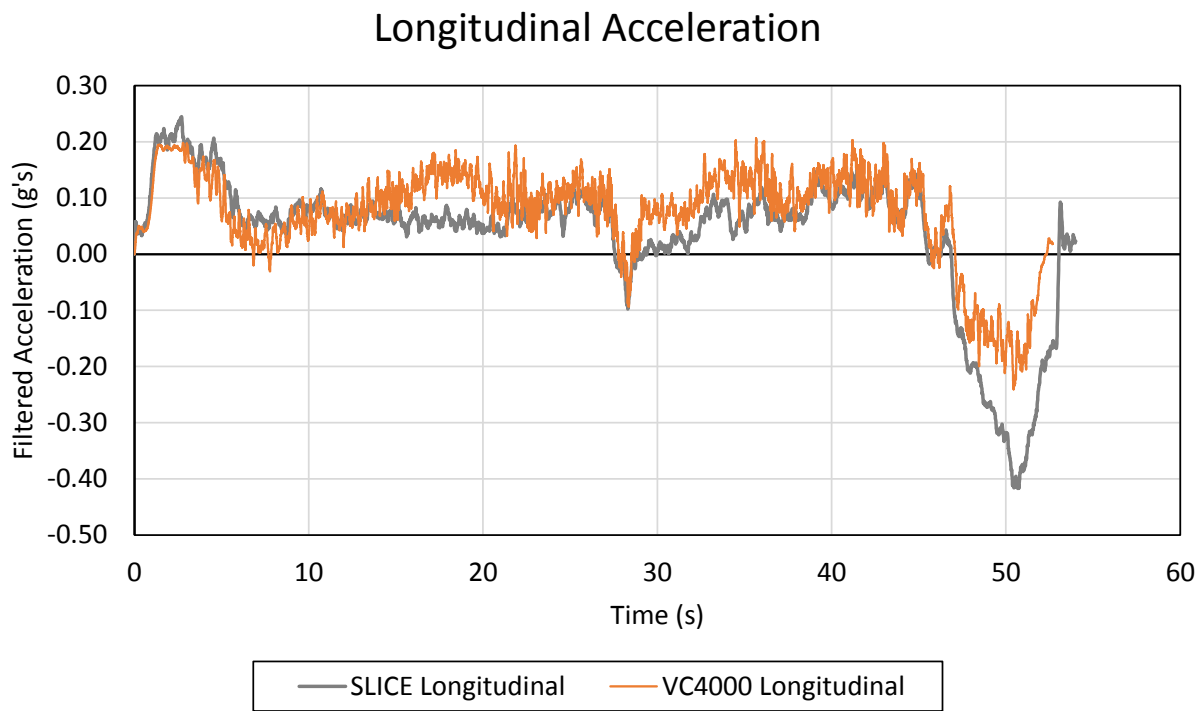


Figure H-1. Longitudinal Acceleration, Test No. CF100-3

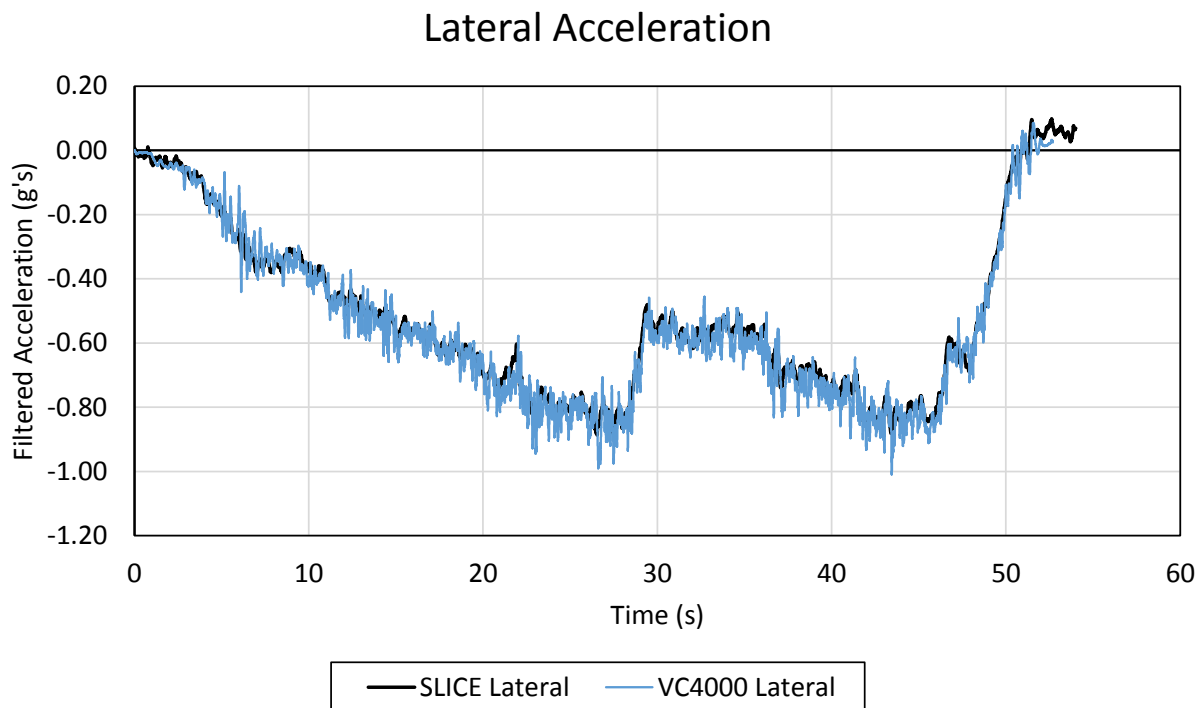


Figure H-2. Lateral Acceleration, Test No. CF100-3

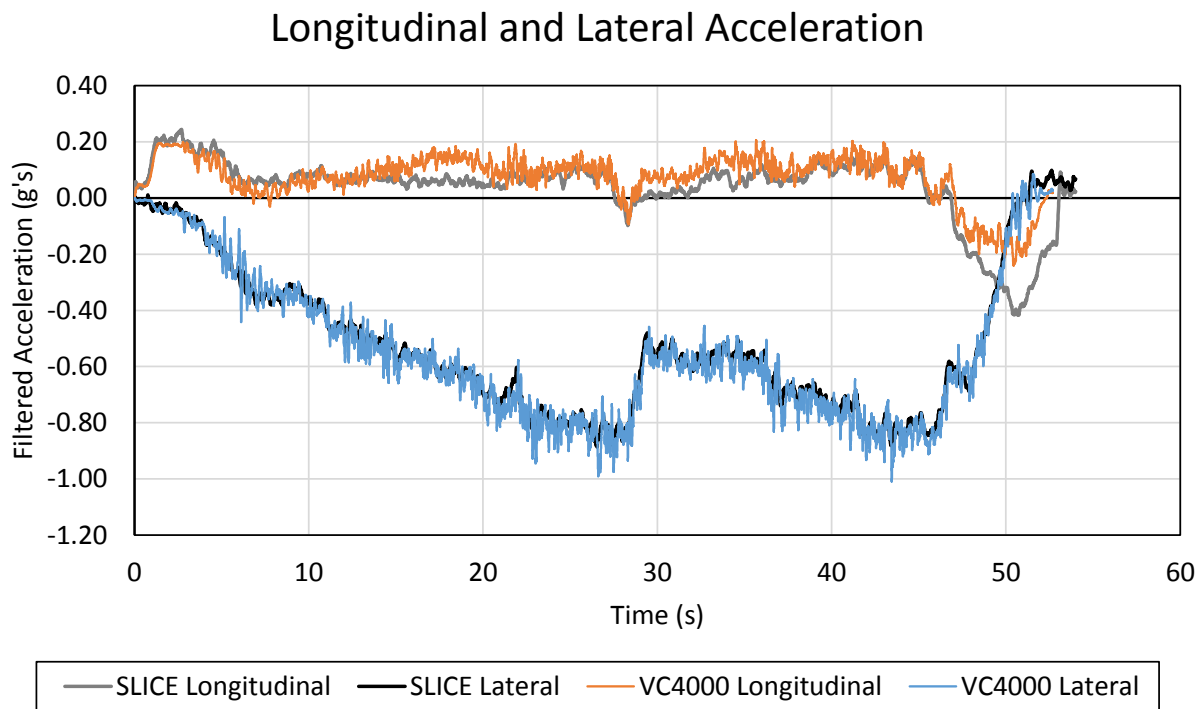


Figure H-3. Longitudinal and Lateral Acceleration, Test No. CF100-3

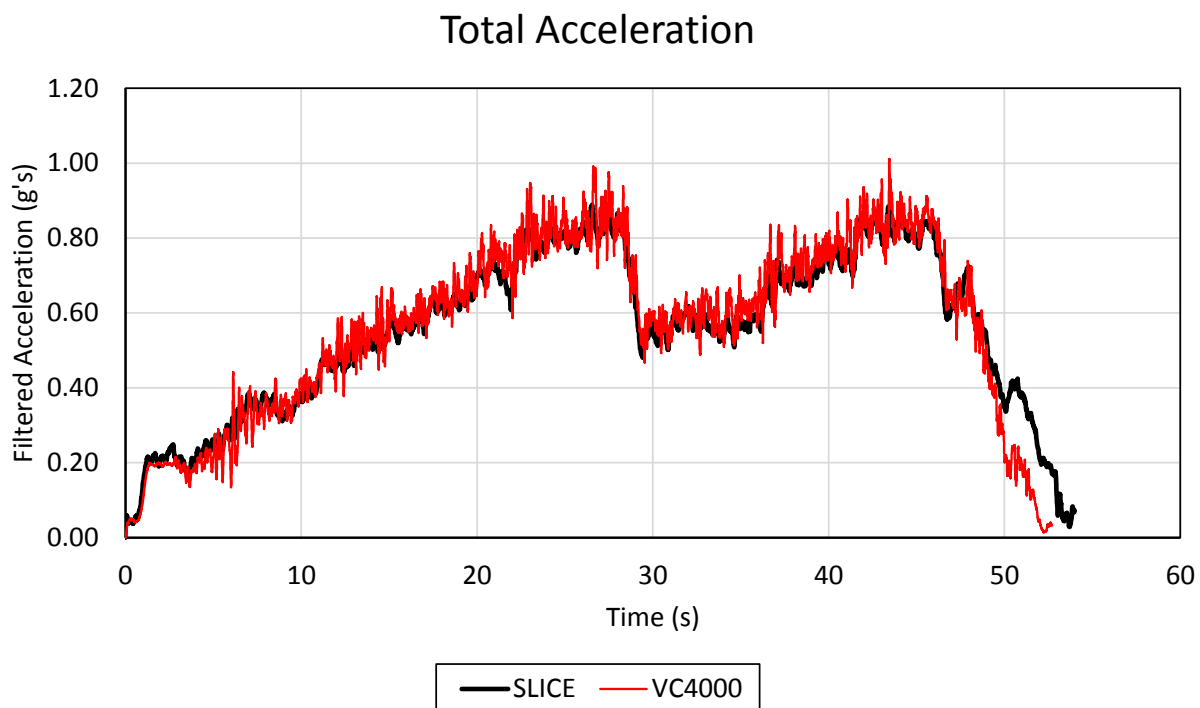


Figure H-4. Total Acceleration, Test No. CF100-3

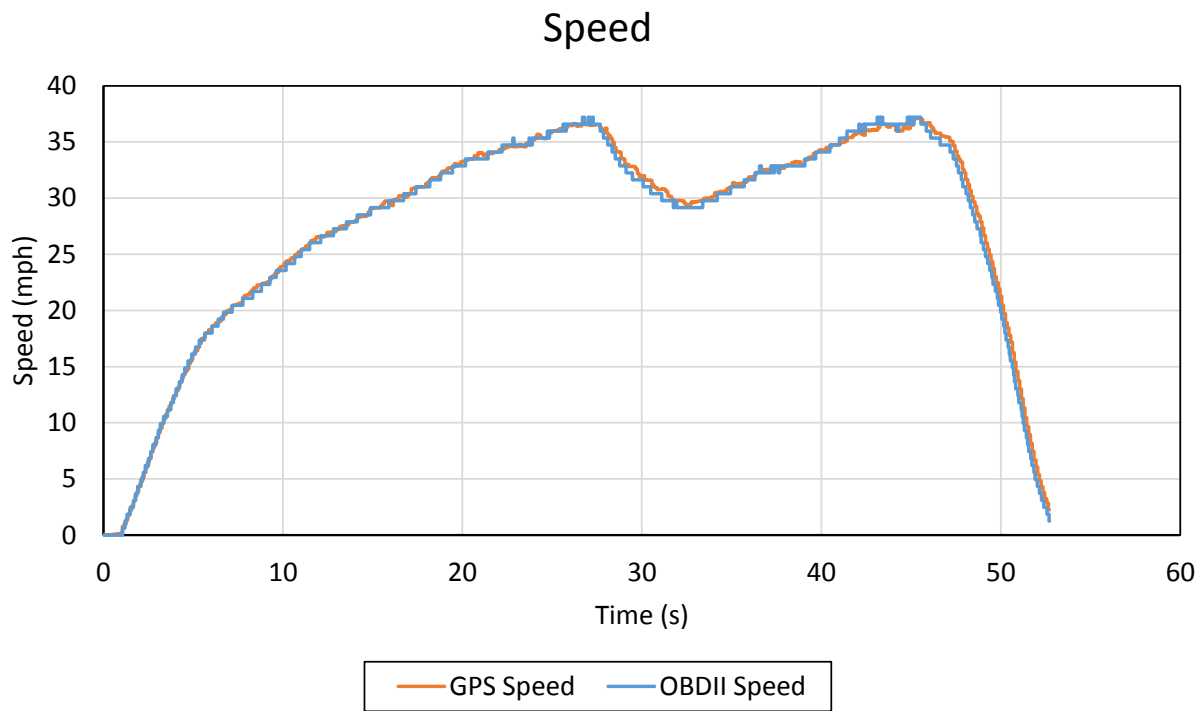


Figure H-5. Speed, Test No. CF100-3

Appendix I. Test Results – Test No. CF100-b

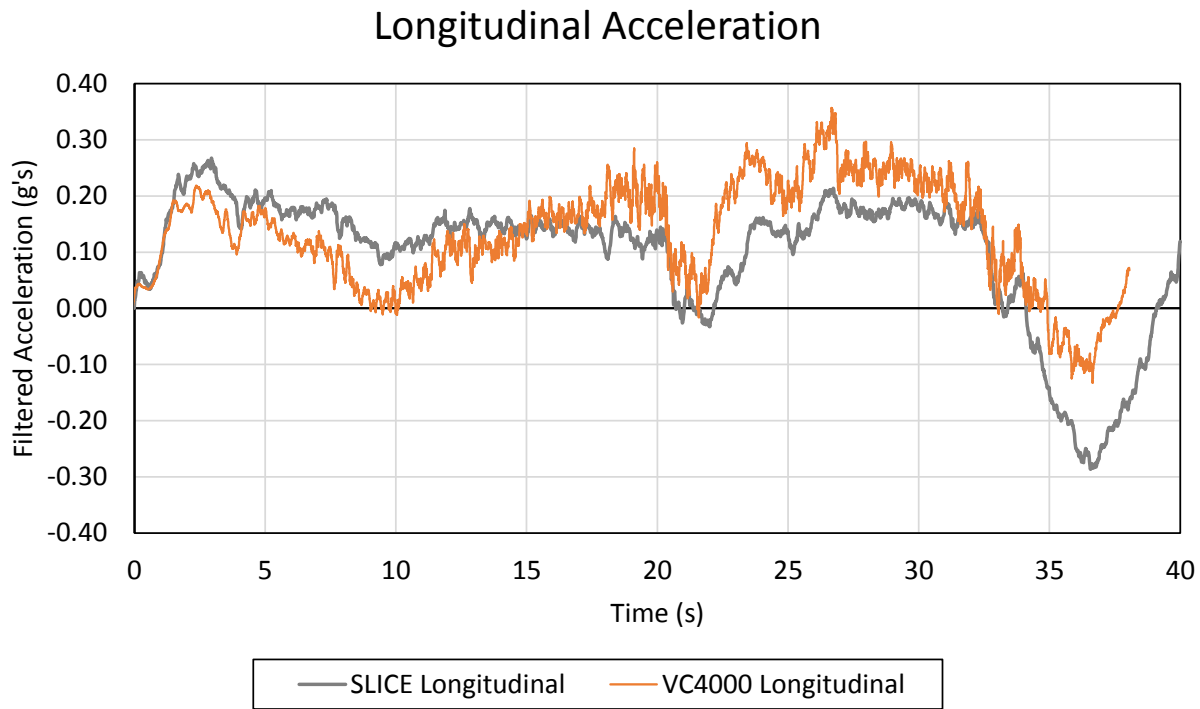


Figure I-1. Longitudinal Acceleration, Test No. CF100-b

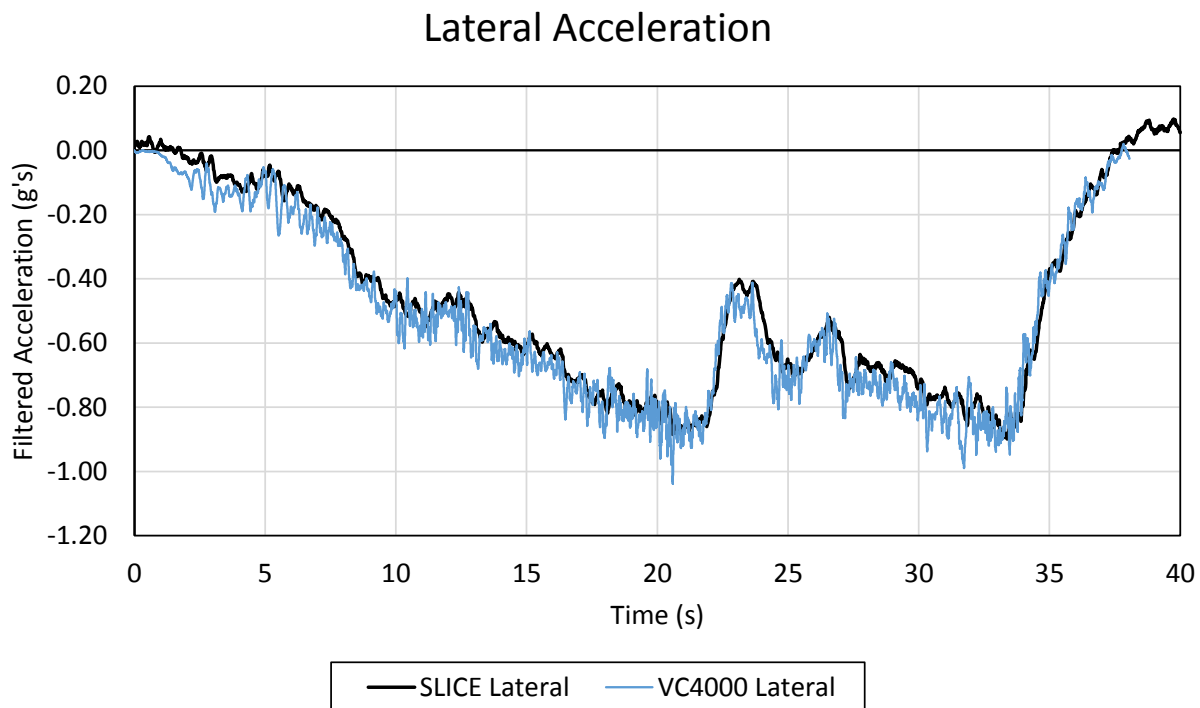


Figure I-2. Lateral Acceleration, Test No. CF100-b

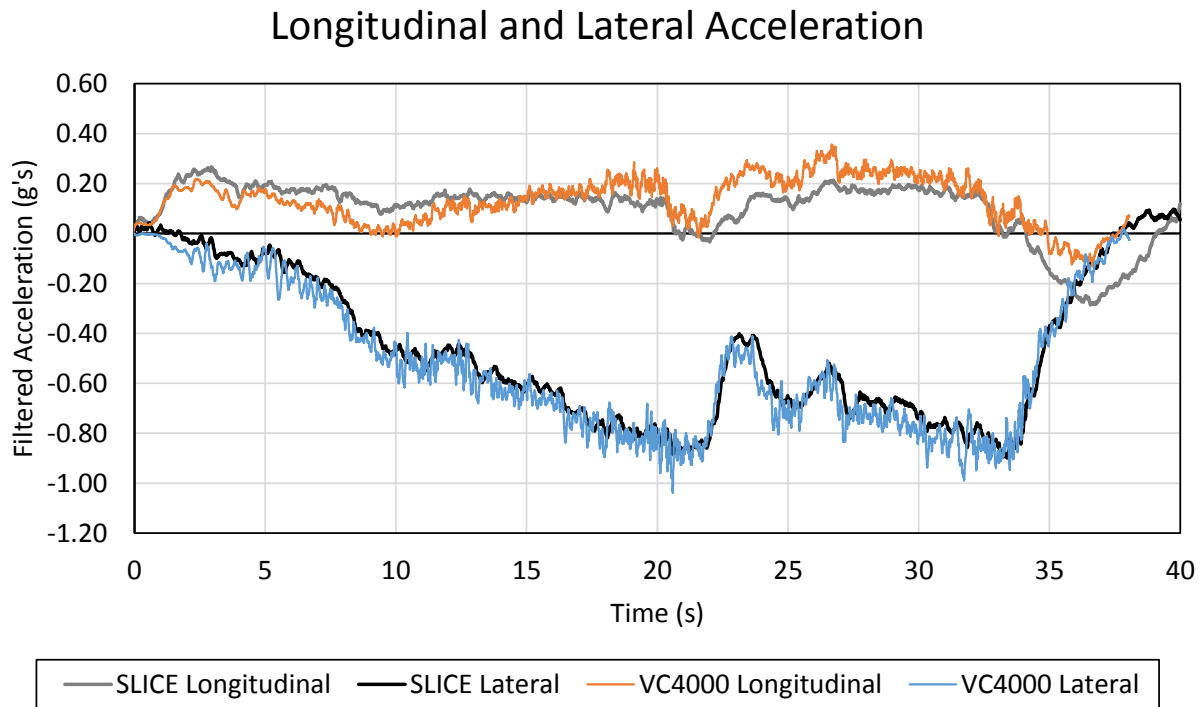


Figure I-3. Longitudinal and Lateral Acceleration, Test No. CF100-b

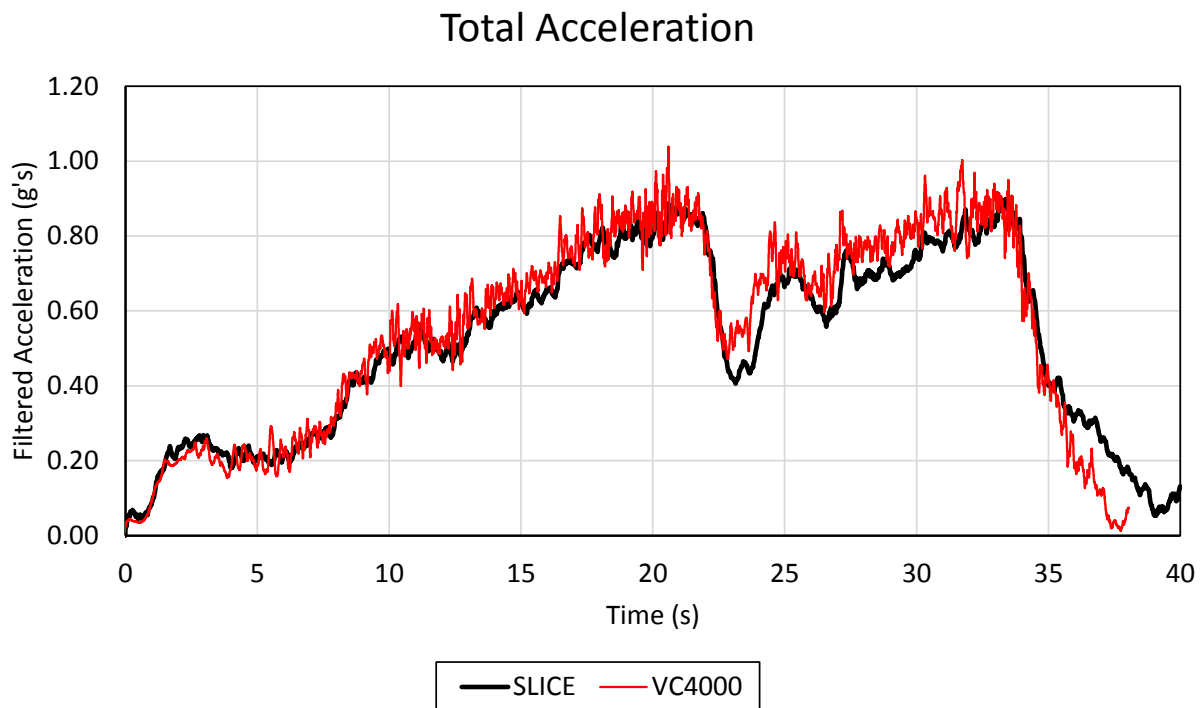


Figure I-4. Total Acceleration, Test No. CF100-b

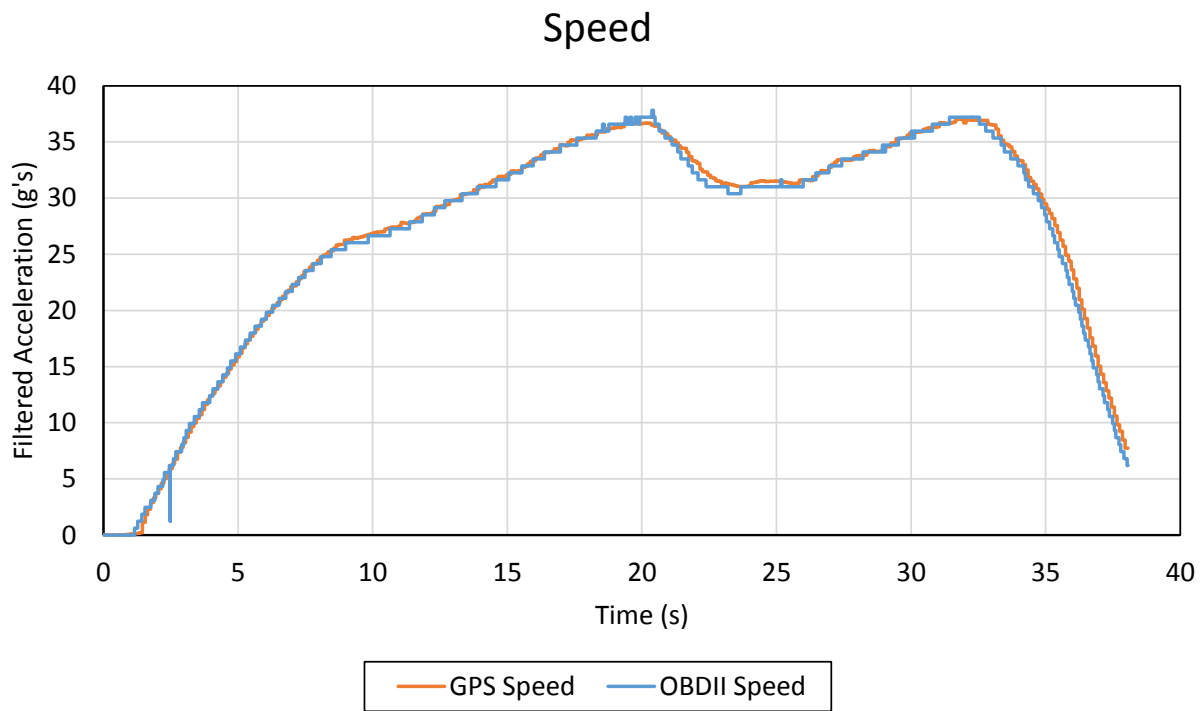


Figure I-5. Speed, Test No. CF100-b

Appendix J. Test Results – Test No. CF200-1

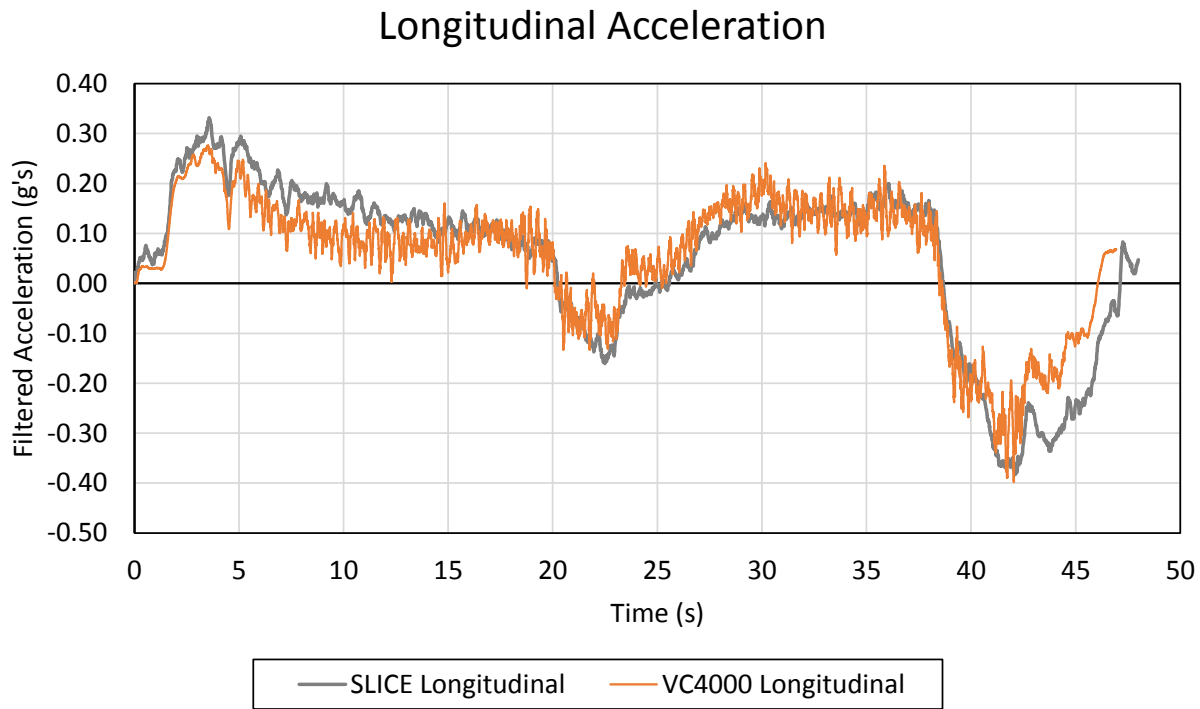


Figure J-1. Longitudinal Acceleration, Test No. CF200-1

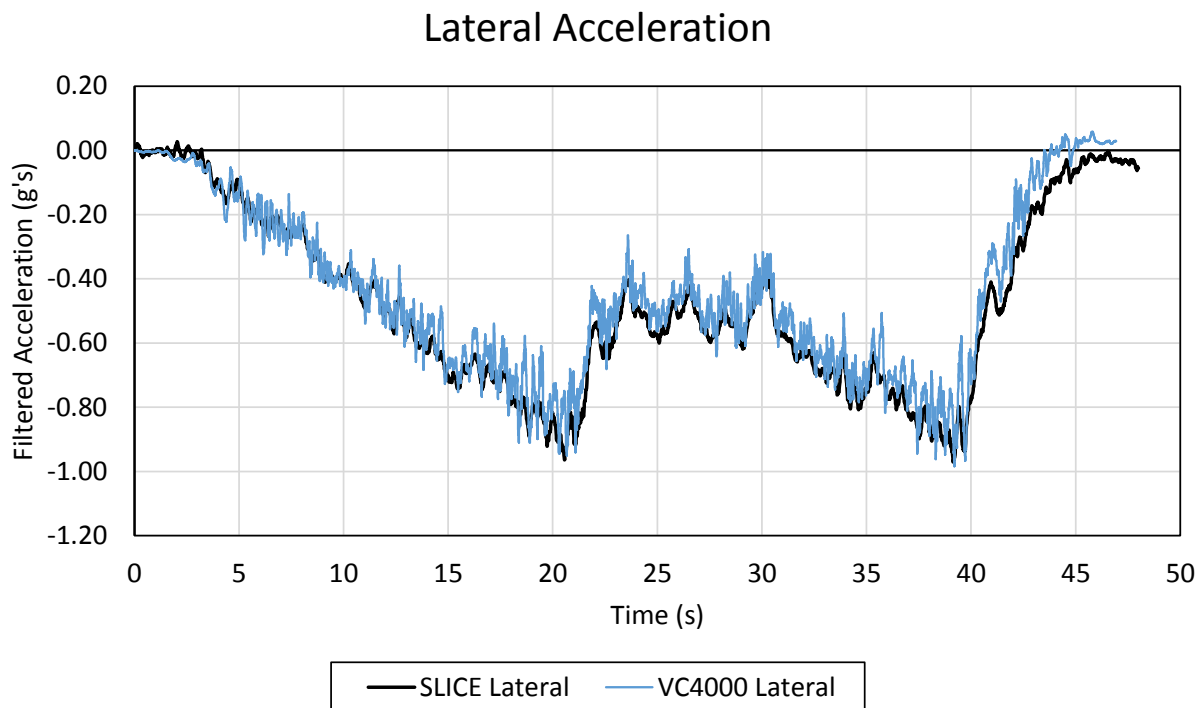


Figure J-2. Lateral Acceleration, Test No. CF200-1

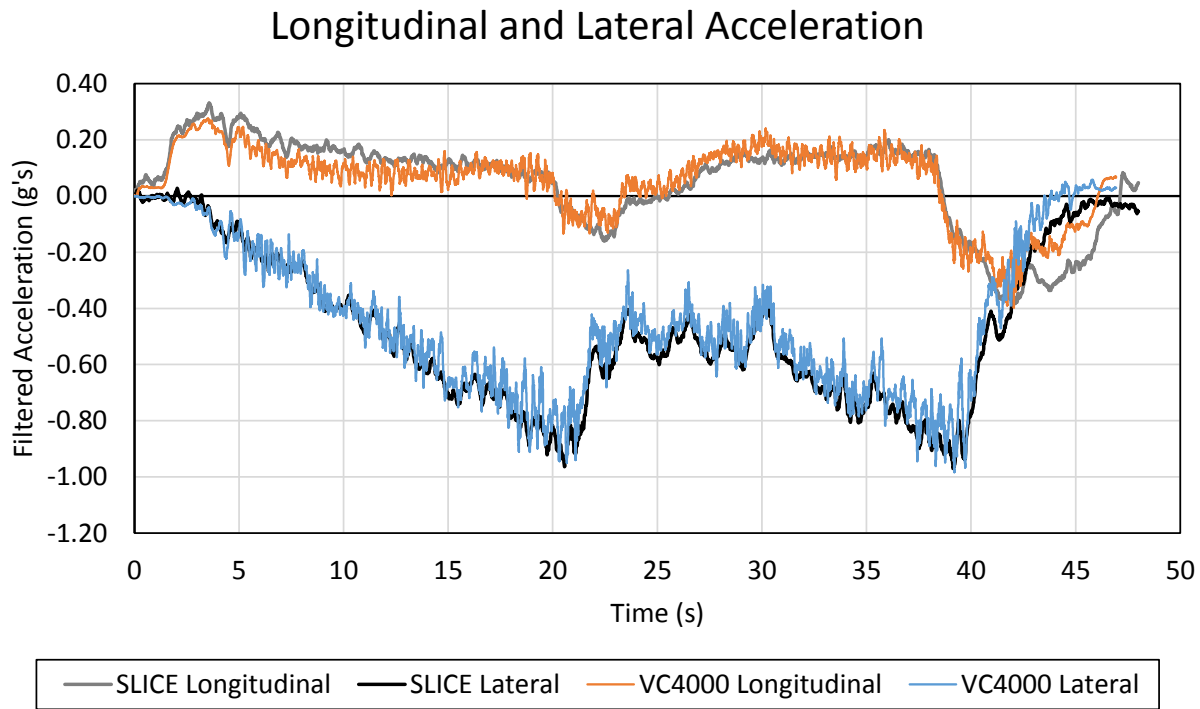


Figure J-3. Longitudinal and Lateral Acceleration, Test No. CF200-1

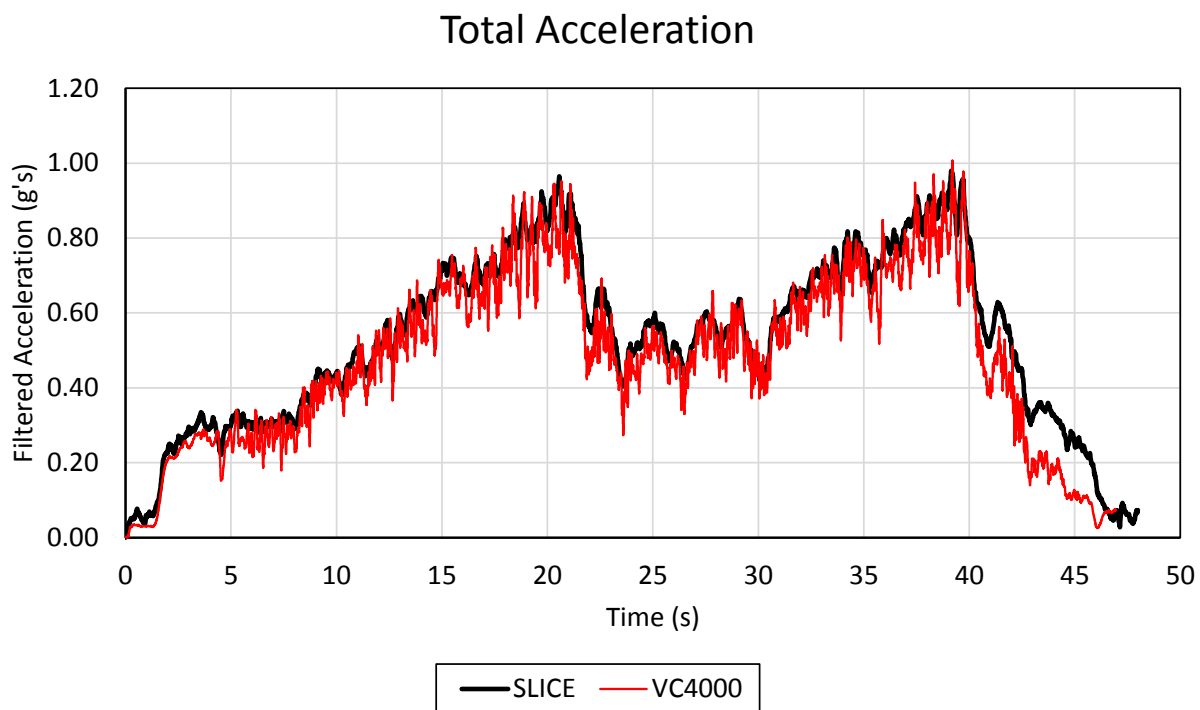


Figure J-4. Total Acceleration, Test No. CF200-1

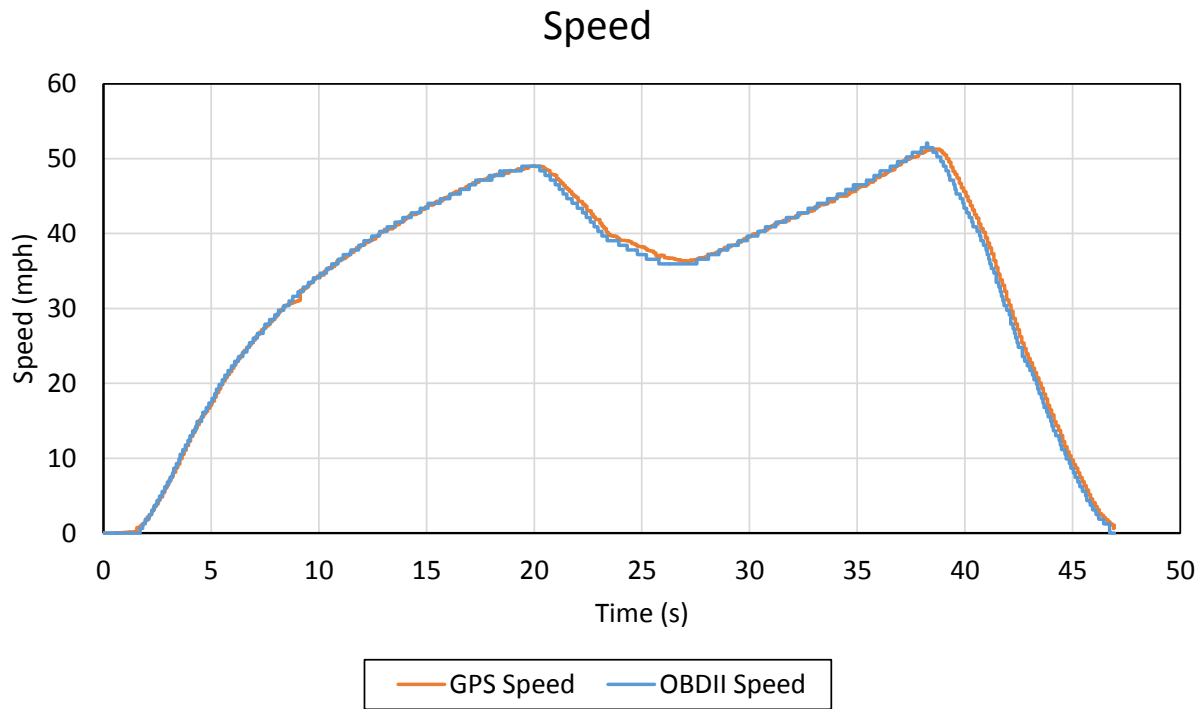


Figure J-5. Speed, Test No. CF200-1

Appendix K. Test Results – Test No. CF200-2

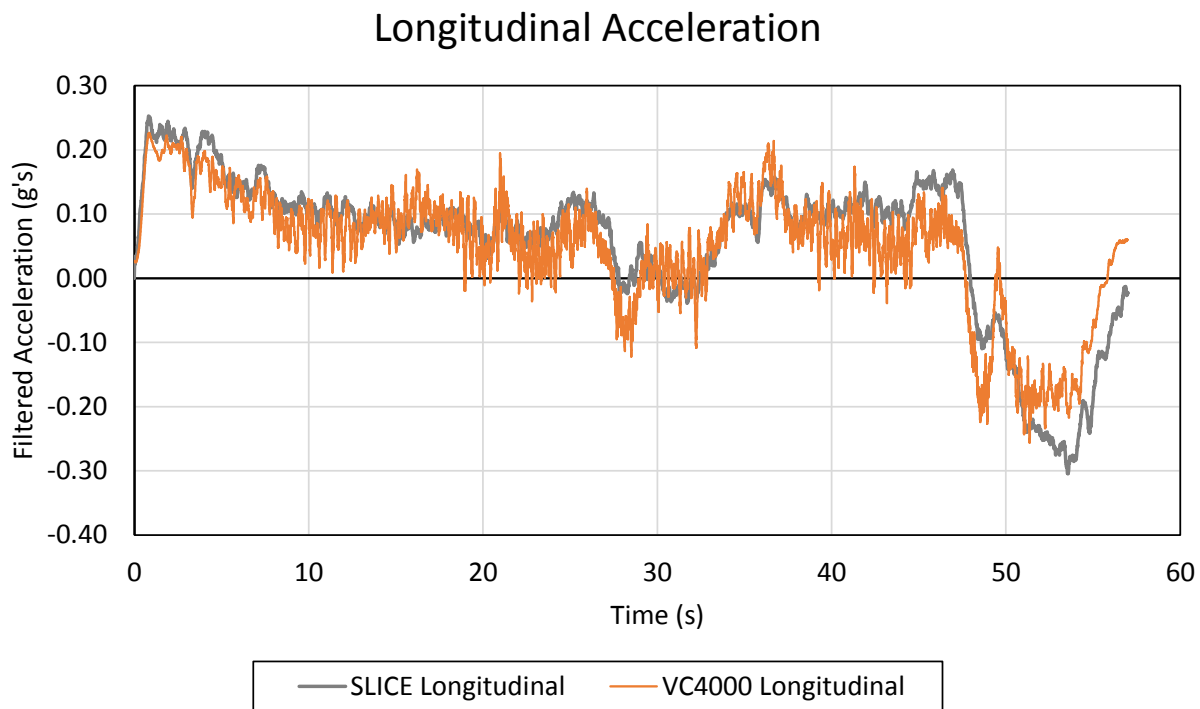


Figure K-1. Longitudinal Acceleration, Test No. CF200-2

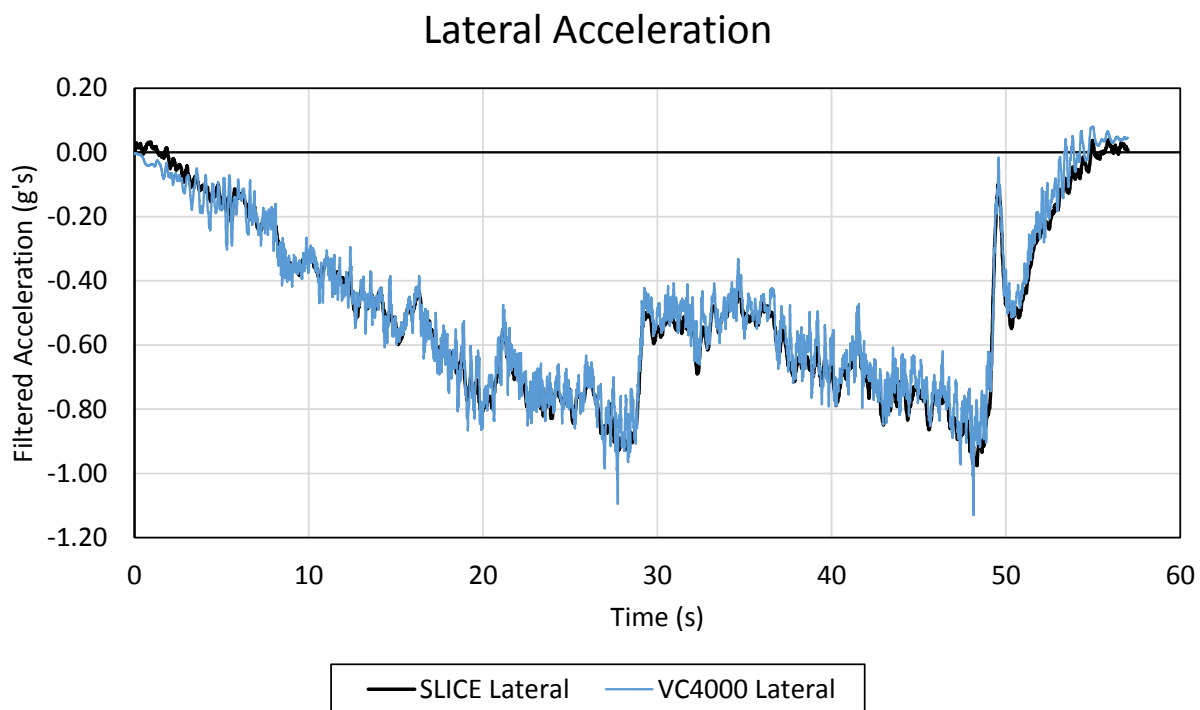


Figure K-2. Lateral Acceleration, Test No. CF200-2

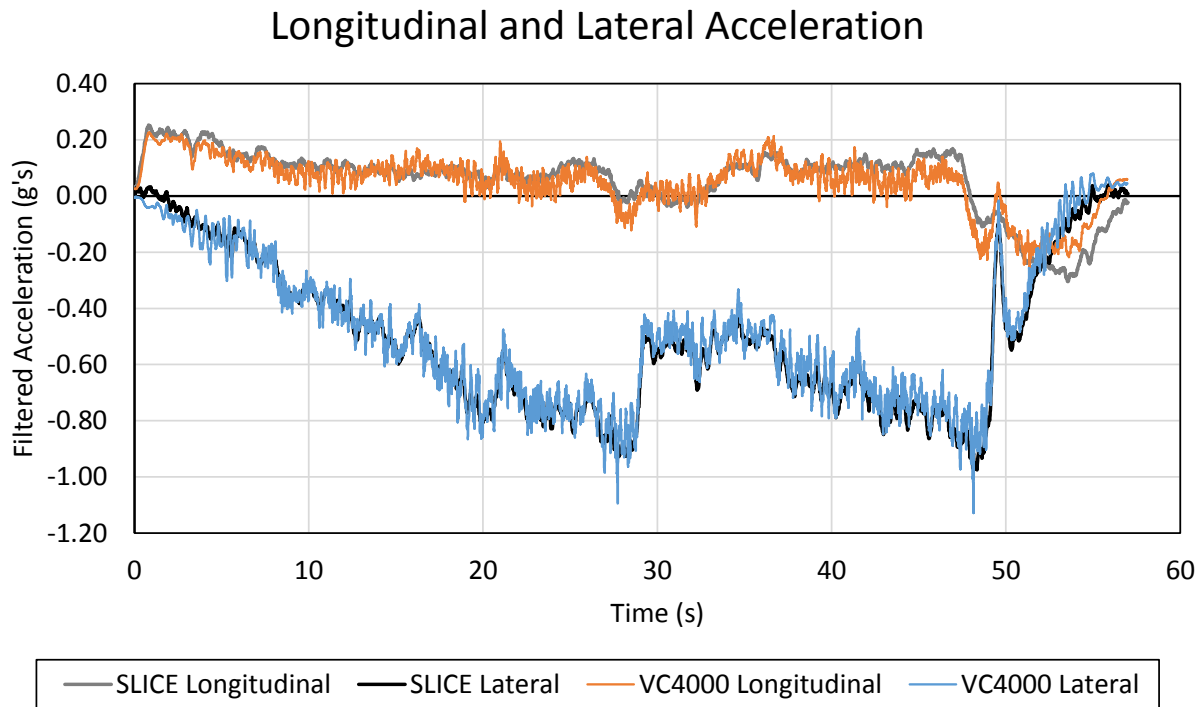


Figure K-3. Longitudinal and Lateral Acceleration, Test No. CF200-2

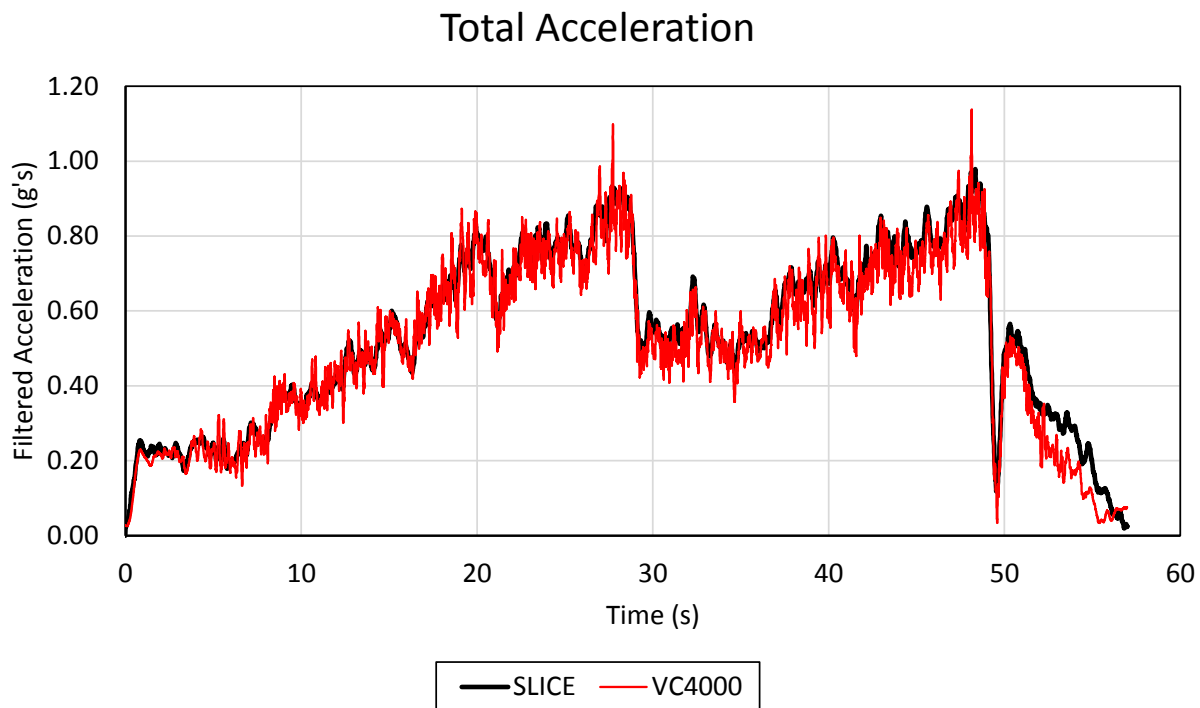


Figure K-4. Total Acceleration, Test No. CF200-2

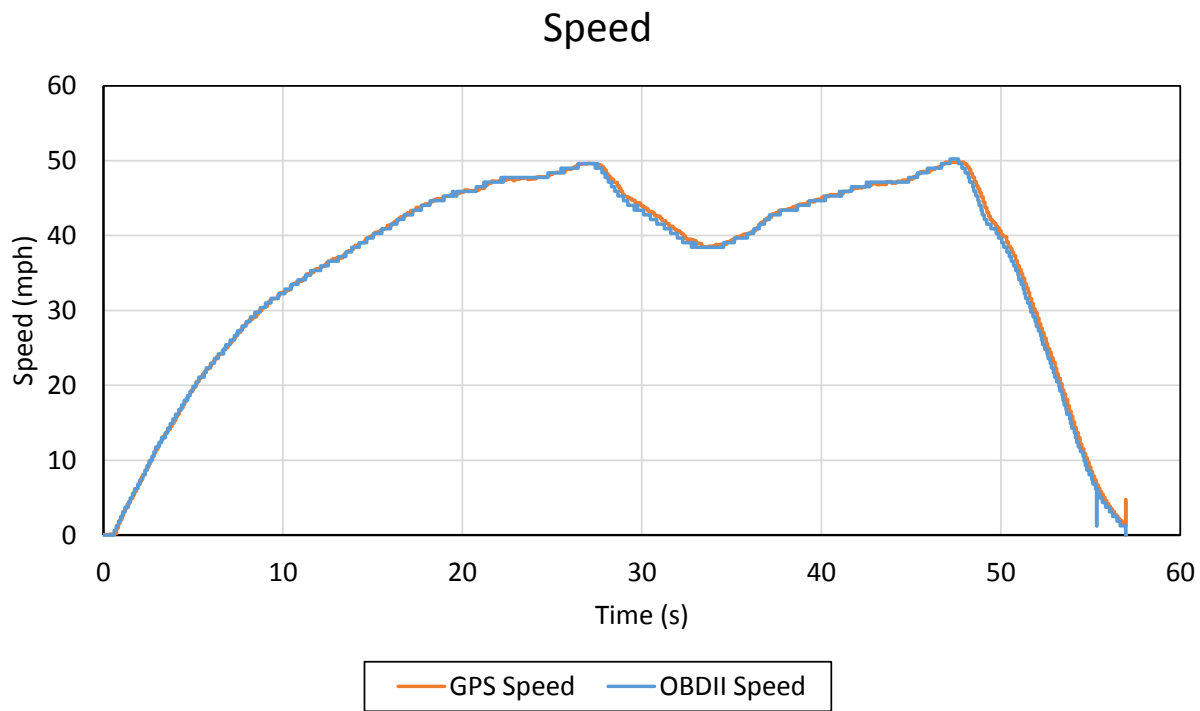


Figure K-5. Speed, Test No. CF200-1

Appendix L. Test Results – Test No. CF200-3

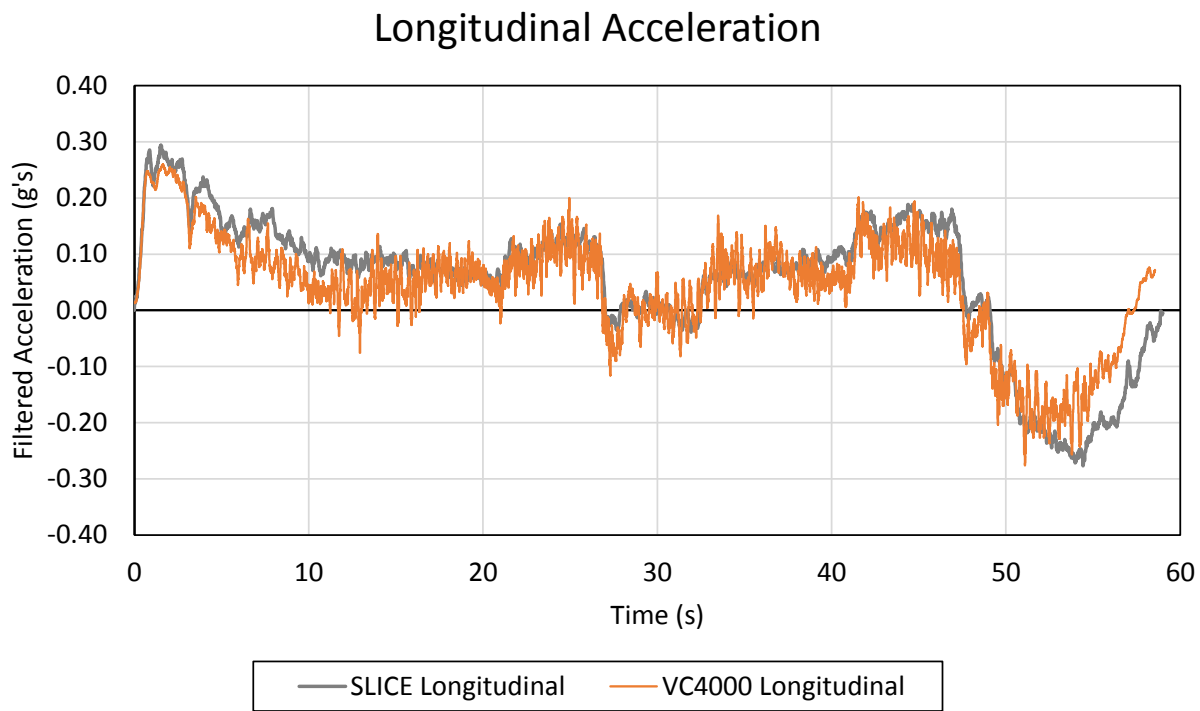


Figure L-1. Longitudinal Acceleration, Test No. CF200-3

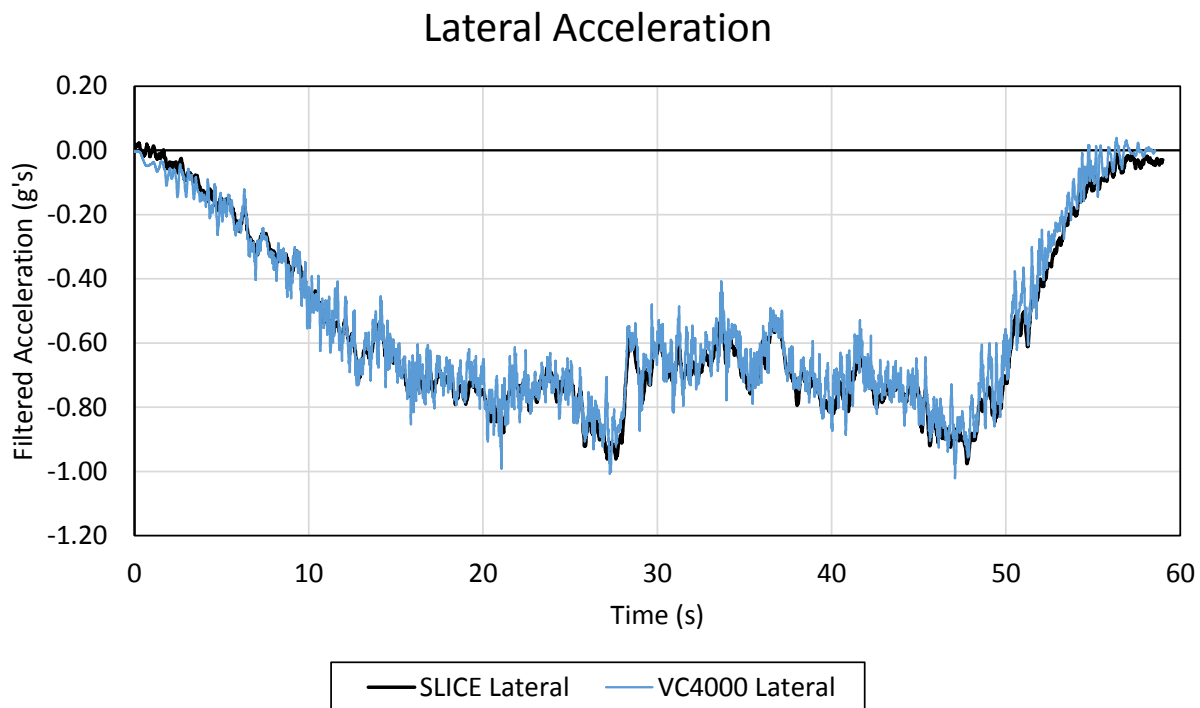


Figure L-2. Lateral Acceleration, Test No. CF200-3

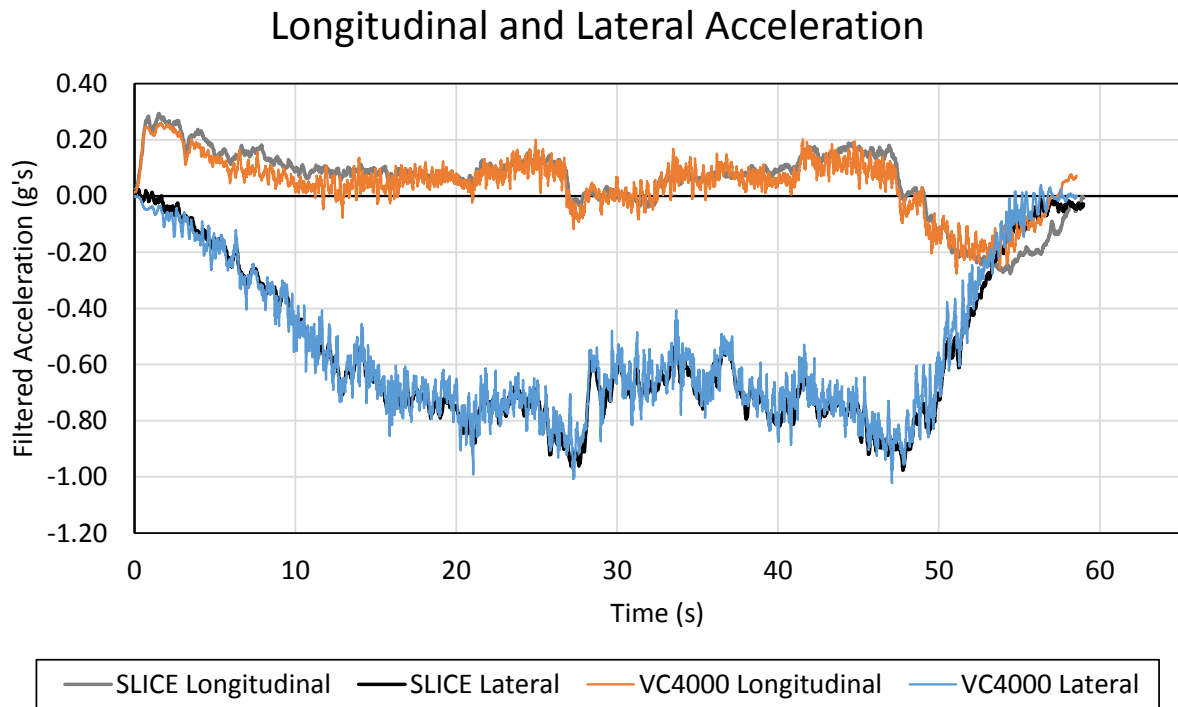


Figure L-3. Longitudinal and Lateral Acceleration, Test No. CF200-3

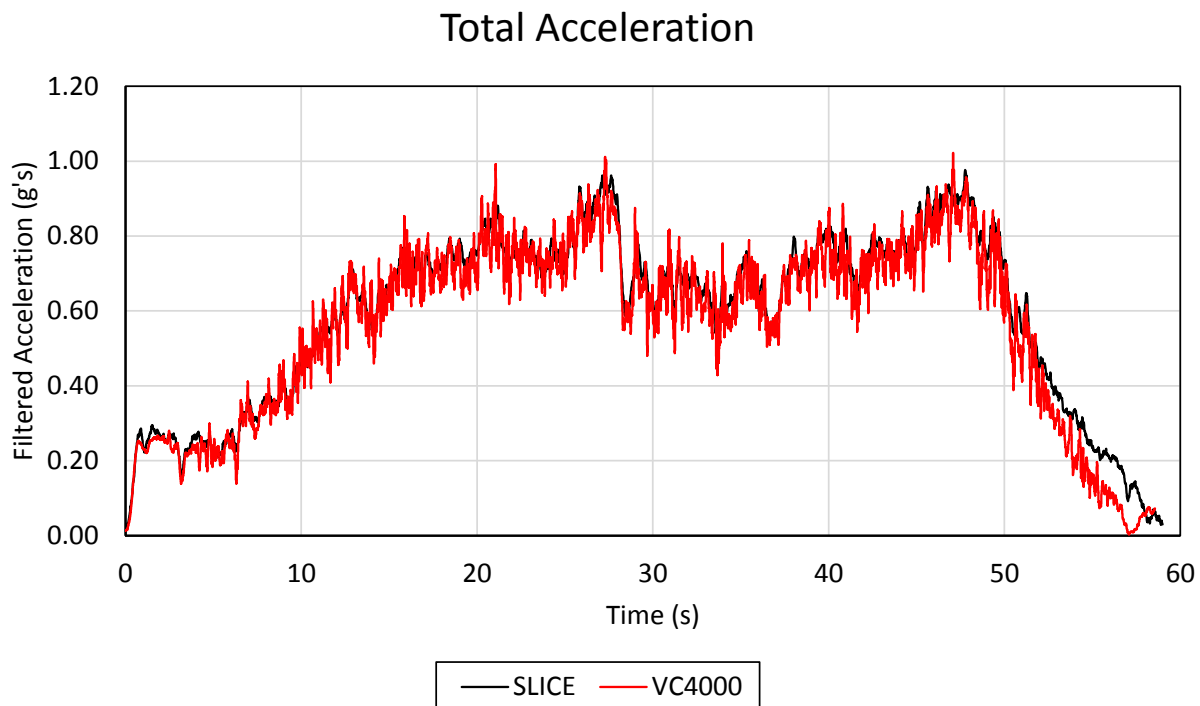


Figure L-4. Total Acceleration, Test No. CF200-3

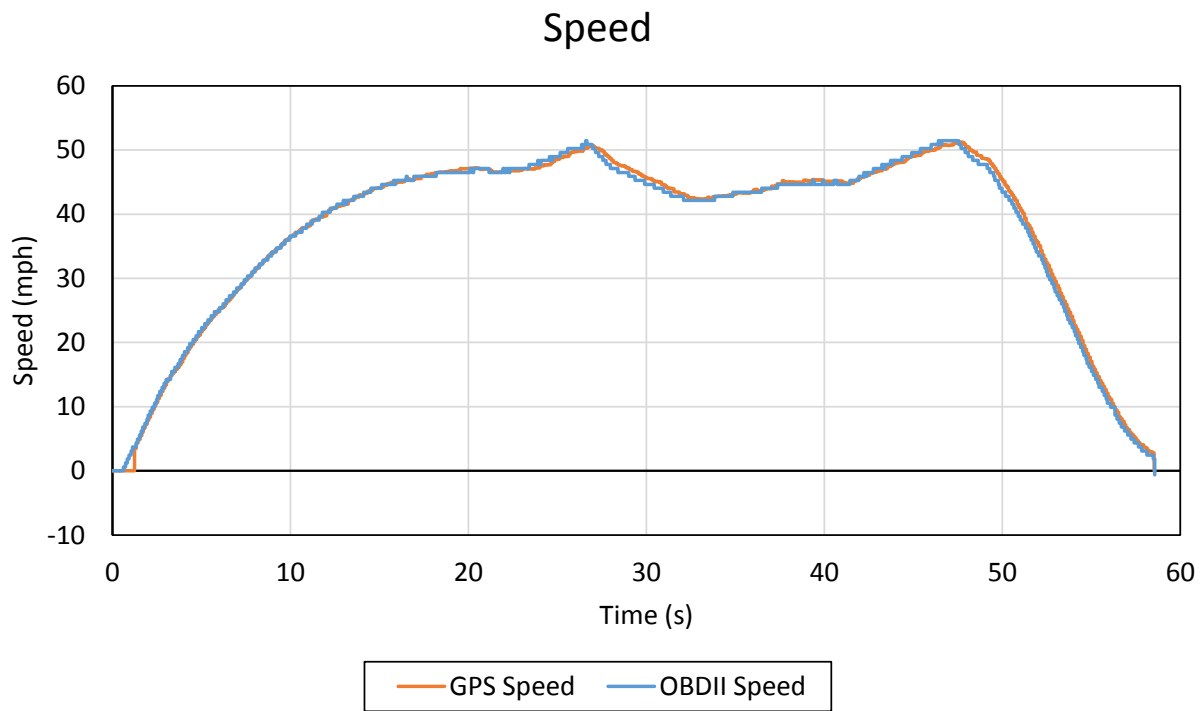


Figure L-5. Speed, Test No. CF200-3

Appendix M. Test Results – Test No. CF200-1b

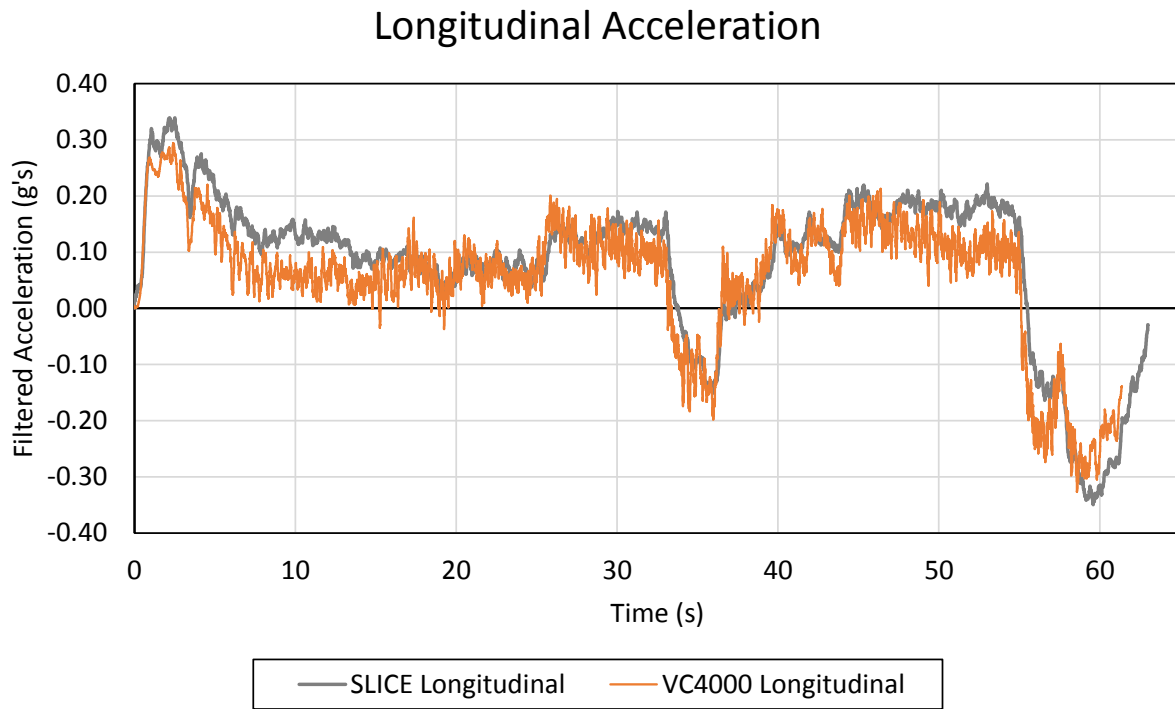


Figure M-1. Longitudinal Acceleration, Test No. CF200-1b

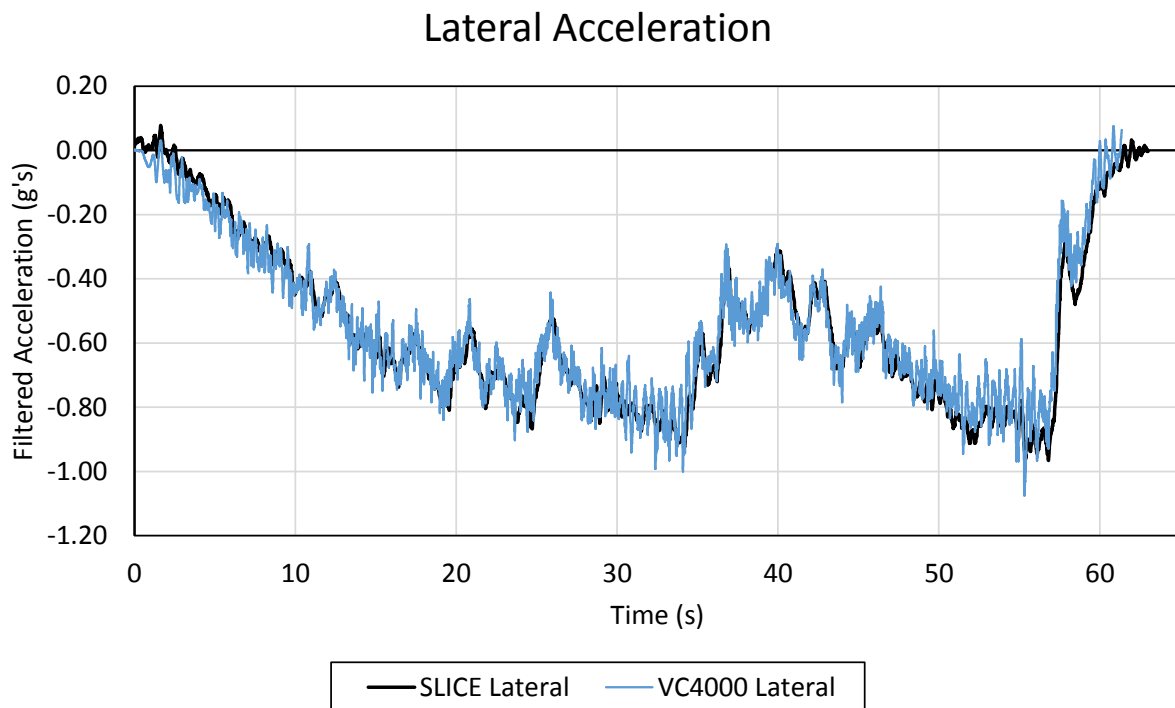


Figure M-2. Lateral Acceleration, Test No. CF200-1b

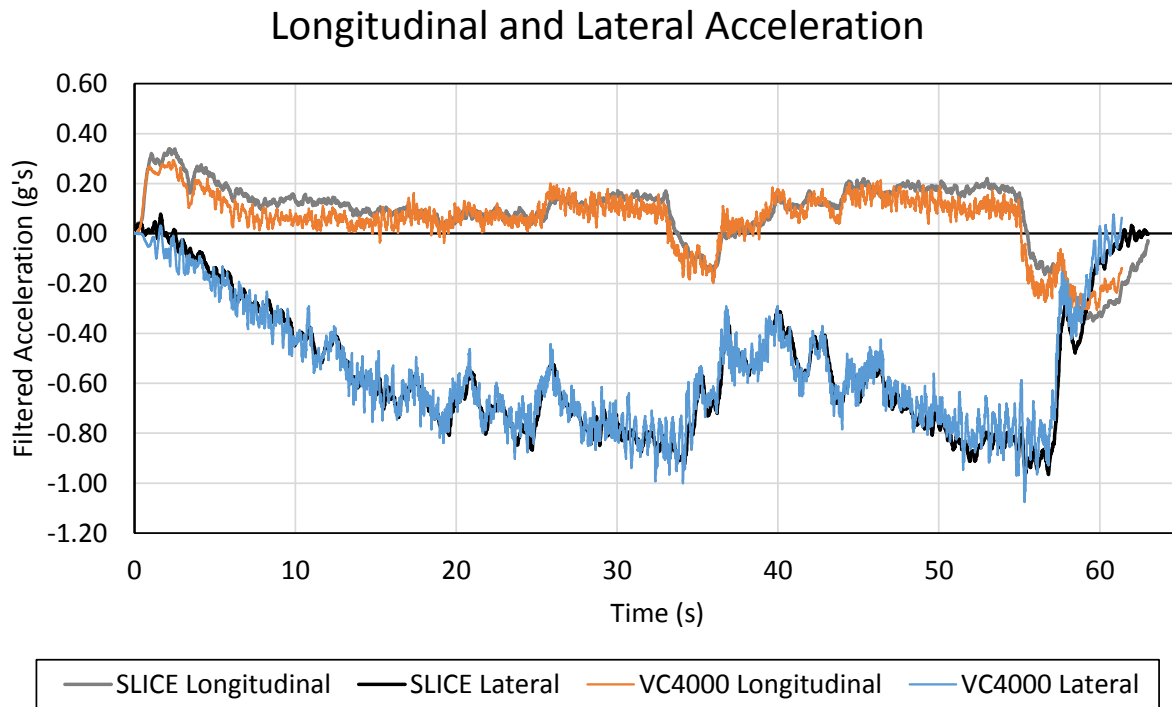


Figure M-3. Longitudinal and Lateral Acceleration, Test No. CF200-1b

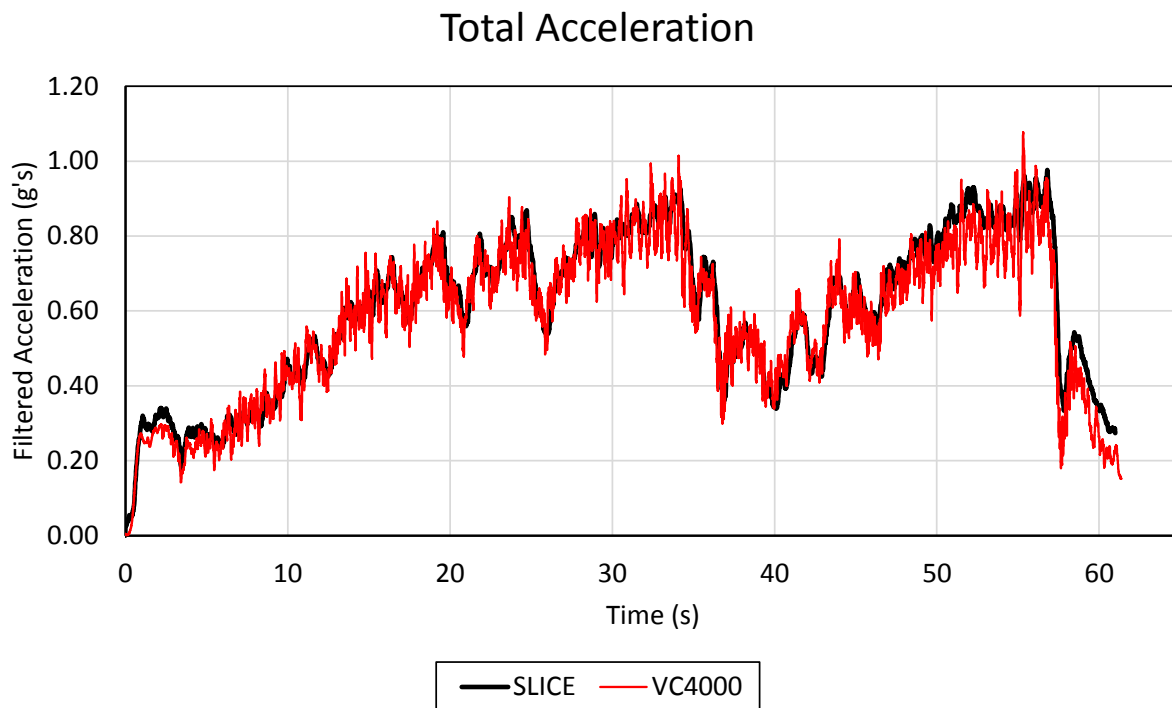


Figure M-4. Total Acceleration, Test No. CF200-1b

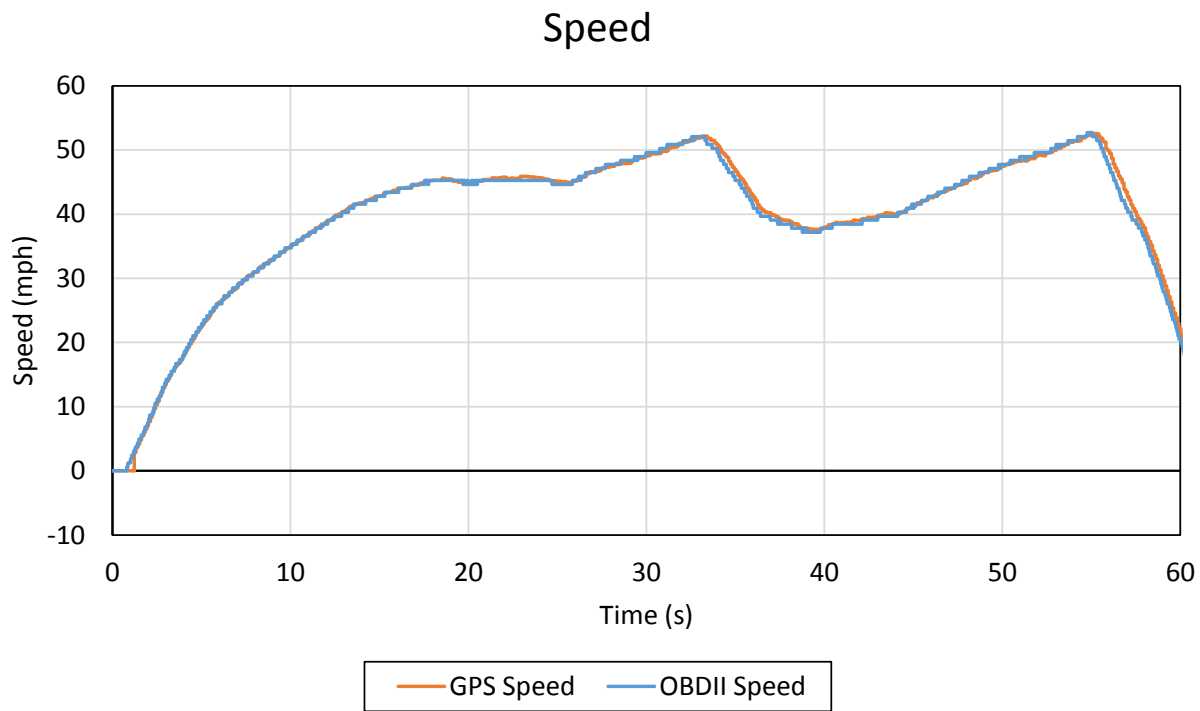


Figure M-5. Speed, Test No. CF200-1b

END OF DOCUMENT